Project 186

Final Technical Report

for

HYDAMP - II

A Joint Industry Program on Hydrodynamic Damping and Combined Motion

by

T. E. Horton
Professor of Engineering
209 St. Andrews Cr.
Oxford, MS 38655
(601)-234-3262

Jointly Sponsored by:

Agip, Milano, ITALY
Mobil R & D Corp. Dallas, TX
Minerals Management Service, Washington, D.C.
Naval Facilities Eng. Ser. Center, Port Hueneme, CA
Texaco Inc. Houston, TX

February 1995

PREFACE

Recall that the objectives of both HYDAMP studies have been:

1. Demonstrating the utility of the IPM in the combined motion hydrodynamic loading,
2. Provide an understanding of combined motion problems, and
3. Provide Morison based data.

At the conclusion of HYDAMP-I the observation was made: "...that the I-T Effect is the major source of uncertainty in the HYDAMP data and that it can be understood and quantified. With the IPM and SSPA data we have the technique and the data to achieve this." Thus the focus of HYDAMP-II has been:

1. A comparative study of the rough and smooth cylinder data and
2. A quantitative treatment of the I-T Effects observed in the data.

The plan for HYDAMP-II was to use the techniques of HYDAMP-I, which meant using the Inertial Pressure Methodology (IPM) as a guide subject to the constraint of the Morison formula.

Because of the coupling of these two studies, we have practiced certain economies in the preparation of this document. We have tried to avoid excessive replication of material. Nomenclature and reference material are the same, and we should refer the reader to the first report for background on concepts and techniques. Thus, the HYDAMP-I report may prove to be a necessary reference to this report.

In the preparation of this report we have tried to focus on the I-T Effect and a Data Correlation that arose from our understanding of the I-T Effect. The Data Correlation was a surprising consequence, which was not considered a possibility when this study was initiated. As a record of combined motion issues, this document is as complete as I could envision. I hope that my exposition of these issues has been clear, as I have addressed the major questions that I have encountered in the past decade of combined motion work.

The data presented in the Appendix also represents a complete record of all unidirectional combined motion data from the SSPA experiment. In this compilation are several Runs which were not available for the HYDAMP-I study.

T. E. Horton
February, 1995

LIST OF SYMBOLS

A_x	Amplitude of motion in the x or in-line direction
A_o	Amplitude of low frequency motion
A'	Amplitude of high frequency motion
a	Radius of the cylinder
C_a	Inertial coefficient for Morison equation
C'_a	The inertial correction coefficient for Morison equation, $C_a = 1\text{-}C'_a$
C_d	The drag coefficient for Morison equation
C'_d	The high frequency drag coefficient
$(C_f - C_r)$	The IPM coefficient
$(C_f + C_r)$	The IPM inertial coefficient
C'	The amplitude of the perturbation of the IPM coefficient
D	Cylinder diameter
DF_x	D-Force, in-line hydrodynamic force less the ideal inertial force
F_d	Drag or damping force
$\tilde{F}_d$	Normalized drag or damping force $F_d/\rho DL$
$(\tilde{F}_d)'$	High frequency component of the normalized drag or damping force
$(\tilde{F}_d)_o$	Low frequency component of the normalized drag or damping force
F_x	Hydrodynamic force on a moving cylinder
f	Frequency of periodic motion
f'	Frequency of high frequency motion
f_o	Frequency of low frequency motion
R	Interaction force term in IPM
T	Period of motion
$\dot{U}$	Acceleration of the cylinder
U	Velocity of the cylinder
U_s	Steady motion velocity
U_p	Periodic velocity amplitude
U_o	Mean velocity of cylinder
U'	Perturbation velocity amplitude
δ	Deviation of pressure coefficients from ideal
θ	Angular position on the cylinder
θ_{min}	Theta-min, position on the cylinder surface were the ideal pressure distribution is a minimum
ρ	Density of fluid
ω	Vorticity

CHAPTER I
INTRODUCTION

HYDAMP is a hydrodynamic loading study based on "Inline Combined Motion" tests conducted on a 1 meter diameter cylinder in the SSPA tank. These SSPA tests involved combinations of periodic and steady motions as well as combinations of two periodic motions. HYDAMP has focused on those tests in which the two combined motions were unidirectional. The data involving the combination of steady and periodic motions were intended to simulate loading from combinations of waves and currents. In this report these are referred to as LF data as they represent "low frequency" tests. The data involving combinations of periodic motions were intended to simulate combinations of wave motion and higher frequency structural motion. For identification we have referred to these as HF data, as they represent "high frequency" effects.

The SSPA experimenters and subsequent investigators of these data have considered the HF and LF tests to be at least distinctive or at most unrelated. However in HYDAMP-I, Chapter 5, we observed similar patterns in the IPM coefficient time series for the LF and HF tests. In the LF tests the steady motion can be viewed as a very low frequency motion with the low frequency contribution appearing as a perturbation. In the HF tests the low frequency motion is similar to the steady motion with the high frequency contribution appearing as a perturbation. The results of this study support this observation and lead to an empirical correlation involving both test conditions.

HYDAMP-I and HYDAMP-II were proposed as companion studies treating the smooth cylinder tests and the rough cylinder tests, respectively. Both studies were intended to supply Morison coefficient data compatible with current practice. The author's Inertial Pressure Methodology (IPM) was to be used as a guide in these studies.

Because of the close relationship between these two studies we have chosen to rely on the Report of HYDAMP-I for background and details on many items, which have not been reproduced in this document. However, to facilitate comparisons of the smooth and rough cylinder data, we have redone all the smooth cylinder data and have presented both smooth and rough cylinder data in this report in a side by side format.

Thus, this HYDAMP-II report represents a complete and comprehensive presentation of all data; however, it does not represent a complete record of all concepts and ideas introduced in the studies. Therefore, it is advantageous at this point to review briefly some of those concepts and ideas presented in HYDAMP-I and to indicate their relationship to this document.

REVIEW OF HYDAMP-I

In this review we are focusing on items which have not been repeated in this document. The two aspects of this exclusion are: (1) those ideas which are common to both studies and which have not been repeated in HYDAMP-II and (2) significant items presented in HYDAMP-I which were not pursued further in HYDAMP-II. Note, in identifying the Chapters in the two reports, Arabic numerals identify Chapters in HYDAMP-I while Roman numerals are used in the current report.

Reviewing HYDAMP-I on this comparative basis:

(a) The background on the IPM was provided in Chapter 3. A supplementary IPM presentation has been included as Appendix D in this report.

(b) Background on the SSPA experiment is reviewed in Chapter 3 and is not considered in this report.

(c) The procedure for converting IPM coefficient data into Morison coefficient data is developed in detail in Chapter 4 page 25. This procedure has been used in both studies and was not repeated in this document.

(d) The concept of a "hierarchy of Morison coefficient approximations" was presented in Chapter 4 , page 27. This presentation on the levels of the hierarchy has not been included in this report. However, recall the successive levels of the hierarchy enable constant Morison coefficient representations to more closely approximate the IPM coefficient. Level I approximation uses the same Morison coefficient values for all test conditions. Level II uses Morison coefficients particular to the test conditions with different coefficient values for the low and high velocity portions of the flow cycle. Chapters 3 and 4 presented the approach to LF data, the hierarchy of coefficient data, and an appraisal of their ability to reproduce the observed LF forces. In this document Chapter III is a similar focus on LF data. In Chapter III, coefficient data is found with a graded appraisal of Level I and Level II applied to both smooth and rough cylinders. The time series of both smooth and rough force predictions for these approximation levels are presented in detail in Appendix A of this report.

(e) Chapter 5 presented examples of the complex relationship between damping force and velocity. Experimental realizations of these representations were presented; however, as they could not be achieved with constant coefficient Morison constraint, they have not been developed further. Clearly, this presents a dilemma for the knowledgeable designer. This subject deserves further study outside the Morison constraint and entails questions of validity of the RV (relative velocity) and IF (independent flow field) representations for the combined motion problem. In HYDAMP-I Chapter 5 presented the HF and damping data. Chapter V serves a similar role but also presents a more comprehensive interpretation of the these data for both smooth

and rough cylinder tests.

(f) Two ideas critical to the success achieved in this report are the "I-T Effect" and the "Correlation KC Number". The correlation KC Number (Chapter 3, page 22) arises from the IPM formulation and is related to the ratio of the velocity squared and the acceleration. The I-T Effect (Chapter 3, page 24), an abbreviation for "inline force contribution related to the transverse force", is associated with vortex dynamics. As a vortex moves in the inline direction it results in a transverse force, and as it is swept in a transverse direction it gives rise to an inline force contribution, the I-T Effect. We shall present more on these two ideas later.

EVOLUTION OF HYDAMP-II

HYDAMP-II was proposed as an adjunct to HYDAMP-I, utilizing the data processing techniques developed in the earlier study to achieve a companion analysis of rough cylinder data. The completion of this data processing task was straight forward and was completed on schedule as planned. Large inline and transverse forces were observed in the rough cylinder data.

The increase in transverse forces provided a clear insight on the I-T Effect. These data confirmed our earlier speculation that the I-T Effect represented a series on inline force impulses with amplitude, frequency, and phase related to the transverse force. Furthermore, rather than oscillating about a "base" pattern, the observed I-T impulses appeared atop the "base" pattern. The "base" pattern is associated with zero I-T force.

At the conclusion of the proposed work the HF and LF data provided only a conjectural data base for establishing a "base" pattern of drag coefficients. The problem was that only during a few cycles, usually in the early portions of a test, was the transverse force sufficiently small to allow the base pattern to be quantified. To establish a correlation pattern we needed a significant data base in which transverse forces were suppressed.

Data for constructing the needed data base are to be found in each Run, in the interval in which the test cylinder is accelerated up to test conditions. This is a classic problem in unsteady hydrodynamics, the "starting problem", which has been studied analytically at lower Reynolds Numbers. Using the IPM, coefficient data can be easily extracted from these test conditions. These data have been "thrown away" by others who analyzed only fully established conditions. During this interval, because the cylinder is moving through a quiescent fluid, there is no return wake to complicate the issue.

Thus, late in the HYDAMP-II effort we saw an opportunity for a significant "break through"; therefore, the objective shifted to examining the coefficient data from the "starting problem" interval. The result was a coefficient data set sufficient to establish the "base" pattern for the drag coefficient. These data have been used with the HF and LF data to establish a comprehensive correlation using the IPM KC Number.

So, in the end, our objective had shifted to the possibility of establishing a comprehensive correlation pattern from the full set of combined motion data. We were able to achieve this objective. The comprehensive pattern indicates that the I-T Effect is a major source of disparity in the test data studied. We have shown that if the transverse force can be suppressed a minimum coefficient is found and as the I-T Effect is enhanced the coefficient increases above this minimum base.

In this report we have provided both (1) the data specified in the original proposal and (2) the most comprehensive view of these data yet achieved. We have been able to fit together on a comprehensive correlation plot both the HF and LF data, as well as conventional periodic and more exotic "starting problem" data. This correlation plot is far more than I had felt possible when this study commenced.

To all designers, hydrodynamic loading coefficients are important, and the SSPA data are especially important in that they match design conditions for many structures. Certainly the values for these specific test conditions are important; however, a comprehensive understanding of such data is more important. Such an understanding not only enhances the level of confidence within the range of the tests but also enables one to extrapolate the data intelligently to conditions not included in the tests. This understanding also allows one to see why for the same KC Number, the drag coefficients for a random sea state and for the simple periodic motion can differ dramatically.

REPORT ORGANIZATION

Chapter II serves as an introduction to the data and reviews two important concepts: the I-T Effect and the IPM based KC Number.

Chapter III is devoted to the LF data. Morison coefficients with force predictions based on these data are presented. A correlation of the LF drag coefficients with IPM based KC Numbers concludes the chapter.

Chapter IV treats the "Starting Problem" data. These data yield a coefficient data base which is free from the I-T Effect. Composite correlation plots of the LF and Starting Problem data are presented.

Chapter V is devoted to the HF data. A detailed explanation of the behavior of the inline and transverse data patterns for these test conditions is given. Damping coefficient data for both smooth and rough cylinders are presented. Correlation plots of drag coefficients for periodic data, with and without high frequency perturbations, are presented.

Chapter VI presents additional conclusions on the study and a complete correlation plot comprised of data from all SSPA unidirectional test conditions: LF, HF, Periodic, and Starting Problem.

In drafting this report we have: (1) relied on the previous report to supply background material, (2) presented detailed compilations of data in self contained Appendices, and (3) introduced meaningful ID Numbers and formatted data so that side by side comparisons could be easily made.

In examining the self contained Appendices of this report, one might feel that they have been arranged in reverse order, with Appendix D containing introductory review material on the IPM. Appendix C presents detailed time series data for all SSPA unidirectional tests: LF, HF, and Periodic. Appendix B presents a close-up of the LF data and Appendix A presents force predictions for the LF cases and coefficients. At the beginning of each of Appendix is a detailed guide to its contents.

CHAPTER II
REVIEW OF DATA AND CONCEPTS

This chapter provides a review of ideas and data which are used later in this study. The first section covers how data were processed and serves as an introduction to the data format and location in the Appendix. The second section illustrates the development of time series inline and transverse data patterns for different KC Numbers. This review assists in understanding the observations on HF data in Chapter V. Illustrations of the I-T Effect are given in the third section. The final sections treat the question of the proper correlation KC Number for combined motion and the character and role of roughness in the SSPA tests.

REVIEW OF DATA

In this report we have compiled the smooth and rough cylinder time series of all 39 SSPA Inline Combined Motion test conditions. Before introducing the IPM data, we shall cover how the data were reviewed before IPM processing.

The preliminary review consisted of plotting every point, Figure 2.1, for each of the 78 runs. These plots are recorded data for inline and transverse forces and for inline and transverse accelerations as a function of the point number (time between points 0.02 seconds). These plots were used to appraise the quality and to determine significant amplitudes. They indicate that each record contains a lengthy interval before movement starts and after motion has been terminated. On the small scale of the transverse acceleration plot (4th frame) one can detect the 0.004 meters/sec^2/bit digitizing resolution. Also, note on the inline acceleration plot (3rd frame) the initial impulse that starts the motion and a similar impulse that terminates it. After this preliminary review, these intervals at the beginning and end of the Run can be deleted from the record.

To determine the precise start and stop points for further processing, plots such as Figure 2.2 were constructed. These zoomed in on the starting (right column) and terminal (left column) impulses. Suitable new Initial and Final Points, which define the "Significant Test Interval", are indicated on the inline acceleration plots. These points become the basis for the computation of velocity by integration of the inline acceleration.

Because the digital resolution of the acceleration imposes a limit on zeroing the acceleration, the computed velocity will have an apparent drift component. For example, in Run 132, which has a Significant Test Time of 66 seconds, an acceleration uncertainty of .004 meters/sec^2 results in a velocity component which would

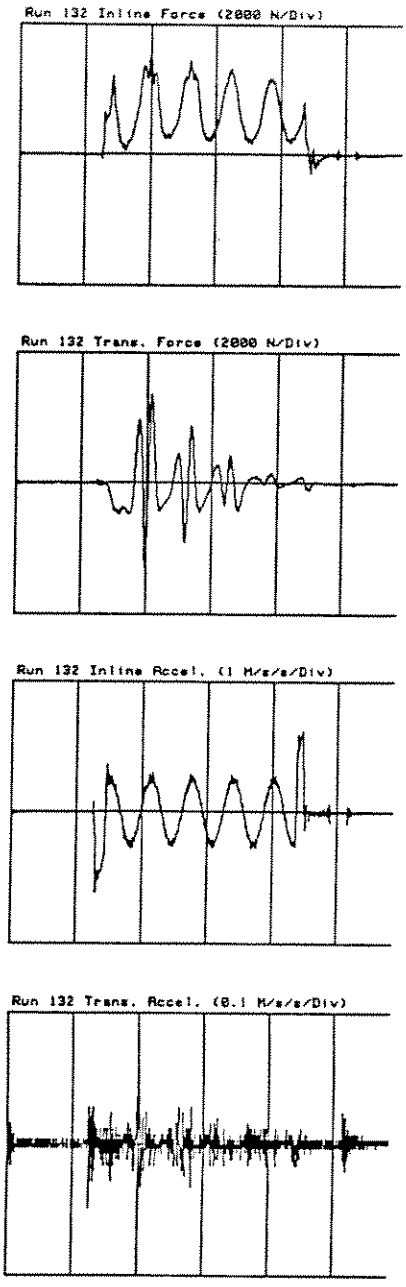

RAW DATA for RUN 132 points 1 to 5840

FIGURE 2.1
INITIAL PLOT OF TEST DATA

Times Series Plot of Full Test Interval
Time scale: 1000 points/div or 20 sec/div

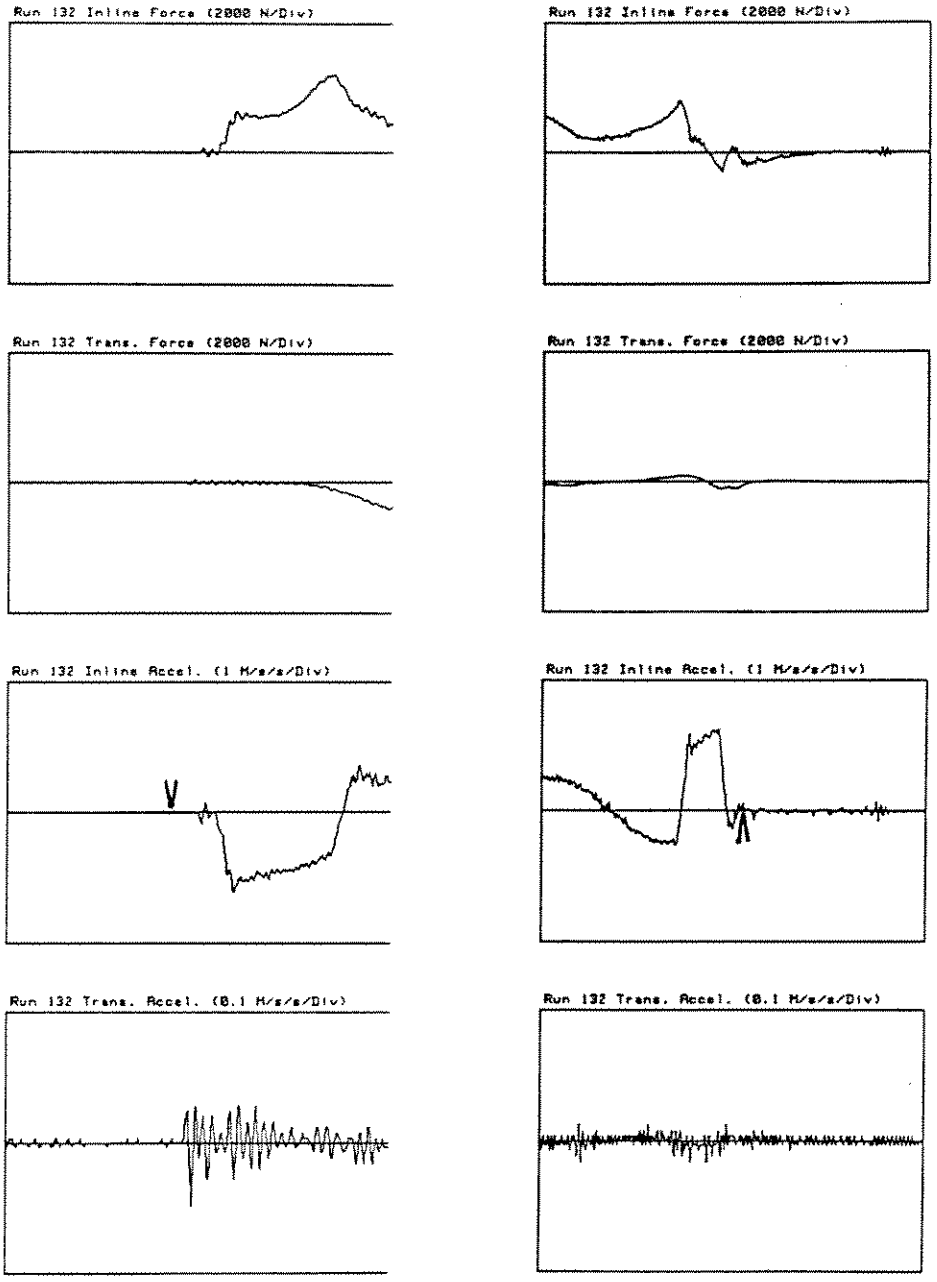

RAW DATA for RUN 132 points 1000 to 1500

RAW DATA for RUN 132 points 4000 to 5000

FIGURE 2.2
ZOOM PLOTS OF STARTING AND TERMINAL IMPULSES

Time series plots of test data widowing the Starting (Left) and Terminal (Right) Impulses of the run. Marks on the Inline Acceleration plots are chosen as Initial Point (1230) and Final Point (4535) which determine the Significant Test Interval. Data rate: 0.02 sec/pt.

increase linearly to 0.264 meters/sec by the end of this 66 second interval. With test velocities of the order of 1 meter/sec this apparent drift is certainly significant. So, the computed velocity consists of the periodic or the combined motion component and the linearly increasing "apparent" drift component. As the velocity should be zero at the Final Point, the computed velocity at this point is used as the basis for a linear drift correction which is applied at each point to the associated velocity. The validity of this corrected velocity was achieved by checking the replication of zero crossings and extremum amplitudes.

In this Figure, the time scale of the transverse acceleration plot allows one to observe the very high frequency (VHF) components, at approximately 4.5 Hz, which is likely a structural resonance. We shall have other opportunities to observe the VHF Effects which appears as a noise component in both inline and transverse data of all the Runs.

Figure 2.3 illustrates the two force and acceleration plots formatted to the Significant Test Interval and with the computed and corrected velocity shown on each plot. This Figure also contains an excellent illustration of the I-T force component topping off the inline force. Note its frequency, phase, and amplitude relationship to the transverse force. In this example there are 4 high velocity time intervals in which the effective amplitudes of the transverse forces are different. These differences are seen in the I-T components. This Figure also supplies a view of the starting interval which can be contrasted to the total test interval. Note that these time series data are plotted "windowing" the Significant Test Interval and retaining the original SSPA point numbers and grid.

Although compilations of data in the formats of Figures 2.1 to 2.3 have not been included in this report, the Significant Test Interval format has been used for the IPM Processed Data Plots compiled in Appendix C. A review of the IPM and the processing procedure are presented in Appendix D.

The Appendix C data includes all LF, HF, and Periodic test conditions in the SSPA experiment. At the beginning of Appendix C is a "Guide to Time Series Plots" which supplies a complete description of the data format and serves as a guide to locations of data sets. The illustrative Run 132, which is a rough cylinder test, is found on page 18 of Appendix C. On the opposing page is Run 381, the smooth cylinder counterpart.

For cycle-to-cycle comparison of data, a "folded" data plot is more convenient. A folded time series plot consists of superimposing successive cycles of a Run using the velocity for alignment. This allows a better plotting scale and is useful in portraying cycle to cycle variations in the data as well as the average pattern for the data. Appendix B, presents each of the 18 LF test conditions in a folded format. In Appendix A, the folded format is used for comparisons of the Morison force predictions with the observed forces. The folded format is also used to present HF data in Chapter V.

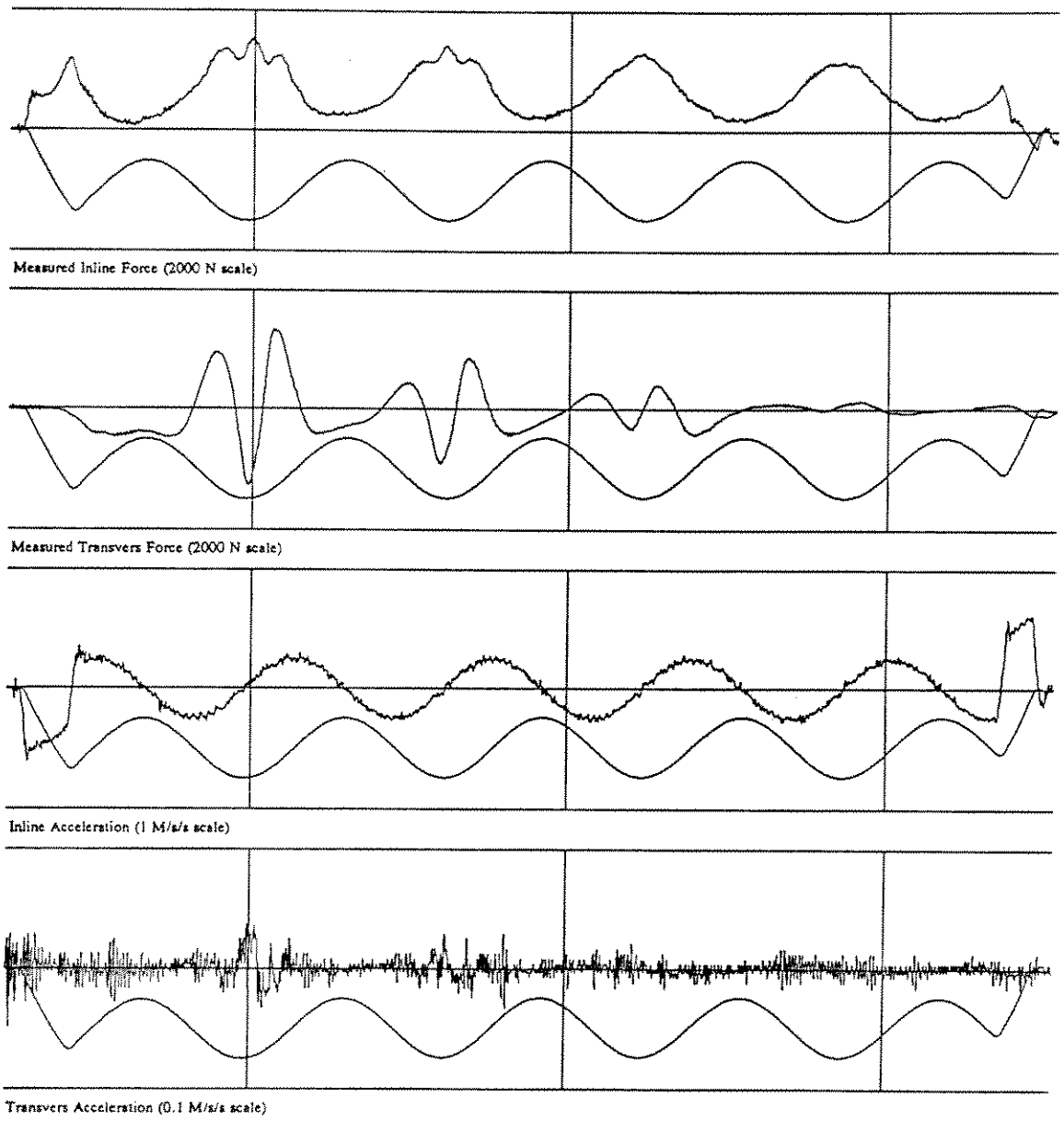

DATA for RUN 132 points 1230 to 4535

FIGURE 2.3
SIGNIFICANT TEST INTERVAL OF TEST DATA
PLOTS WITH VELOCITY PRIOR TO IPM PROCESSING

Time series plots of test data widowed to the Significant Test Interval. Velocity is shown on each plot. The Point Position of the Original Data Record has been retained. Thus the first grid line in this plot is 2000 and corresponds to 2000 on Figure 2.1. Time scale: 1000 pt/div.

Considering again our illustration Run 132, as it is presented on page 18 of Appendix B in a folded format. Here are superimposed the 4 cycle intervals, cited earlier. The smooth cylinder data are found on the same page. On the opposite page are Runs 380 and 133, which are companions to Runs 381 and 132, with steady motion components in opposite directions. In Appendix A, such "duplicate" runs are not necessary so only Runs 380 and 133 were compiled. Appendix A and Appendix B were intended to be autonomous with their own introductions and guides.

COMPARISON OF TIME SERIES

The format and abundance of data in Appendix C allows one to perform a myriad of comparative studies. In this section we have chosen to construct a simple but illustrative comparison. The data are not for combined motion tests but rather for simple periodic tests. The data format of Figure 2.1 for the raw inline and transverse data is used. Comparison plots of smooth and rough cylinders for 4 test conditions are compiled in Figure 2.4. The force scale and time grid are the same for all plots. The periodic test conditions have the same Reynolds Number so that the Figure indicates the influence of KC Number change. The size of the plot allows one to discern only gross features, which is our intent. The upper left quadrant portrays a "low" KC Number of 6.3 and the upper right a "mid-range" KC Number of 12.6. The lower left quadrant portrays a "high" KC Number of 62.8 and the lower right a high KC Number of 94.3. Within each quadrant the smooth test is on the left and the rough test is on the right.

The first aspect to note is the significant difference in both inline and transverse force levels between the smooth and rough cylinders. The only exception is the low KC inline data, which are inertial dominated. The impression is that the type of roughening applied to the cylinder results in a significant increase in the drag and transverse forces, and results in only a modest change in the inertial force.

Next, note the low and mid-range transverse force patterns. In both cases the frequency is twice that of the inline motion. For the mid-range, the transverse force requires a significant number of cycles to build-up to a fully established level. This fully established level exceeds that of both low and high KC Number tests. For the low KC Number test, the transverse force pattern appears to suffer from a stability problem. The pattern beats on and off at a modest amplitude. The exception is the last half of the rough cylinder test where the transverse force builds-up to amplitudes comparable to the mid-range values. For the mid-range KC Number condition, large transverse forces are achieved at twice the inline frequency. For KC Numbers above the mid-range, as the KC Number increases the transverse force pattern diminishes in amplitude while the frequency increases relative to the inline frequency. The I-T Effects are difficult to discern on a figure of this scale; however the larger transverse forces observed with the rough cylinder should yield enhanced I-T values.

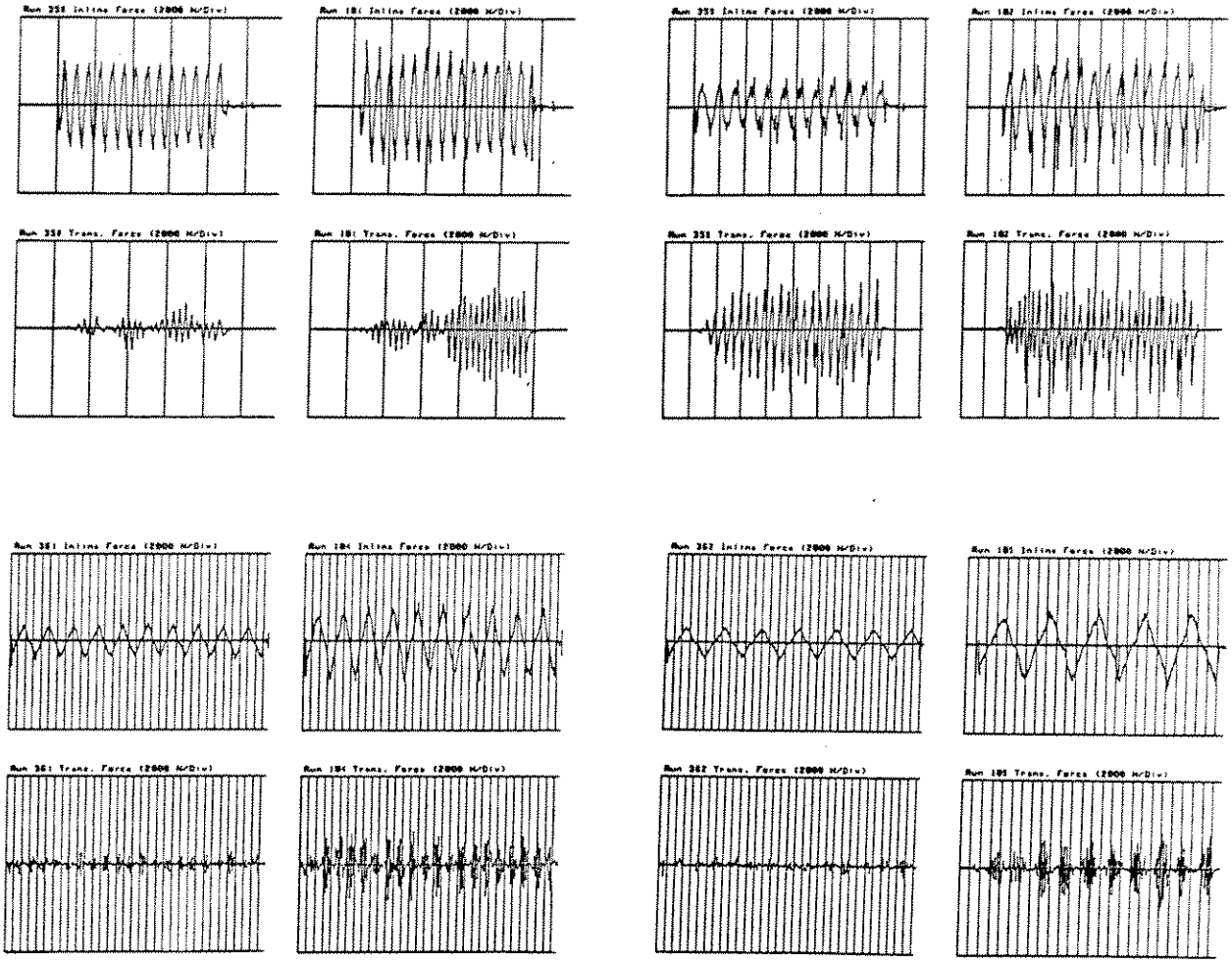

FIGURE 2.4
VARIATION OF TIME SERIES PATTERNS WITH KC NUMBER

In the quadrants of this Figure are presented Initial Test Data Plots of inline and transverse forces for Periodic Tests at 4 KC Numbers. For each quadrant the test parameters - Amplitude of Oscillation, Period of Oscillation, and KC Number - are: (Upper Left) 1 meter, 6.25 sec, and 6.3; (Upper Right) 2 meters, 12.5 sec, and 12.6; (Lower Left) 10 meters, 62.5 sac, and 63; and (Lower Right) 15 meters, 94.3 sec, and 94. Within each quadrant smooth cylinder plots are on the left and rough cylinder plots are on the right. Time scale: 20 sec/div.

I-T EFFECT

We originated the term "I-T Effect" to identify a force component that has been observed by many others. This Inline-Transverse Effect is observed as a periodic component of the inline force which correlates with the transverse force. The correlation is such that it is observed at twice the Strouhal frequency. Because it occurs as an even frequency, it is clearly beyond the odd frequency spectra of the Morison equation.

Our interest in the I-T Effect is based on our observation that it can be enhanced or suppressed by the history of the fluid-structure motion and that it can be a sizable contributor to the inline force. The easiest example to cite is the significant increase in the drag coefficient observed with mid range KC Numbers. This increase would be an I-T contribution associated with the development of sizable transverse forces. In studying test data from a variety of sources we have observed that it may take multiple cycles for large transverse force patterns to develop and that these force patterns can be controlled by combined motion.

There are several models for explaining the I-T Effect. Pressure perturbations and vortex shedding are a simple dichotomy. As the IPM is based on pressure distribution arguments, the former would seem to be preferred; however, a more insightful model is based on the vorticity transport concept, Horton and Feifarek (1981) and developed further by Feifarek (1985). Recall that vorticity is the rotational characteristic of fluid motion which originates in the sheared flow of the boundary layer and forms the core of a vortex.

The vorticity transport idea can be represented by the three orthogonal vectors, depicted in Figure 2.5, for a two dimensional flow. The vectors are the transport velocity, the vorticity which is perpendicular to the page, and the resulting force. The force is given by the vector cross-product relation of velocity and vorticity. In the drawing, the spiral curl represents the direction of rotation of the vorticity with counterclockwise rotation associated with a vorticity vector directed out of the page. Changing the direction of the velocity changes the direction of the resulting force, and reversing the direction of the vorticity reverses the direction of the force. Clearly a force component on the body arises from each element of vorticity.

In the figure, the first of three circles represents a cylinder experiencing a flow from right to left. Two shed vortices are shown moving aft of the cylinder, they produce transverse force components which are in opposition and inline components which increase the drag. As these vortices would have been shed alternately they would produce the expected periodic transverse force pattern while introducing inline impulses in the drag. Both impulses would increase the drag above a base level so that the effect would be a periodicity in the drag at twice the transverse force frequency.

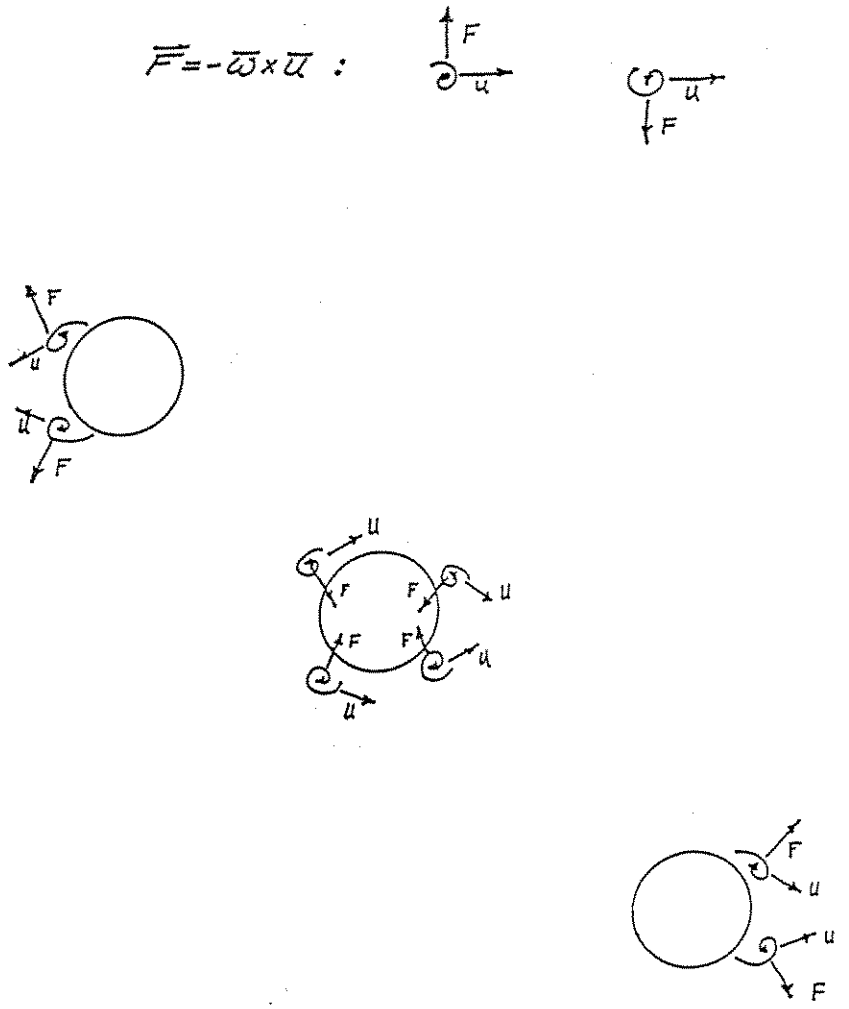

FIGURE 2.5
FORCE ASSOCIATED WITH VORTICITY TRANSPORT

Vector cross-product relationship between the vorticity and the transport velocity yielding the force vector. The vector relationship of this expression is portrayed to its right. Clockwise vorticity transported to the right results in an upward force and counterclockwise vorticity transport to the right results in a downward force. Three illustrations of the usual states of vorticity transport relative to a circular cylinder are shown. The forces associated with each vorticity element should be resolved into inline (horizontal) and transverse (vertical) components. The top cylinder illustrates vorticity behind the cylinder due to flow from the right, and the bottom cylinder illustrates vorticity behind the cylinder due to flow from the left. The middle cylinder depicts sweeping of prior vorticity back over the cylinder.

The second and third circles represent cases with flow from left to right. The middle one represents sweeping of the previous vortices back over the cylinder. At the right we see shedding of new vortices in the aft region.

Inordinately large drag coefficients were observed in the slack flow interval of those LF test conducted with large steady velocities. This anomaly is most likely associated with the shed vortex being swept across the aft region. From the vorticity transport viewpoint the force vector would be swept across the aft region, contributing a large component to the inline force. Clearly, this model has intriguing qualities which regrettablely need not be pursued further here.

The 5 figures that follow provide several realizations of the I-T Effect.

Shown in Figure 2.6, are the results from a computational fluid dynamics study by Jordan and Fromm (1972) for an impulsively started cylinder at the relatively low Reynolds Number of 400. The complete viscous flow problem was treated. Flow and pressure distributions were presented with drag, lift, and torque data. The lower plot is a conventional time series plot, and above it is a cross plot of inline vs transverse effects. These plots show the inline contribution at twice the Strouhal frequency. The torque arises from the asymmetry in the shear distribution which is associated with the alternate vortex shedding.

A second illustration, in Figure 2.7, consists of inline and transverse periodic time series data from Sarpkaya's U-Tube apparatus. We have projected the extrema positions of the transverse force plot on the inline plot to indicate the frequency and phase relationship between the two plots.

A third companion illustration, at the same KC Number of 27, is presented in Figure 2.8. These are folded plots of several cycles of inline and transverse IPM coefficients for a SSPA periodic test. The plot at the top of the figure is for early cycles in the test in which the transverse forces and the I-T Effect are small. In the lower plot the transverse force has increased and we see the impulses indicative of the I-T Effect.

The final illustrations are taken from the LF data of this study. In Figures 2.9 and 2.10 are shown conventional and folded time series plots for data sets with different periodic KC Numbers and steady velocity test conditions. The alignment of inline and transverse forces on the conventional plots shows the phase and frequency relationship noted in the previous figures. The folded plots show the I-T impulses above the base curve which corresponds to negligible transverse and I-T forces.

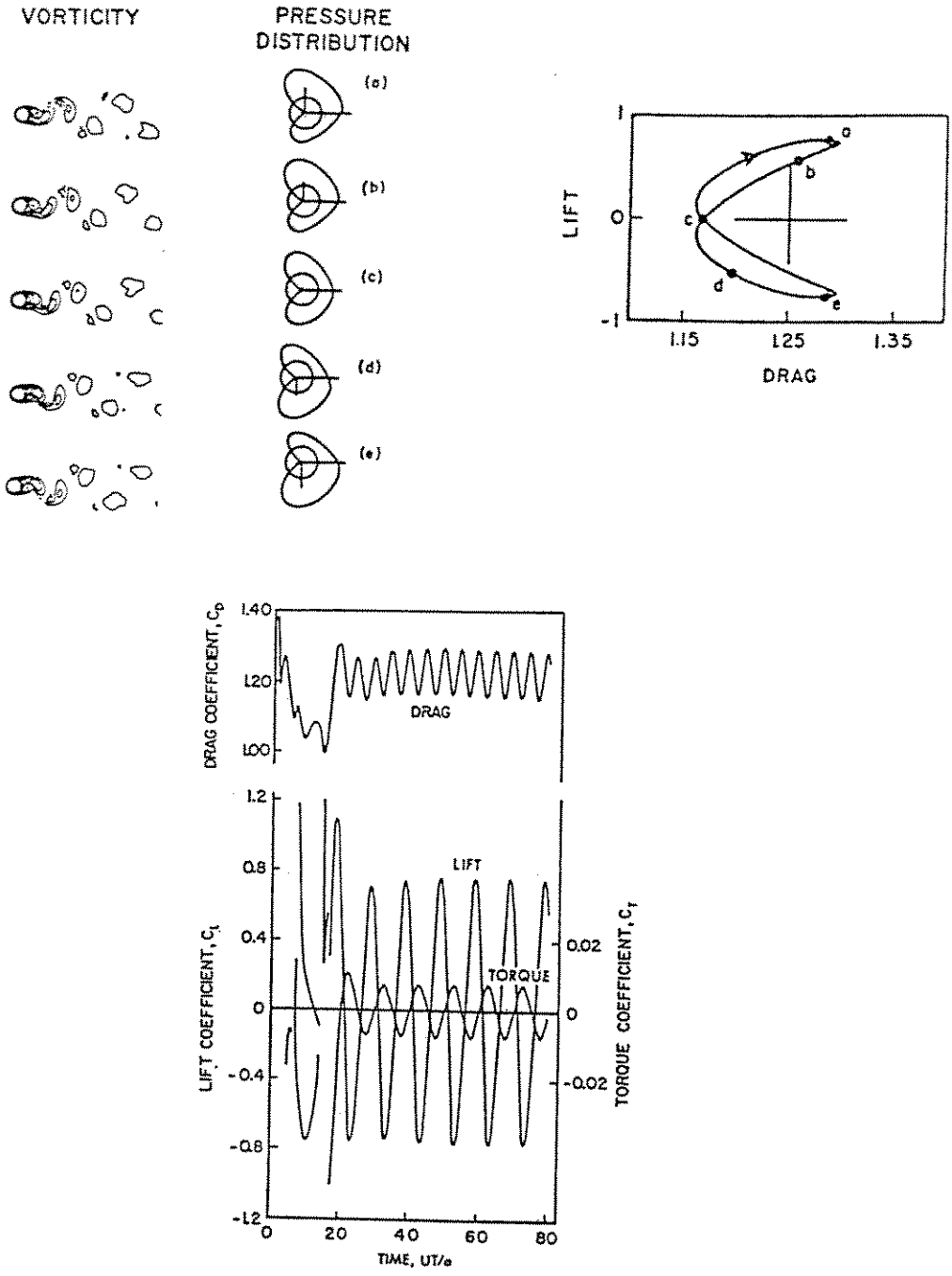

FIGURE 2.6
ILLUSTRATION OF THE I-T EFFECT

CFD data illustrating the Impulsive Start of a cylinder to a Reynolds Number of 400. In the upper part are the vorticity field and the pressure distribution at 5 times. The resulting inline (drag) and transverse (lift) forces are shown at the right for these time points. Conventional time series plots of the transverse coefficient and the inline drag coefficient are shown in the lower plot. The plots of this figure indicate the relationship between vorticity, pressure distribution and the resulting forces. Reproduced from the March 1972 *Physics of Fluids* paper of Jordan and Fromm.

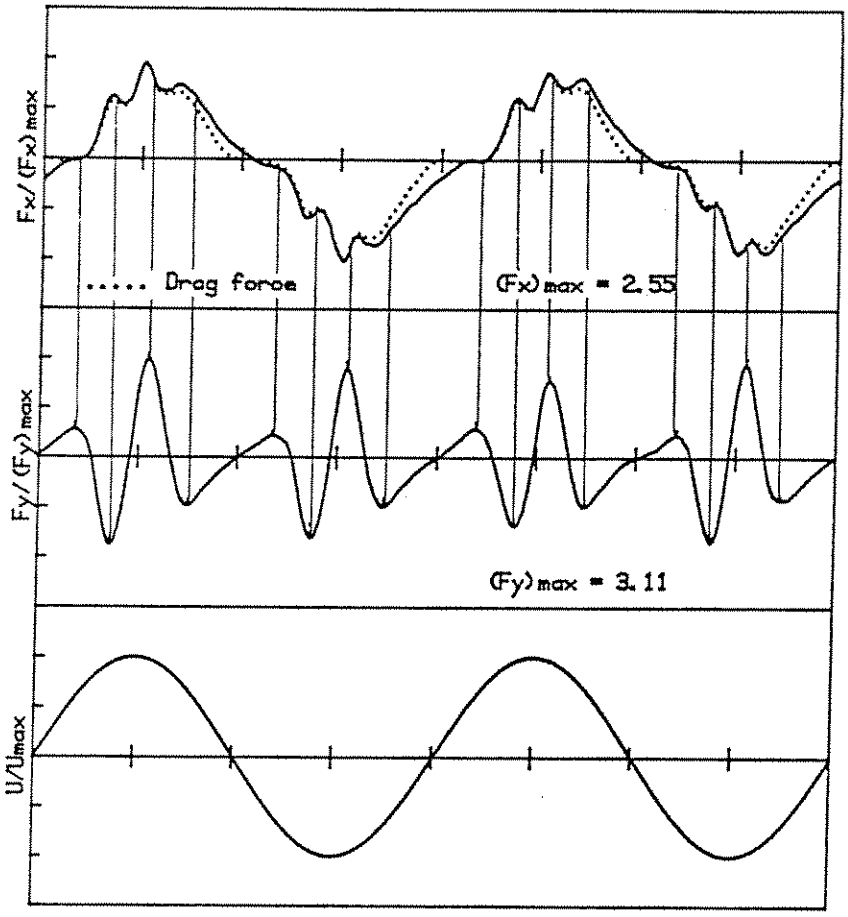

RUN # 8
Ko = 27.1
Re = 34200

Fx = (Fx)raw - Ideal Inertial force

FIGURE 2.7
ILLUSTRATION OF THE I-T EFFECT

Time series of inline and transverse forces with velocity for a simple periodic test in the Naval Postgraduate School U-Tube Facility at a KC Number of 27. Note alignment of extreme values of the transverse force with the inline D-Force. Perturbations of the inline force correlate with the transverse force. The frequency of the inline perturbations (I-T) are at twice the transverse frequency.

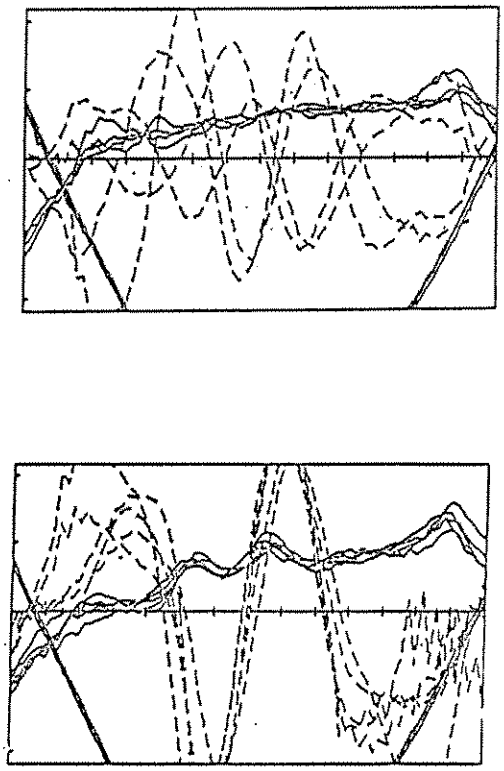

FIGURE 2.8
ILLUSTRATION OF THE I-T EFFECT

Folded time series plots of Periodic SSPA data with KC Number of 27. In each plot the velocity is shown with the inline and transverse IPM coefficients. The transverse coefficients are the dashed curves. In the upper frame, 4 early cycles are presented in which the transverse pattern is modest. The lower frame shows a well developed transverse pattern and perturbations of the inline IPM coefficient. Data from Run 363 (S-27-190-0-0).

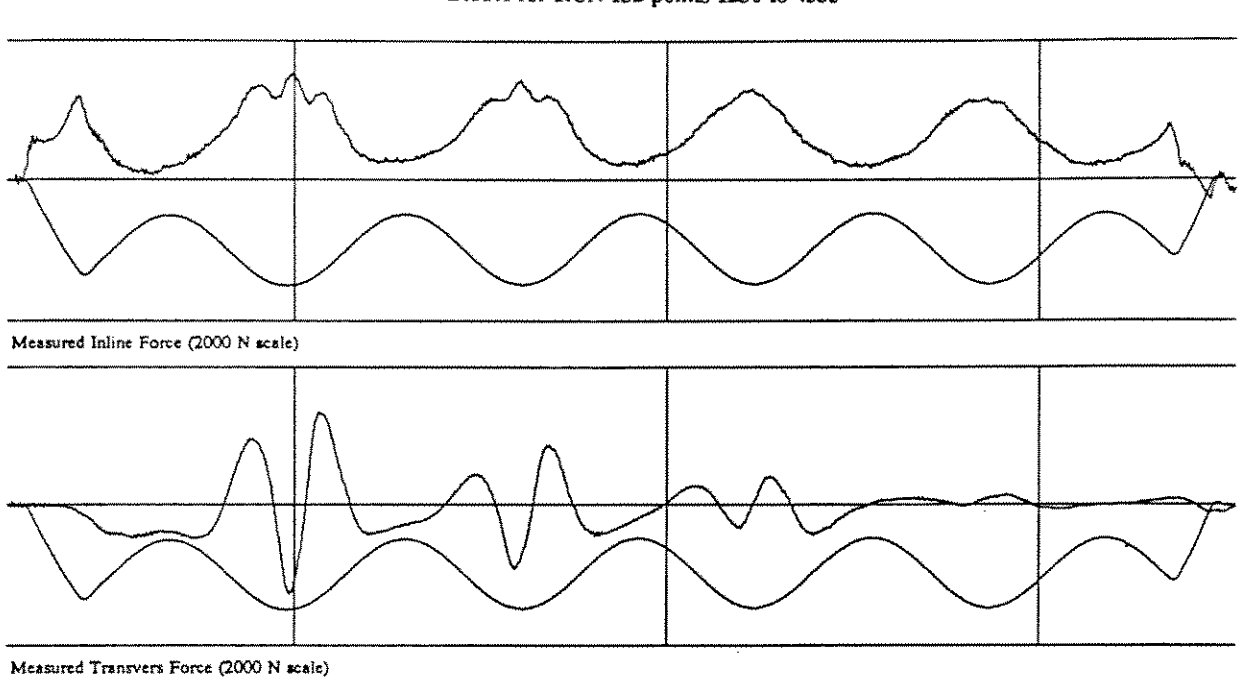

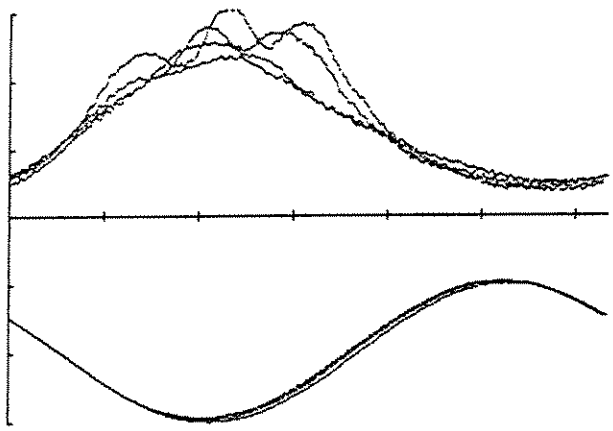

```
Periodic Amplitude in meters.....,  1
Frequency in Hz.................  .08
Steady Velocity in m/sec.........  1
Velocity Ratio (steady/periodic)....  2
KC number.......................  6.3
Reynolds number/10^6............  .44
        PLOT FOR DATA FROM 4 TO 12
```

FIGURE 2.9
ILLUSTRATION OF THE I-T EFFECT

Data from SSPA Combined Motion tests: Run 132 (R-6-44-0-2.0). Time series of velocity with inline and transverse forces for the complete significant test interval. A folded plot presents inline force and velocity for the 4 significant cycles of the test. The time series shows the frequency and the phase relationship between the transverse and I-T patterns. The character of the change in amplitudes of the I-T perturbations with reduction of the transverse amplitudes is clear in the folded plots. This folded plot shows the relationship between the base* force curve and the I-T impulses imposed on it.

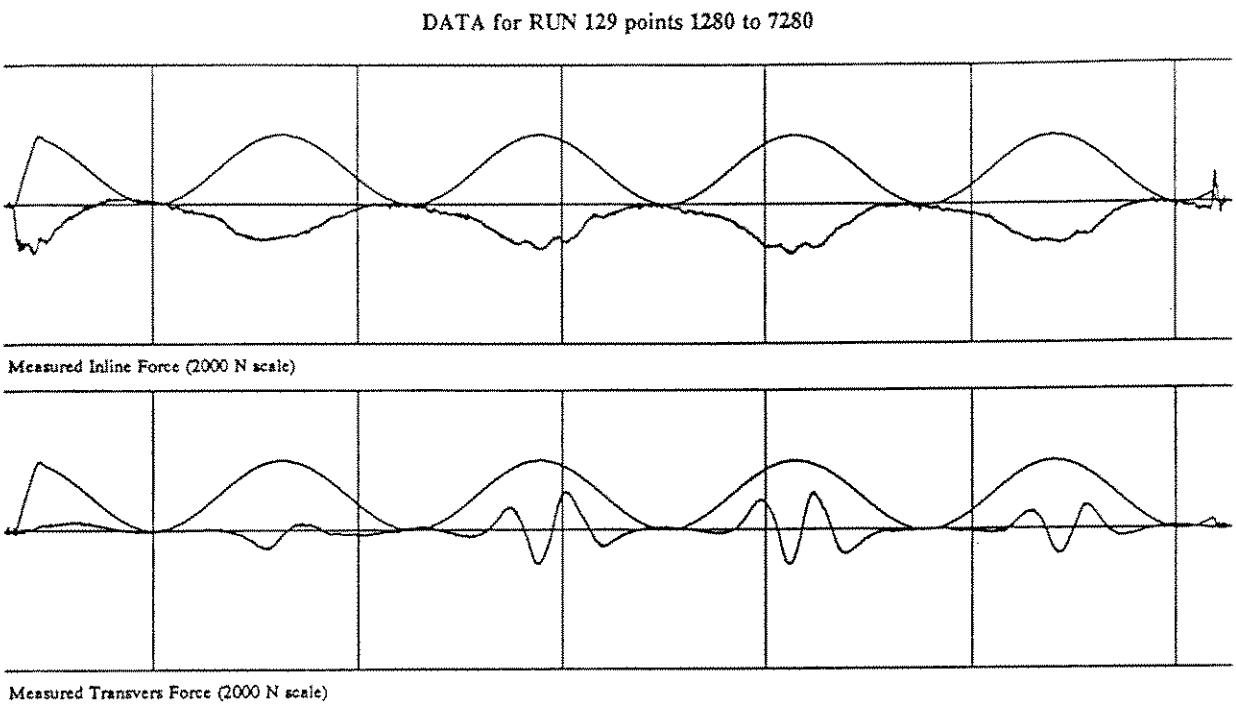

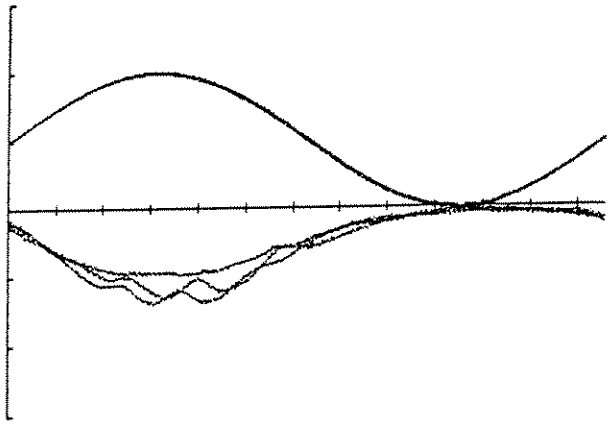

FIGURE 2.10
ILLUSTRATION OF THE I-T EFFECT

Data from SSPA combined motion tests: Run 129 (R-12-44-0-1.0 +). Time series of velocity with inline and transverse forces for the complete significant test interval. A folded plot presents inline force and velocity for the 4 significant cycles of the test. The time series shows the frequency and the phase relationship between the transverse and I-T patterns. The character of the change in amplitudes of the I-T perturbations with reduction of the transverse amplitudes is clear in the folded plots. This folded plot shows the relationship between the base* force curve and the I-T impulses imposed on it.

CORRELATION KC-NUMBERS

In HYDAMP-I we refrained from presenting data correlated with the IPM based KC Number despite the evidence that the pattern of the IPM coefficient, as well as the Morison coefficient data, correlates with an IPM based KC Number:

$$2\pi U^2/D\dot{U}.$$

This quantity arises in the IPM formulation, see Appendix D. The inverse of this quantity is related to the IPM's Theta-min angle (the minimum pressure location on the test cylinder). Instantaneous values of Theta-min correlate with the instantaneous values of the IPM coefficient, the Theta-min Correlation Figure 3 Appendix D.

The author has encountered this quantity: (1) in the literature as Iverson's modulus, Iverson (1951), and (2) in general dimensional analysis studies in fluid dynamics where it represents a measure of the steadiness of a flow, the ratio of the convective and temporal inertial terms in the Navier-Stokes equations.

For a simple periodic flow the quantity yields the familiar KC Number representations:

$$U_p T/D$$

and

$$2\pi A_x/D\,.$$

In the above T is the period of the motion, A_x is periodic amplitude, and U_p is the periodic velocity amplitude of the cylinder of diameter D.

Note that these periodic KC Numbers follow logically from our IPM based KC Number. However, most investigators have taken the reverse approach in using these two periodic KC forms to speculate on forms applicable to combined motion data.

In one approach UT/D is used with the velocity replaced by the combined velocities and the period replaced by the zero crossing periods of the combined flow. This approach yields an expression consistent with the amplitude to diameter argument for a KC Number.

The other combined motion KC-Number, based on UT/D, is:

$$(U_s + U_p)T/D$$

which is a simple combination of the periodic KC-Number and Reduced Velocity. Despite the frequent uses of this expression in data presentations it does not appear to have a rational origin.

Using the IPM based KC Number for the LF case yields:

$$(KC) \cdot (1 \pm U_p/U_s)^2$$

where (KC) is the usual periodic KC-Number. This correlation KC Number is used with the LF data in the next chapter.

Curves relating these three approaches to their modified KC-Numbers for LF type combined motion test are presented in Figure 2.11. In this figure $(KC)_c/(KC)$ is the ratio of correlation to periodic KC Numbers and U_p/U_s is the ratio of periodic to steady velocity amplitudes.

One problem with the non-IPM based approaches is that they do not provide a correlation KC-Number for $U_s > U_p$. Another dilemma is that they provide no guidance for the HF cases or for the starting problem cases. Thus the IPM KC Number expression:

$$2\pi U^2/D\dot{U}$$

is the only source of consistent and rational correlation parameters for all the data considered in this study. We shall show that it provides a basis for a correlation plot involving all the data considered in this study.

ROUGH CYLINDER TESTS

During half the SSPA tests on a 1 meter diameter cylinder, the surface was covered with artificial roughness elements. The individual roughness elements, which were stamped from 1mm sheet metal, were right conical frusta of 2 cm height with 1.5 and 3 cm diameters. The elements were glued to a 1 mm rubber backing and held in place by a 0.8 mm perforated sheet metal skin. The elements were located on 4 cm centers in

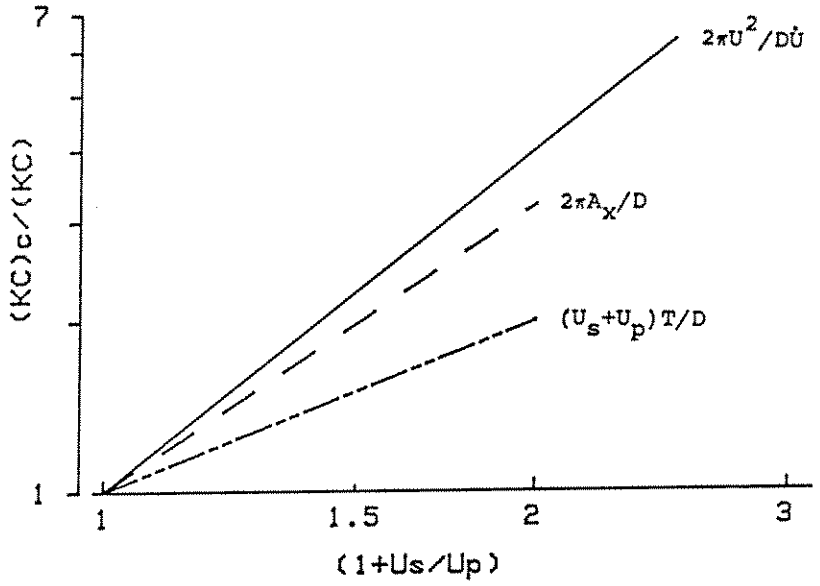

FIGURE 2.11
CORRELATION KC NUMBER

Shift in correlation KC Number with steady velocity. The ratio of correlation KC Number to periodic KC Number is plotted vs the ratio of steady to periodic velocity amplitudes for 3 different descriptions of the KC Number. The top curve is the IPM base KC Number for combined motion. The middle curve is based on amplitude of motion arguments. The lowest curve is based on the simple addition of Periodic KC Number and Reduced Velocity.

horizontal rows with each row offset by 2 cm and separated by 3.5 cm. The mass of the smooth test section was 103 kg and 140 kg with roughness added. The displaced mass was 785 kg for the smooth cylinder and the displaced volume of the roughness elements added less than 2%.

For further details on the SSPA test apparatus consult the HYDAMP-I report.

How did the rough cylinder data differ from the smooth cylinder data for the same test conditions? We have seen in Figure 2.4 the increase in the inline and the transverse forces. Examination of the plots in Appendix B indicate that the force is not only larger but that it develops more rapidly within a half cycle. This rapid development extends the time interval for the transverse force pattern. So we see a slightly different pattern for the transverse forces.

A partial explanation for these differences is associated with the establishment of steady flow around the roughness elements very early in a flow cycle. This is due to the 1/50 ratio of diameters of roughness elements to test cylinder. This ratio assures the KC Number on the roughness elements being at least 50 times the nominal value of the test. The Reynolds Number is lower by the same ratio which means the higher drag coefficients associated with subcritical conditions as in the Keulegan and Carpenters experiments. This would explain the larger drag and more rapid development. As the roughness elements are vorticity generators this should also increase the transverse force and lead to earlier separation of the flow on the test cylinder.

SUMMARY OF CONCEPTS

Above we have presented three important ideas which are critical to this study. The first is the I-T force component which rides atop a base force pattern. The base pattern is associated with zero transverse force. The combined motion conditions can be used to enhance or suppress transverse and the associated I-T forces. The second idea is the IPM based KC Number which will enable all the data to be correlated. The third is how the flow around and separation on the roughness elements gives rise to the rapid development of an apparent surface force. This force contribution is the source of the increased drag with roughness in the SSPA experiments.

CHAPTER III
STUDY OF LF DATA

Recall that the LF designation is derived from the Low Frequency descriptive and refers to the set of SSPA tests in which unidirectional steady and periodic velocities are combined. The addition of a steady velocity to a periodic motion results in an increase in one velocity extrema while decreasing the other. We shall identify the fractions of the flow cycle associated with each extrema as the "high velocity" fraction and "low velocity" fraction of the flow cycle.

The periodic motion is low frequency, 0.016 to 0.16 Hz, corresponding to periodic KC Numbers of the range 3 to 63. Tests were conducted at 12 combined motion conditions involving steady velocity to periodic velocity amplitude ratios of 0.1, 0.5, 1, and 2. An additional set of 6 duplicate tests were conducted with the direction of the steady velocity reversed in the test tank. A catalogue of LF test conditions is found in the Appendix C with conventional time series plots of the 18 smooth cylinder Runs and the companion 18 rough cylinder Runs.

The subject of this chapter corresponds to the material presented in HYDAMP-I in Chapters 3 and 4, "Analysis of Low Frequency Data" and "Low Frequency Predictions". These chapters of the previous report provide the reader with background concepts, data analysis procedures, and miscellaneous observations on the data set.

To streamline this chapter, we have chosen not to duplicate text material from the previous study. Also, voluminous presentations of data have been shifted to Appendices A and B.

In this chapter we introduce the processed LF data, present the Morison force coefficient data derived from the IPM coefficients, present the force predictions based on the Morison coefficient data, present an appraisal of the force predictions, and conclude with a correlation plot of LF coefficient data using the IPM based KC Number.

INTRODUCTION OF LF DATA

The time series for the significant test interval of all LF data, processed with the IPM, is presented in Appendix C. To aid the user in making comparisons of these data, an ID number has been supplied with each figure. For example on page C 1a, one finds at the bottom of the page **S-6-88-0-0.1** . This identifies the data

as a smooth cylinder test at a periodic KC Number rounded to 6 with a steady to periodic velocity ratio of 0.1 . A full explanation of the ID number is supplied at the beginning of each appendix. Using these ID numbers one can thumb through the plots identifying and comparing data by their test parameters without the intermediary of the Run number and Page number catalogue. Of particular note on such plots is the development of the transverse force and the associated change in the inline force and IPM coefficient. Clearly, for low and mid range KC Number tests, several cycles are required to achieve a "fully-established" time series pattern.

In Appendix B, the LF data have been presented as folded time series with companion smooth and rough tests on the same page. These folded plots differ from the time series of Appendix C in two ways that we shall note. First, we shall note the "flipping" of plots for duplicated test conditions which differ because the steady velocities had been reversed. The tests with positive steady velocities were plotted flipped to facilitate comparisons with other data. These plots are identified by a + appended to its ID. Velocity is presented on each plot, and the orientation is such that the "high velocity" is in the negative direction. The second item to note is that not all the cycles from the significant test interval were used for these folded plots. In selecting the interval for these plots, we followed the convention, used by Shell and others, of selecting an interval of "fully-established" conditions. Recall that in earlier illustrations of the I-T Effect a more extensive interval was used which included cycles in which the transverse force was small.

These fully-established IPM coefficient plots in Appendix B were used in quantifying the Morison coefficients. The corresponding force plots provide the data band to which the Morison force predictions are compared in Appendix A. Clearly, in using such plots, one will tend to average through the data bands and consequently the I-T contribution. Although this approach is conventional practice, it is contrary to the vision presented later in this report.

Theta-min, the IPM kinematic quantity, has been presented in plots of Appendix B for each test condition. Recall the Theta-min angle is the minimum pressure location on the cylinder surface and is related to the KC Number. Its pattern on the plots shows how the minimum pressure point sweeps over the cylinder surface. So, a long dwell time at 90°is indicative of a high KC Number, and a rapid sweep through the 90° position indicates a low KC Number. Clearly, the Theta-min patterns of these plots indicate increasing the steady velocity shifts the high velocity fraction of the flow cycle to a higher KC Number pattern while shifting the low velocity fraction to a lower KC Number pattern.

The D-Force or Defect Force is presented at the top of each set and is reproduced in Appendix A as the observed force to which the Morison prediction is compared. This force, which is indicative of the drag force, is the difference between the measured inline hydrodynamic force and the ideal inertial force on the cylinder.

MORISON COEFFICIENTS

Following the procedures of HYDAMP-I, the time-dependent IPM coefficient data was used to achieve a hierarchy of constant coefficient Morison approximations. In the original work the different levels of approximation were achieved by considering the values of C_a', the inertial corrective coefficient, and C_d, the drag coefficient, to be constant in selected time series intervals. Three levels in this approximation hierarchy were considered in the original work.

For companion smooth and rough cylinder tests, the difference in their inertial corrective coefficients was found to be insignificant. Therefore, a formal tabulation of the values found in the previous report has not been included here; however, C_a' values for the Level I and Level II approximations have been listed on the force prediction plots.

For the Level I approximation, a C_a' value of 0.67 is applied to both smooth and rough cylinders, and C_d values of 0.67 and 1.3 are applied to the smooth and rough cylinders, respectively. Recall that for Level I these coefficients are applied to the full flow cycle and to all test conditions.

For the Level II approximation the values applicable to the high velocity and low velocity fractions of the flow cycle may differ and these values are expected to be a dependent on the test conditions. The drag coefficient values for the smooth and rough cylinders are presented in Figures 3.1 to 3.4. Recall these values are applicable to both Levels II and III.

Each figure presents data of a different steady to periodic velocity ratio with data applicable to the high and low velocity portions of the test cycle in upper and lower plots, respectively. On each plot both rough and smooth cylinder data can be identified without distinguishing symbols. The rough cylinder data is the higher curve on each plot.

The solid line represents the effective mean value of the drag coefficient, and the dashed lines are derived from the extreme values observed in the IPM coefficient data. This presentation quantifies the uncertainty in the coefficient data.

We have chosen to present these data in this conventional format in terms of the test cylinder's periodic amplitude to diameter ratio. Recall the periodic KC Number is 2π times this ratio.

At this point our only comment on these data is that for $U_s/U_p \geq 0.5$ the coefficients applicable to the low velocity portion of the flow cycle are inordinately large and erratic.

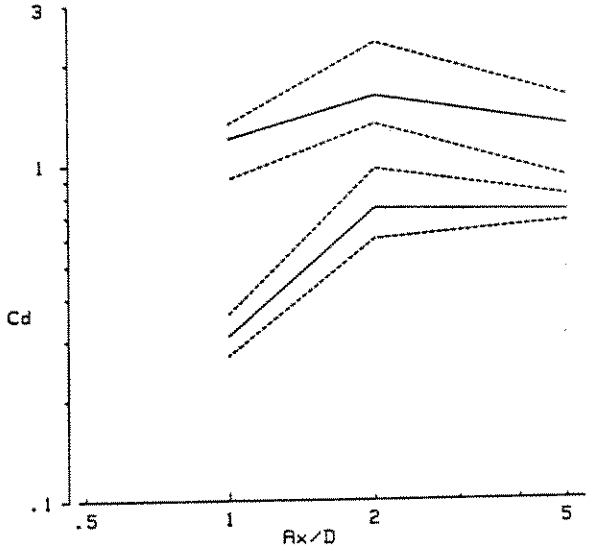

Us/Up=0.1 for High Velocity Part of Cycle

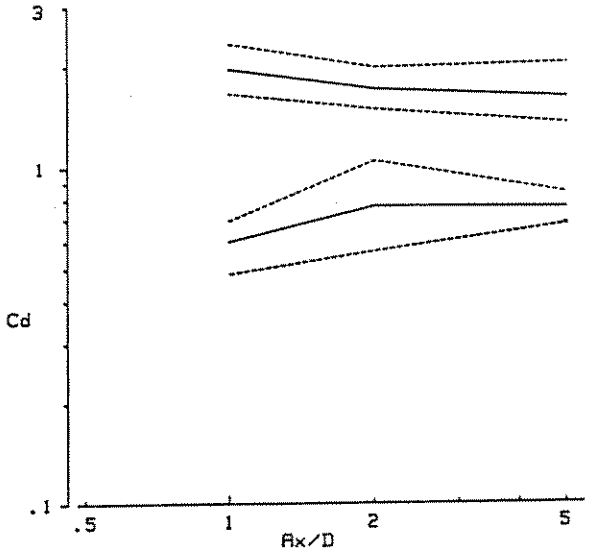

Us/Up=0.1 for Low Velocity Part of Cycle

FIGURE 3.1
LEVEL II DRAG COEFFICIENT DATA

Morison drag coefficients applicable to the high velocity and low velocity parts of a combined motion flow cycle. Rough and smooth coefficient data are presented on the same plot; rough cylinder data is identified as the larger value. The solid curves represent "effective mean values" and the dashed curves are from extreme values which indicate uncertainty. Data are plotted as a function of the ratio of periodic motion amplitude to diameter. The Steady Velocity to Periodic Velocity ratio for these LF data is 0.1 .

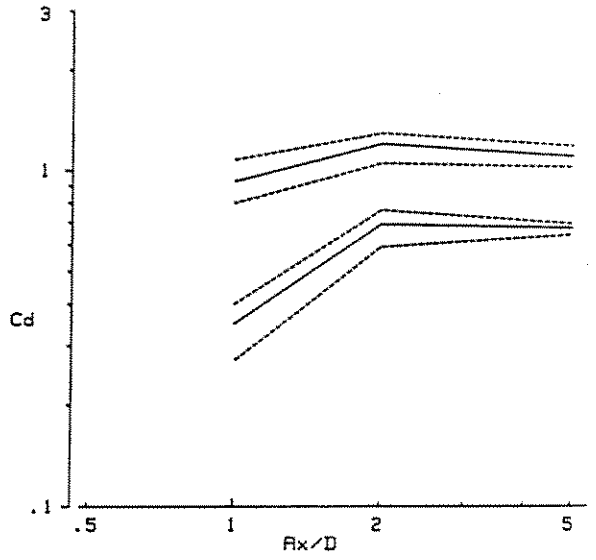

Us/Up=0.5 for High Velocity Part of Cycle

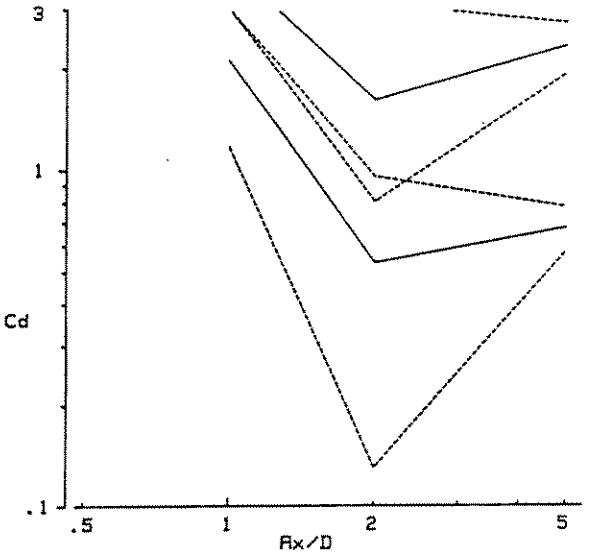

Us/Up=0.5 for Low Velocity Part of Cycle

FIGURE 3.2
LEVEL II DRAG COEFFICIENT DATA

Morison drag coefficients applicable to the high velocity and low velocity parts of a combined motion flow cycle. Rough and smooth coefficient data are presented on the same plot; rough cylinder data is identified as the larger value. The solid curves represent "effective mean values" and the dashed curves are from extreme values which indicate uncertainty. Data are plotted as a function of the ratio of periodic motion amplitude to diameter. The Steady Velocity to Periodic Velocity ratio for these LF data is 0.5 .

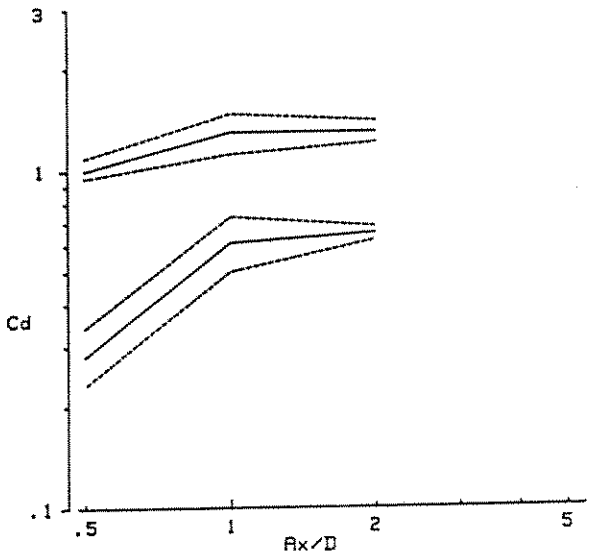

FIGURE 3.3
LEVEL II DRAG COEFFICIENT DATA

Morison drag coefficients applicable to the high velocity and low velocity parts of a combined motion flow cycle. Rough and smooth coefficient data are presented on the same plot; rough cylinder data is identified as the larger value. The solid curves represent "effective mean values" and the dashed curves are from extreme values which indicate uncertainty. Data are plotted as a function of the ratio of periodic motion amplitude to diameter. The Steady Velocity to Periodic Velocity ratio for these LF data is 1.0 .

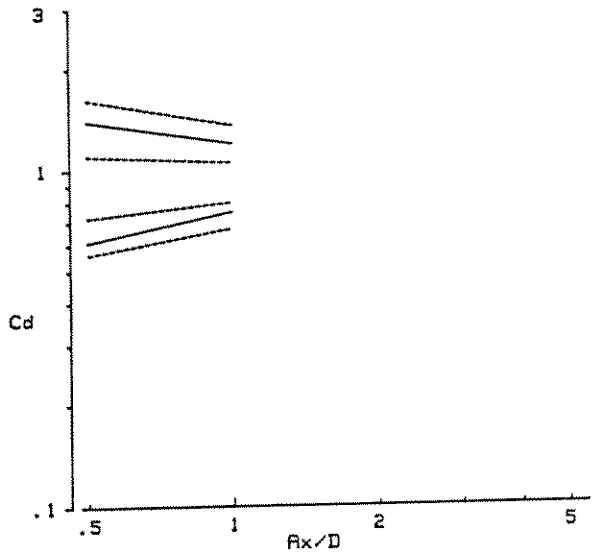

Us/Up=2 for High Velocity Part of Cycle

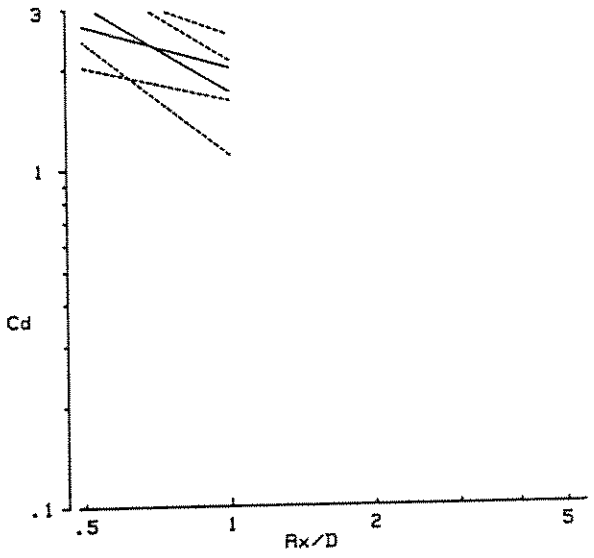

Us/Up=2 for Low Velocity Part of Cycle

FIGURE 3.4
LEVEL II DRAG COEFFICIENT DATA

Morison drag coefficients applicable to the high velocity and low velocity parts of a combined motion flow cycle. Rough and smooth coefficient data are presented on the same plot; rough cylinder data is identified as the larger value. The solid curves represent "effective mean values" and the dashed curves are from extreme values which indicate uncertainty. Data are plotted as a function of the ratio of periodic motion amplitude to diameter. The Steady Velocity to Periodic Velocity ratio for these LF data is 2.0 .

MORISON FORCE PREDICTIONS

The adequacy of the coefficient data and of the level of approximation in achieving accurate force predictions is demonstrated in the plots of Appendix A. In these folded plots the "observed" D-Force data have been reproduced as a band formed by the individual data points. This band is the target for the force prediction. Force predictions based on the measured kinematics and the noted coefficients appear as the solid curve on each plot. A guide to these data plots is provided at the beginning of Appendix A.

A semiquantitative appraisal of these predictions is given if Table 3.1. For the matrix of test conditions we have assigned a grade to each force prediction. The grade for the smooth cylinder is above the diagonal of the test condition box, and the grade for the rough cylinder prediction is below the diagonal. The grades represent 10% increments; so an "A" is associated with a prediction that falls within the data band more than 90% of the time.

This table shows that rough cylinder predictions are better than those for the smooth cylinder. The explanation for this observation is seen in the time series of IPM coefficient data. The rough cylinder data have an early "turn-on", so that they are a better approximation to a constant value.

The table shows a diagonal pattern of increasingly inadequate performance for both smooth and rough predictions. Thus high current and high KC Number combine to yield good predictions, and increasing the current for a fixed periodic motion results in improved predictions. From working with the force prediction plots, I have concluded that for some test condition and some parts of the flow cycle it is impossible to predict forces with a constant coefficient Morison equation. The problem is more acute in the low velocity fraction of the flow cycle. The "LV" notation on some of the test matrix conditions indicate such a low velocity problem.

CORRELATION OF LF DATA

A key to understanding the "diagonal pattern" of Table 3.1 is the IPM based KC Numbers tabulated in the matrix of test parameters in Table 3.2. This tabulation indicates a similar diagonal pattern for the combined motion KC Numbers. Now if we consider acceptable predictions to be those with a grade of B and above, we see from Tables 3.1 and 3.2 that these acceptable predictions, with mixed exceptions, correspond to correlation KC Numbers above 30. The relationship between the quality of a Morison force prediction and correlation KC Number is similar to the observation frequently noted by others for simple periodic tests: at low and mid range KC Numbers the Morison equation does a poor job of reproducing the force time series; however, above the mid range it can provide a satisfactory prediction.

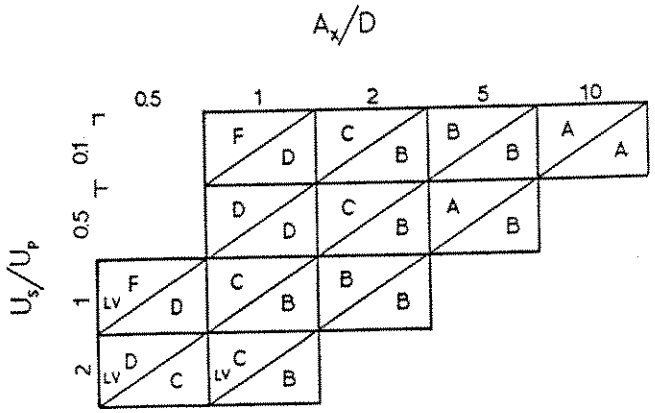

TABLE 3.1
APPRAISAL OF MORISON FORCE PREDICTIONS FOR LF TEST

Two letter Grades (A, B, C, D, or F) were assigned to each Test Matrix Element. These Grades indicate how well the Morison predictions fit the D-Force time series data. For each test matrix element the upper Grade is for the smooth cylinder and the other is for the rough cylinder.

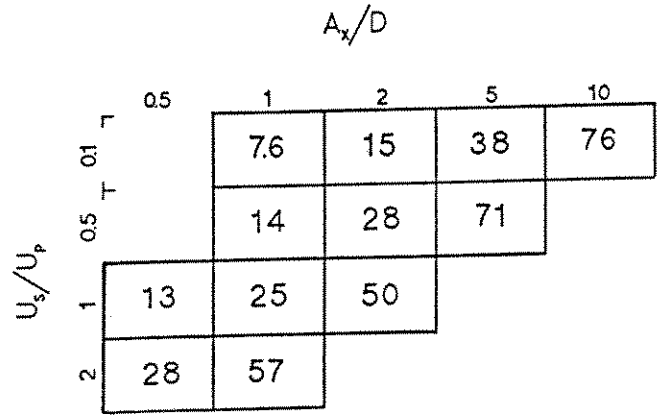

TABLE 3.2
IPM BASED KC NUMBERS FOR LF TEST MATRIX

The values of the Correlation KC Number, $2\pi\ U^2/\ D\dot{U}$, computed with high velocity and acceleration amplitudes of the LF test conditions.

In Figure 3.5, the correlation KC Numbers from this table have been used to replot the data of Figures 3.1 to 3.4. The curves are the solid line data, "the effective mean" drag coefficient. We have chosen not to reproduce the dashed curves for several reasons. Foremost is elimination of the confusion of multiple overlapping curves. Second is the belief these curves of the effective mean make the case for the correlation. One can envision the uncertainty bands and see that their overlap would provide the conventional, but less sophisticated, argument supporting the correlation. We can achieve a finer resolution than the uncertainty bands of Figures 3.1 to 3.4.

The primary disparity in the correlation occurs for the mid range KC Number points. To understand the probable cause of this disparity, recall that these are effective mean data which are afflicted with an I-T contribution. Furthermore in the mid KC Number range this contribution can achieve maximum values.

A measure of the transverse force for the test conditions is provided in Table 3.3. Here are tabulated the amplitudes of the IPM transverse force coefficients with the correlation KC Numbers from Table 3.2. Note the transverse coefficient values along the diagonal of mid range correlation KC Numbers: 1.2 at 15, 0.4 at 14, and 0.3 at 13. The highest transverse coefficient corresponds to the largest drag coefficient in the mid KC Number range. The other two mid range points correspond to conditions in which a significant diminution of the transverse and attendant I-T Effect is observed.

In this illustration we see the addition of a current to a periodic motion not only significantly shifting the correlation KC Number but also interfering with the symmetry which provides feedback between the positive and negative part of the flow cycle. This is necessary to fully establish the transverse force pattern. One can call this "interference". However, stated quantitatively the Strouhal and KC Numbers are illconditioned to support vortex shedding during that cycle fraction.

This illconditioning explains the erratic behavior of the low velocity drag coefficients for test conditions with $U_s/U_p \geq 0.5$. For these test conditions the low velocity correlation KC Numbers are less than 8 and inadequate to achieve vortex shedding. So the vorticity shed in the high velocity part of the cycle is swept back over the cylinder or meanders about the cylinder during the low velocity part of the cycle. Thus vorticity transport dominates the force in low velocity interval. As the Morison equation is incapable of describing this situation, inordinately large and erratic inline and transverse coefficients are associated with this low velocity portion of the flow cycle for these test conditions.

Because effective mean data were used, all the data used in compiling the correlation shown in Figure 3.5 involve an I-T contribution. Clearly this correlation would be enhanced if more data were available with transverse and I-T Effects reduced.

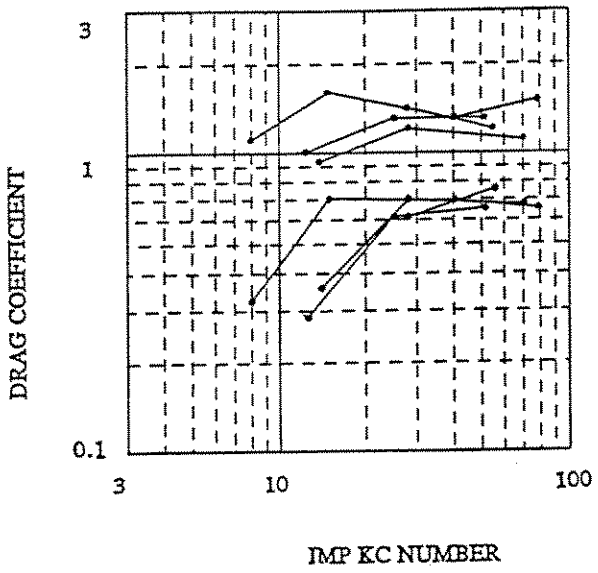

FIGURE 3.5
CORRELATION OF LF DRAG COEFFICIENT DATA WITH IPM BASED KC NUMBER

Curves represent the High Velocity Effective Mean Coefficient Data from Figures 3.1 to 3.4 plotted using the IPM based KC Number of Table 3.2.

A_x/D

U_s/U_p \ T	0.5	1	2	5	10
0.1		0.7 / 7.6	1.2 / 15	1.2 / 38	1.0 / 76
0.5		0.4 / 14	1.0 / 28	0.5 / 71	
1	0.3 / 13	0.9 / 25	0.8 / 50		
2	0.9 / 28	0.8 / 57			

TABLE 3.3
IPM TRANSVERSE COEFFICIENT AMPLITUDES AND IPM BASED CORRELATION KC NUMBERS FOR LF TEST MATRIX

CHAPTER IV
THE STARTING PROBLEM

Our search for data to establish a zero I-T Effect data base led to the consideration of the unsteady flow associated with starting the motion of the test cylinder in each SSPA test. We have used the term "starting problem" to identify and describe these data.

There are two starting problems which have been addressed by numerous analytical and experimental studies. One is the impulsive start in which a cylinder initially at rest instantaneously achieves a constant velocity. The second is the uniform acceleration start in which a cylinder initially at rest is subjected to a constant acceleration resulting in a linear increase in velocity. The second is our "starting problem" as it closely approximates the process used to initiate the motion of the test cylinder in the SSPA experiments.

Initially we examined the early cycles in test runs, those prior to the"fully established" test interval, in the search for a zero I-T data base. Illustrations of such data have been presented in Chapter II. These were sufficient to establish the concept of the I-T Effect but were insufficient in number and diversity to establish an irrefutable data base for a correlation. In examining the data from the early stages of each run one becomes aware of the starting interval which appears to be free from transverse forces. The matching of the IPM coefficients from the starting interval with those from early cycles, which were free from transverse development, encouraged the exploration of the full set of data associated with the starting interval of each LF run.

This chapter is devoted to the presentation of an I-T free data base derived form instantaneous IPM coefficients and IPM based KC Numbers.

OBSERVATION FROM ANALYTIC SOLUTIONS

For the case of a uniformly accelerated cylinder, analytic solutions for the development of a laminar boundary-layer can be traced back to the classic work of Blasius (1908). This work yields an expression for calculating the instantaneous position of the flow separation point on the cylinder surface. This expression indicates that the instantaneous separation angle can be expressed as a function of the instantaneous IPM KC Number, $2\pi U^2/D\dot{U}$. Recall that the IPM Theta-min is also a function of the IPM KC Number. In Figure 4.1 these two angles are plotted as a function of time for a case similar to the starting of the SSPA tests in

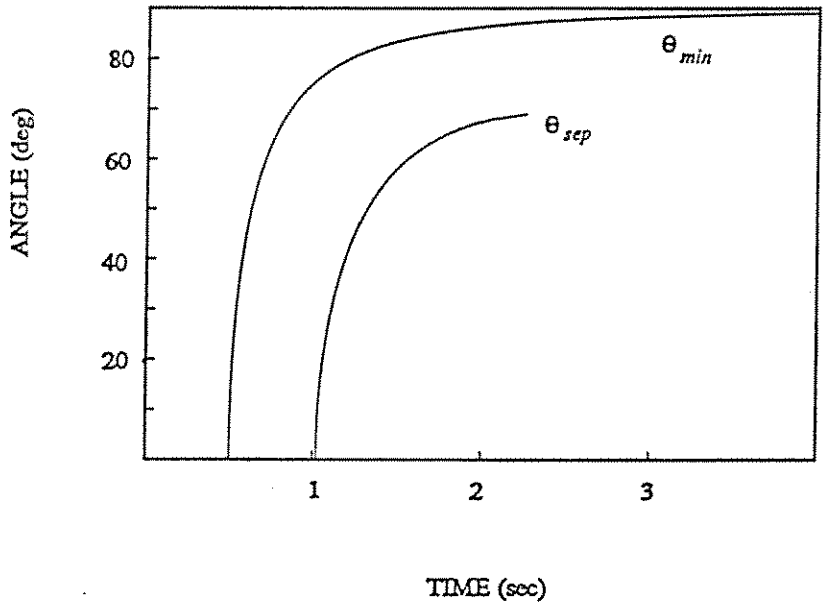

FIGURE 4.1
THETA-MIN AND SEPARATION ANGLE

Time series showing the change of the Theta-min angle and the angular position of the Separation Point for the Starting Problem of a 1 meter cylinder subjected to a uniform 0.5 meter/sec^2 acceleration. Theta-min is the IPM minimum pressure point on the surface of the cylinder. The associated separation angle was computed using the Blasius expression.

which the constant acceleration was 0.5 meters/sec^2. Although this separation analysis is for a laminar boundary-layer the plot is significant in that it shows explicitly several points that we have been contending for the IPM. First, it shows a similar pattern for the two quantities. Second, it shows that Theta-min is a precursor for separation. Third it shows that for an initial fraction of the test time no separation has occurred. Thus during this interval the drag can only be due to surface resistance. The "turn on" of the drag is associated with the development of flow separation.

With the analytical relationship of Blasius relating the IPM KC Number and the separation angle, the known relationship between separation and drag, and the IPM relationship between the KC Number and Theta-min, it is logical that there should be a relationship between instantaneous values of Theta-min and the IPM drag coefficient. This logical relationship is supported by the empirical evidence we have presented as the Theta-min Correlation (Appendix D pages 10 & 11).

Furthermore, if the IPM KC Number is the correlation parameter for starting interval drag coefficients, it should be used in relating the starting problem data to other data such as the LF.

The starting problem data set has many fascinating aspects. However, the constraints of time and objectives will limit us to mentioning three. (1) Evidence of high frequency "ringing" could be studied, (2) Very high frequency damping and combined motion could be studied, and (3) The examination of the initial fraction of starting problem interval. There are other problems that can be examined with other "trash data" intervals involving deceleration such as the companion terminal interval at the end of the test and the transition from the starting interval to the first quarter cycle.

COMPARISON OF TIME SERIES DATA

With the IPM algorithm we can convert any hydrodynamic force and attendant kinematic time series to a IPM coefficient time series which when multiplied by 8/3 becomes a drag coefficient time series. This process was used with the starting interval data. IPM processed data from 18 such time series are superimposed in Figure 4.2. In constructing these plots the Theta-min turn on condition was used for alignment. For these test conditions, with nearly constant acceleration, the longer the test interval the larger the velocity and consequently the higher the KC Number.

The individual drag coefficient time series when superimposed reveal surprisingly similar patterns. In the first 0.5 seconds, the pattern for both rough and smooth tests are similar in amplitude and the dominance of high frequency ringing. It is surprising that the ringing patterns are similar in amplitude ,frequency , and phase.

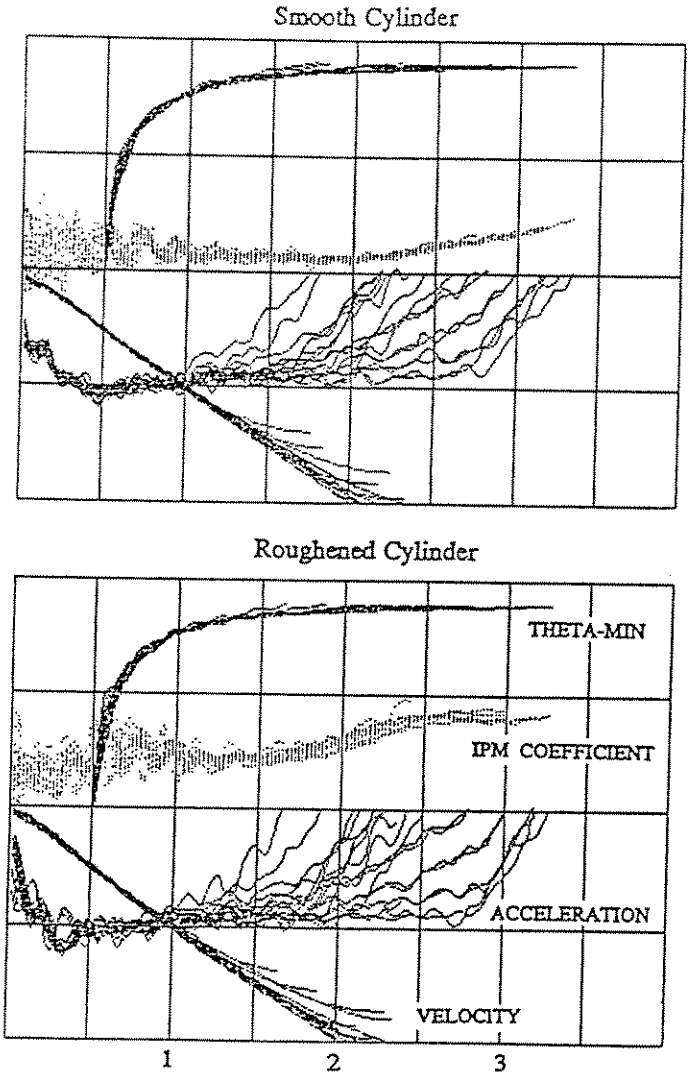

FIGURE 4.2
COMPOSITE TIME SERIES PLOT OF STARTING PROBLEM DATA

The composite of 18 sets of Starting Problem data from the SSPA experiment. The IPM drag coefficient scale is 0.5/div. The Velocity and Acceleration scales are 0.5 meters/sec/div and 0,5 meters/sec^2/div. The Theta-min scale is 50°/div.

One would expect at least a random phase. For this interval, separation has not occurred as Theta-min is at the rear stagnation point. However, during this interval, the Theta-min patterns on the individual roughness elements (treated as small cylinders) reveals that separation on these elements is in progress. Thus, by the end of the half second interval, the roughened cylinder drag has risen significantly above that of the smooth cylinder. During the next one second interval, it is doubtful that separation has occurred in view of the Theta-min values and the nearly constant levels of the damped ringing pattern of the coefficient. Separation behind the rough test cylinder develops sooner than on the smooth cylinder. For the rough cylinder separation begins after the 1.5 second point, and for the smooth cylinder after the 2 second point.

This pattern is well illustrated in the Theta-min Correlation plots of Figure 4.3. Here we see the constant levels before the ramping up as separation turns-on. Two sets of test data were used in creating each curve.

CORRELATION PLOT

Using coefficient values from the 90° Theta-min position and the associated IPM KC Numbers, the correlation plot of the starting problem data was constructed, Figure 4.4. In Figure 4.5 we have superimposed the LF plot of Figure 3.5 with the starting problem data of Figure 4.4. The correlation between these two supplementary data sets is encouraging.

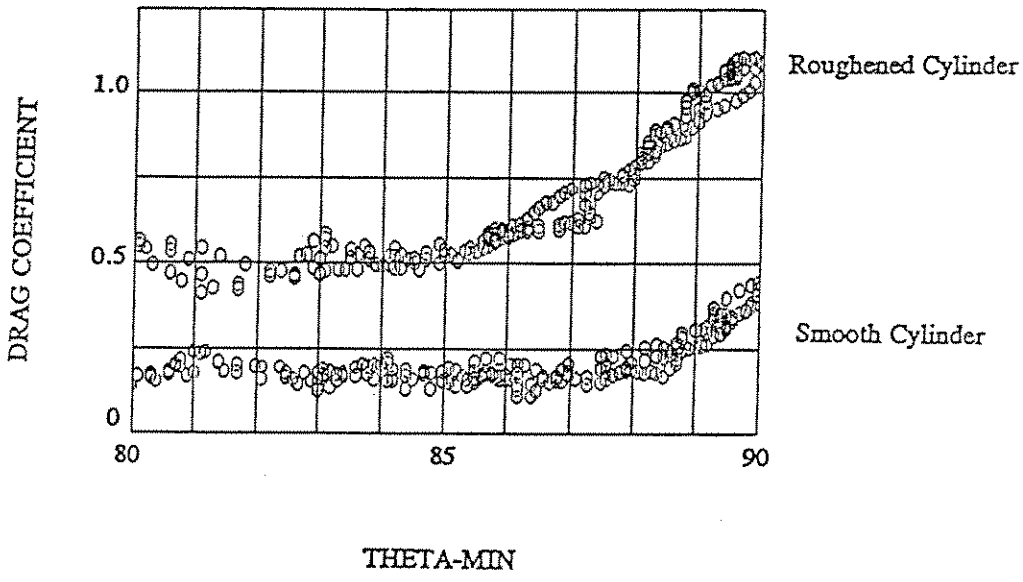

FIGURE 4.3
THETA-MIN CORRELATION PLOT FOR STARTING PROBLEM DATA

Recall the Theta-min Correlation (Appendix D page 10) is the empirically observed relationship between instantaneous values of Theta-min and IPM Coefficient. In this plot the IPM coefficient has been converted to an instantaneous Morison drag coefficient using 8/3. Data from the start of Runs 130 and 131 were used for the roughened cylinder. Data from the start of Runs 378 and 379 were used for the smooth cylinder.

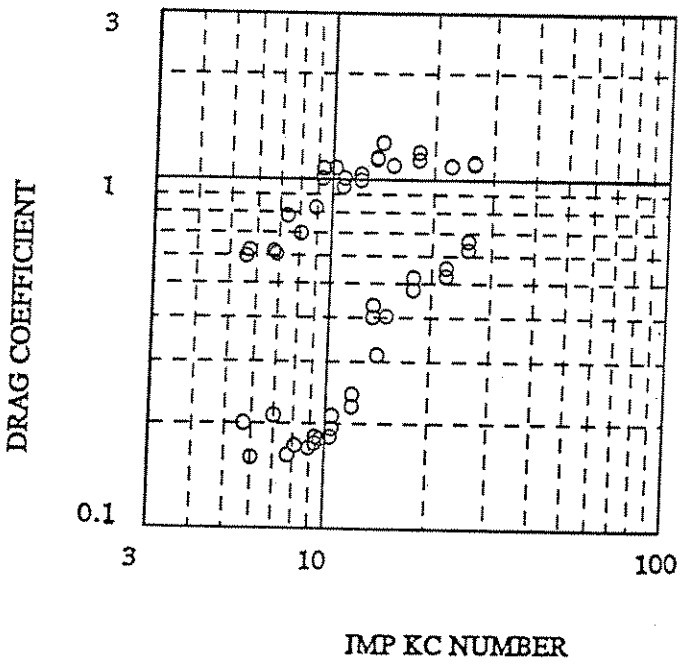

FIGURE 4.4
CORRELATION PLOT OF STARTING PROBLEM DATA

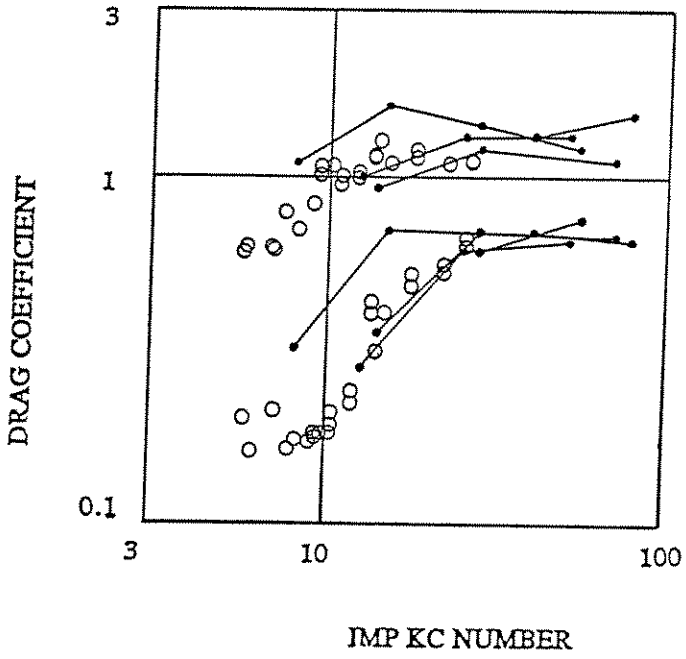

FIGURE 4.5
COMPOSITE CORRELATION OF LF AND STARTING PROBLEM DATA

CHAPTER V
STUDY OF HF DATA

In the previous study, in the comparable chapter which dealt with the HF Data, two subjects were introduced which have not been developed further in this study. The first was the dilemma presented by the RV and IF forms of the Morison equation, and the second was the question of the functional dependance of the damping force on velocity. On the first subject, recall that an analysis based upon the perturbation of the IPM coefficient led to an Applicability Map. On the second, evidence was presented for rather complex damping force patterns. These subjects are both interesting and significant; however, it was felt that a meaningful pursuit of them was beyond the intent of this study.

The previous study, with some justification, presented data based upon the linear damping approximation as exemplified by Equation (15) of HYDAMP-I. The current study is based on that approximation and provides a comparable appraisals of both smooth and rough cylinder tests.

The objective of this Chapter is to provide quantitative damping data and a qualitative understanding of the influence of combined high and low frequency motions on hydrodynamic forces. Although these coefficient data are important, our knowledge of damping will be confined to the meager range of the tests, unless we achieve an understanding of the HF problem. As a minimum, an understanding of these data enables one to extrapolate intelligently.

In examining the HF data we shall see the role of the I-T Effect in masking damping forces so that negative damping occurs in some tests for portions of the flow cycle. We shall also confront the dilemma of transverse forces which can be enhanced or diminished by high frequency motion. In these pursuits the rough data provides confirmation of subtle relationships seen previously in the smooth data.

A dividend presented in this Chapter is additional data supporting the correlation pattern established thus far with the LF and Starting Problem data. The IPM KC Number has been a key ingredient in establishing this correlation. For some HF test data, the IPM KC Number provides the only reasonable basis for a correlation.

The end result is a set of damping coefficients and additional data supporting a comprehensive correlation of drag coefficients in which the relative contribution of separation and I-T Effect are understood and quantified. As presented in the next Chapter, this correlation can encompass all the inline combined motion SSPA data.

RETROSPECTIVE

A brief retrospective of transverse force patterns, the I-T Effect, and how they might be influenced by HF motion is appropriate here. In an earlier Chapter the variation of transverse force patterns with KC Number was reviewed for simple periodic motion. The picture was presented in terms of a high, low, and mid KC Number behavior, with the mid range approximately 10 to 20. In the mid range the transverse forces occur as a 2nd harmonic and buildup after several cycles to achieve the largest observed amplitudes. Attendant to the buildup of the transverse force is a peaking of the inline drag force in the mid KC range, which is a manifestation of the I-T Effect.

As the KC Number increases the transverse force occurs at progressively higher frequencies and with reduced amplitudes. For these conditions the I-T Effect appears as a perturbation in the IPM inline coefficient time series at twice the transverse frequency. For the low KC range the transverse force may not develop at all but when it does it occurs as a 2nd harmonic.

The transverse and I-T patterns have been qualitatively described in terms of vortex motion and a force associated with vector cross product of the velocity and the strength of the vorticity.

How does combined motion modify this picture? We have seen the significant modifications which occur with the addition of a steady velocity. For the LF data the dramatic modification of the force patterns and correlation of the drag coefficient has been attributed to (1) modification of the KC Number and (2) interference. The shift in the KC Number by the modification of the velocity has been established. The retardation of transverse force development for mid range IPM KC Numbers is attributed to "interference". The opposing fractions of a cycle no longer reinforce each other, and the periods are illconditioned.

What should we expect with HF data? (1) Modification of the KC Number. Here acceleration modification creates the possibility of shifts to a lower KC Number. (2) Both retardation and enhancement of I-T Effect can now occur. The high frequency motion clearly can interfere with vortex shedding, but also it has the possibility of resonance with it.

PRESENTATION OF HF DATA

The test conditions of the HF data are summarized in Table 5.1. Included in this Table are Periodic Runs which shall provide a useful basis for comparisons. This Table list the Run Numbers of both the smooth and rough tests followed by the frequency, motion amplitude, and velocity amplitude of the low frequency periodic

motion (LF motion). The conventional Reynolds and Keulegan-Carpenter Numbers for the LF motion are also listed. The primed quantities refer to the HF (high frequency) perturbation and are the frequency, motion amplitude, and velocity amplitude followed by a KC Number for the high frequency periodic motion. The last two columns compare the relative amplitudes of velocities and acceleration of the two periodic motions. For Runs 445 and 199 only the high frequency motion was used in the tests.

TABLE 5.1

SUMMARY OF TEST CONDITIONS FOR HIGH FREQUENCY DATA

	Low frequency motion					*High frequency motion*					
Run No.	f_o	A_o	U_o	*Re-No.*	*KC-No.*	f'	A'	U'	*KC-No.*	U'/U_o	$\dot{U}'/\dot{U}_o$
smooth/rough	*(Hz)*	*(meters)*	*(m/s)*			*(Hz)*	*(meters)*	*(m/s)*			
437/192	0.079	2	1	0.88×10^6	12.6	0.3	0.1	0.2	0.63	0.2	0.76
438/193	0.032	5	1	0.88×10^6	31.4	0.3	0.1	0.2	0.63	0.2	1.9
439/194	0.016	10	1	0.88×10^6	63	0.3	0.1	0.2	0.63	0.2	3.8
440/195	0.079	1	0.5	0.44×10^6	6.3	0.3	0.1	0.2	0.63	0.4	1.5
441/196	0.016	5	0.5	0.44×10^6	31.4	0.3	0.1	0.2	0.63	0.4	7.5
443/197	0.079	1	0.5	0.44×10^6	6.3	0.3	0.15	0.3	0.94	0.6	2.3
442/198	0.016	5	0.5	0.44×10^6	31.4	0.3	0.15	0.3	0.94	0.6	11.3
445/199						0.3	0.1	0.2	0.63		

TEST CONDITIONS FOR ASSOCIATED PERIODIC DATA

Low frequency motion

Run No.	f_o	A_o	U_o	*Re-No.*	*KC-No.*
smooth/rough	*(Hz)*	*(meters)*	*(m/s)*		
359/102	0.079	2	1	0.88×10^6	12.6
360/103	0.032	5	1	0.88×10^6	31.4
361/104	0.016	10	1	0.88×10^6	63
352/96	0.079	1	0.5	0.44×10^6	6.3
354/98	0.016	5	0.5	0.44×10^6	31.4

To aid in the examination and comparison of these data they have been organized, using the low frequency motion KC Number, into 5 sets which are identified as Cases 1, 2a, 2b, 3, and 4. The respective rounded low frequency KC Numbers, low and high frequencies are listed with Run numbers in Table 5.2. The last 3 columns are the smooth/rough Run numbers of the Periodic runs, $A'/D = 0$, and the 2 amplitudes of high frequency motion.

TABLE 5.2

CASE GUIDE TO PERIODIC AND HF RUNS

	LF *KC*	f_o	f'	$A'/D = 0$	$A'/D = 0.1$	$A'/D = 0.15$
Case 1	63	0.016	0.3	361/104	439/194	-
Case 2a	31	0.032	0.3	360/103	438/193	-
Case 2b	31	0.016	0.3	354/98	441/196	442/198
Case 3	12	0.079	0.3	359/102	437/192	-
Case 4	6	0.079	0.3	352/96	440/195	443/197

Note that the periodic Reynolds Numbers of Cases 2b and 4 are half the values of Cases 1, 2a, and 3. Despite the modest number of test Cases this array represents a very meaningful basis for a HF study.

Plots of the Runs by Cases are found in Figures 5.1 to 5.5. Each Figure is comprised of a set of folded time series plots of the IPM inline force coefficient and the velocity, in the upper half, and plots of the inline vs transverse IPM coefficients in the lower half. The right side presents smooth cylinder data. At the top of each half page sequence of plots are the simple periodic Runs.

The time series plots show the magnitude and perturbations of the inline (drag) coefficient. The inline vs transverse plot is equally graphic in illustrating the I-T Effect and the significant changes in the transverse coefficient with test conditions.

REVIEW OF HF DATA

Let us first examine these data to ascertain significant patterns, then review these Cases a second time providing qualitative explanations for the patterns, and conclude with a quantitative presentation of how drag coefficients are influenced by HF motion.

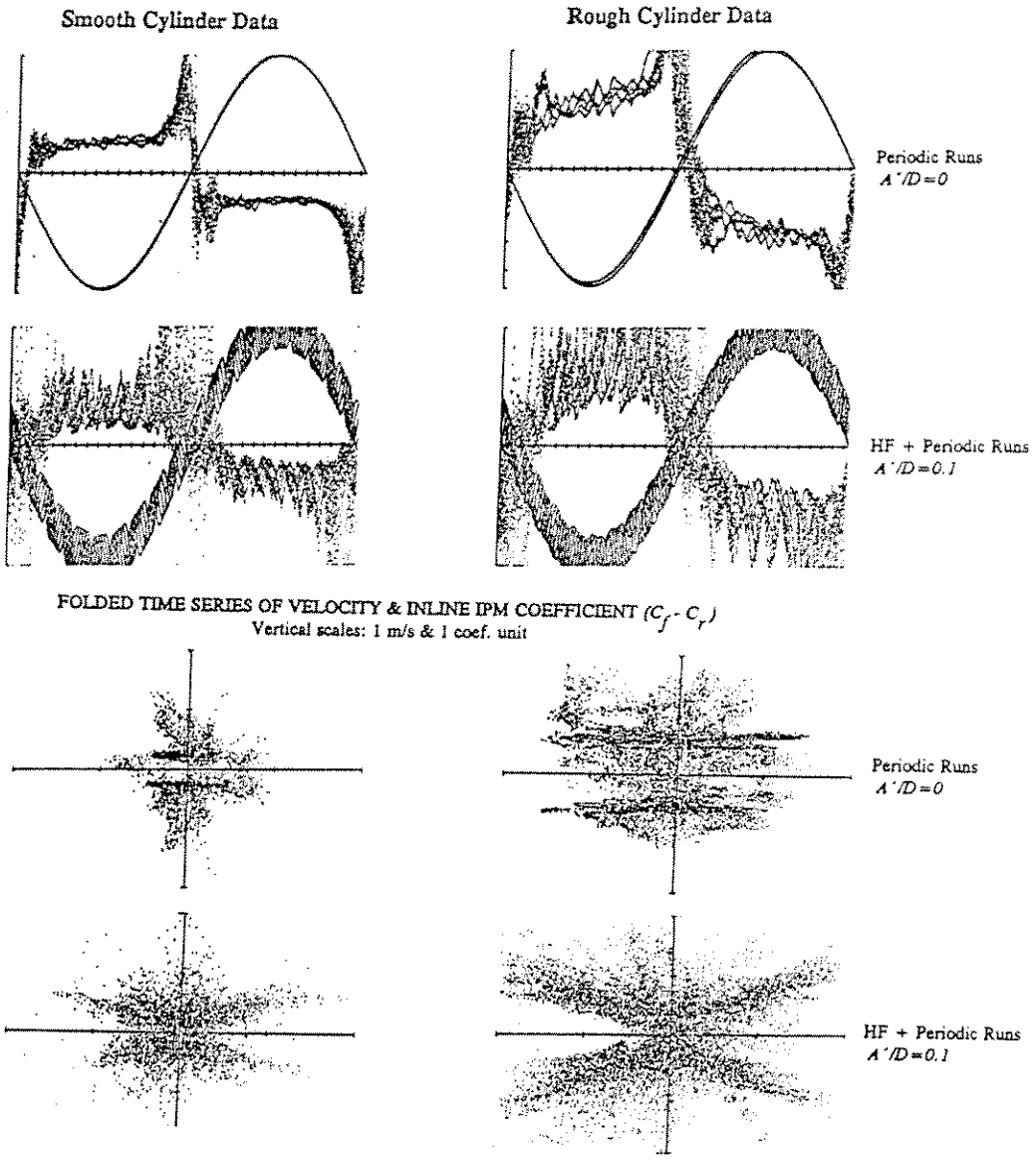

FIGURE 5.1
Smooth Runs 361 and 439 compared to Rough Runs 104 and 194
COMPARATIVE DATA FOR HF CASE 1: $N_{KC}= 63$, $N_{Re}/10^4= 88$

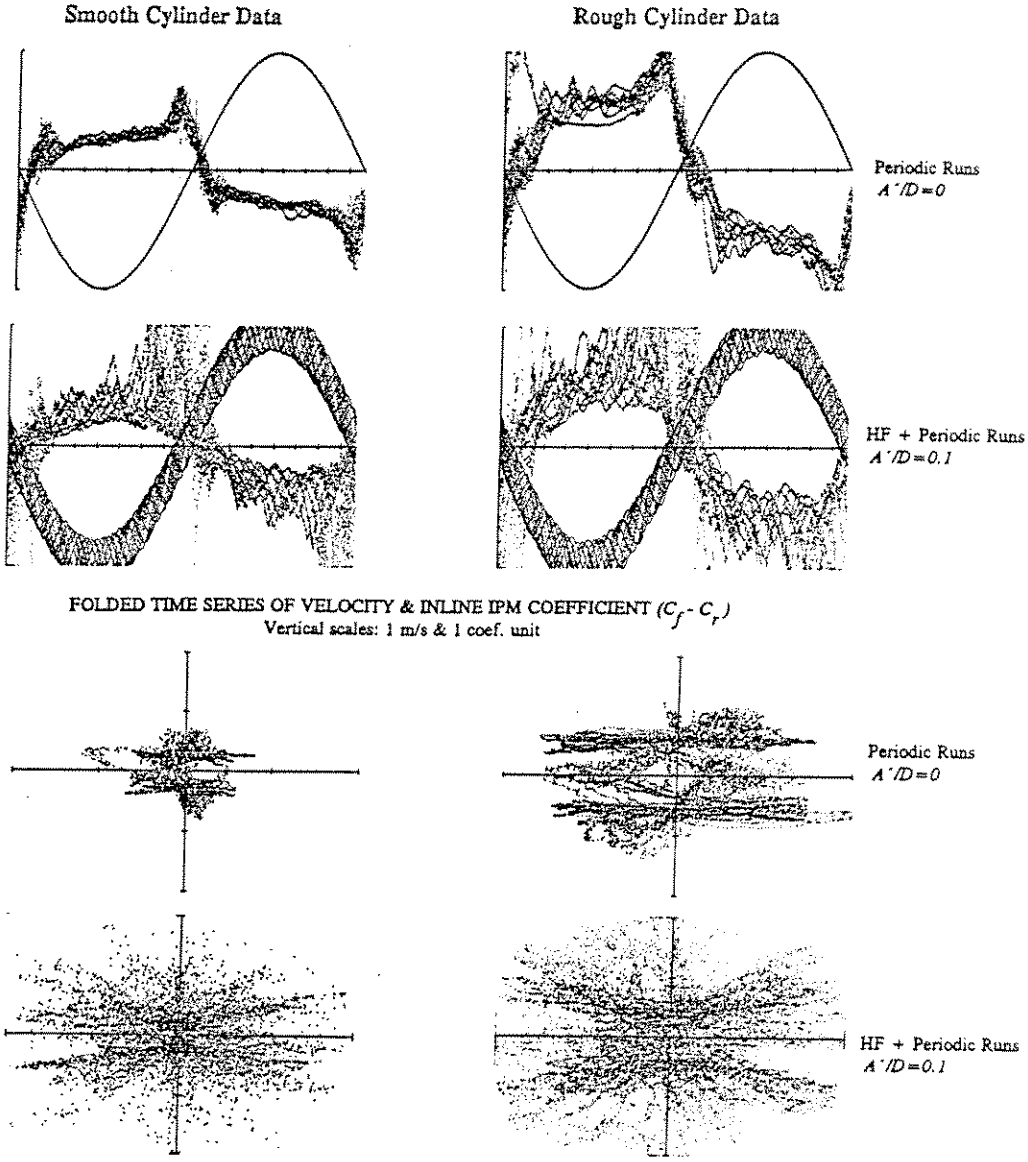

FIGURE 5.2
Smooth Runs 360 and 438 compared to Rough Runs 103 and 193
COMPARATIVE DATA FOR HF CASE 2a: $N_{KC}=31.4$, $N_{Re}/10^4 = 88$

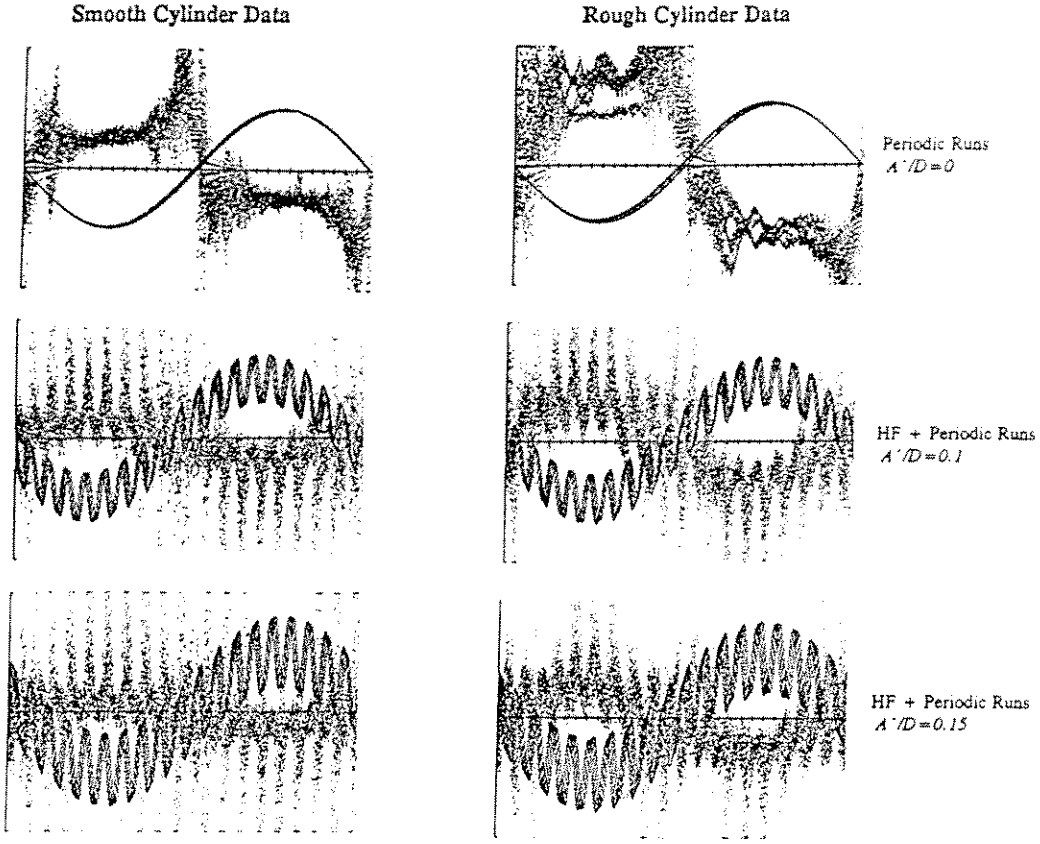

FOLDED TIME SERIES OF VELOCITY & INLINE IPM COEFFICIENT (C_f - C_r)
Vertical scales: 1 m/s & 1 coef. unit

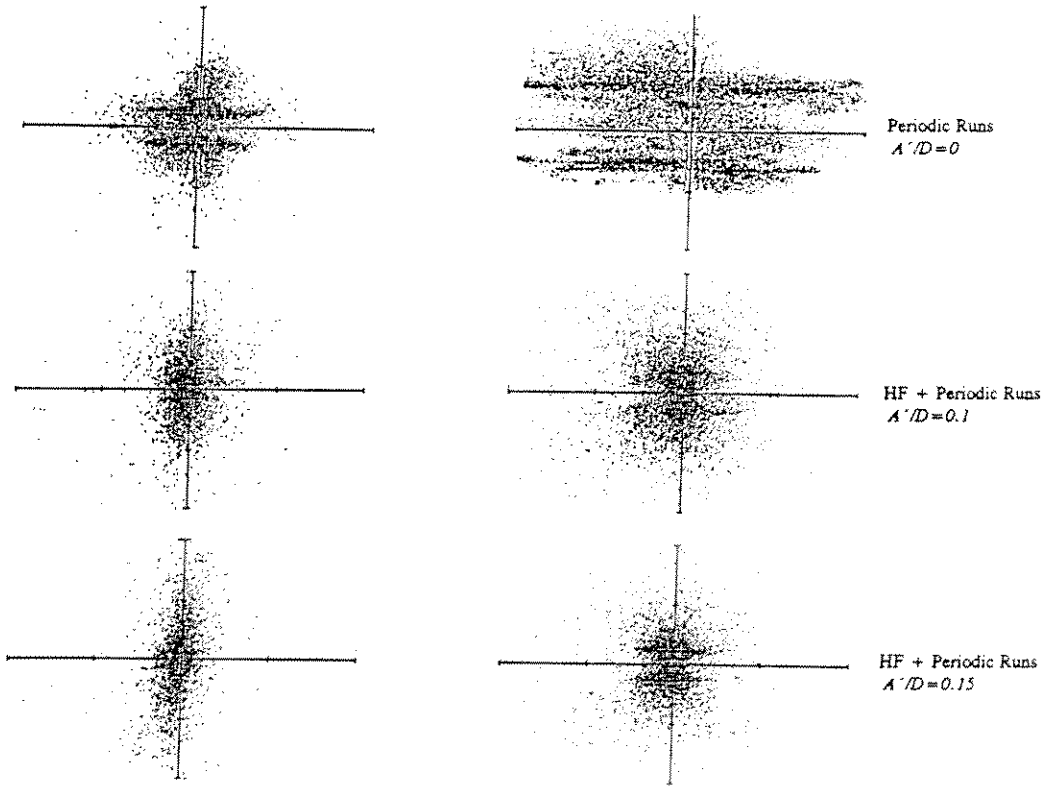

Scales: 1 coef. unit/division
INLINE (vertical scale) vs TRANSVERSE (horizontal scale) IPM COEFFICIENTS

FIGURE 5.3

Smooth Runs 354, 441, and 442 compared to Rough Runs 98, 196 and 198
COMPARATIVE DATA FOR HF CASE 2b: $N_{KC}=31.4$, $N_{Re}/10^4=44$

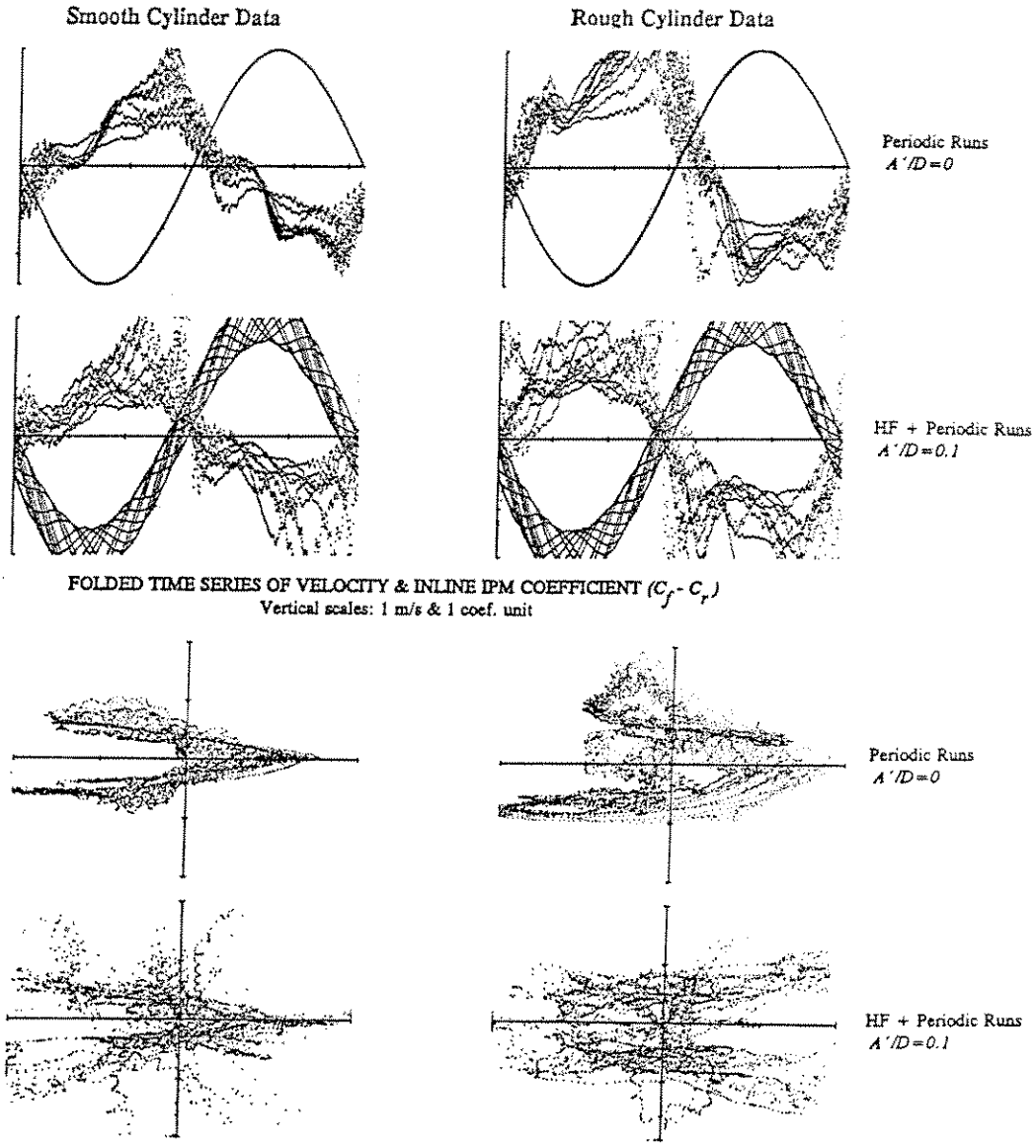

FIGURE 5.4
Smooth Runs 359 and 437 compared to Rough Runs 102 and 192
COMPARATIVE DATA FOR HF CASE 3: $N_{KC}=12.6$, $N_{Re}/10^4 = 88$

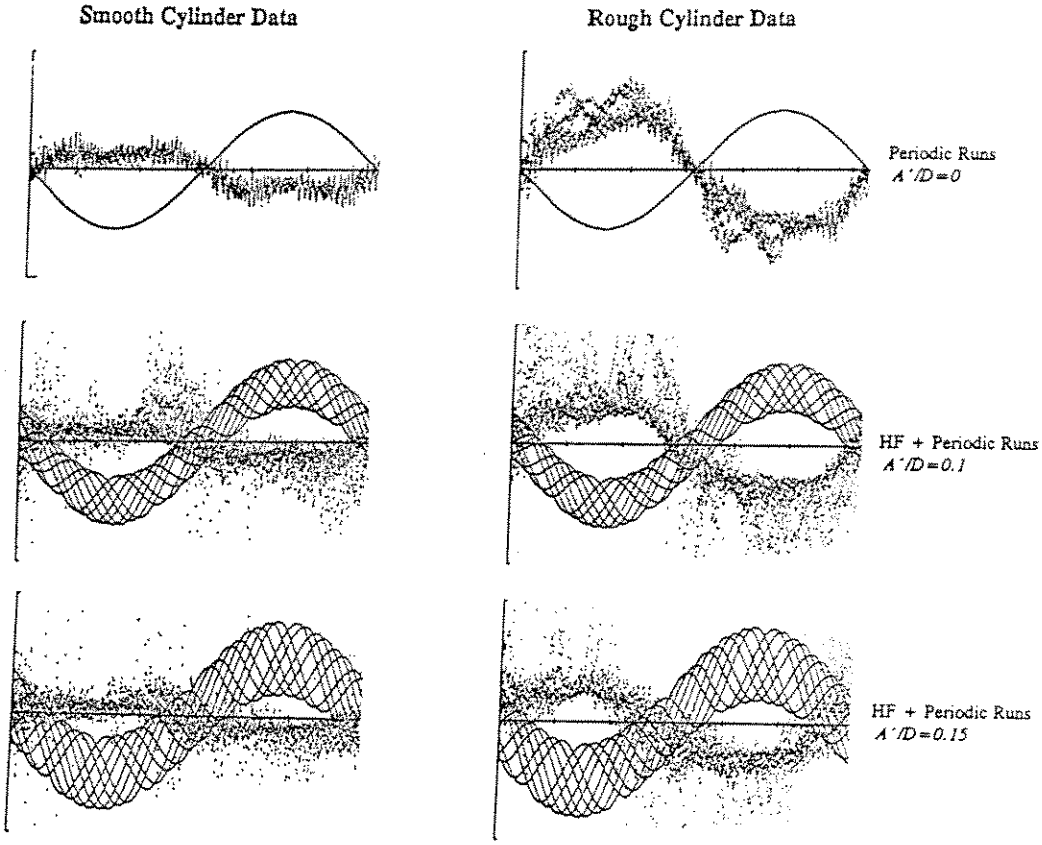

FOLDED TIME SERIES OF VELOCITY & INLINE IPM COEFFICIENT $(C_f - C_r)$
Vertical scales: 1 m/s & 1 coef. unit

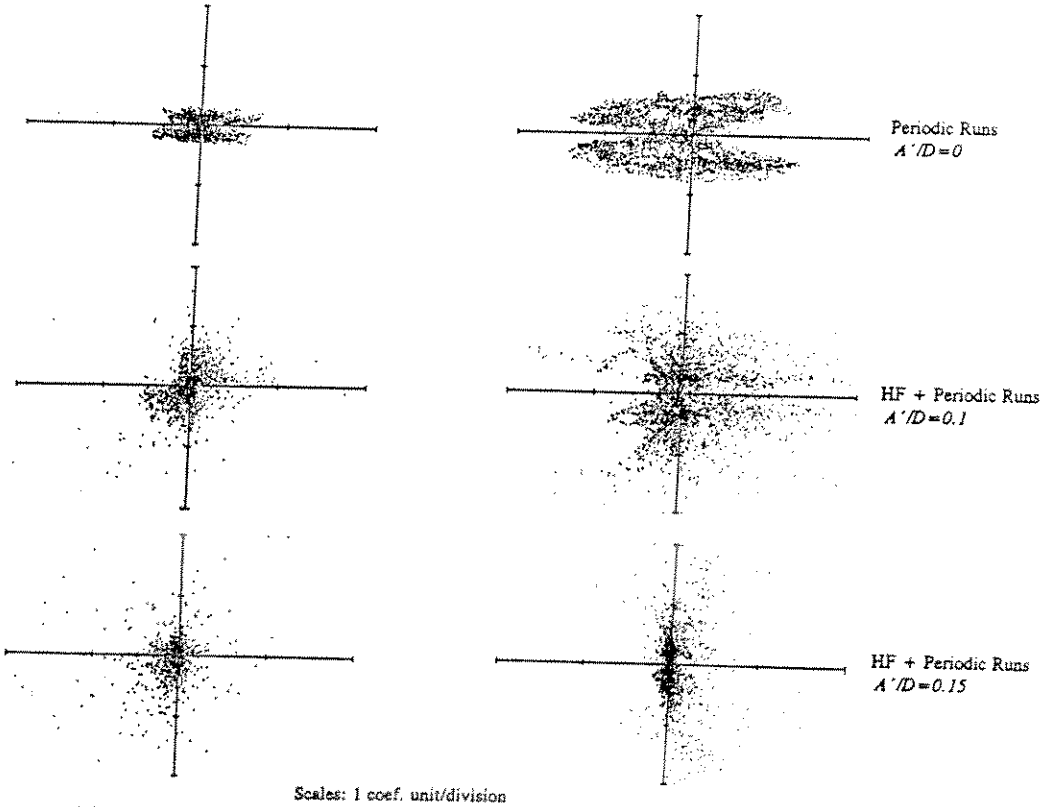

Scales: 1 coef. unit/division
INLINE (vertical scale) vs TRANSVERSE (horizontal scale) IPM COEFFICIENTS

FIGURE 5.5
Smooth Runs 352, 440, and 443 compared to Rough Runs 96, 195 and 197
COMPARATIVE DATA FOR HF CASE 4: $N_{KC} = 6.3$, $N_{Re}/10^4 = 44$

For the first look, focus on the Periodic Runs and note the significant increase in the inline coefficient when the smooth and rough data are compared; also note the more significant transverse force for the rough cylinder data. The periodic data of Cases 1, 2a, and 2b are almost identical (2b is the fuzzier of the three as one should expect a more significant signal to noise problem with the lower velocity). For the Periodic Runs of Case 3, the inline and the transverse coefficients are in the robust pattern expected with the mid KC range. The V pattern of the inline vs transverse plots are indicative of a 2nd harmonic in the transverse coefficient. For the low KC data of Case 4 we see modest values of both inline and transverse coefficients for the smooth cylinder and enhanced values for the rough cylinder.

Now examining the HF + Periodic data. The pattern for Cases 1 and 2a are similar, a high frequency perturbation of the inline coefficient with larger coefficient perturbations associated with the rough cylinders and very energetic inline vs transverse patterns in the form of a double V. For Case 2b, a distinctly different pattern is seen with both the inline and the transverse coefficients greatly reduced. Case 3 is only moderately influenced by the HF addition. For this Case the HF Runs have inline vs transverse patterns which are slightly more erratic than the Periodic Runs. For Case 4 the reduction of the transverse coefficient is clear.

The questions now are: Why was the transverse force enhanced in some Cases and diminished in others, and why the dramatic reduction in the inline coefficient for Case 2b?

EXPLANATION OF HF DATA

Our answers to the above questions and explanation of the HF Data patterns are aided by a cycle-by-cycle spectral analysis of each Run. A cycle-by-cycle analysis is useful in quantifying changes during the test time and in showing the development of patterns at the start of the test. In the following discussion, reference will be made to harmonics rather than frequency. The 1st or primary reference harmonic is at the frequency of the LF Periodic. For all the Cases, the HF component of motion was not an integer multiple of the LF, which is very significant; however, we shall refer to it as a 18.75 harmonic or a 3.75 harmonic in the discussion below.

Starting with Case 1 at a KC Number of 63, the Periodic Runs indicate transverse force components occurring at harmonics 5 to 13. Although the dominant component shifts during the test it is centered around the 9th harmonic. The HF motion appears as a 18.75 harmonic which would reinforce an 18 harmonic I-T component and it's derivative 9th harmonic in the transverse force. The result is a significant increase in the transverse coefficient seen at the bottom of Figure 5.1. An attendant significant increase in the I-T Effect, at approximately the 18th, is coupled to the transverse force pattern. Thus it is equally likely to be in phase or 180° out of phase with the HF velocity and damping force. The result is a sizable I-T component that

dominates a small damping component. So when damping is examined for each HF cycle, a very large statistical variance in the damping force is observed for Case 1. The magnitude of the variance correlates with the I-T amplitude. Clearly, a large variance around a small value leads to a high probability of negative values.

The explanation for Case 2a at a KC Number of 31 is similar. However, the transverse harmonic components occur in the 2 to 8 range centered at the 5th. The HF motion appears as the 9.4th, which would reinforce a 4th or 5th harmonic in the transverse. The build up of the transverse results in significant I-T components in which the damping effect is easily lost.

For Case 3 at a KC of 12 the explanation follows a similar line but with and additional provision. For these Runs the transverse forces occur as strong 2nd harmonics and the HF motion as a 3.75th which should reinforce a 4th harmonic I-T and associated 2nd harmonic transverse. However, the 1/4 harmonic dissonance for this Case is more significant than in those discussed above. Now the 1/4 harmonic is a more significant fraction of the LF flow cycle. For this Case we see the onset of conditions in which the HF motion interferes with the transverse force rather than reinforcing it. Thus at the bottom of Figure 5.4, the Inline vs Transverse pattern becomes more irregular when the HF is added.

For Case 4 the entire harmonic relationship of Case 3 applies. The difference is that Case 4 is comprised of low KC Number Runs in which the transverse force pattern tends to be nonexistent or at best less stable. Thus it is not surprising to see the 1/4 cycle dissonance, associated with the HF motion, suppress a 2nd harmonic transverse forces pattern. With the transverse and I-T components suppressed, the problem of extracting the small damping force becomes more accurate and less confused, with statistical variance now reduced to the order of the quantity to be measured.

To this point our explanation has focused on the interference/resonance effects, now consider the possibility of KC Number shifts for the HF Runs. As a first approximation of the correlation KC Number that might be applied to the HF Runs consider the IPM KC Number, $2\pi\ U^2/D\dot{U}$, evaluated using the dominant velocity and acceleration for each Run. To this approximation Case 1 with Periodic KC Number of 63 would shift to 17. Case 2a with KC Number of 31 would also shift to 17 and the 12 for Case 3 would not change. For Case 4 the KC Number of 6 would be shifted to 4 for the smaller HF amplitude. If the velocities and accelerations of both periodic and HF motions are combined in this expression the shifts would not be as large. In terms of the correlation of drag coefficient with IPM KC Number presented in the previous Chapter, these shifts would not result in a significant change in the correlation pattern. Such shifts would not provide as decisive an explanation of the HF data as "interference" does.

If we compute the IPM KC Number for Case 2b using the above approximation, the Periodic KC Number of

31 shifts to 4. A shift from the high to the low KC range should entail a significant change in the drag coefficient and transverse force pattern. Effects we have just seen in the data of that Case.

For Case 2b the Periodic Runs have the same spectral characteristics as those of Case 2a, i.e. transverse forces around the 5th harmonic with the I-T at the 10th. For this Case the HF appears as a 18.2th harmonic. The difference between the 10th and 18th is too great to achieve a resonance reinforcement other than as a 9th harmonic transverse force. A 9th harmonic is sustainable only at much higher KC Numbers.

So for Case 2b both a KC Number shift and interference are significant in reducing the drag coefficient and suppressing the transverse force. We shall see more on this Case in the next section as we quantify these data.

DRAG COEFFICIENTS FOR HF DATA

The IPM based procedure of HYDAMP-I was used to determine drag coefficients for the 24 Runs which comprised the Cases we have just examined.

The data for the Periodic Runs are presented in Figure 5.6 and data from the HF Runs are presented in Figure 5.7. With one exception these data have been presented as bands. These represent the limits of the cycle-to-cycle variation, as with the presentation of the LF Data in Chapter III. As with the LF Data, the bands are attributable to: (1) the VHF (very high frequency $\approx$ 4.5 Hz) noise and (2) the I-T contribution.

In Figure 5.6 we chose not to present the data at KC Number 63. The triangles represent cycles in which transverse and I-T Effect are minimal. These points, as we shall show in the next Chapter, fit nicely into the correlation pattern presented earlier. As a convenient reference, these points are included on Figure 5.7 . Note, that with the exception of the smooth cylinder at a KC Number of 6.3, the data bands are slightly above the triangles. For the smooth 6.3 test conditions the drag force is small, thus allowing the VHF noise to determine the band limits. In the other test conditions the I-T Effect is the dominant source of cycle to cycle variation and the relationship between band and triangle point is indicative of the magnitude of the I-T Effect.

The data bands for the HF Runs and the Periodic Runs are quite similar and would overlap if superimposed. However. the thickness of the bands of Figure 5.7 are greater as would be expected with the increased I-T Effect associated with most of the HF tests. For the low Reynolds Number data at 6.3 and 31 we have two test conditions corresponding to the two amplitudes of the HF motion. The larger amplitude of motion is associated with the smaller drag coefficients.

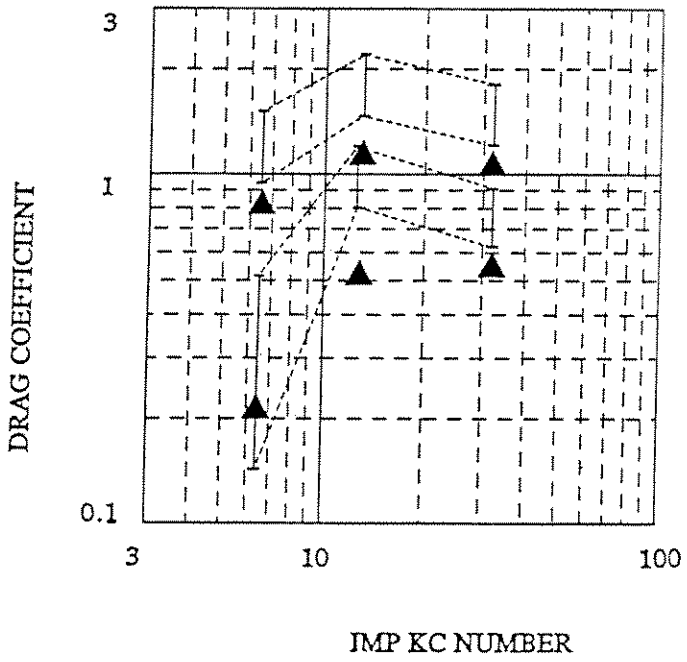

FIGURE 5.6
DRAG COEFFICIENTS FOR PERIODIC MOTION RUNS
ROUGH CYLINDER DATA (UPPER BAND) AND SMOOTH CYLINDER DATA (LOWER BAND)

All Data Bands show the cycle-to-cycle variation which is attributed to the I-T Effect. The Triangular Data Points are taken from cycles in which transverse forces were minimal. The I-T Effect is an inline force component which is induced by the transverse force and correlates with the transverse force amplitude and frequency.

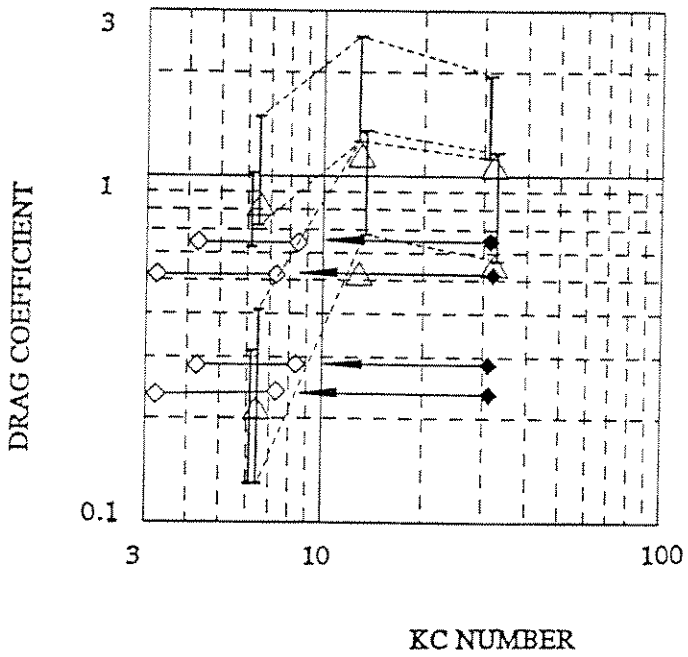

FIGURE 5.7
DRAG COEFFICIENTS FOR COMBINED MOTION - HF RUNS
ROUGH CYLINDER DATA (UPPER BAND) AND SMOOTH CYLINDER DATA (LOWER BAND)

These combined motion test conditions involved a Low Frequency (LF) periodic motion combined with a High Frequency (HF) periodic motion. Data Bands show the cycle-to-cycle variation which is attributed to the I-T Effect. The Triangular Data Points, from Figure 5.6, were taken from periodic test cycles in which transverse forces were minimal. The I-T Effect is an inline force component which is induced by the transverse force and correlates with the transverse force amplitude and frequency. At a Keulegan-Carpenter Number of 6.3 two data bars are shown with the first from the left representing a HF amplitude of 0.15 m and other an amplitude of 0.1 m. At a KC Number of 31 the data from Case 2b are shown as solid diamonds with the upper point in each pair representing a HF amplitude of 0.1 m and the lower an amplitude of 0.15 m. The arrows indicate shifts in these points for an IPM based KC Number ($2\pi U^2/D\dot{U}$). The shifted points are the open diamonds. The low KC Number end of each shift is for a combination of LF velocity with HF acceleration and the other end is for combined values for velocity and acceleration. Only Case 2b data have been shifted; all other data are plotted at the LF KC Number.

Data bands were not used with the Case 2b HF data which are presented as solid diamonds. Clearly, these points are out-of-line with the overall data pattern. However, if IPM KC Number shift, indicated by the arrows, is applied then these points fall within the correlation pattern. The horizontal bars, associated with the shifted data, are indicative of two different interpretations of the IPM KC Number expression. The larger shift is associated with a combination of dominant velocity and acceleration and the smaller shift with a combined velocity and dominant acceleration.

HF MOTION TESTS

Runs 445 and 199 represent test conditions in which only the HF motion was applied to the test cylinders. These test provide a view of hydrodynamic behavior for a periodic KC Number of 0.63.

For these tests Drag Coefficients of 0.23 ± 0.06 and 0.74 ± 0.06 were determined for the smooth and rough cylinders respectively. Shell in their SSPA Study reported values of 0.42 and 1.34 based on conventional Morison analysis.

The folded time series of the IPM Coefficient, Theta-min and the velocity for these Runs may be contrasted in Figure 5.8. The presence of the VHF component can be seen as a source of significant uncertainty for these data. The full time series for these tests are presented in Appendix C, and as one might expect they show no transverse forces.

We have chosen to contrast the initial portions of the starting problem time series with these data in Figure 5.9. The two sets are presented on identical scales and represent the superposition of multiple records. In contrasting the plots the average amplitude and behavior of the IPM Coefficients are comparable and indicative of the surface resistance drag argument presented in an earlier Chapter.

We should also note the repetitive character of the VHF pattern. It would appear that with the IPM, one could analyze these data also. This is but another indication of the deeper insight achieved with the IPM.

DAMPING COEFFICIENTS

In the HYDAMP-I study, linear damping was argued to be the only appropriate approximation to represent damping forces in the SSPA combined motion context. This argument follows from the IF and RV ideas which have not been pursued further in this study.

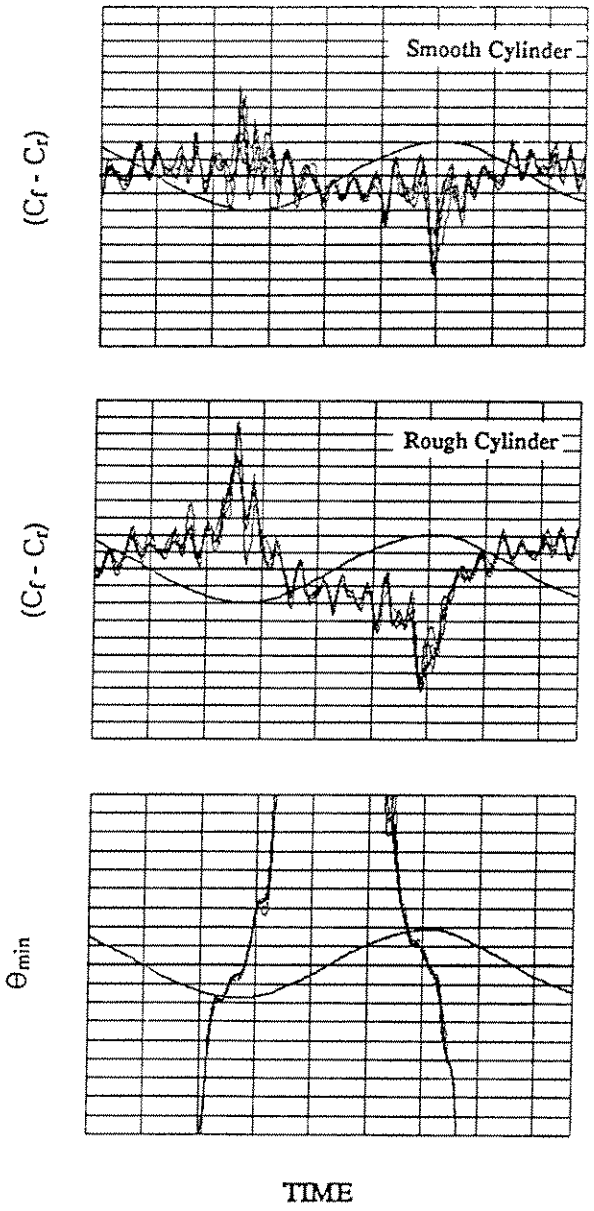

FIGURE 5.8
TEST WITH HF MOTION ONLY
IPM COEFFICIENT, THETA-MIN, AND VELOCITY TIME SERIES

Folded time series plots of 12 cycles from tests with simple periodic motion of amplitude 0.1 meters oscillating at 0.3 Hz yielding a periodic Keulegan-Carpenter Number of 0.63. Velocity is shown on all plots.
Scales: 0.5 sec/div, 0.1 coefficient units/div, 10°/div, and 0.1 meters/sec/div.

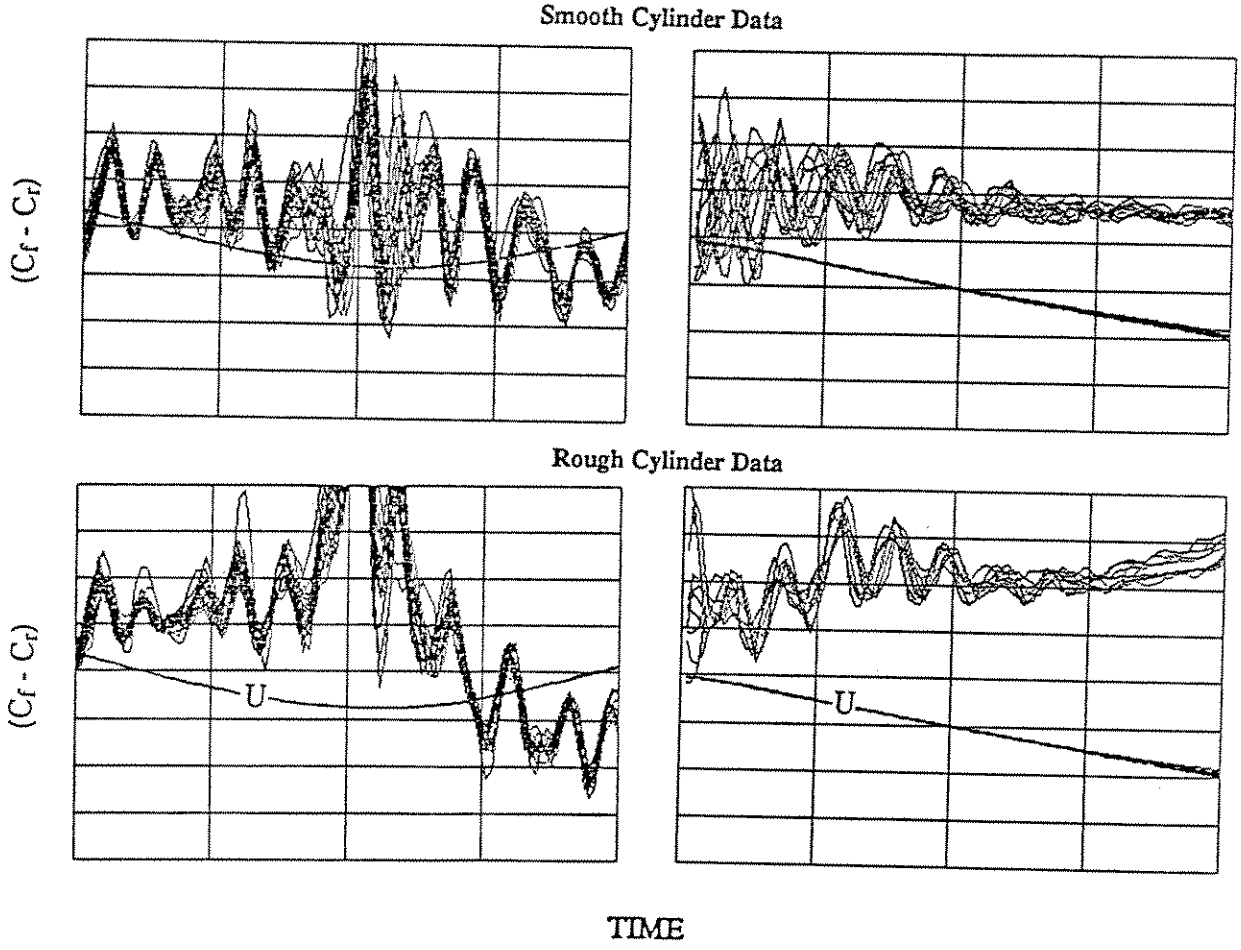

FIGURE 5.9
COMPARISON OF IPM COEFFICIENT TIME SERIES FOR KC NUMBERS < 1

Plots at the left portray superposition of multiple cycles from tests with HF periodic motion only. Plots at the right portray superposition of many SSPA Runs in which only the early portion of the Starting Problem is shown. Velocities are shown on all plots. Scales common to all plots are 0.1 coefficient units/div and 0.5 sec/div. The VHF noise (very high frequency ≈ 4.5 Hz) is clearly repetitive and not random.

However, we shall review the arguments briefly. Recall, the IPM drag term (comprised of the product of the IPM coefficient and the velocity squared) was expressed as a polynomial using low frequency terms and high frequency perturbations for both coefficient and velocity. In the resulting expression, consideration was given to the cubic and quadratic terms; however, for the HF data of this study their inclusion was not justified considering: (1) the small contribution of these terms with these data and (2) the errors imposed by the constant coefficient constraint. The result indicated only a linear approximation was plausible.

The realization of the linear approximation for HYDAMP-I was Equation (15):

$$(\bar{F}_d)' = \bar{F}_d - (\bar{F}_d)_o = -1/2 \left[2 C_d' U_o U' \right]$$

where the $(\,)_o$ referrers to the low frequency contribution and $(\,)'$ referrers to the high frequency contribution. The expression states that the damping force is the difference between the observed forces from the HF tests and the corresponding periodic test. The quantity U_o represents the low frequency velocity amplitude.

For the HYDAMP-I this expression was the implicit basis for determining damping coefficients. Two procedures were used. One used a spectral analysis for the difference in forces. This procedure was also used in the Shell SSPA Study. It suffers from the HF motion not being a harmonic of the LF motion. The second procedure considered the amplitude of the coefficient perturbations. As we have seen above the IPM coefficient perturbations can be compromised by I-T contamination.

A different approach was used in this study, one which uses the above expression explicitly to compute a damping coefficient for each cycle of the HF motion. The procedure involves first aligning the velocity records of the corresponding HF and Periodic Runs so that their difference yields the high frequency velocity. Accurate alignment can be achieved by monitoring the amplitude of the resultant time series as one record is shifted relative to the other. With this alignment, the difference in the force or IPM coefficient records provides the HF perturbation. This perturbation record is comprised of I-T, damping, and VHF contributions. Using the properties of orthogonal functions, one can project out of this time series the drag/damping contribution which is phased to the velocity. This procedure yields the force difference and the velocities for computing the damping coefficient with the above expression. The resulting set of cycle-by-cycle damping coefficients could be analyzed statistically. The average and standard deviation (variance) are reported in Table 5.3.

For portions of LF cycles negative damping coefficients were observed. This occurs when the I-T contribution is in phase with the velocity. The large values of the statistical variance are indicative of the I-T Effect. For the Cases 1, 2a, and 3a (Runs 438, 194, 438, 193, 437, and 192) significant transverse and I-T forces occur.

And large σ values are associated with these data. For the other Runs the transverse forces were reduced as were the values σ.

TABLE 5.3

LINEAR DAMPING COEFFICIENTS WITH STANDARD DEVIATION FOR HF DATA

Case	*Run No. smooth/rough*	*KC*	*Re/10⁴*	*A′/D*	*Smooth*		*Rough*	
					C_d'	σ	C_d'	σ
1	439/194	63	88	0.1	.0027	.11	.097	.32
2a	438/193	31	88	0.1	.028	.19	.145	.39
3	437/192	12	88	0.1	.02	.5	.29	.78
4	440/443	6	88	0.1	.079	.105	.21	.28
4	443/197	6	44	0.15	.088	.066	.27	.17
2b	441/196	31	44	0.1	.026	.047	.142	.098
2b	442/198	31	44	0.15	.051	.028	.199	.05

Note the similar damping coefficient values for the comparable Cases 2a and 2b, Runs 438 and 441 and Runs 193 and 196. Recall these are Cases for similar test conditions in which drastically different transverse and I-T Effects were observed. This is reflected in the significantly different values of σ.

A logical question is: Does the I-T Effect cause the damping coefficient to be physically modified, or does it just make it more difficult to determine by presenting a signal to noise problem? The favorable comparison of the above paragraph would indicate the latter.

How consistent are these data? If we assume the damping force for the HF Data is equal to the drag force of Runs 445 and 199, tests with the HF motion only, then the above expression yields a conversion of a HF only drag coefficient to a damping coefficient:

$$C_d' = 1/2\, C_d U'/U_o$$

Values computed with this expression fall within error bands, σ , for all Runs.

The table below contrasts the previously reported values with the current values. On average, the current values are 1/3 the values of the previous HYDAMP study and 1/5 the value reported in the Shell SSPA study. We shall comment on the significance of this difference in the next Chapter.

TABLE 5.4

COMPARISON OF DAMPING COEFFICIENTS WITH THOSE OF PREVIOUS SSPA STUDIES

Run Number	*437*	*438*	*439*	*440*	*441*	*443*
Shell SSPA Study	.12	.07	.03	.26	.10	.28
HYDAMP-I	.07	.09	.02	.16	.07	.18
HYDAMP-II	.02	.028	.0027	.079	.026	.088

CHAPTER VI
CONCLUSIONS

In providing Morison coefficient data and an understanding of combined motion problems, the stated objectives of HYDAMP have been attained using the IPM as an invaluable guide. We are gratified that far more has been achieved than was envisioned in the proposal.

By quantifying both the uncertainty in the coefficients and their ability to predict loads for several levels of approximation, we have gone further than most studies, which seem content with lists of coefficient data for the test conditions. Illustrations of the I-T Effect have been presented, which demonstrate how its variability is the source of coefficient correlation problems with combined motion. The roles of interference, illconditioned periods, and KC Number shifts on I-T Effect variability have been detailed. These led not only to our understanding of how combined motions modify structural loading but also to a correlation of coefficient data including the I-T Effect.

This Chapter is not intended as a summary or review of the previous material. Rather, the intent is to provide additional concluding statements on the following: the IPM, correlation of data, quantifying the I-T Effect, and observations on damping coefficients.

ON THE IPM

We have demonstrated the utility of the IPM for many things, but not force predictions. In that regard we took a sharp tool, the IPM, and used it on a not-so-sharp tool, the Morison equation.

The generation and correlation of the Morison coefficient set has been a significant accomplishment. These Morison coefficients were base on IPM coefficients. Thus the same correlation could be used directly with the characteristics of the IPM coefficient set. With the IPM accurate force predictions have been demonstrated without undue complexity. This potential for improved force predictions using correlated "instantaneous" coefficients is one of the important but implicit messages of this study.

Our study has provided unique opportunities to use the IPM. The first was the IPM based KC Number which is the basis for the coefficient correlation. The second was the ability of the IPM to process the entire data record. From that attribute several items follow. First it allowed us to compare records on a cycle-by-cycle basis and to look closely, almost microscopically, at effects within a cycle. This led to our understanding of

the I-T Effect. Recall, this was done without any filtering, smoothing, or averaging. Second it allowed an examination of the "starting data", which was a crucial data set in the correlation presented in this study. Without the IPM it would have been difficult to compute coefficients for these data. Without the IPM it would have been difficult to know what to do with these data, i.e. how to correlate them with the other data.

In the course of the study there were other more subtle demonstrations of the utility of the IPM, which we have chosen not to enumerate. The list above should be sufficient to impress one with the power of the IPM.

COMPREHENSIVE COEFFICIENT CORRELATION

Composite correlations of rough and smooth cylinder tests are compiled respectively in Figures 6.1 and 6.2. The LF data from Figure 3.5 was transferred directly to these plots, as were the starting problem data from Figure 4.4. The triangular data points, representing minimal I-T Effect for Periodic Tests, were taken from Figure 5.6. For the HF Data of Figure 5.7, the data bars have been transferred at their LF Periodic KC Numbers and the Case 2b data as the shifted points. In addition, the "HF only" data, which should be portrayed at a KC Number of 0.63, were plotted in the margin of each plot. Some additional points at low KC Numbers have been add. These were taken from the early portion of the starting process records, Figure 4.2.

Recall that most of the points, which comprised the "base" patterns on these two plots, are minimally influenced by the I-T Effect. The bars of HF data indicate the extent of the I-T Effect, which is clearly superimposed on our base pattern.

A rather simple portrayal of this base pattern is comprised of 3 straight line segments. These are: constant low and high KC Number segments which are connected by a sloping line. The rough and smooth patterns are identical but shifted.

Thus, for the smooth cylinder the drag coefficient is 0.2 up a KC Number of 8. It then ramps up to 0.6 at a KC Number of 15, and for the rough cylinder the drag coefficient is 0.7 up to a KC Number of 6 and then ramps up to 1.1 at a KC Number of 13. The coefficient scatter bands for both representations is $\pm$ 0.1. Clearly the patterns are the same with the rough cylinder pattern shifted 2 KC Number units to the left and 0.5 coefficient units upward.

The low KC Number drag coefficient for the smooth cylinder is indicative of the minimum drag coefficient reported in the literature for steady flow in the trans-critical range. The region of linear increase with KC Number corresponds to the type of Wake Volume Scaling presented by Horton et al *J of OMAE* 1994.

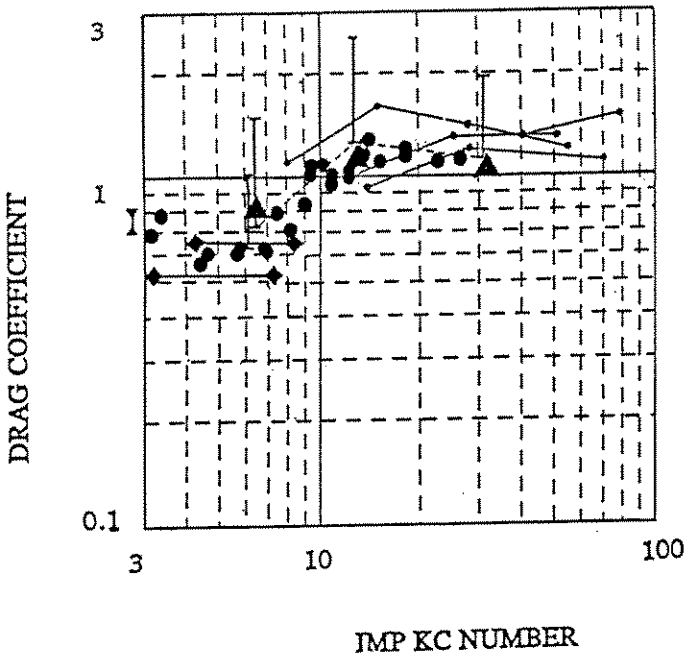

FIGURE 6.1
COMPILATION OF DRAG COEFFICIENT DATA
FROM THE SSPA INLINE COMBINED MOTION TESTS OF THE ROUGHENED CYLINDER

Compilation and Correlation of data from Periodic motion tests, LF (Periodic + Steady Tow) tests, HF (combined high and low frequency periodic) tests, and "Starting" test. Bars are indicative of the maximum I-T contribution.

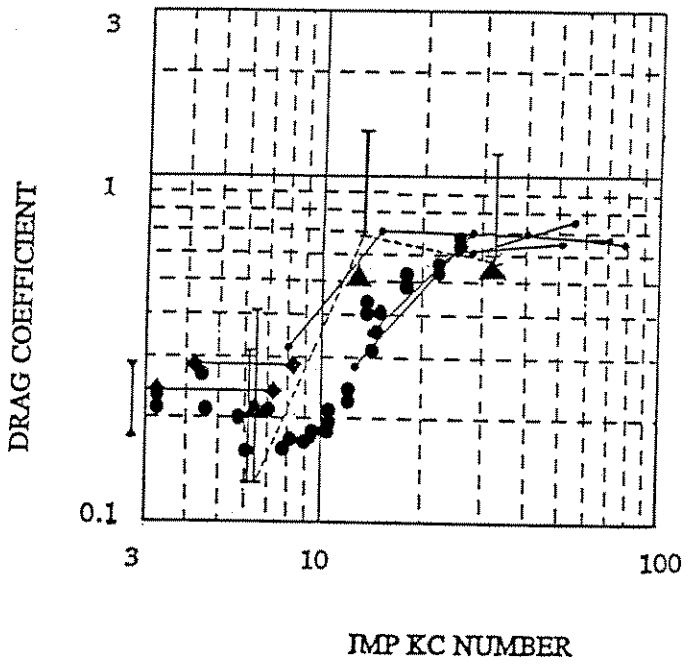

FIGURE 6.2
COMPILATION OF DRAG COEFFICIENT DATA
FROM THE SSPA INLINE COMBINED MOTION TESTS OF THE SMOOTH CYLINDER

Compilation and Correlation of data from Periodic motion tests, LF (Periodic + Steady Tow) tests, HF (combined high and low frequency periodic) tests, and "Starting" test. Bars are indicative of the maximum I-T contribution.

The differential shifts between the smooth and the rough patterns are attributable to: (1) earlier separation for the rough tests (the 2 unit KC Number shift) and (2) the "apparent surface" force for the drag coefficient shift. This "apparent surface" force, as discussed earlier, is due to the flow separation on each of the small frustum elements on the rough test cylinder. The cumulative effect, of the high drag coefficient forces on each frustum, is an apparent shear force tangent to the roughened test cylinder's surface.

I-T CONTRIBUTION

To the above pattern any I-T contribution must be added. The time series view presented in this study, Figures 2.9 and 2.10, is that the I-T Effect occurs as a periodic series of impulses which mathematically could be represented as the combination of a negative cosine term and a constant term, both of equal amplitude. The I-T Effect drag coefficient contribution reported in this study is the total impulse amplitude which is clearly twice the periodic amplitude.

For some test conditions the I-T Effect adds a negligible contribution. For test conditions which reinforce the transverse force, the I-T can become quite large. For smooth cylinders its maximum contribution, which occurs in the mid KC range, is 0.8 ± 0.15 and it decreases to 0.5 ± 0.15 in the high KC range. The corresponding I-T contributions for rough cylinders are 1.4 ± 0.2 and 0.8 ± 0.2 .

The periodic I-T pattern is consistent with the vorticity transport model presented earlier. Moreover it is superior to the usual view of a high frequency periodic contribution, which is usually ignored or filtered, oscillating about a supposed average drag coefficient. Clearly, a conventional average drag coefficient is comprised of our base coefficient and half the I-T contribution. Because of the sensitivity of the I-T to test conditions, this conventional representation yields a multiplicity of average coefficient curves. One for each set of test conditions.

DAMPING COEFFICIENTS

Our work in this study has clarified the connection between the I-T and negative damping. An improved set of damping coefficients has been presented for both the smooth and rough tests. Because these coefficients are lower than those of previous studies of the SSPA data, some remarks on the implications of smaller damping coefficients are appropriate.

Recall, first that a characteristic of an oscillatory system is its Q-factor, which is inversely proportional to the

damping coefficient. This Q is a direct measure of the ring time of the system.

Second on the issue of dynamic loading. Consulting standard amplification factor plots, one finds that changing a damping coefficient by a factor of 3 for a system which was at 1/2 critical damping results in deflections which are over 3 times those predicted by a static analysis.

And on the bottom-line issue of fatigue life, Truestad et al *OMAE* 1987 have indicated reducing damping values from 0.02 to 0.01 resulted in a 5 to 10 fold reduction in fatigue life.

Finally as damping relates back to the combined motion problem and the appropriateness of the RV Morison equation, we should note that the more sophisticated simulation programs are based on the RV Morison equation and thus use it to account for damping effects. Rosenbusch & Gutierrez in their 1983 Shell SSPA Report questioned this practice by indicating: "...that in a number of tests combining high frequency motion with other flows to simulate structural motion. The damping predicted by the Morison equation was higher than that inferred from the measurements. For the smooth cylinder, over prediction greater than a factor of 10 is common...".

SUGGESTIONS

Figures 6.1 and 6.2 provided a simple and accurate portrayal of drag coefficients for inline combined motion situations. I feel it would be difficult to improve on this portrayal, other than with a careful statistical reexamination of the data. However, there are two important questions that have not achieved a similar state of clarity. These are RV vs IF descriptions and the treatment of combined non-inline motions.

The inadequacy of guidelines for using the RV (relative velocity) form of the Morison equation as opposed to the IF (independent flowfield) form has been demonstrated in HYDAMP-I. That previous study presented a promising criteria for establishing the needed guidelines. Clearly, further development of this promising approach is desirable.

The inadequacy of the guide lines for treating the real world flows, which are not simple unidirectional motions, has been pointed out by numerous authors. The IPM is capable of proving the insight to this problem, and the SSPA tests contain adequate data covering various levels of complexity. The treatment of the simple case of combining skewed steady and periodic motions would represent the desired starting point.

APPENDIX A

COMPARISON OF COMBINED MOTION FORCES MORISON PREDICTIONS AND SSPA EXPERIMENT

The data are presented in a "folded" format (successive cycles of data are superimposed using velocity as a basis for alignment). Similar plots including the velocity are presented in Appendix B. The experimental data is presented as individual data points so that in the folded format they provide a picture of both the pattern and it's variation. For each test condition it's experimental data band is repeated in each of the three frames comprising a column on the page.

Three different Morrison predictions are presented for each test condition. The folded format was used for the predictions which were based on the observed acceleration and velocity for the same number of cycles as the experimental data. The Morrison equation coefficients for each prediction are listed above the frame.

The Level I prediction uses the same pair of coefficients for all test conditions, i.e. (0.67 & 0.67) for smooth and (1.3 & 0.67) for rough. Level I predictions are presented in the bottom frame.

The Level II predictions use two pair of coefficients for each test condition. These coefficients are chosen as the best approximation to the observed force in the high and low velocity fractions of the flow cycle. The upper frame presents the "high velocity" prediction in which periodic and steady velocities are in the same direction. High velocity conditions are representative of the data in the upper half of the frame as noted in the accompanying illustrative figure where the lower half is not shown. The middle frame presents the "low velocity" prediction which is appropriate to the portion of the flow cycle in which the steady and periodic velocities are in opposition. All data plots with the exception of those in Appendix C are plotted so maximum forces appear in the upper half of the fame attendant with maximum velocities in the lower half. This has been achieved by flipping some of the data sets as noted by the + appended to the ID number for these data.

GUIDE TO DATA IN APPENDIX A

The accompanying Table serves as a guide to the test conditions, Run and ID numbers, and presentation pages. The quantities tabulated are: Page number in Appendix A, SSPA Run Numbers for smooth and rough cylinders, amplitude of the periodic motion in meters, frequency of the periodic motion, periodic motion Reynolds number and Keulegan-Carpenter number, the steady tow velocity in meters/second, and the ratio of the steady and periodic velocity amplitudes. The final item is a useful ID Number which is comprised of 4 numbers. The numbers are derived form the test condition parameters and are: (1) a rounded KC number, (2) a representation of the periodic Reynolds number, (3) the ratio of the high frequency motion amplitude to cylinder diameter, and (4) the ratio of steady to periodic velocity amplitudes. A prefix S or R distinguishes between smooth and rough data. The terminal " + " identifies data for which the steady tow velocity was in the positive direction.

Page	Run No. smooth/rough	A_o meters	f_o Hz	$Re/10^6$	KC	U_s m/s	U_s/U_o	ID Number
1	364/106	1.0	0.16	0.88	6.3	0.1	0.1	S/R- 6-88-0-0.1
2	365/107	2.0	0.08	0.88	12.6	0.1	0.1	S/R-12-88-0-0.1
3	366/108	5.0	0.032	0.88	31.4	0.1	0.1	S/R-31-88-0-0.1
4	367/109	10.0	0.016	0.88	63.0	0.1	0.1	S/R-63-88-0-0.1
5	368/117	1.0	0.16	0.88	6.3	0.5	0.5	S/R- 6-88-0-0.5+
6	370/115	2.0	0.08	0.88	12.6	0.5	0.5	S/R-12-88-0-0.5+
7	372/111	5.0	0.032	0.88	31.4	0.5	0.5	S/R-31-88-0-0.5+
8	373/116	0.5	0.16	0.44	3.1	0.5	1.0	S/R- 3-44-0-1.0
9	375/112	1.0	0.08	0.44	6.3	0.5	1.0	S/R- 6-44-0-1.0
10	376/129	2.0	0.04	0.44	12.6	0.5	1.0	S/R-12-44-0-1.0+
11	378/131	0.5	0.16	0.44	3.1	1.0	2.0	S/R- 3-44-0-2.0+
12	380/133	1.0	0.08	0.44	6.3	1.0	2.0	S/R- 6-44-0-2.0+

Smooth Cylinder Data, Cycles between Zero Crossings 9 & 27

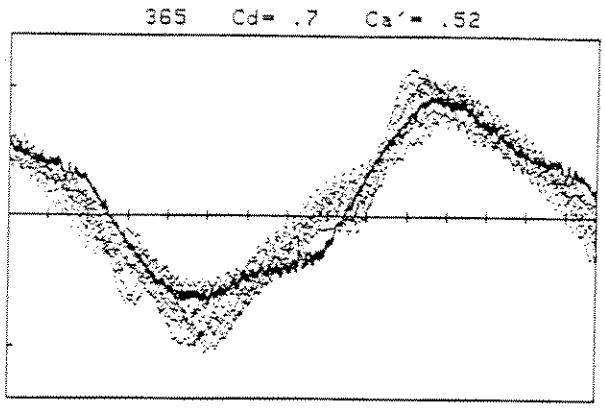

Rough Cylinder Data, Cycles between Zero Crossings 11 & 29

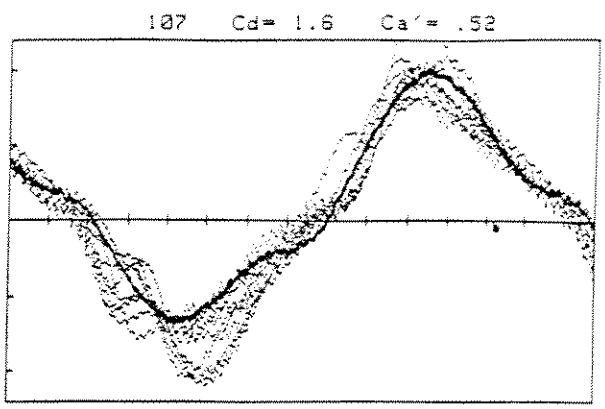

High Velocity Prediction (Upper Half)

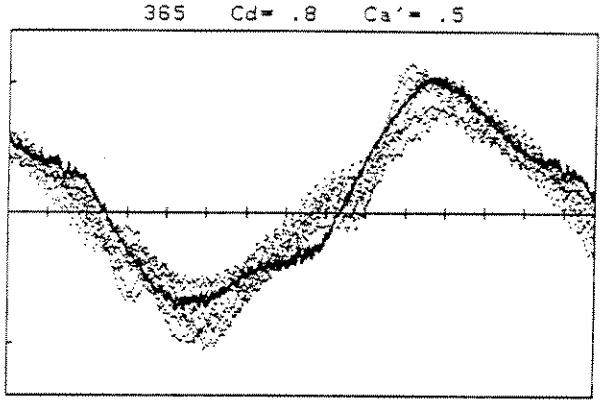

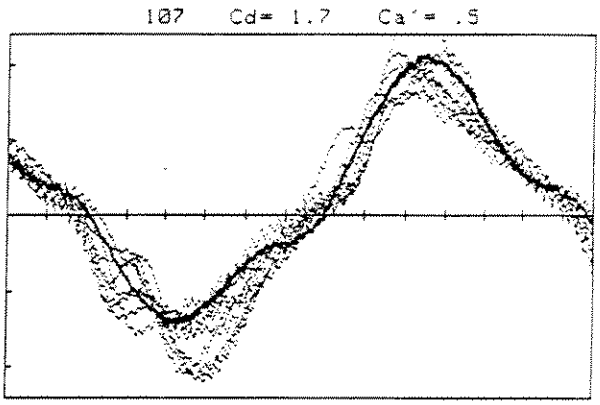

Low Velocity Prediction (Lower Half)

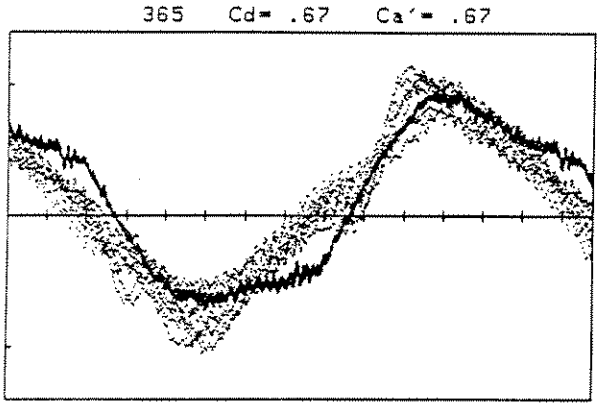

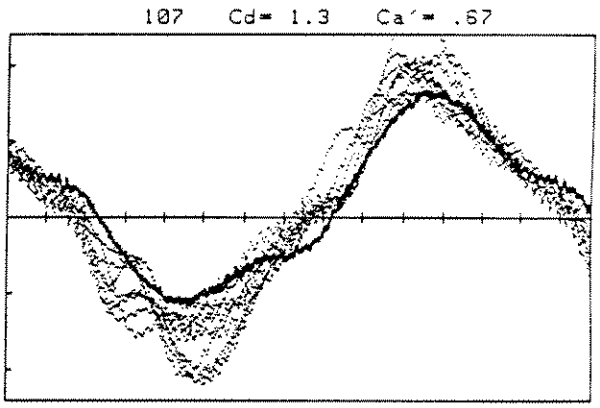

Level I Prediction

FOLDED TIME SERIES OF D-FORCE, COMPARISON OF OBSERVED & MORISON PREDICTION

LEVEL II Predictions on 1st & 2nd Pair, LEVEL I Predictions on 3rd Pair

DEFECT FORCE (500 N/div.), TIME (1 sec/div.)

Periodic Amplitude/Diameter..... 2

Velocity Ratio (steady/periodic)..... .1

Reynolds number/1,000,000..... .88

KC number (Periodic)..... 12.6

12-88-0-0.1

Smooth Cylinder Data, Cycles between Zero Crossings 6 & 16

Rough Cylinder Data, Cycles between Zero Crossings 6 & 16

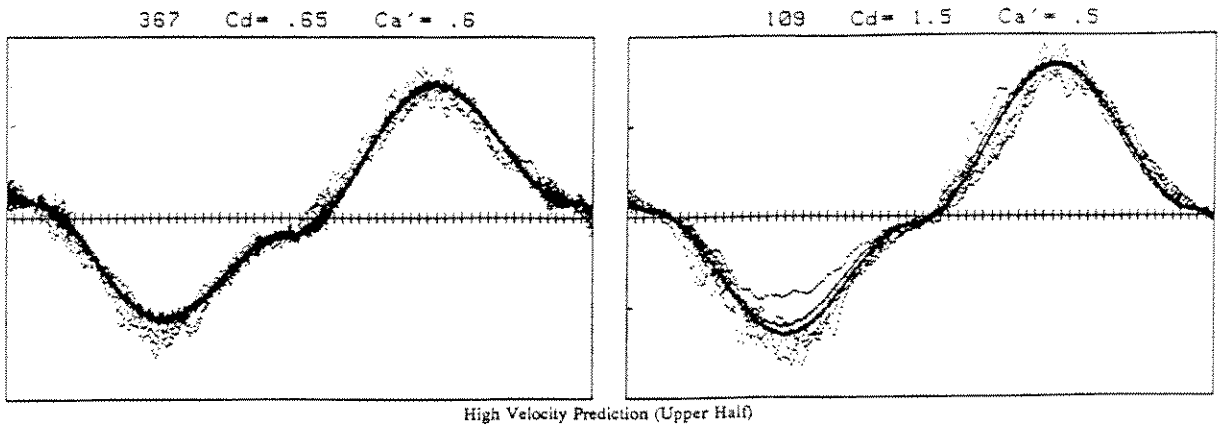

High Velocity Prediction (Upper Half)

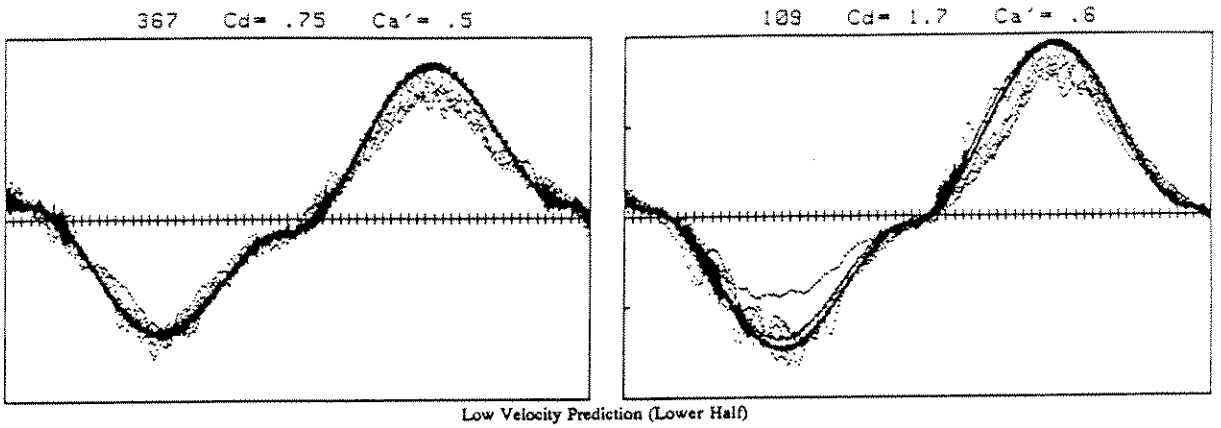

Low Velocity Prediction (Lower Half)

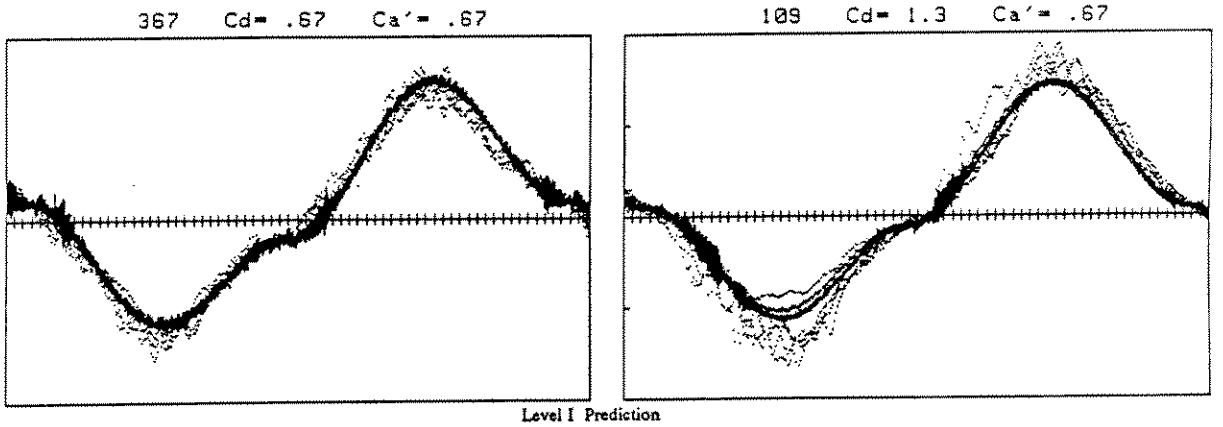

Level I Prediction

FOLDED TIME SERIES OF D-FORCE, COMPARISON OF OBSERVED & MORISON PREDICTION

LEVEL II Predictions on 1st & 2nd Pair, LEVEL I Predictions on 3rd Pair

DEFECT FORCE (500 N/div.), TIME (1 sec/div.)

Periodic Amplitude/Diameter..... 10

Velocity Ratio (steady/periodic)..... .1

Reynolds number/1,000,000..... .88

KC number (Periodic)..... 63

Smooth Cylinder Data, Cycles between Zero Crossings 7 & 21

Rough Cylinder Data, Cycles between Zero Crossings 9 & 23

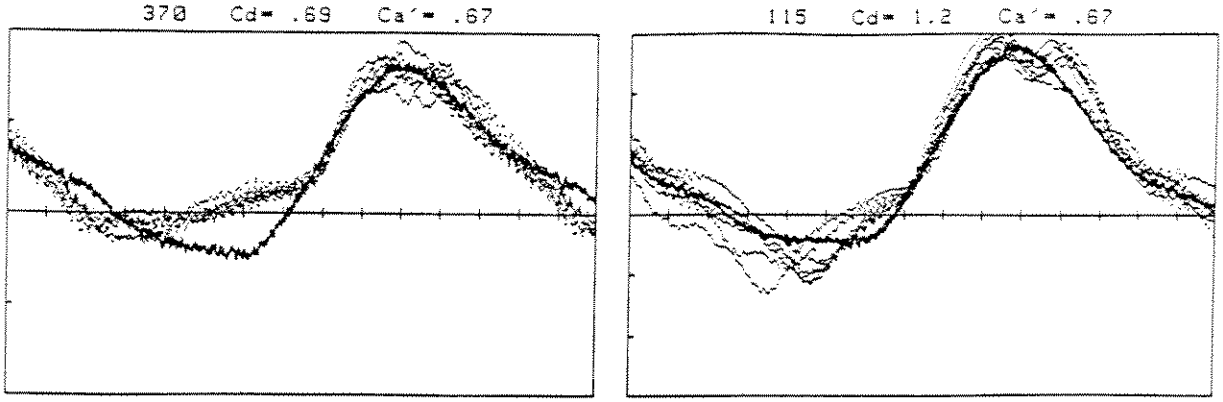

High Velocity Prediction (Upper Half)

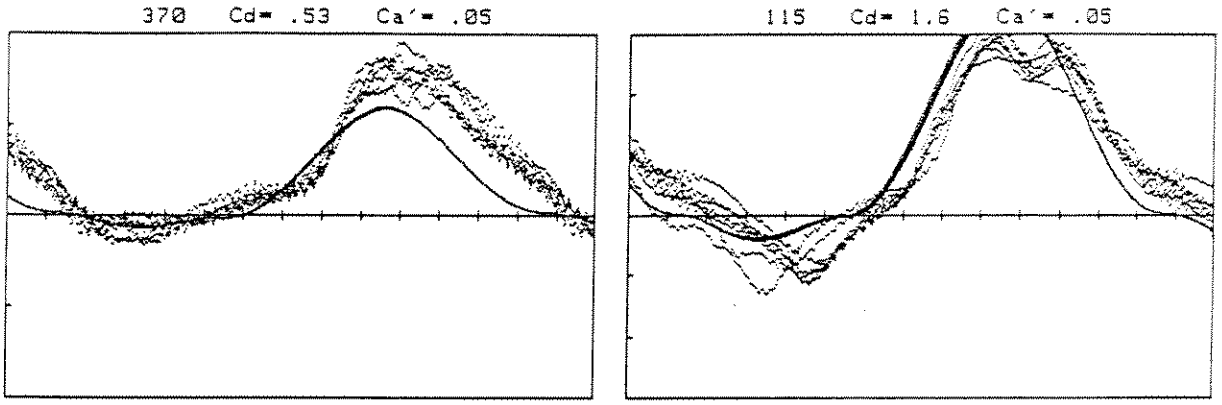

Low Velocity Prediction (Lower Half)

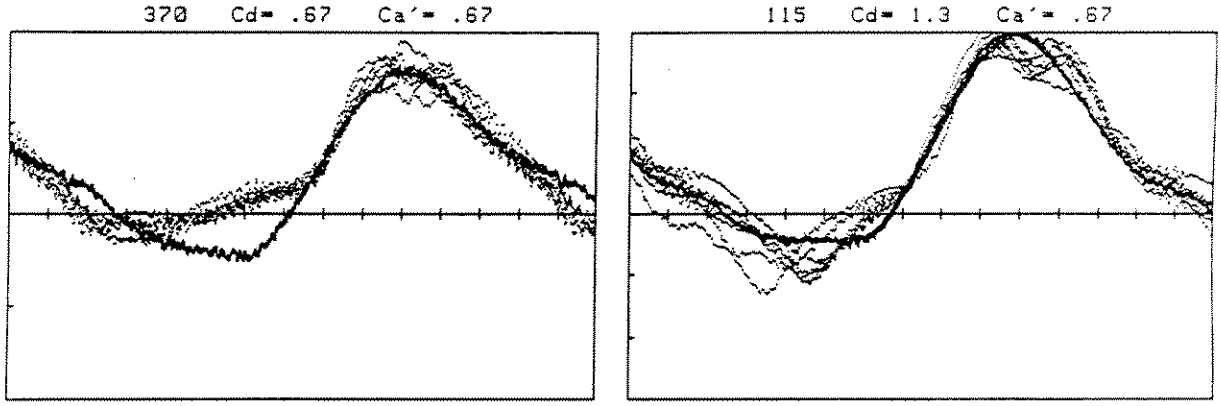

Level I Prediction

FOLDED TIME SERIES OF D-FORCE, COMPARISON OF OBSERVED & MORISON PREDICTION

LEVEL II Predictions on 1st & 2nd Pair, LEVEL I Predictions on 3rd Pair

DEFECT FORCE (500 N/div.), TIME (1 sec/div.)

Periodic Amplitude/Diameter..... 2

Velocity Ratio (steady/periodic)..... .5

Reynolds number/1,000,000..... .88

KC number (Periodic)..... 12.6

12-88-0-0.5+

Smooth Cylinder Data, Cycles between Zero Crossings 5 & 21

Rough Cylinder Data, Cycles between Zero Crossings 5 & 21

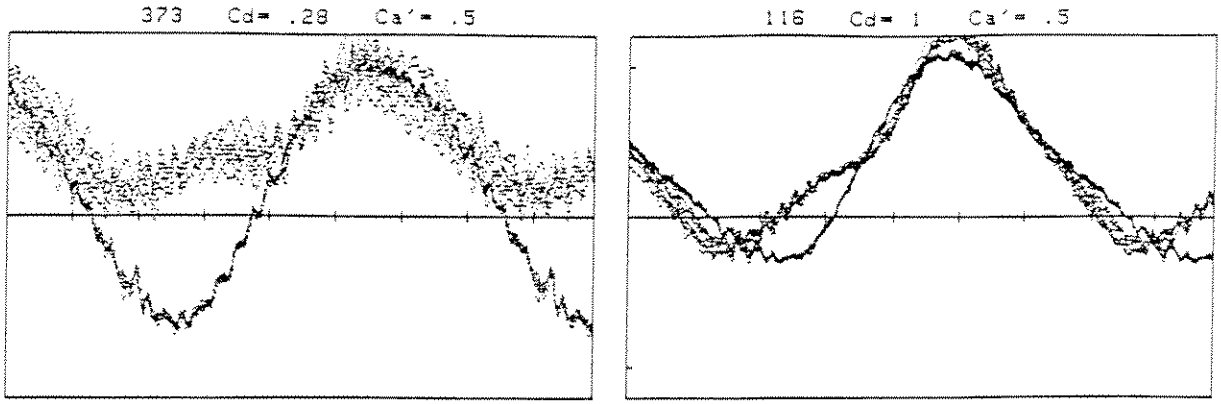

High Velocity Prediction (Upper Half)

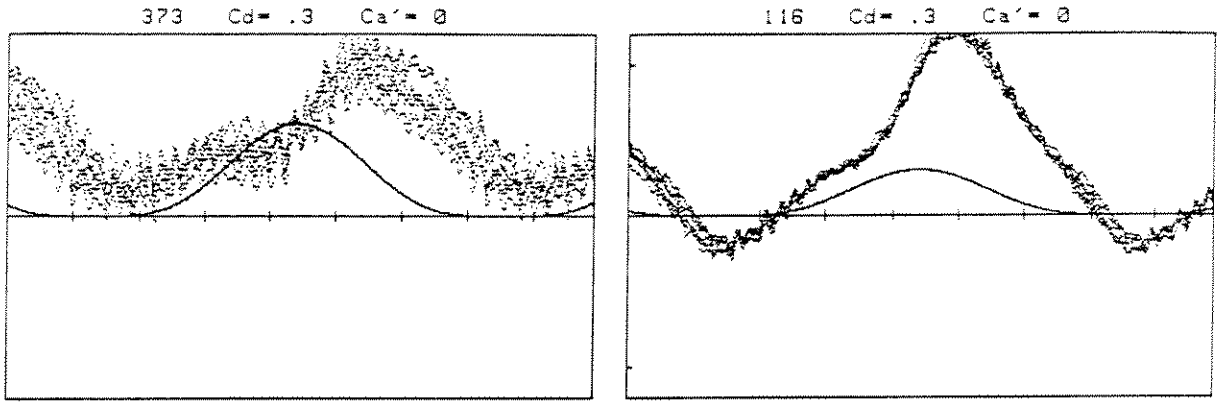

Low Velocity Prediction (Lower Half)

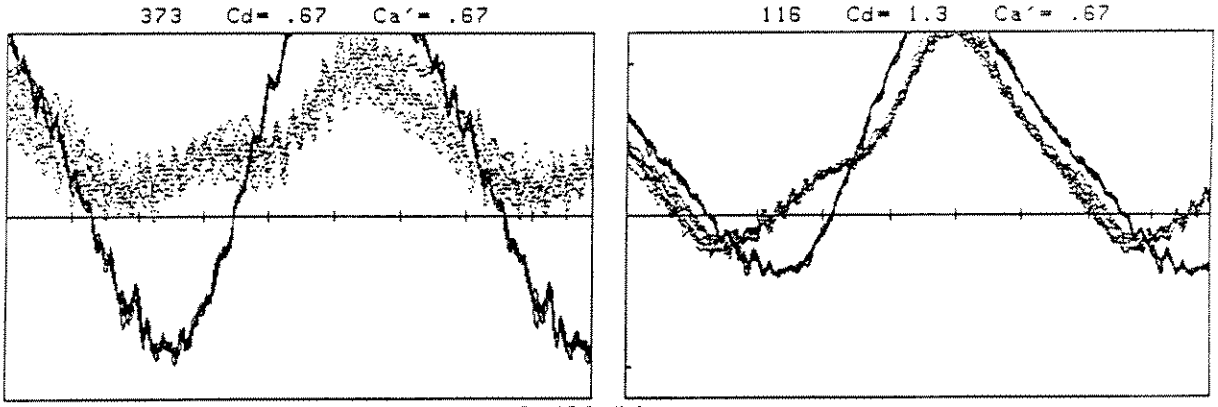

Level I Prediction

FOLDED TIME SERIES OF D-FORCE, COMPARISON OF OBSERVED & MORISON PREDICTION

LEVEL II Predictions on 1st & 2nd Pair, LEVEL I Predictions on 3rd Pair

DEFECT FORCE (500 N/div.), TIME (1 sec/div.)

Periodic Amplitude/Diameter..... .5

Velocity Ratio (steady/periodic)..... 1

Reynolds number/1,000,000..... .44

KC number (Periodic)..... 3.1

Smooth Cylinder Data, Cycles between Zero Crossings 5 & 9

Rough Cylinder Data, Cycles between Zero Crossings 5 & 9

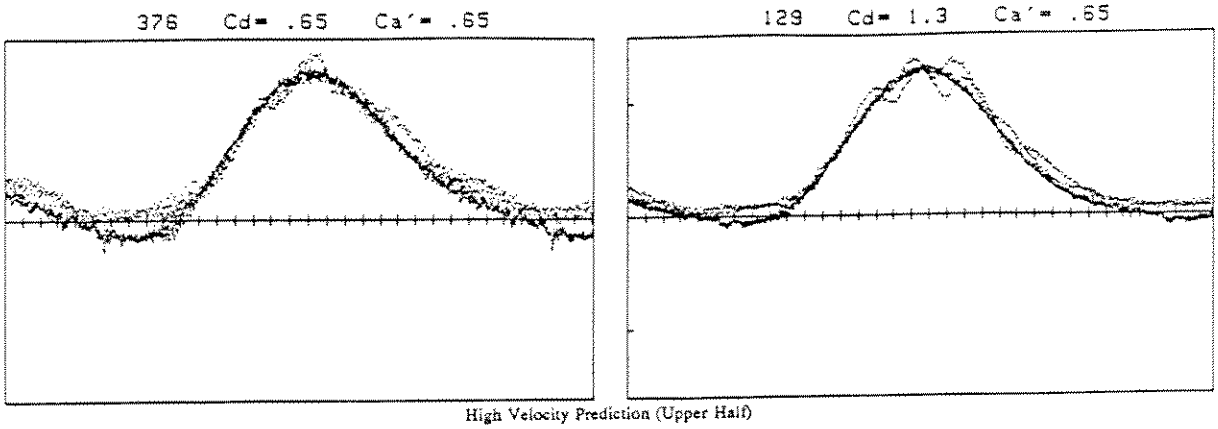

High Velocity Prediction (Upper Half)

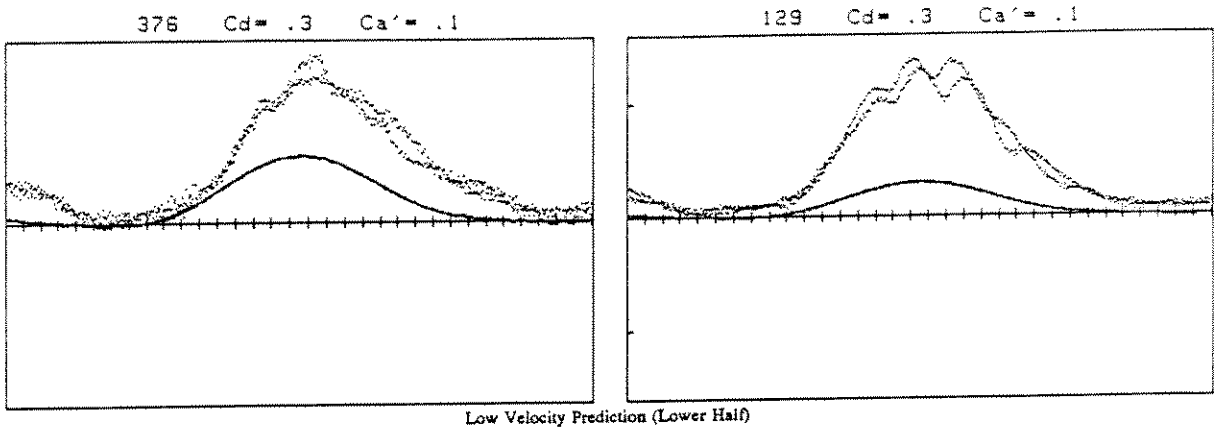

Low Velocity Prediction (Lower Half)

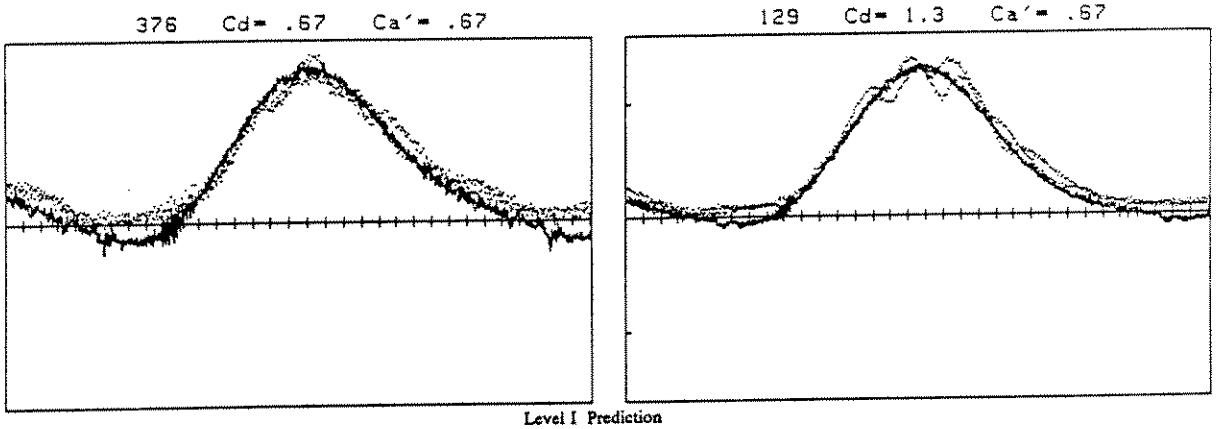

Level I Prediction

FOLDED TIME SERIES OF D-FORCE, COMPARISON OF OBSERVED & MORISON PREDICTION

LEVEL II Predictions on 1st & 2nd Pair, LEVEL I Predictions on 3rd Pair

DEFECT FORCE (500 N/div.), TIME (1 sec/div.)

Periodic Amplitude/Diameter..... 2

Velocity Ratio (steady/periodic)..... 1

Reynolds number/1,000,000..... .44

KC number (Periodic)..... 12.6

12-44-0-1.0+

Smooth Cylinder Data, Cycles between Zero Crossings 3 & 11

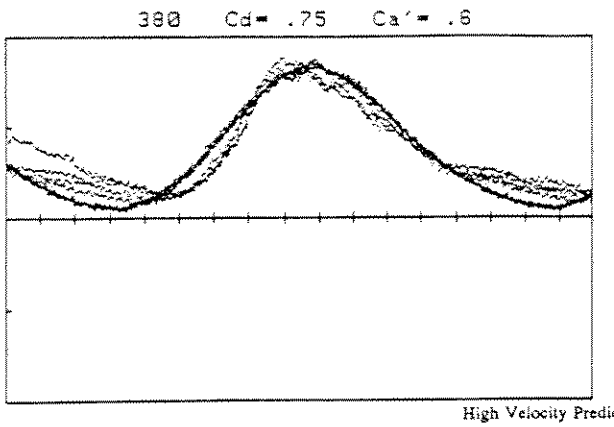

Rough Cylinder Data, Cycles between Zero Crossings 3 & 11

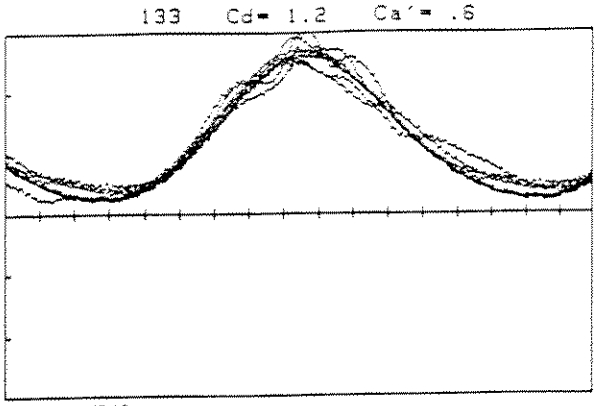

High Velocity Prediction (Upper Half)

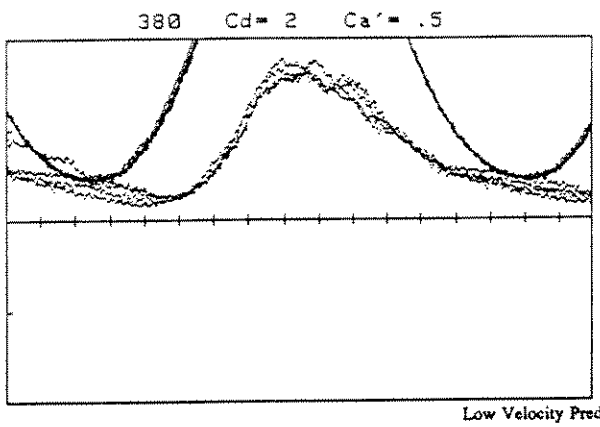

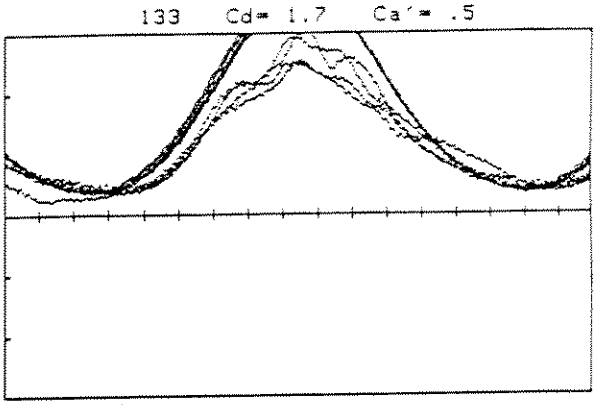

Low Velocity Prediction (Lower Half)

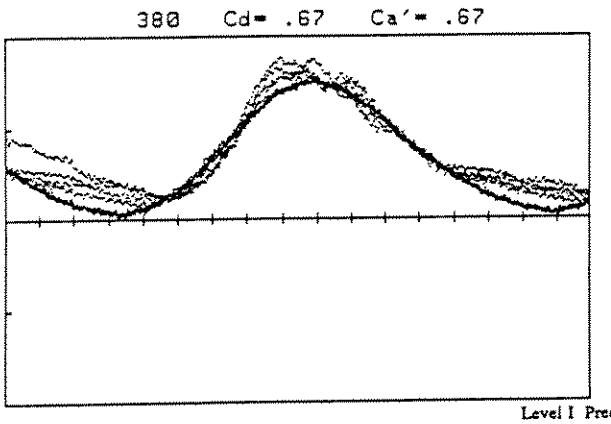

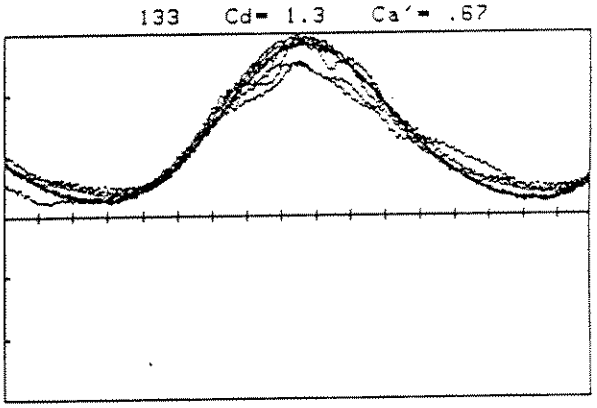

Level I Prediction

FOLDED TIME SERIES OF D-FORCE, COMPARISON OF OBSERVED & MORISON PREDICTION

LEVEL II Predictions on 1st & 2nd Pair, LEVEL I Predictions on 3rd Pair

DEFECT FORCE (500 N/div.), TIME (1 sec/div.)

Periodic Amplitude/Diameter..... 1

Velocity Ratio (steady/periodic)..... 2

Reynolds number/1,000,000..... .44

KC number (Periodic)..... 6.3

6-44-0-2.0+

APPENDIX B

PRESENTATION OF ALL LF DATA IN A FOLDED FORMAT
(Low Frequency periodic + steady tow)

GUIDE TO THE LF DATA PLOTS

The Table below lists page location and test parameters for all LF Runs. These have been organized so smooth and rough cylinder data can be compared on the same page. When comparable test conditions (test parameters are identical but steady tow velocities are opposite) are available they are presented on opposing pages with the data flipped so the dominant velocity is in the negative direction on all plots. Runs which have been flipped are noted by a + appended to the ID Number.

The folded format is achieved by superimposing successive cycles using the velocity for alignment. The folded velocity pattern is presented on each of the frames.

The four frames for each Run present the D-Force and 3 IPM Quantities: Theta-min (minimum pressure location of the cylinder surface), the Inline Force Coefficient, and the Transverse Force Coefficient.

The D-Force (Defect Force) is the difference between the observed inline hydrodynamic force and the ideal hydrodynamic inertial force on the 1 meter length of the test cylinder.

The coordinate for Theta-min runs from 0°to 180° with the time axis at 90°. On the time axis the interval is 1 second/division.

In the Table the quantities are: Page number in Appendix B, SSPA Run Numbers for smooth and rough cylinders, amplitude of the periodic motion in meters, frequency of the periodic motion, periodic motion Reynolds number and Keulegan-Carpenter number, the steady tow velocity in meters/second, and the ratio of the steady and periodic velocity amplitudes.

The final item is an ID Number which is comprised of 4 numbers. The numbers are derived from the test condition parameters and are: (1) a rounded KC number, (2) a representation of the periodic Reynolds number, (3) the ratio of the high frequency motion amplitude to cylinder diameter, and (4) the ratio of steady to periodic velocity amplitudes. A prefix S or R distinguishes between smooth and rough data. The terminal + identifies data for which the steady tow velocity was in the positive direction.

Page	Run No. smooth/rough	A_o meters	f_o Hz	$Re/10^6$	KC	U_s m/s	U_s/U_o	ID Number
1	364/106	1.0	0.16	0.88	6.3	0.1	0.1	S/R- 6-88-0-0.1
2	365/107	2.0	0.08	0.88	12.6	0.1	0.1	S/R-12-88-0-0.1
3	366/108	5.0	0.032	0.88	31.4	0.1	0.1	S/R-31-88-0-0.1
4	367/109	10.0	0.016	0.88	63.0	0.1	0.1	S/R-63-88-0-0.1
5	368/117	1.0	0.16	0.88	6.3	0.5	0.5	S/R- 6-88-0-0.5+
6	369/114	2.0	0.08	0.88	12.6	0.5	0.5	S/R-12-88-0-0.5
7	370/115	2.0	0.08	0.88	12.6	0.5	0.5	S/R-12-88-0-0.5+
8	371/110	5.0	0.032	0.88	31.4	0.5	0.5	S/R-31-88-0-0.5
9	372/111	5.0	0.032	0.88	31.4	0.5	0.5	S/R-31-88-0-0.5+
10	373/116	0.5	0.16	0.44	3.1	0.5	1.0	S/R- 3-44-0-1.0
11	374/113	1.0	0.08	0.44	6.3	0.5	1.0	S/R- 6-44-0-1.0+
12	375/112	1.0	0.08	0.44	6.3	0.5	1.0	S/R- 6-44-0-1.0
13	376/129	2.0	0.04	0.44	12.6	0.5	1.0	S/R-12-44-0-1.0+
14	377/128	2.0	0.04	0.44	12.6	0.5	1.0	S/R-12-44-0-1.0
15	378/131	0.5	0.16	0.44	3.1	1.0	2.0	S/R- 3-44-0-2.0+
16	379/130	0.5	0.16	0.44	3.1	1.0	2.0	S/R- 3-44-0-2.0
17	380/133	1.0	0.08	0.44	6.3	1.0	2.0	S/R- 6-44-0-2.0+
18	381/132	1.0	0.08	0.44	6.3	1.0	2.0	S/R- 6-44-0-2.0

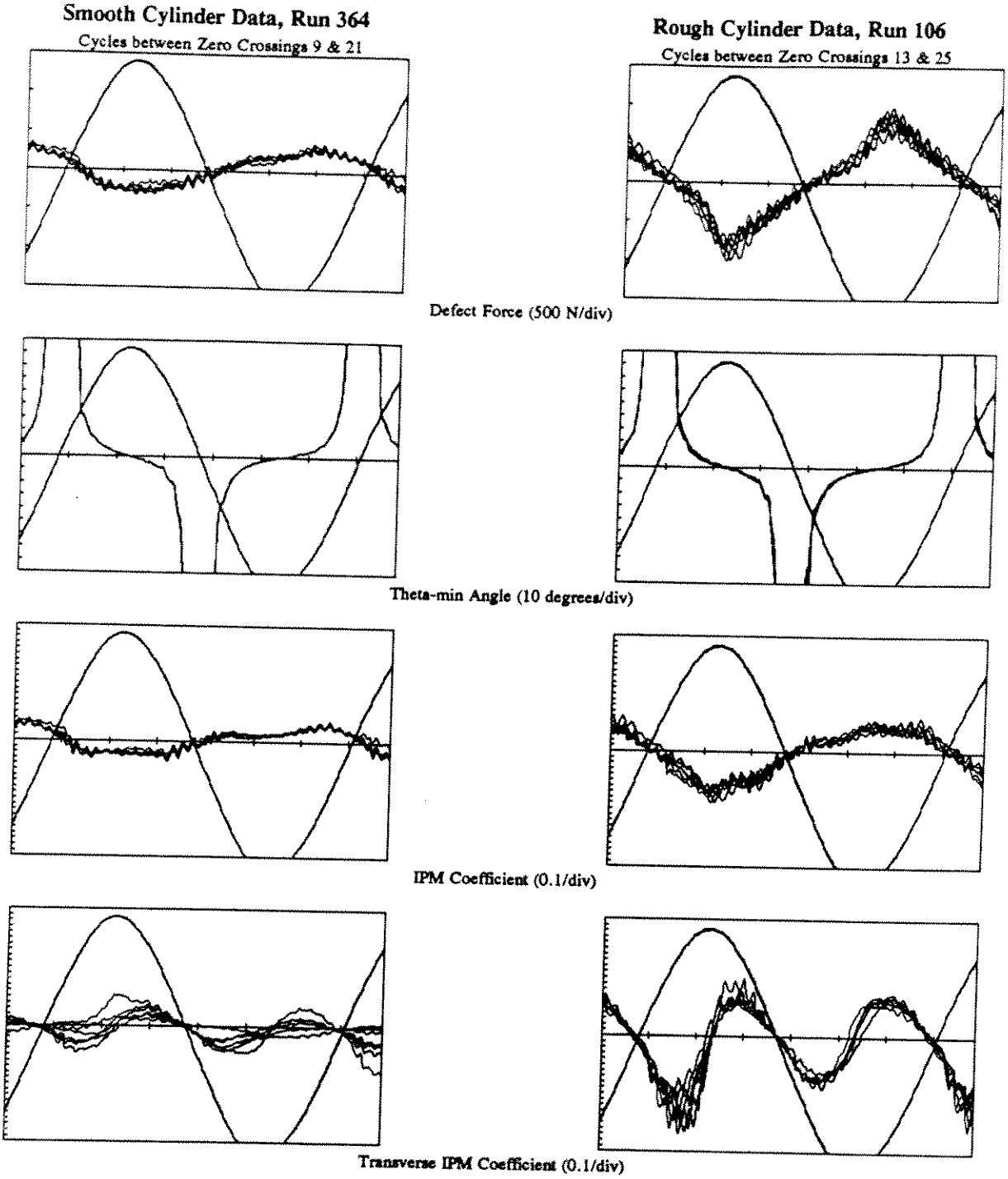

FOLDED TIME SERIES PLOTS OF D-FORCE, THETA-MIN, & IPM COEFFICIENTS WITH VELOCITY SHOWN ON EACH PLOT

Periodic Amplitude (meters)	1
Frequency (Hz)	.16
Steady Velocity (m/sec)	.1
Velocity Ratio (steady/periodic)	.1
Reynolds number/1,000,000	.88
KC number	6.3

6-88-0-0.1

Smooth Cylinder Data, Run 365

Cycles between Zero Crossings 9 & 27

Rough Cylinder Data, Run 107

Cycles between Zero Crossings 11 & 29

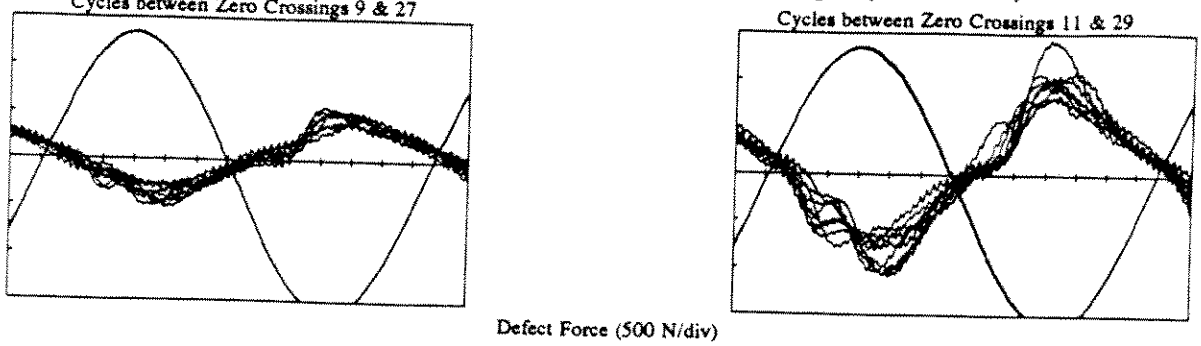

Defect Force (500 N/div)

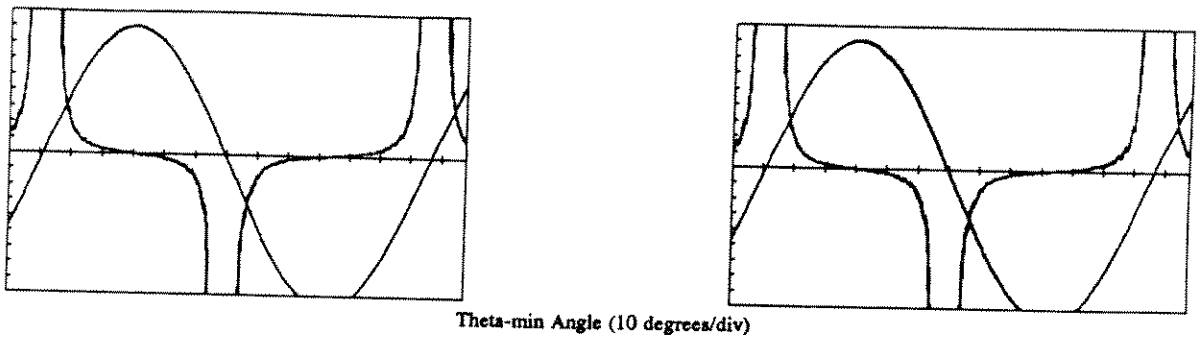

Theta-min Angle (10 degrees/div)

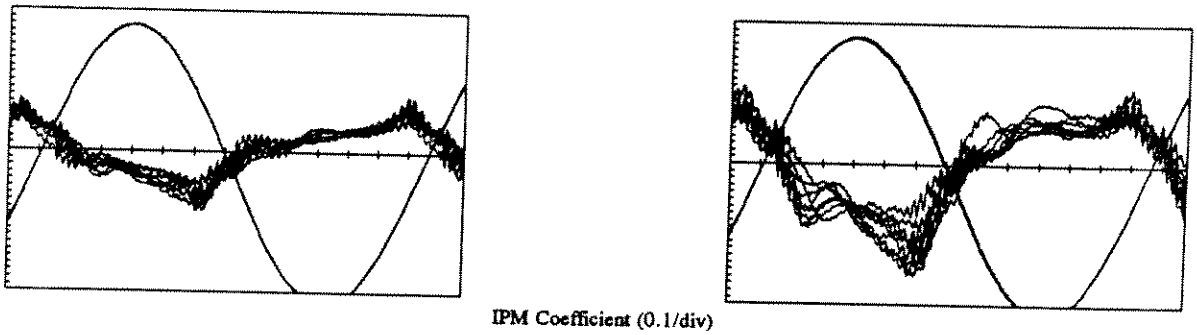

IPM Coefficient (0.1/div)

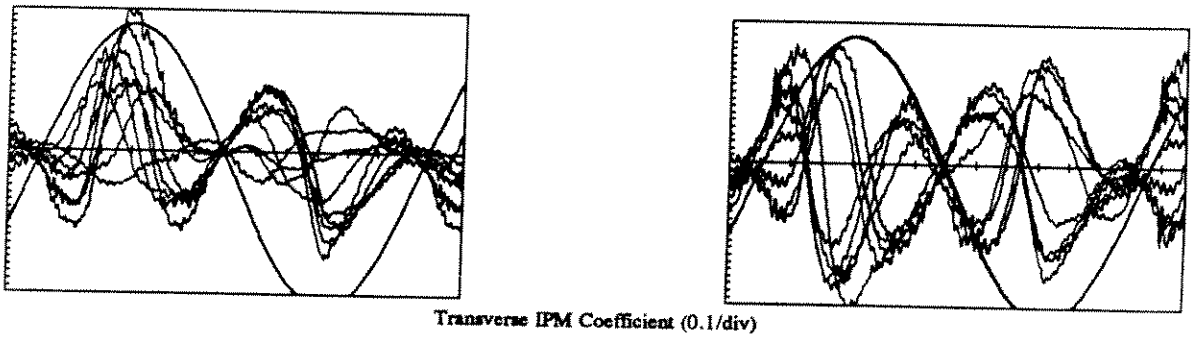

Transverse IPM Coefficient (0.1/div)

FOLDED TIME SERIES PLOTS OF D-FORCE, THETA-MIN, & IPM COEFFICIENTS WITH VELOCITY SHOWN ON EACH PLOT

Periodic Amplitude (meters)..... 2
Frequency (Hz)..... .08
Steady Velocity (m/sec)..... .1
Velocity Ratio (steady/periodic)..... .1
Reynolds number/1,000,000..... .88
KC number..... 12.6

12-88-0-0.1

Smooth Cylinder Data, Run 366

Cycles between Zero Crossings 9 & 27

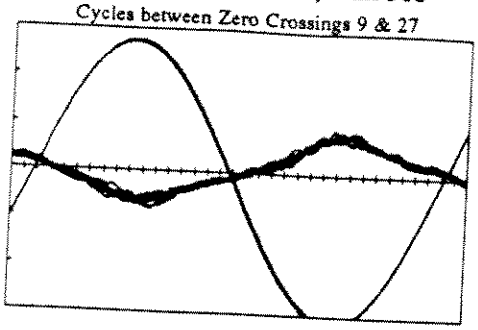

Rough Cylinder Data, Run 108

Cycles between Zero Crossings 9 & 27

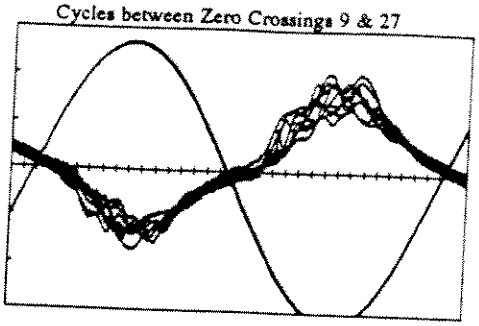

Defect Force (500 N/div)

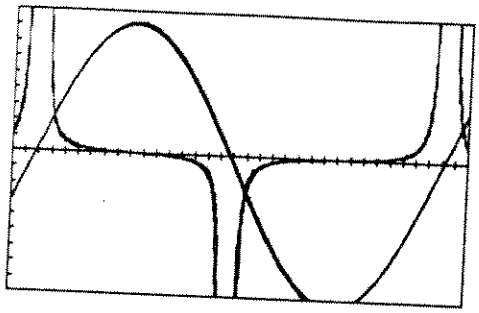

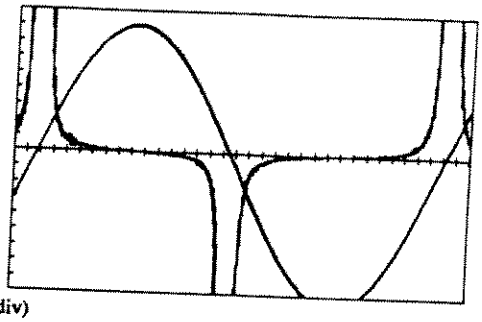

Theta-min Angle (10 degrees/div)

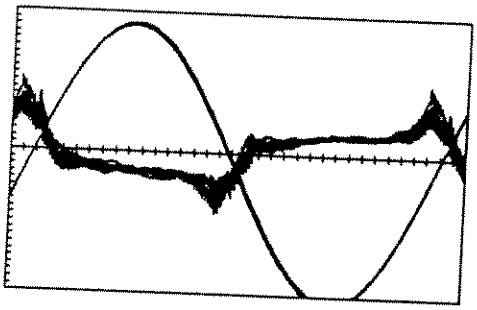

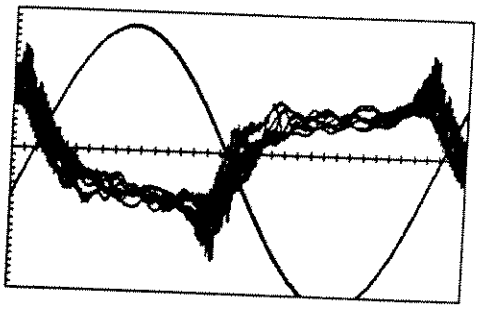

IPM Coefficient (0.1/div)

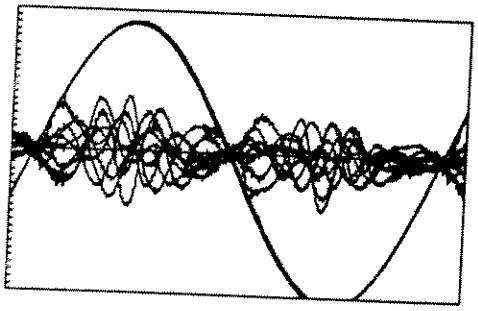

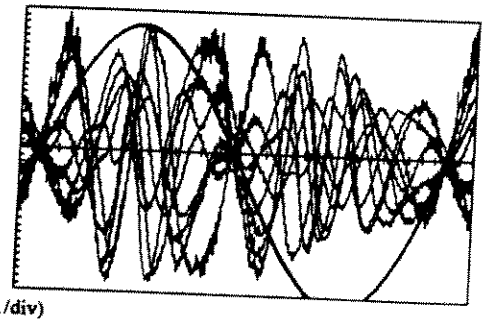

Transverse IPM Coefficient (0.1/div)

FOLDED TIME SERIES PLOTS OF D-FORCE, THETA-MIN, & IPM COEFFICIENTS WITH VELOCITY SHOWN ON EACH PLOT

Periodic Amplitude (meters)..... 5
Frequency (Hz)..... .032
Steady Velocity (m/sec)..... .1
Velocity Ratio (steady/periodic)..... .1
Reynolds number/1,000,000..... .88
KC number..... 31.4

Smooth Cylinder Data, Run 367

Cycles between Zero Crossings 6 & 16

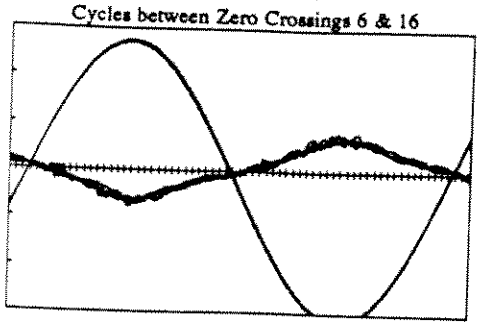

Rough Cylinder Data, Run 109

Cycles between Zero Crossings 6 & 16

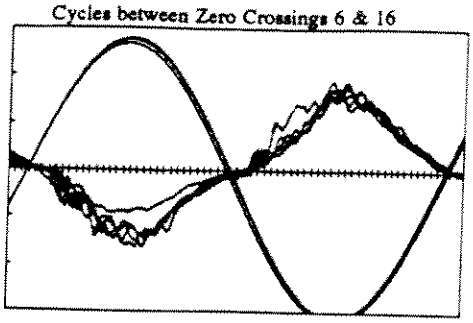

Defect Force (500 N/div)

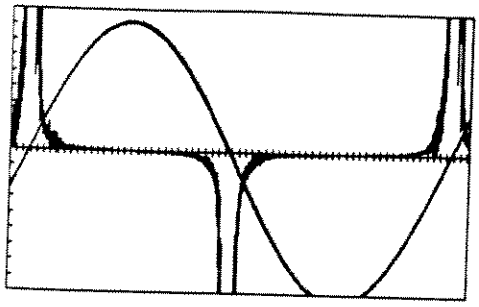

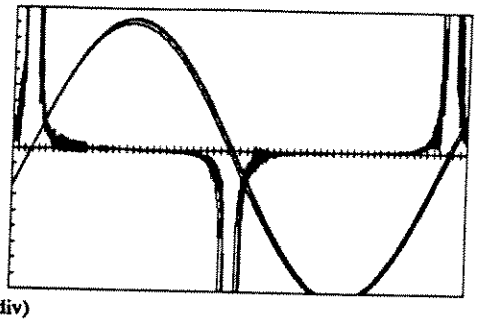

Theta-min Angle (10 degrees/div)

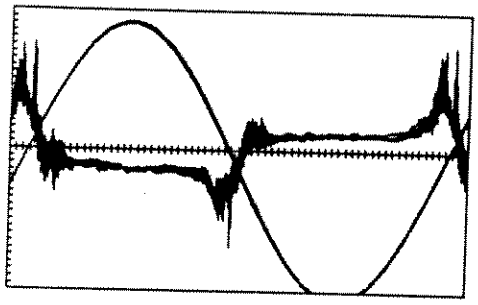

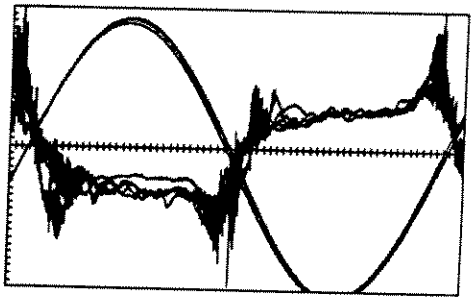

IPM Coefficient (0.1/div)

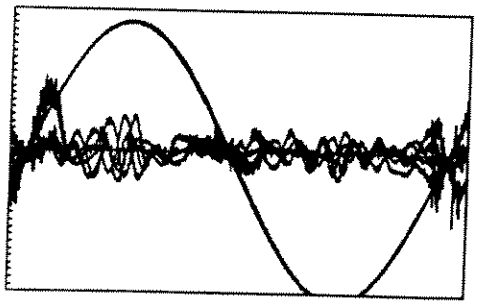

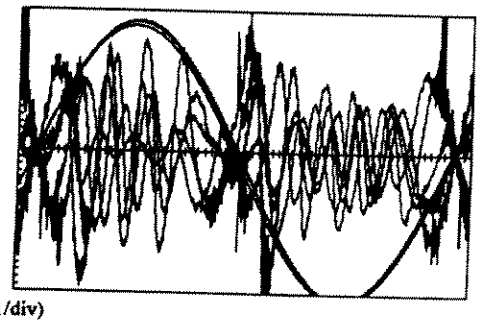

Transverse IPM Coefficient (0.1/div)

FOLDED TIME SERIES PLOTS OF D-FORCE, THETA-MIN, & IPM COEFFICIENTS WITH VELOCITY SHOWN ON EACH PLOT

Periodic Amplitude (meters)..... 10
Frequency (Hz)..... .016
Steady Velocity (m/sec)..... .1
Velocity Ratio (steady/periodic)..... .1
Reynolds number/1,000,000..... .88
KC number..... 63

63-88-0-0.1

Smooth Cylinder Data, Run 368

Cycles between Zero Crossings 9 & 33

Rough Cylinder Data, Run 117

Cycles between Zero Crossings 9 & 39

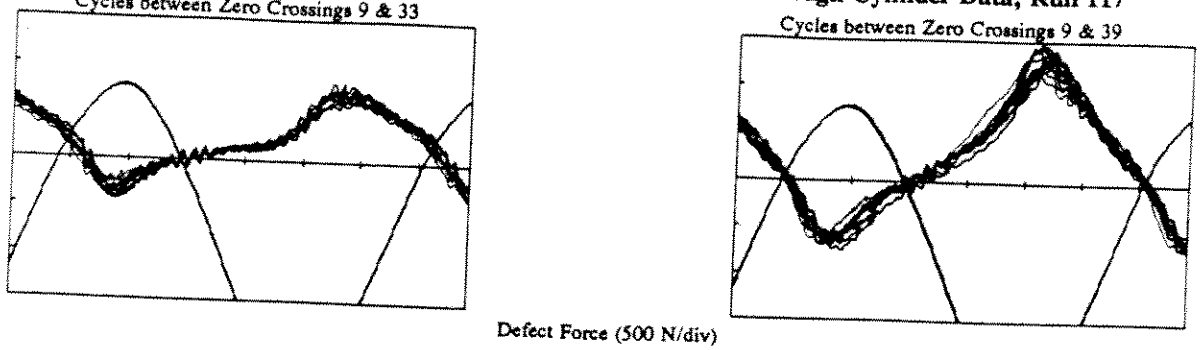

Defect Force (500 N/div)

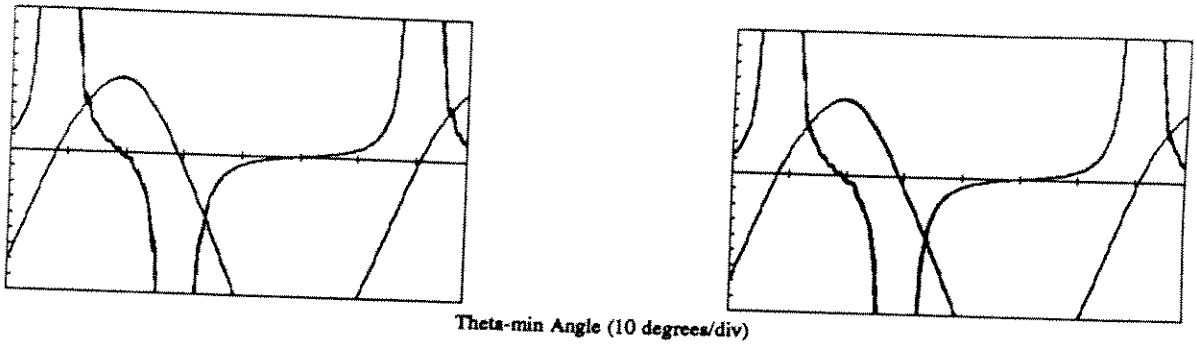

Theta-min Angle (10 degrees/div)

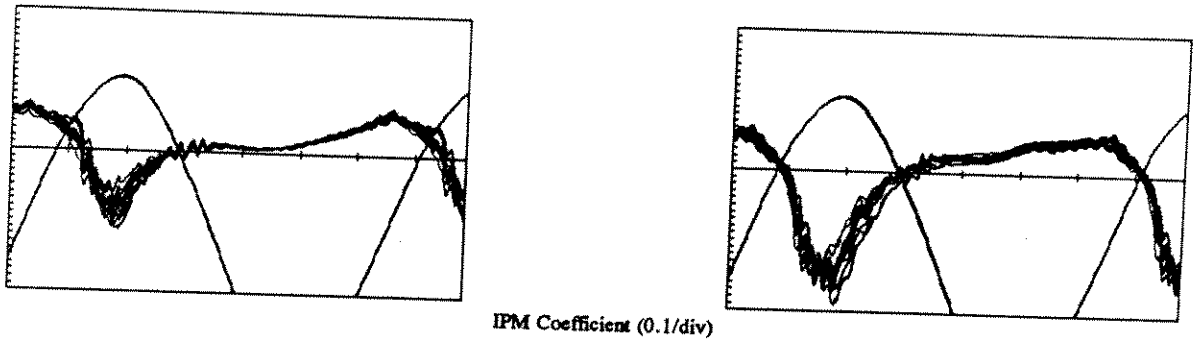

IPM Coefficient (0.1/div)

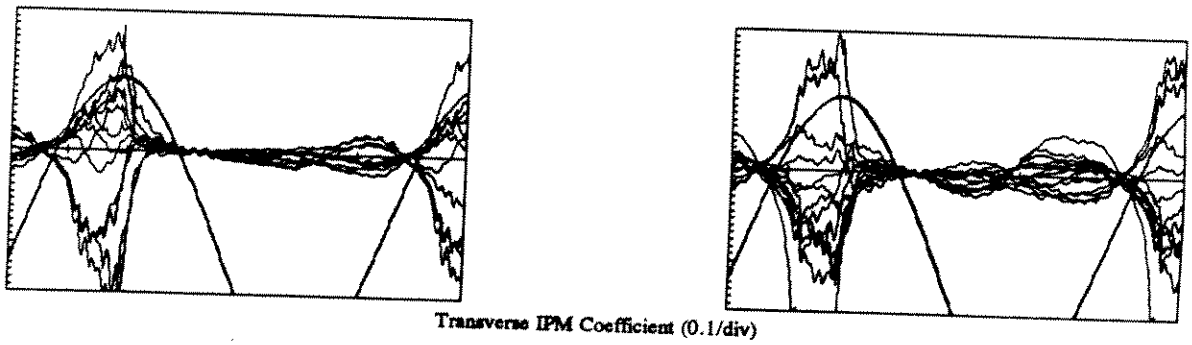

Transverse IPM Coefficient (0.1/div)

FOLDED TIME SERIES PLOTS OF D-FORCE, THETA-MIN, & IPM COEFFICIENTS WITH VELOCITY SHOWN ON EACH PLOT

Periodic Amplitude (meters)..... 1
Frequency (Hz)..... .16
Steady Velocity (m/sec)..... .5
Velocity Ratio (steady/periodic)..... .5
Reynolds number/1,000,000..... .88
KC number..... 6.3

6-88-0-0.5

Smooth Cylinder Data, Run 369

Cycles between Zero Crossings 4 & 20

Rough Cylinder Data, Run 114

Cycles between Zero Crossings 5 & 19

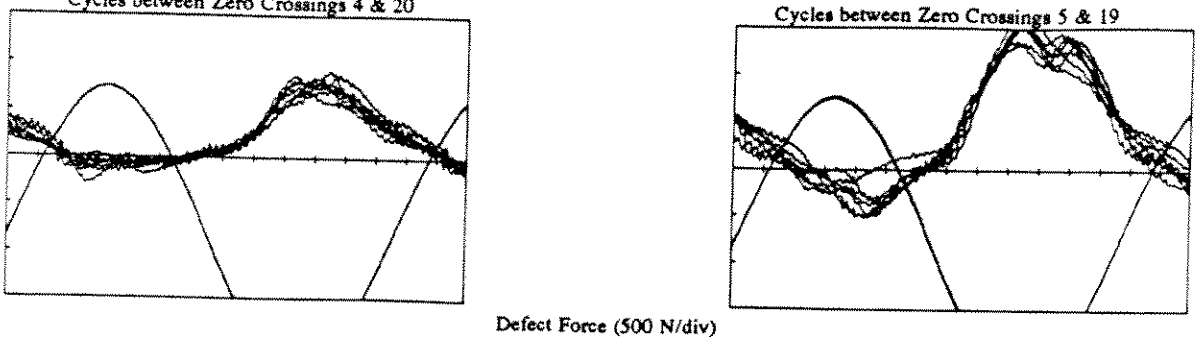

Defect Force (500 N/div)

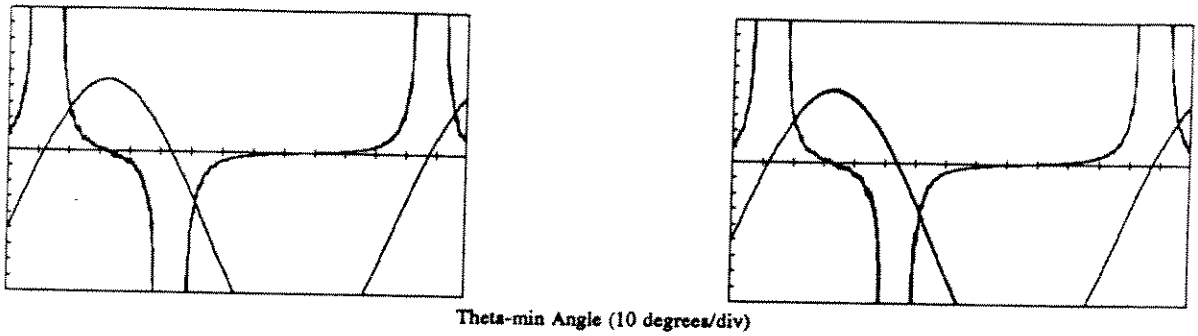

Theta-min Angle (10 degrees/div)

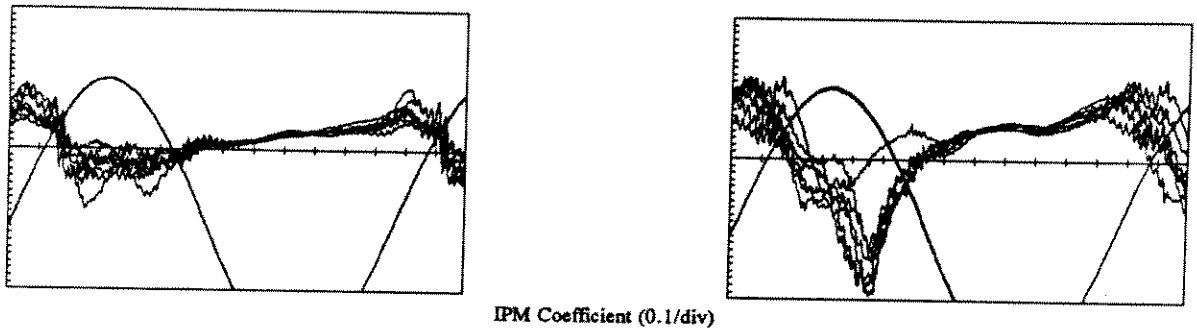

IPM Coefficient (0.1/div)

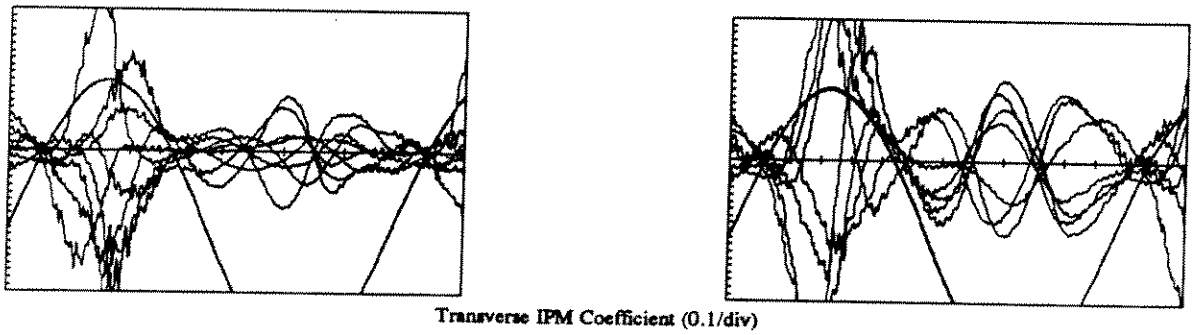

Transverse IPM Coefficient (0.1/div)

FOLDED TIME SERIES PLOTS OF D-FORCE, THETA-MIN, & IPM COEFFICIENTS WITH VELOCITY SHOWN ON EACH PLOT

Periodic Amplitude (meters)..... 2

Frequency (Hz)..... .08

Steady Velocity (m/sec)..... .5

Velocity Ratio (steady/periodic)..... .5

Reynolds number/1,000,000..... .88

KC number..... 12.6

12-88-0-0.5

Smooth Cylinder Data, Run 370

Cycles between Zero Crossings 7 & 21

Rough Cylinder Data, Run 115

Cycles between Zero Crossings 9 & 23

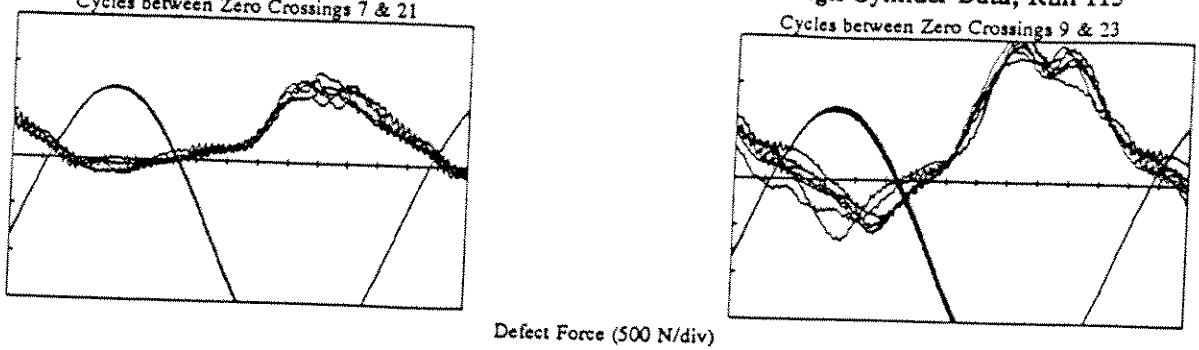

Defect Force (500 N/div)

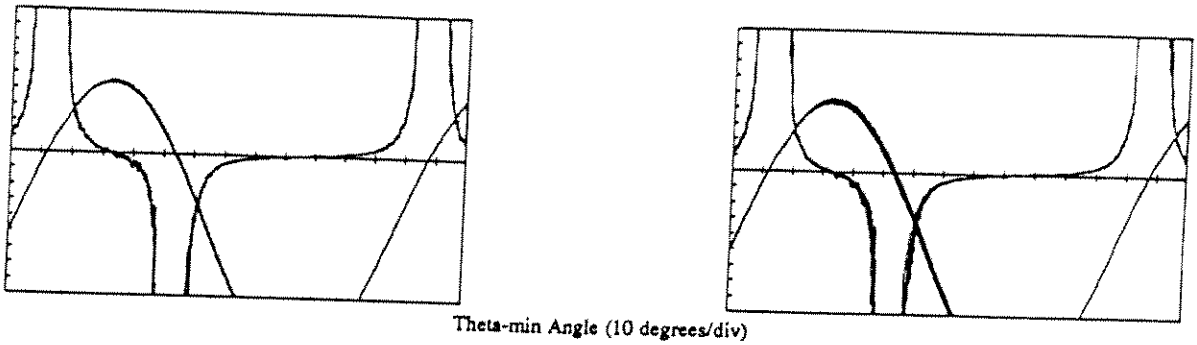

Theta-min Angle (10 degrees/div)

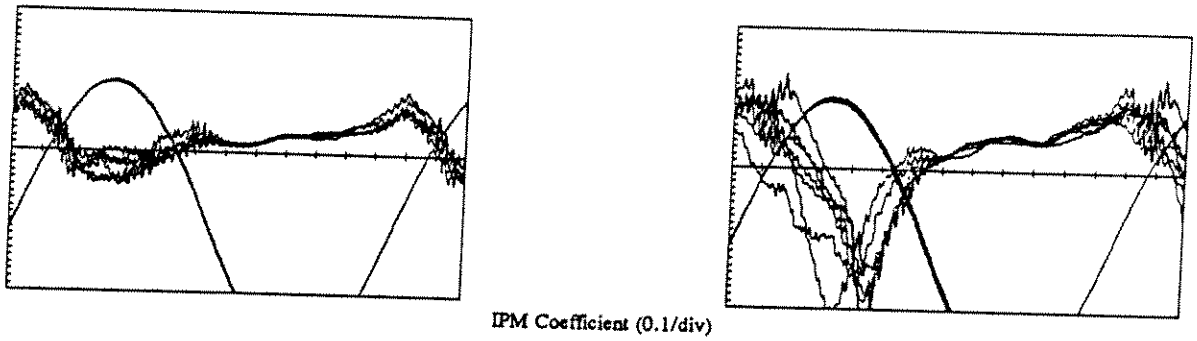

IPM Coefficient (0.1/div)

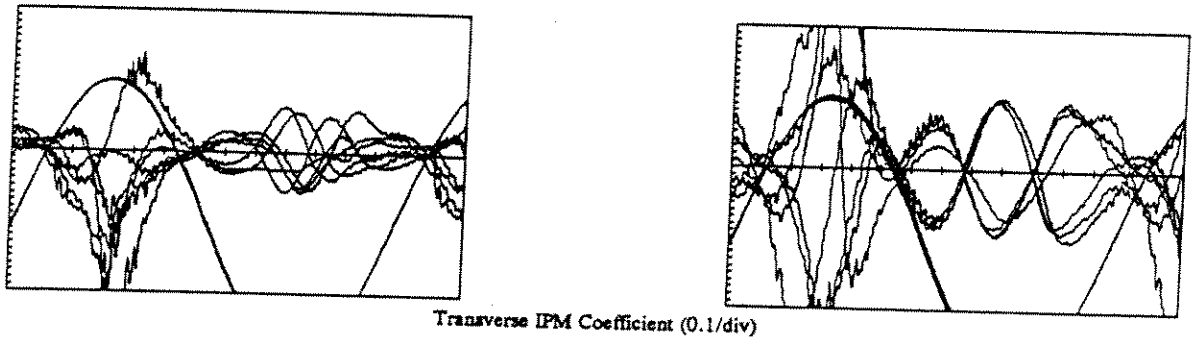

Transverse IPM Coefficient (0.1/div)

FOLDED TIME SERIES PLOTS OF D-FORCE, THETA-MIN, & IPM COEFFICIENTS WITH VELOCITY SHOWN ON EACH PLOT

Periodic Amplitude (meters)..... 2
Frequency (Hz)..... .08
Steady Velocity (m/sec)..... .5
Velocity Ratio (steady/periodic)..... .5
Reynolds number/1,000,000..... .88
KC number..... 12.6

12-88-0-0.5+

Smooth Cylinder Data, Run 371

Cycles between Zero Crossings 3 & 7

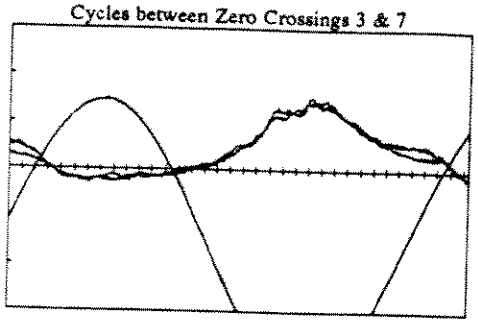

Rough Cylinder Data, Run 110

Cycles between Zero Crossings 3 & 7

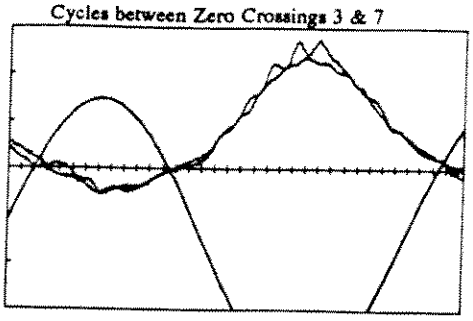

Defect Force (500 N/div)

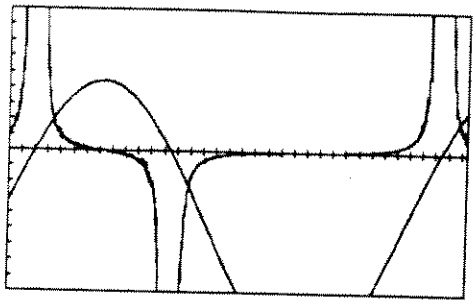

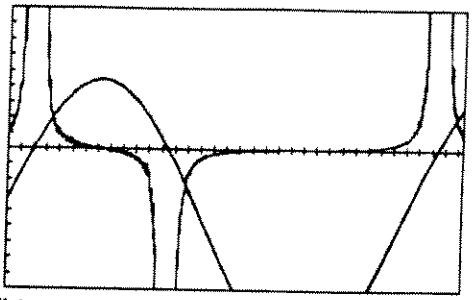

Theta-min Angle (10 degrees/div)

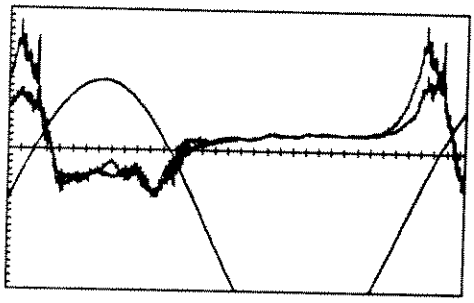

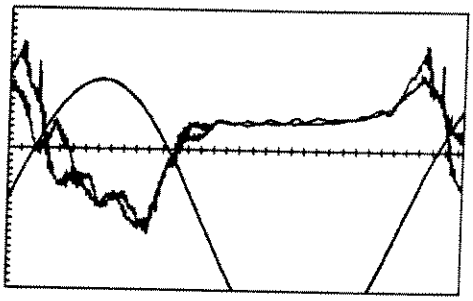

IPM Coefficient (0.1/div)

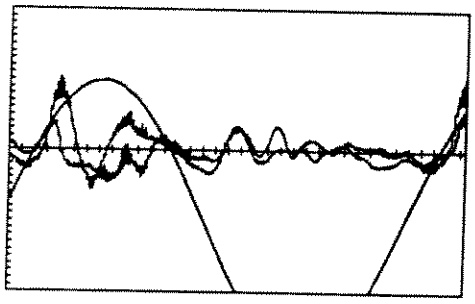

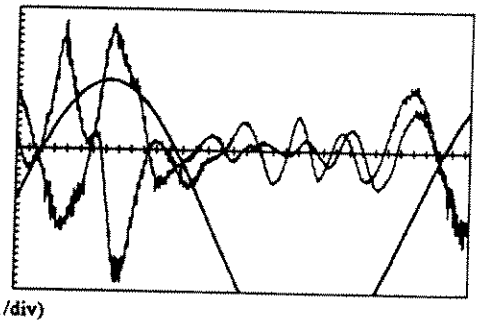

Transverse IPM Coefficient (0.1/div)

FOLDED TIME SERIES PLOTS OF D-FORCE, THETA-MIN, & IPM COEFFICIENTS WITH VELOCITY SHOWN ON EACH PLOT

Periodic Amplitude (meters)..... 5
Frequency (Hz)..... .032
Steady Velocity (m/sec)..... .5
Velocity Ratio (steady/periodic)..... .5
Reynolds number/1,000,000..... .88
KC number..... 31.4

31-88-0-0.5

Smooth Cylinder Data, Run 372

Cycles between Zero Crossings 6 & 10

Rough Cylinder Data, Run 111

Cycles between Zero Crossings 5 & 9

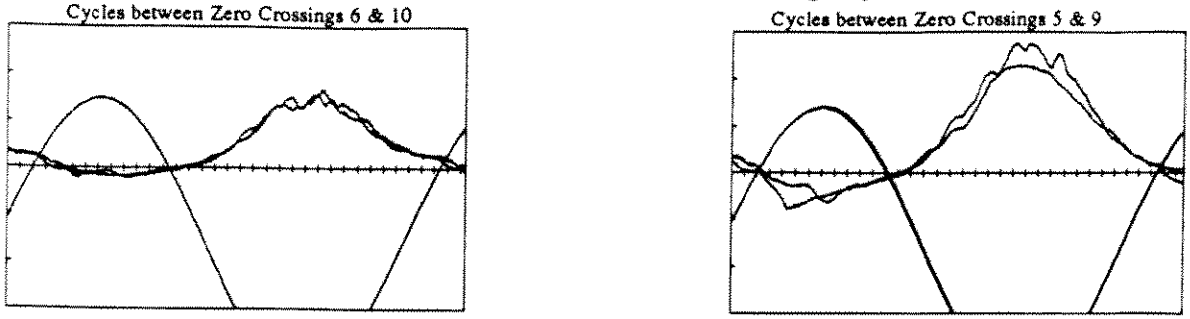

Defect Force (500 N/div)

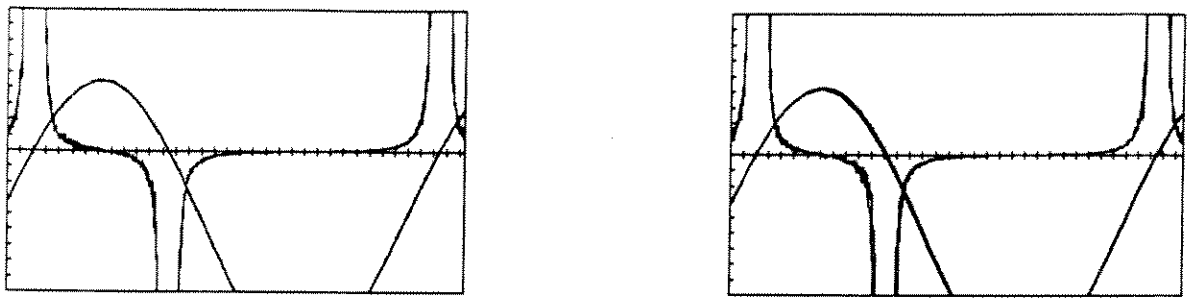

Theta-min Angle (10 degrees/div)

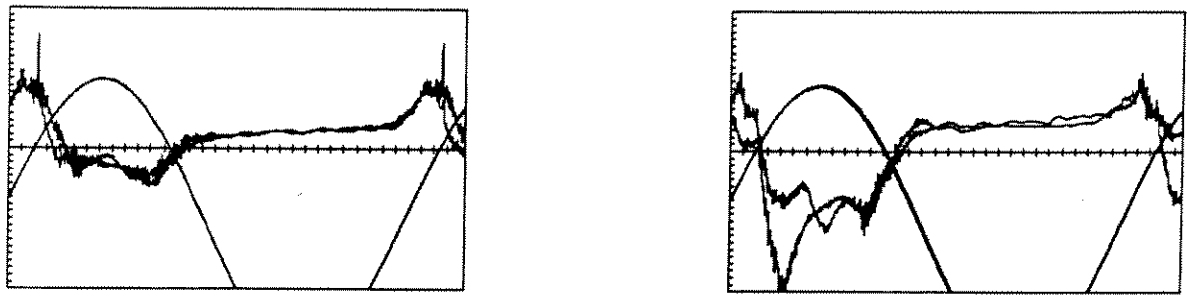

IPM Coefficient (0.1/div)

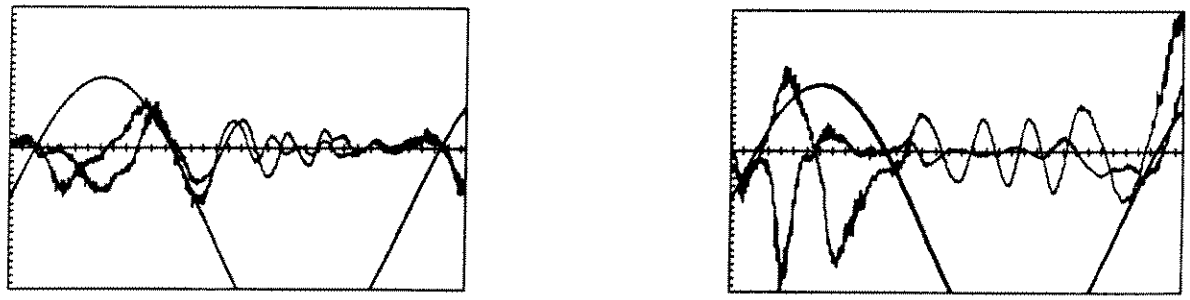

Transverse IPM Coefficient (0.1/div)

FOLDED TIME SERIES PLOTS OF D-FORCE, THETA-MIN, & IPM COEFFICIENTS WITH VELOCITY SHOWN ON EACH PLOT

Periodic Amplitude (meters)..... 5
Frequency (Hz)..... .032
Steady Velocity (m/sec)..... .5
Velocity Ratio (steady/periodic)..... .5
Reynolds number/1,000,000..... .88
KC number..... 31.4

31-88-0-0.5+

Smooth Cylinder Data, Run 373

Cycles between Zero Crossings 5 & 21

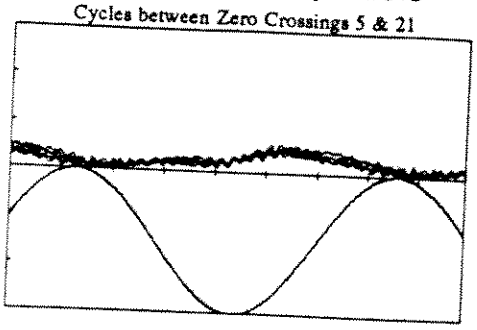

Rough Cylinder Data, Run 116

Cycles between Zero Crossings 5 & 21

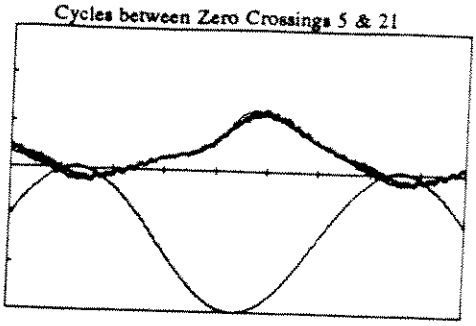

Defect Force (500 N/div)

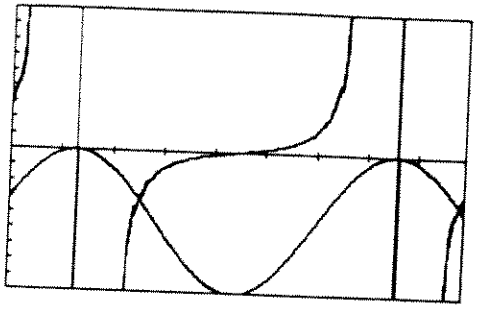

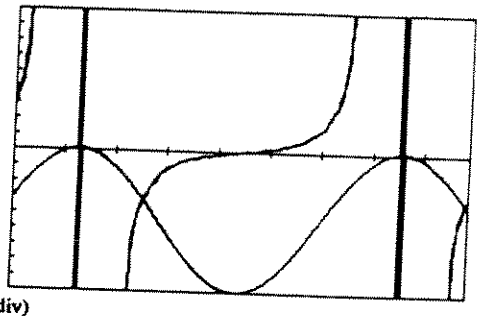

Theta-min Angle (10 degrees/div)

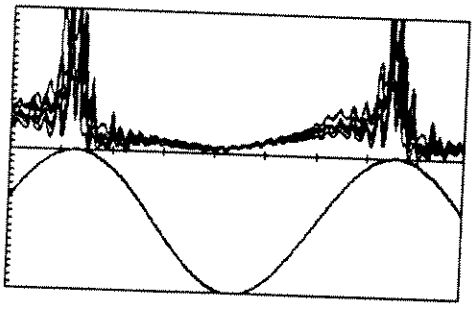

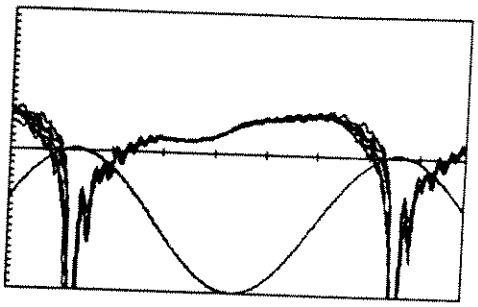

IPM Coefficient (0.1/div)

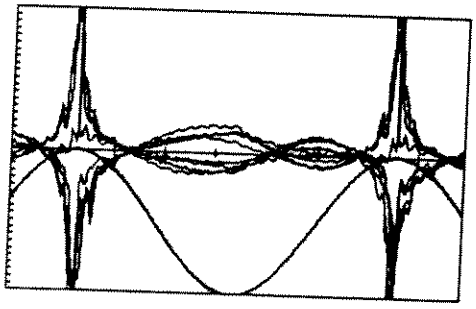

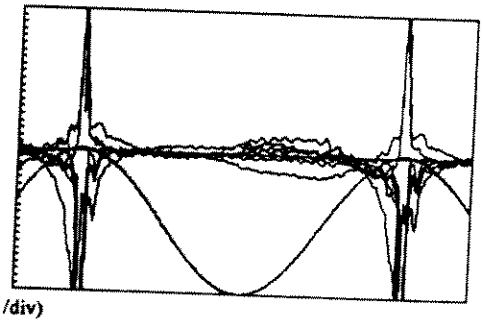

Transverse IPM Coefficient (0.1/div)

FOLDED TIME SERIES PLOTS OF D-FORCE, THETA-MIN, & IPM COEFFICIENTS WITH VELOCITY SHOWN ON EACH PLOT

Periodic Amplitude (meters)..... .5
Frequency (Hz)..... .16
Steady Velocity (m/sec)..... .5
Velocity Ratio (steady/periodic)..... 1
Reynolds number/1,000,000..... .44
KC number..... 3.1

Smooth Cylinder Data, Run 374

Cycles between Zero Crossings 5 & 19

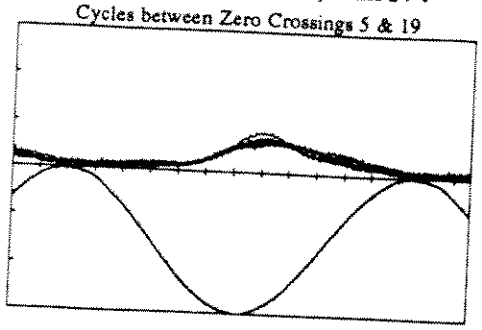

Rough Cylinder Data, Run 113

Cycles between Zero Crossings 5 & 19

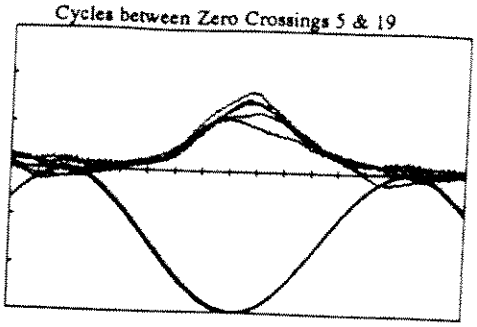

Defect Force (500 N/div)

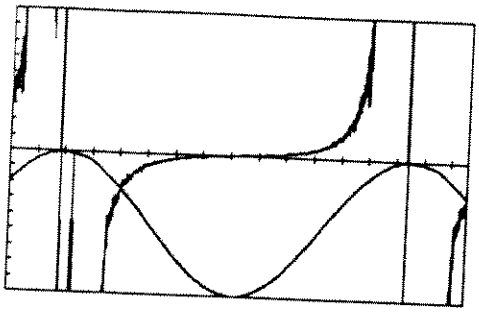

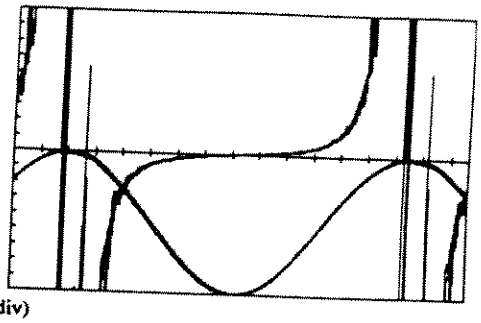

Theta-min Angle (10 degrees/div)

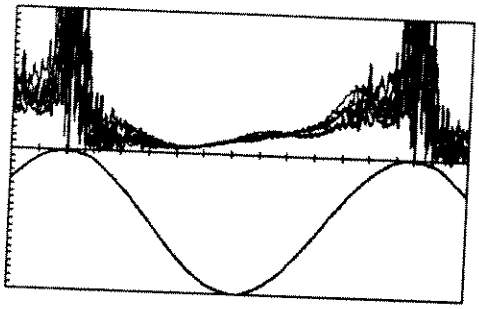

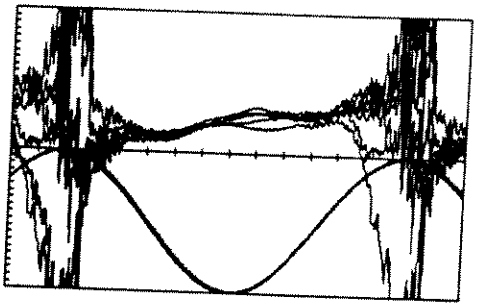

IPM Coefficient (0.1/div)

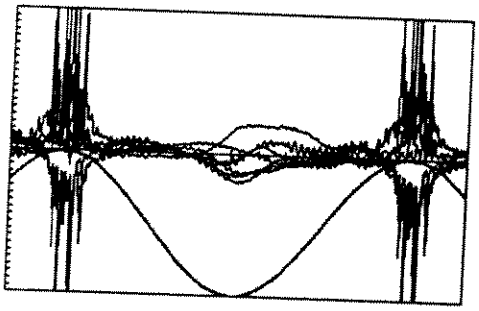

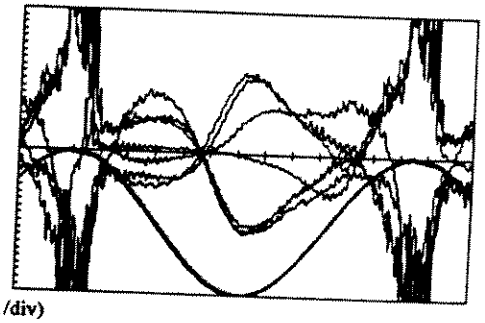

Transverse IPM Coefficient (0.1/div)

FOLDED TIME SERIES PLOTS OF D-FORCE, THETA-MIN, & IPM COEFFICIENTS WITH VELOCITY SHOWN ON EACH PLOT

Periodic Amplitude (meters)..... 1
Frequency (Hz)..... .08
Steady Velocity (m/sec)..... .5
Velocity Ratio (steady/periodic)..... 1
Reynolds number/1,000,000..... .44
KC number..... 6.3

6-44-0-1.0+

Smooth Cylinder Data, Run 375

Cycles between Zero Crossings 5 & 19

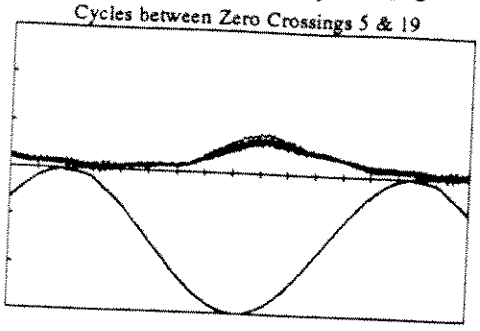

Rough Cylinder Data, Run 112

Cycles between Zero Crossings 5 & 19

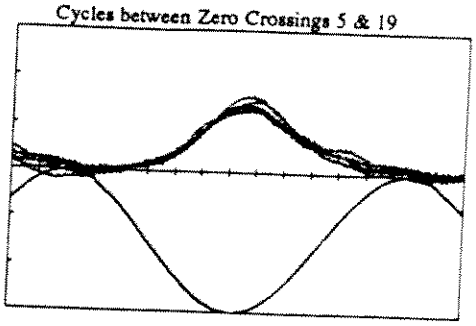

Defect Force (500 N/div)

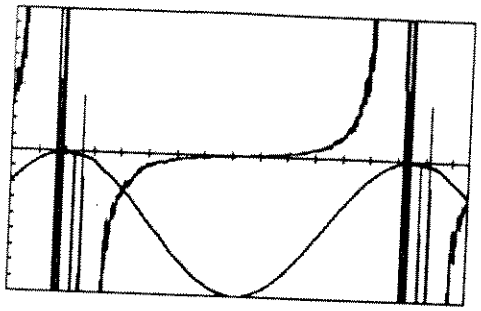

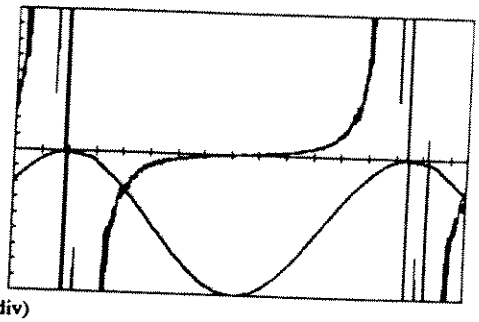

Theta-min Angle (10 degrees/div)

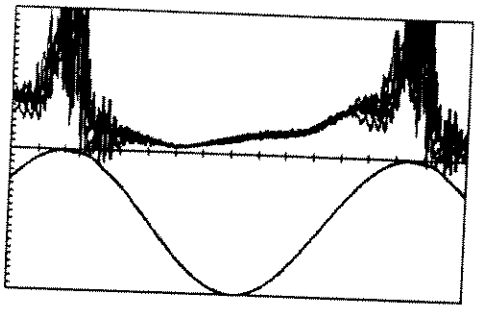

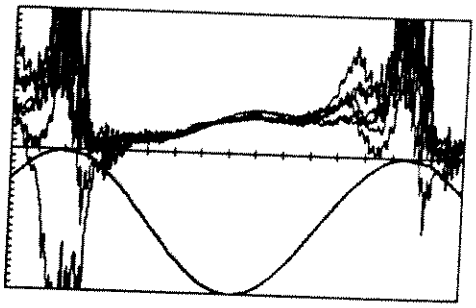

IPM Coefficient (0.1/div)

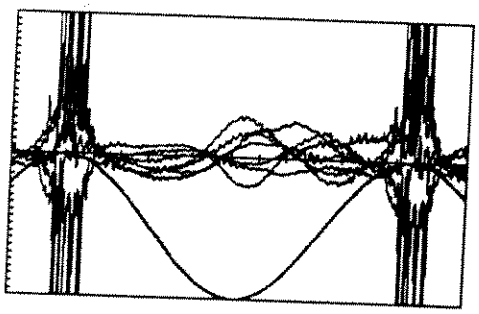

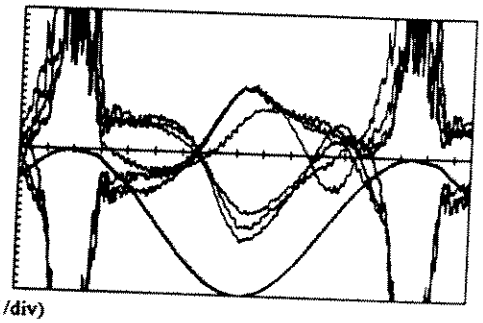

Transverse IPM Coefficient (0.1/div)

FOLDED TIME SERIES PLOTS OF D-FORCE, THETA-MIN, & IPM COEFFICIENTS WITH VELOCITY SHOWN ON EACH PLOT

Periodic Amplitude (meters)..... 1
Frequency (Hz)..... .08
Steady Velocity (m/sec)..... .5
Velocity Ratio (steady/periodic)..... 1
Reynolds number/1,000,000..... .44
KC number..... 6.3

Smooth Cylinder Data, Run 376

Cycles between Zero Crossings 5 & 9

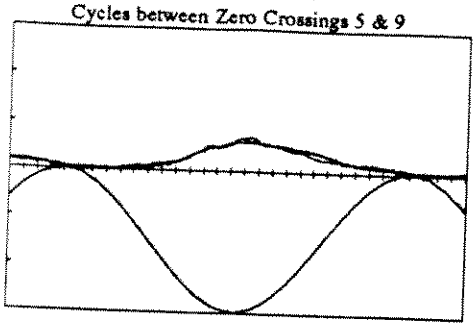

Rough Cylinder Data, Run 129

Cycles between Zero Crossings 5 & 9

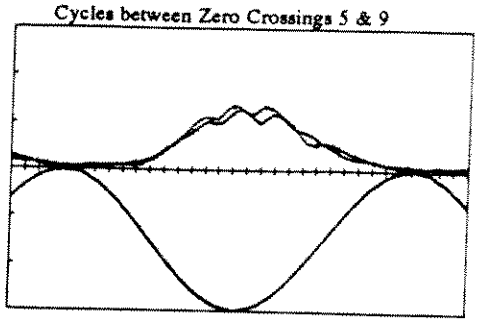

Defect Force (500 N/div)

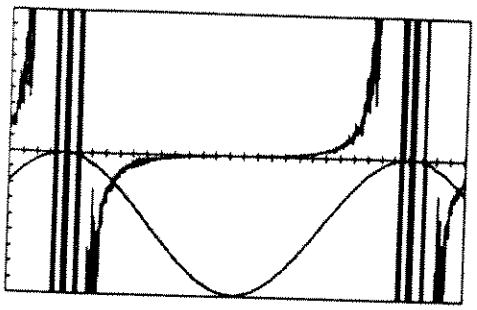

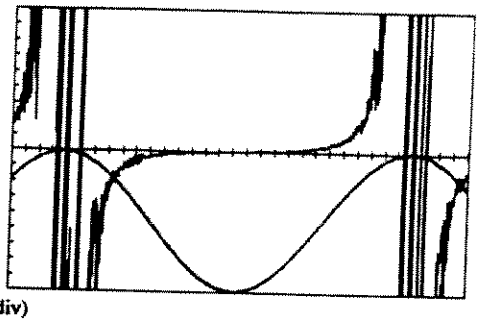

Theta-min Angle (10 degrees/div)

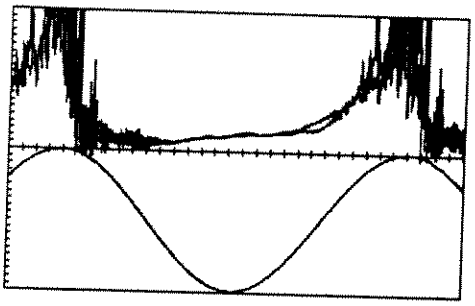

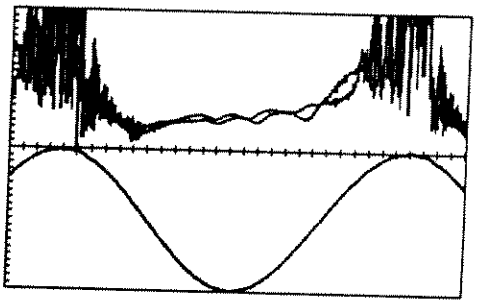

IPM Coefficient (0.1/div)

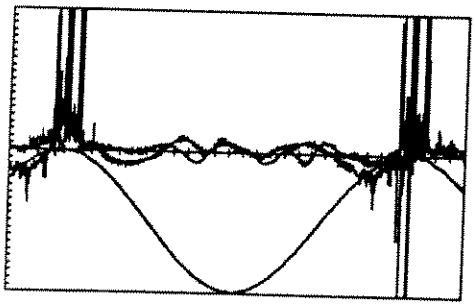

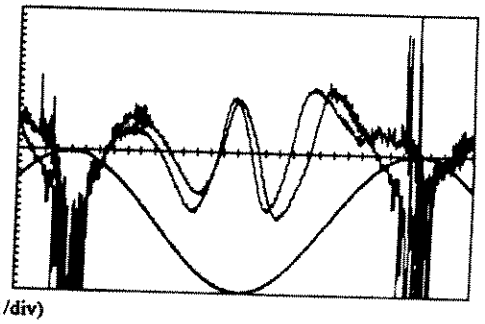

Transverse IPM Coefficient (0.1/div)

FOLDED TIME SERIES PLOTS OF D-FORCE, THETA-MIN, & IPM COEFFICIENTS WITH VELOCITY SHOWN ON EACH PLOT

Periodic Amplitude (meters)..... 2
Frequency (Hz)..... .04
Steady Velocity (m/sec)..... .5
Velocity Ratio (steady/periodic)..... 1
Reynolds number/1,000,000..... .44
KC number..... 12.6

12-44-0-1.0+

Smooth Cylinder Data, Run 377

Cycles between Zero Crossings 5 & 9

Rough Cylinder Data, Run 128

Cycles between Zero Crossings 5 & 9

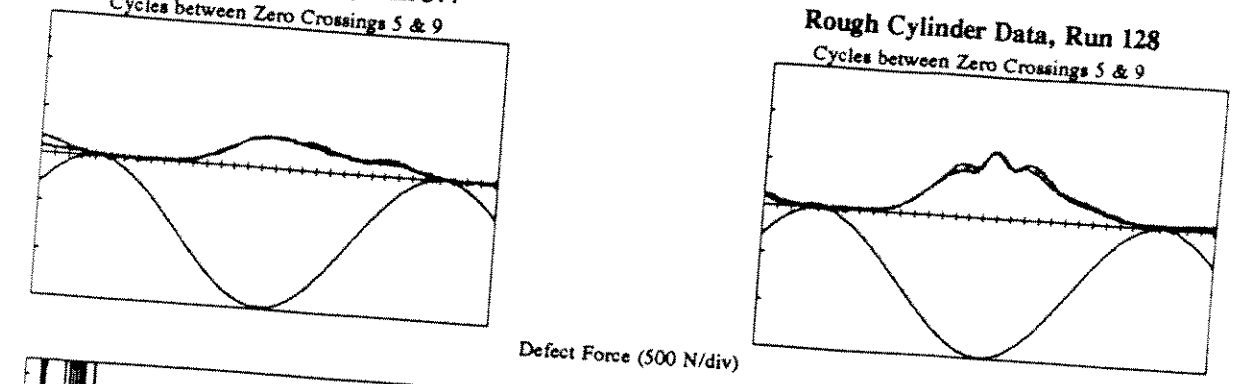

Defect Force (500 N/div)

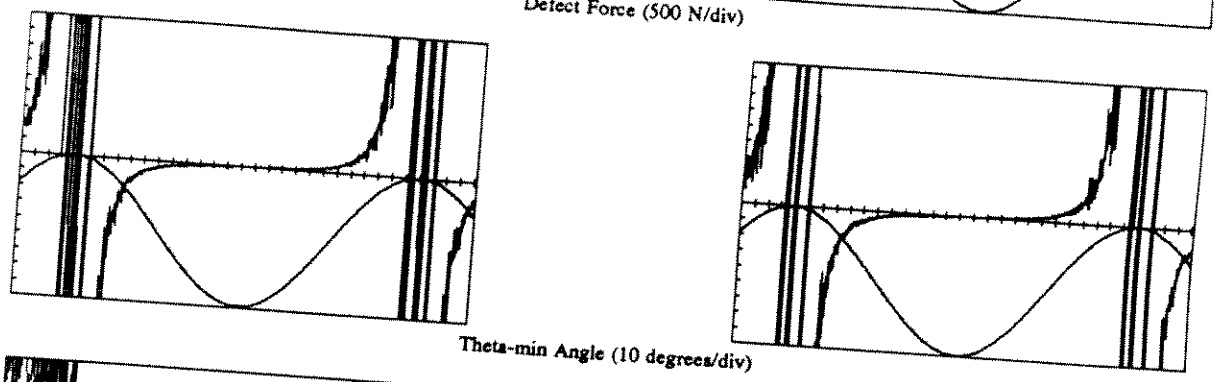

Theta-min Angle (10 degrees/div)

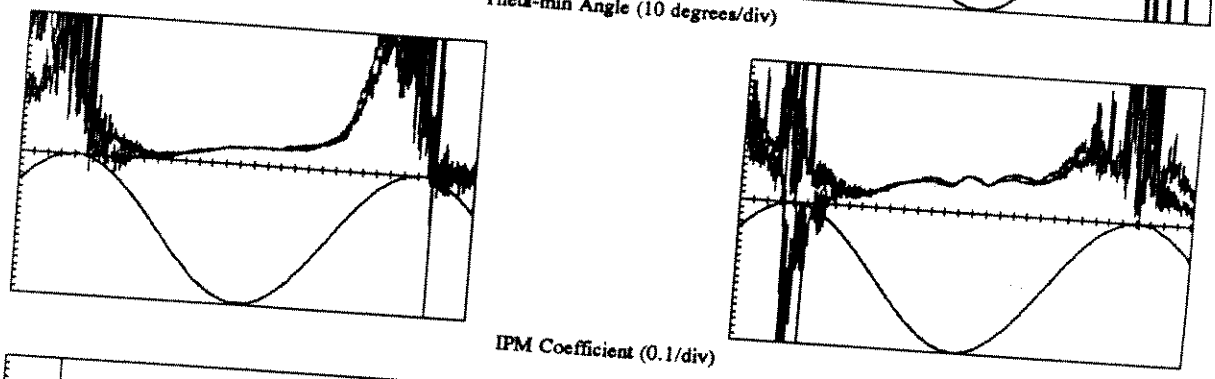

IPM Coefficient (0.1/div)

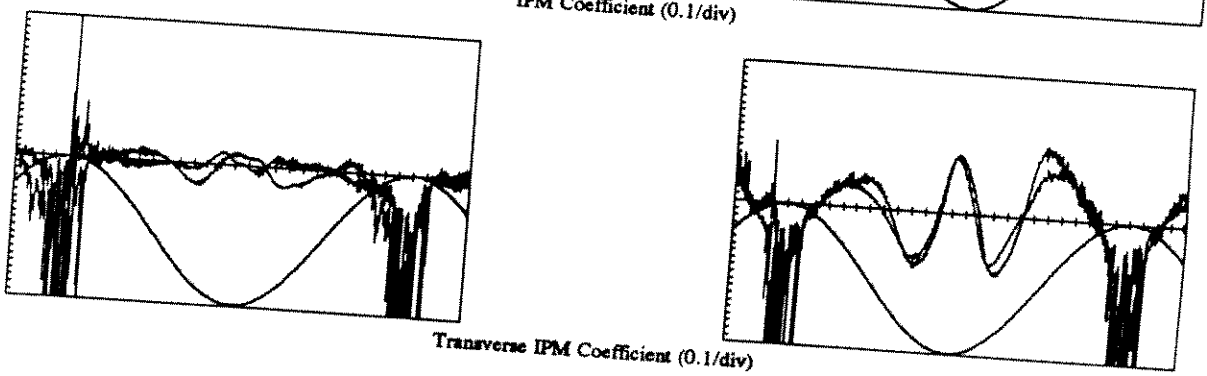

Transverse IPM Coefficient (0.1/div)

FOLDED TIME SERIES PLOTS OF D-FORCE, THETA-MIN, & IPM COEFFICIENTS WITH VELOCITY SHOWN ON EACH PLOT

Periodic Amplitude (meters)..... 2
Frequency (Hz)..... .04
Steady Velocity (m/sec)..... .5
Velocity Ratio (steady/periodic)..... 1
Reynolds number/1,000,000..... .44
KC number..... 12.6

12-44-0-1.0

Smooth Cylinder Data, Run 378

Cycles between Zero Crossings 5 & 19

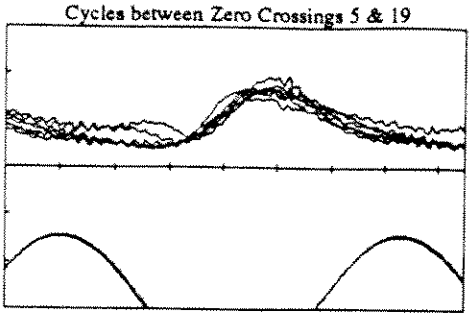

Rough Cylinder Data, Run 131

Cycles between Zero Crossings 5 & 19

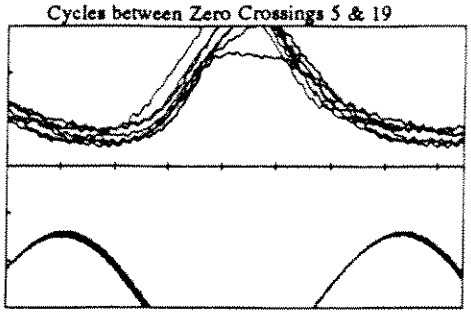

Defect Force (500 N/div)

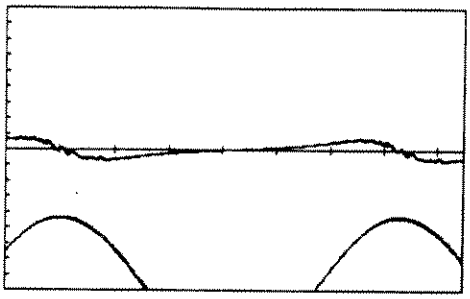

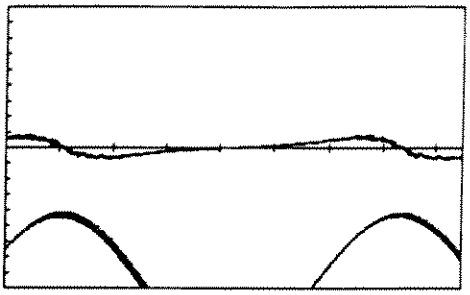

Theta-min Angle (10 degrees/div)

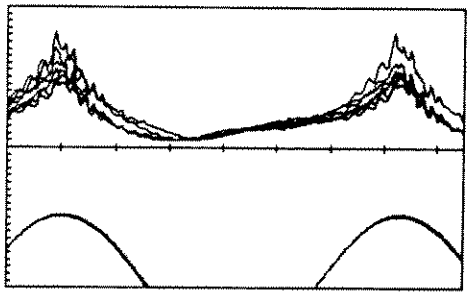

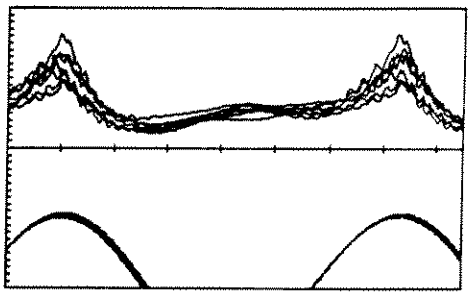

IPM Coefficient (0.1/div)

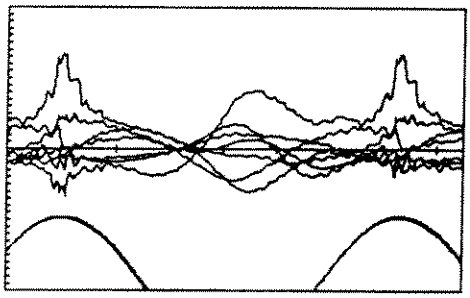

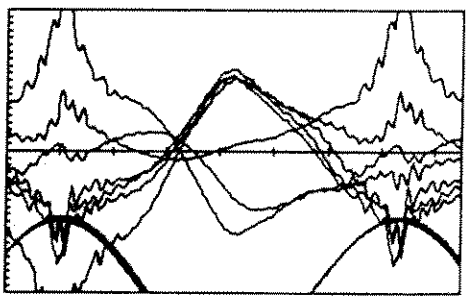

Transverse IPM Coefficient (0.1/div)

FOLDED TIME SERIES PLOTS OF D-FORCE, THETA-MIN, & IPM COEFFICIENTS WITH VELOCITY SHOWN ON EACH PLOT

Periodic Amplitude (meters)..... .5
Frequency (Hz)..... .16
Steady Velocity (m/sec)..... 1
Velocity Ratio (steady/periodic)..... 2
Reynolds number/1,000,000..... .44
KC number..... 3.1

3-44-0-2.0+

Smooth Cylinder Data, Run 379

Cycles between Zero Crossings 5 & 19

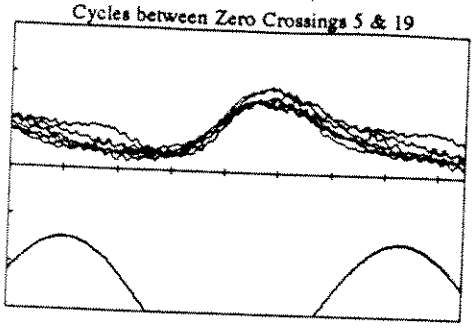

Rough Cylinder Data, Run 130

Cycles between Zero Crossings 5 & 19

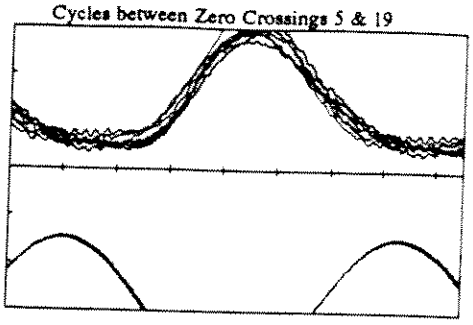

Defect Force (500 N/div)

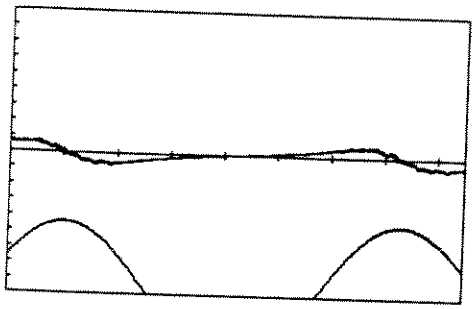

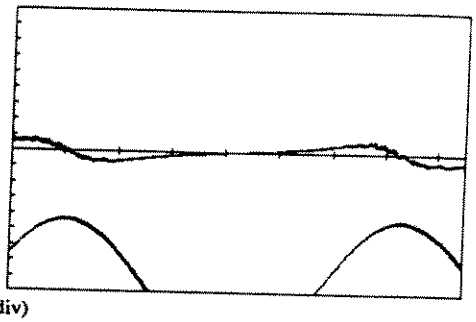

Theta-min Angle (10 degrees/div)

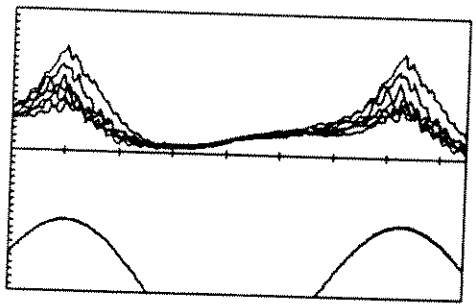

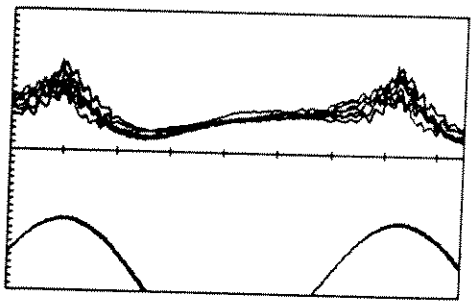

IPM Coefficient (0.1/div)

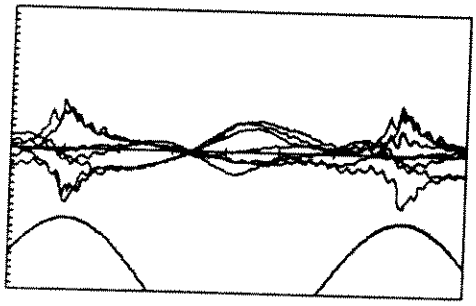

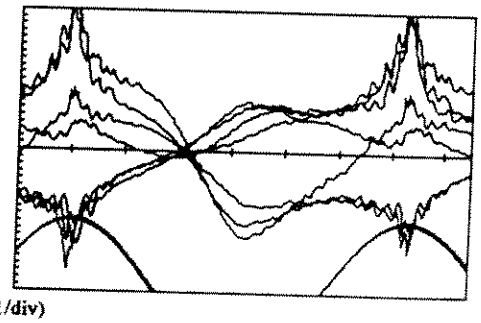

Transverse IPM Coefficient (0.1/div)

FOLDED TIME SERIES PLOTS OF D-FORCE, THETA-MIN, & IPM COEFFICIENTS WITH VELOCITY SHOWN ON EACH PLOT

Periodic Amplitude (meters)..... .5
Frequency (Hz)..... .16
Steady Velocity (m/sec)..... 1
Velocity Ratio (steady/periodic)..... 2
Reynolds number/1,000,000..... .44
KC number..... 3.1

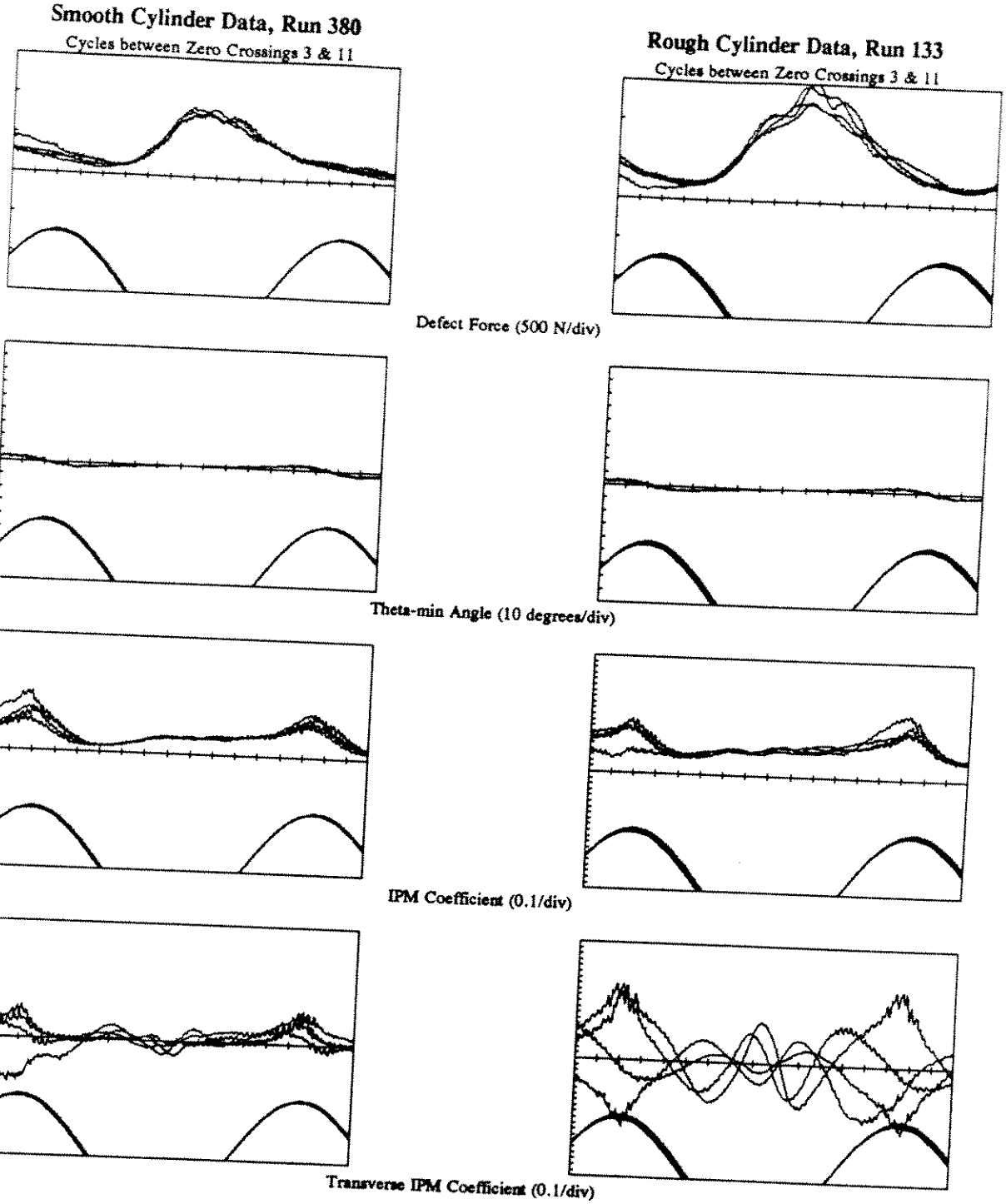

FOLDED TIME SERIES PLOTS OF D-FORCE, THETA-MIN, & IPM COEFFICIENTS WITH VELOCITY SHOWN ON EACH PLOT

Periodic Amplitude (meters)	1
Frequency (Hz)	.08
Steady Velocity (m/sec)	1
Velocity Ratio (steady/periodic)	2
Reynolds number/1,000,000	.44
KC number	6.3

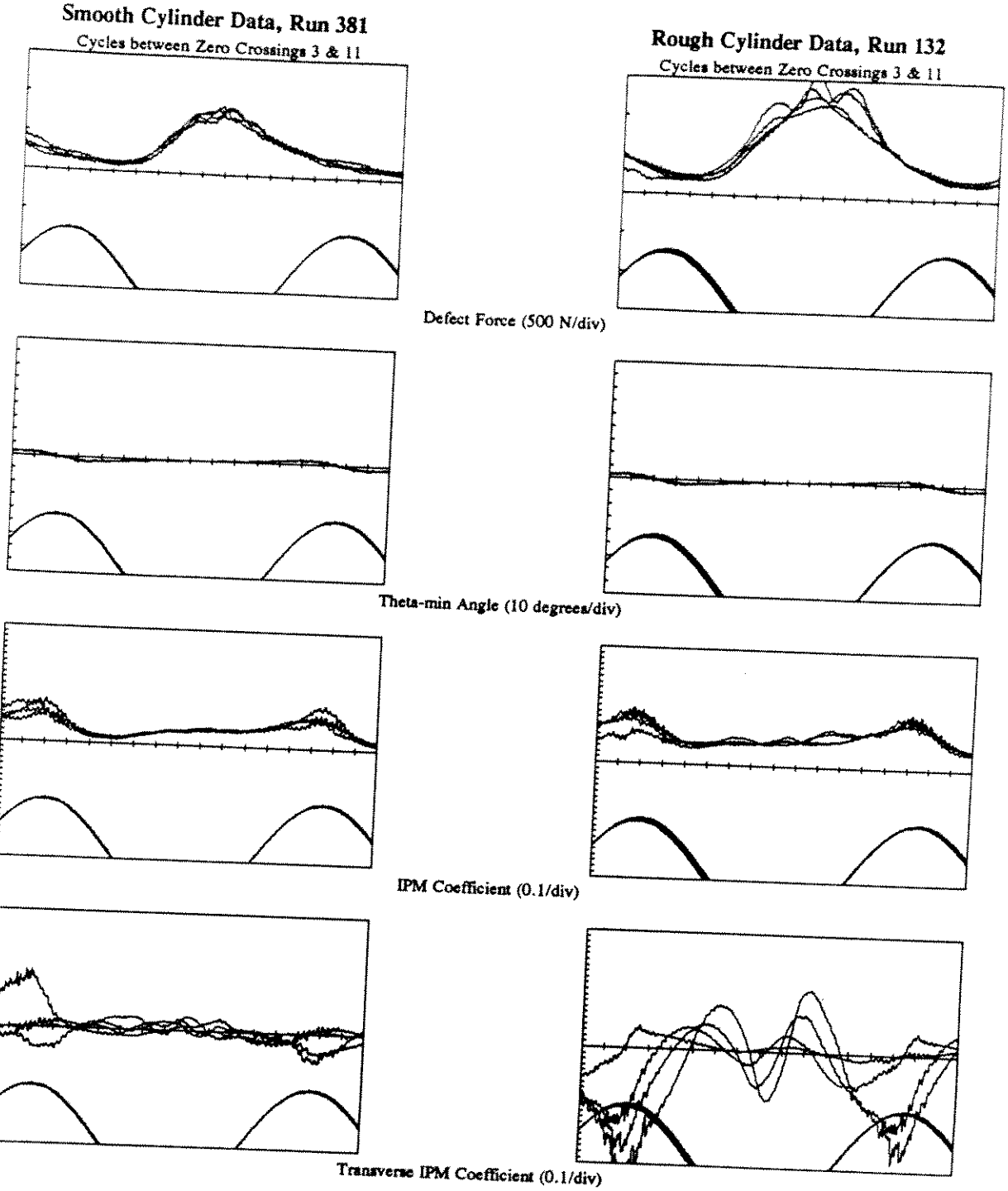

FOLDED TIME SERIES PLOTS OF D-FORCE, THETA-MIN, & IPM COEFFICIENTS WITH VELOCITY SHOWN ON EACH PLOT

Periodic Amplitude (meters)	1
Frequency (Hz)	.08
Steady Velocity (m/sec)	1
Velocity Ratio (steady/periodic)	2
Reynolds number/1,000,000	.44
KC number	6.3

APPENDIX C

TIME SERIES OF ALL INLINE COMBINED MOTION DATA

GUIDE TO TIME SERIES PLOTS

The SSPA Inline Combined Motion Experiments were grouped into 3 categories:

1. LF Tests - combining low frequency periodic motion inline with a steady tow velocity.
2. HF Tests - combining high frequency periodic motion inline with a low frequency periodic motion.
3. Periodic Tests - simple inline periodic motion

The accompanying Tables and annotated Figure serve as a guide to the 78 SSPA Runs displayed on 39 double pages. These time series plots display all the significant SSPA inline combined motion data.

Referring to the numbered items in the illustration below: (1) The page number common to the two pages of data with in Appendix C. Placed on opposing sides the smooth cylinder plots are "a" and the rough cylinder plots are "b". (2) ID Number -"R" or "S" for rough or smooth, "31" is the rounded KC number, "88" is the Reynolds number normalized by 10^4, the third number, which is "0" for this example, is ratio of the HF motion amplitude to cylinder diameter, and the last number "0.5" is the ratio of steady and periodic velocity amplitudes. The terminal + indicates a Run with the steady velocity in the positive direction. (3) The SSPA Run Number followed by the identification numbers of the first and last significant data point in the plot. (4) The cylinder velocity is presented as a reference on each time series plot. Full scale is 2 meters/sec.

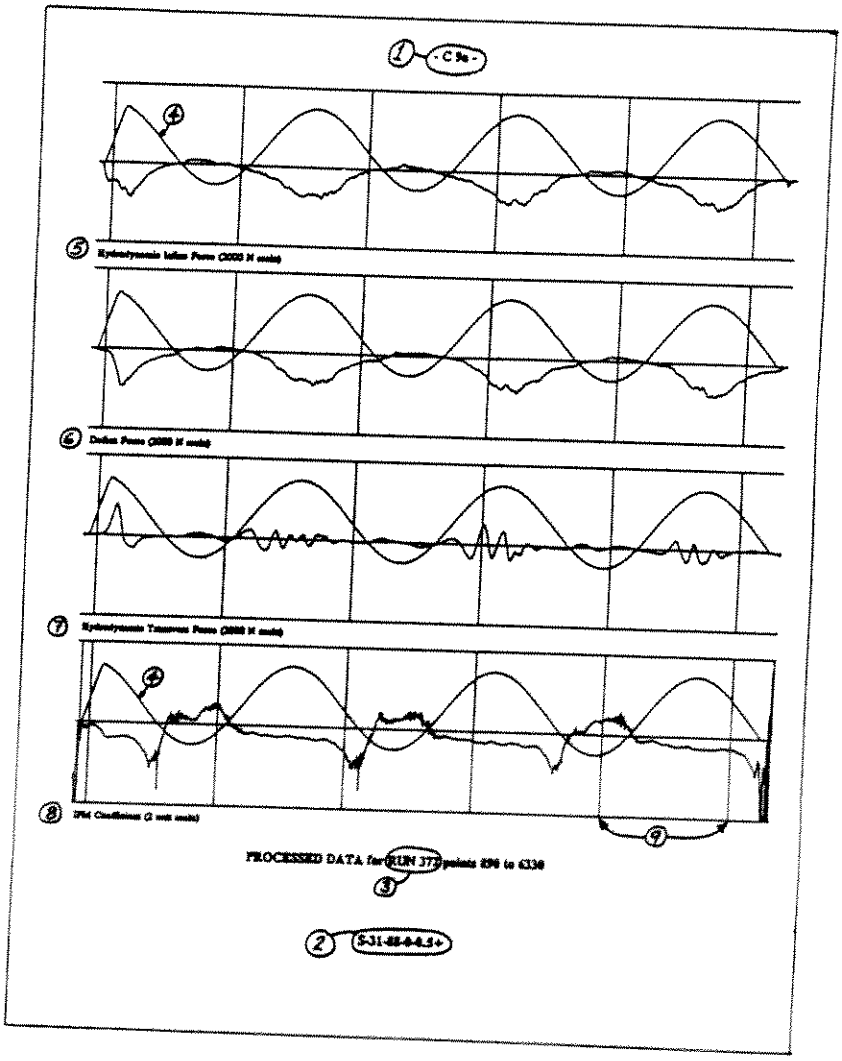

(5) The hydrodynamic force along the axis of motion . (6) The Defect Force is the difference between the inline hydrodynamic force and the ideal hydrodynamic inertial force and is indicative of the drag force. (7) Hydrodynamic force transverse to the axis of motion. Note throughout Appendix C all force plots have used the same scale and represent the load on a 1 meter test length of the cylinder. (8) The IPM inline force coefficient has been computed for every point in the time series. (9) The grid time interval represent 20 seconds, 1000 points. Grid lines occur at 1000 point intervals measured from the zero point of the data tape. For this illustration the first significant data point was at 890 so the first grid line corresponds to 1000.

In the each of the 3 Tables the first 6 columns are: Page number in Appendix C, SSPA Run Numbers for smooth and rough cylinders, amplitude of the periodic motion in meters, frequency of the periodic motion, periodic motion Reynolds number, and Keulegan-Carpenter number. The last column is the ID Number which has been described above. For the LF Tests columns 7 and 8 are the steady tow velocity in meters/second and the ratio of the steady and periodic velocity amplitudes. For the HF Tests columns 7 and 8 are the amplitude of the high frequency motion in meters and the frequency of the high frequency motion.

CATALOGUE OF LF TESTS

Page	Run No. smooth/rough	A_o meters	f_o Hz	$Re/10^6$	KC	U_s m/s	U_s/U_o	ID Number
1	364/106	1.0	0.16	0.88	6.3	0.1	0.1	S/R- 6-88-0-0.1
2	365/107	2.0	0.08	0.88	12.6	0.1	0.1	S/R-12-88-0-0.1
3	366/108	5.0	0.032	0.88	31.4	0.1	0.1	S/R-31-88-0-0.1
4	367/109	10.0	0.016	0.88	63.0	0.1	0.1	S/R-63-88-0-0.1
5	368/117	1.0	0.16	0.88	6.3	0.5	0.5	S/R- 6-88-0-0.5+
6	369/114	2.0	0.08	0.88	12.6	0.5	0.5	S/R-12-88-0-0.5
7	370/115	2.0	0.08	0.88	12.6	0.5	0.5	S/R-12-88-0-0.5+
8	371/110	5.0	0.032	0.88	31.4	0.5	0.5	S/R-31-88-0-0.5
9	372/111	5.0	0.032	0.88	31.4	0.5	0.5	S/R-31-88-0-0.5+
10	373/116	0.5	0.16	0.44	3.1	0.5	1.0	S/R- 3-44-0-1.0
11	374/113	1.0	0.08	0.44	6.3	0.5	1.0	S/R- 6-44-0-1.0+
12	375/112	1.0	0.08	0.44	6.3	0.5	1.0	S/R- 6-44-0-1.0
13	376/129	2.0	0.04	0.44	12.6	0.5	1.0	S/R-12-44-0-1.0+
14	377/128	2.0	0.04	0.44	12.6	0.5	1.0	S/R-12-44-0-1.0
15	378/131	0.5	0.16	0.44	3.1	1.0	2.0	S/R- 3-44-0-2.0+
16	379/130	0.5	0.16	0.44	3.1	1.0	2.0	S/R- 3-44-0-2.0
17	380/133	1.0	0.08	0.44	6.3	1.0	2.0	S/R- 6-44-0-2.0+
18	381/132	1.0	0.08	0.44	6.3	1.0	2.0	S/R- 6-44-0-2.0

CATALOGUE OF HF TESTS

Page	Run No. smooth/rough	A_o meters	f_o Hz	$Re/10^6$	KC	A' meters	f' Hz	ID Number
19	437/192	2.0	0.079	0.88	12.6	0.1	0.3	S/R-12-88-0.1-0
20	438/193	5.0	0.032	0.88	31.4	0.1	0.3	S/R-31-88-0.1-0
21	439/194	10.0	0.016	0.88	63.0	0.1	0.3	S/R-63-88-0-1-0
22	440/195	1.0	0.079	0.44	6.3	0.1	0.3	S/R- 6-44-0.1-0
23	441/196	5.0	0.016	0.44	31.4	0.1	0.3	S/R-31-44-0.1-0
24	443/197	1.0	0.079	0.44	6.3	0.15	0.3	S/R- 6-44-0.15-0
25	442/198	5.0	0.016	0.44	31.4	0.15	0.3	S/R-31-44-0.15-0
26	445/199	0	0	-	-	0.1	0.3	S/R- 0- 0-0.1-0

CATALOGUE OF PERIODIC TESTS

Page	Run No. smooth/rough	A_o meters	f_o Hz	$Re/10^6$	KC	ID Number
27	351/95	.50	0.16	0.44	3.1	S/R- 3-44-0-0
28	352/96	1.0	0.08	0.44	6.3	S/R- 6-44-0-0
29	353/97	2.0	0.04	0.44	12.6	S/R-12-44-0-0
30	356/295	3.0	0.027	0.44	18.8	S/R-18-44-0-0
31	354/98	5.0	0.016	0.44	31.4	S/R-31-44-0-0
32	357/100	10.0	0.008	0.44	63.0	S/R-63-44-0-0
33	358/101	1.0	0.16	0.88	6.3	S/R- 6-88-0-0
34	359/102	2.0	0.08	0.88	12.6	S/R-12-88-0-0
35	360/103	5.0	0.032	0.88	31.4	S/R-31-88-0-0
36	361/104	10.0	0.016	0.88	63.0	S/R-63-88-0-0
37	362/105	15.0	0.0106	0.88	94.0	S/R-94-88-0-0
38	363/293	4.3	0.08	1.90	27.0	S/R-27-190-0-0
39	355/294	5.0	0.064	1.75	31.4	S/R-31-175-0-0

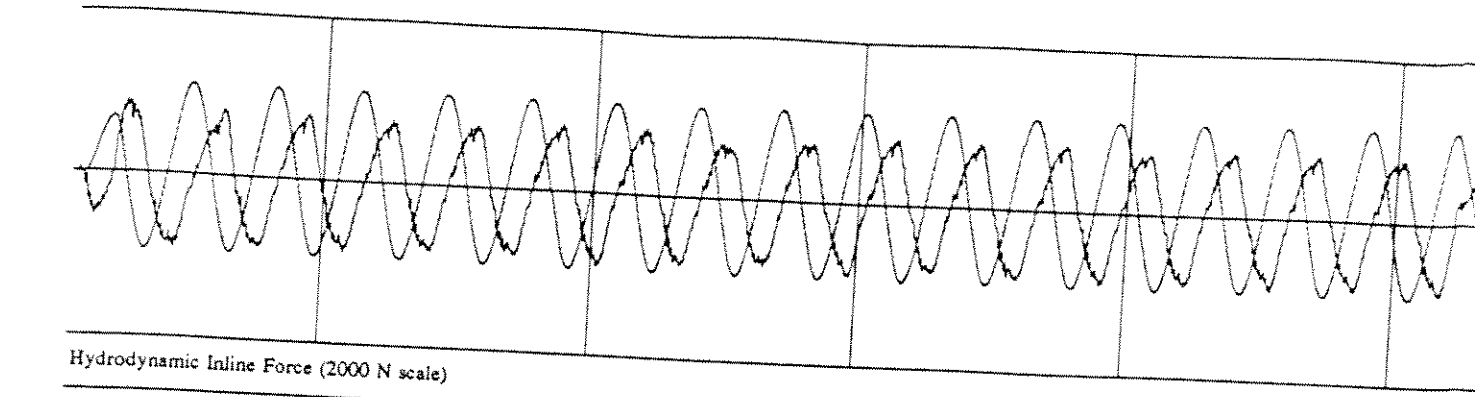

Hydrodynamic Inline Force (2000 N scale)

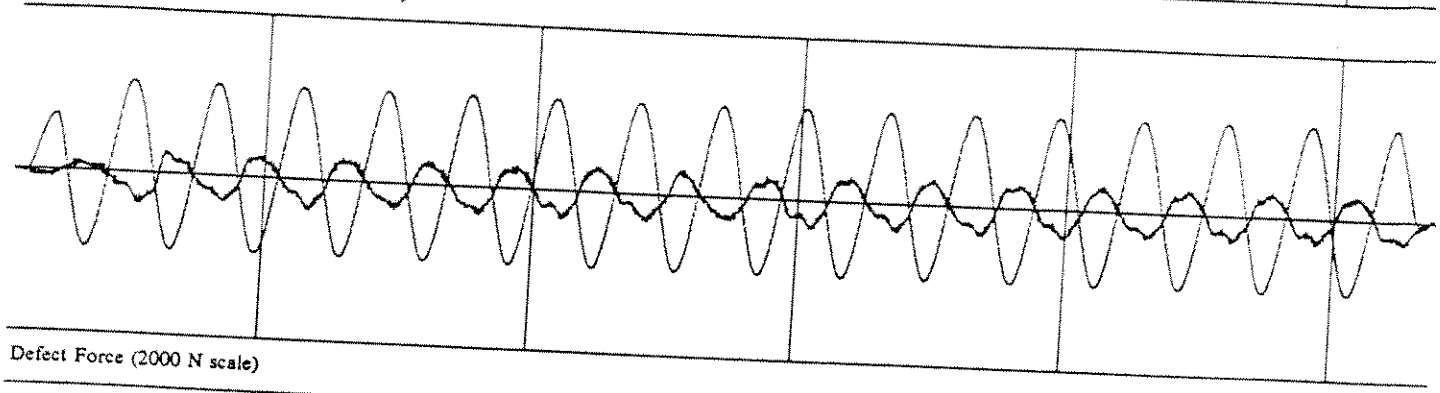

Defect Force (2000 N scale)

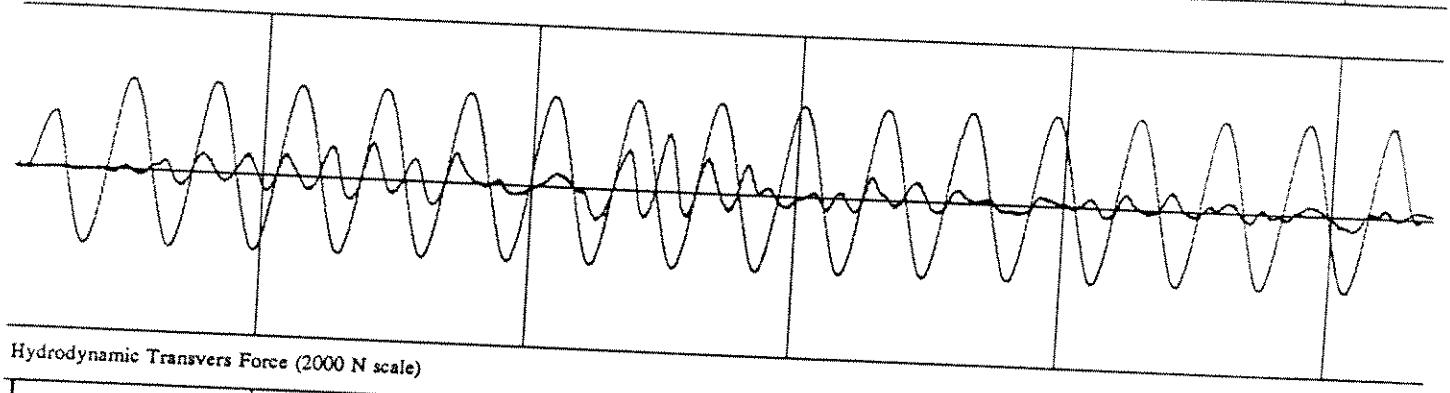

Hydrodynamic Transvers Force (2000 N scale)

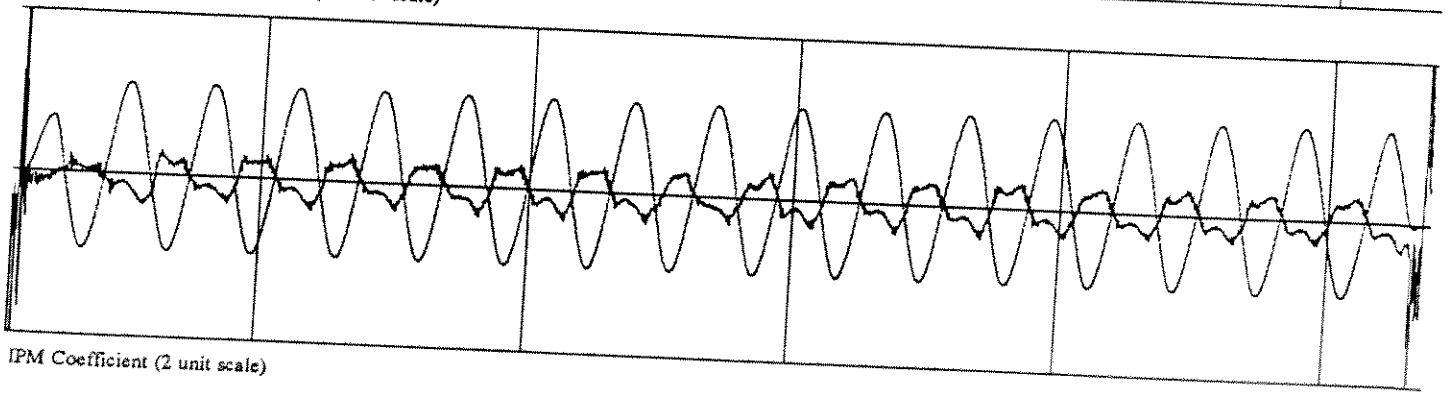

IPM Coefficient (2 unit scale)

PROCESSED DATA for RUN 364 points 1080 to 6370

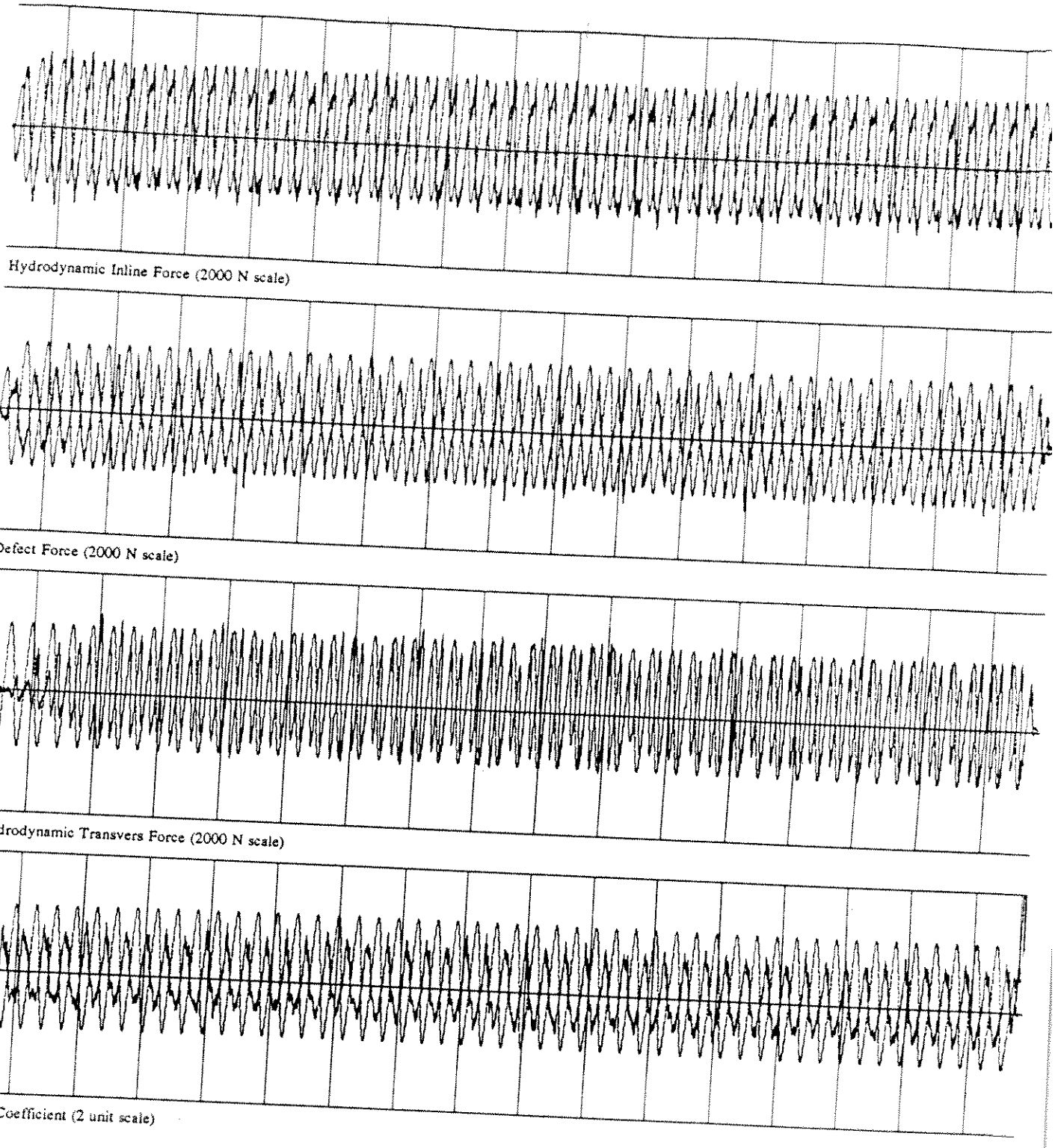

PROCESSED DATA for RUN 106 points 1235 to 17780

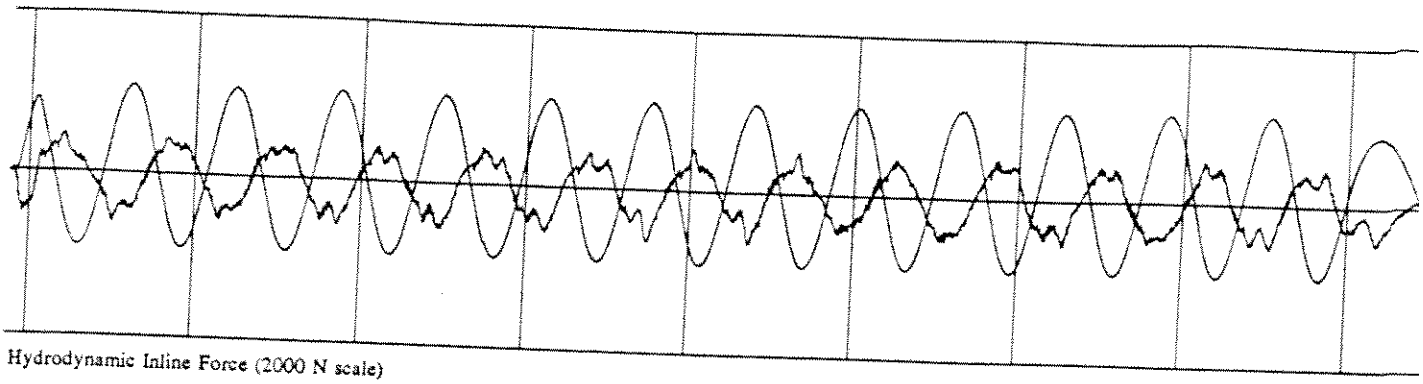

Hydrodynamic Inline Force (2000 N scale)

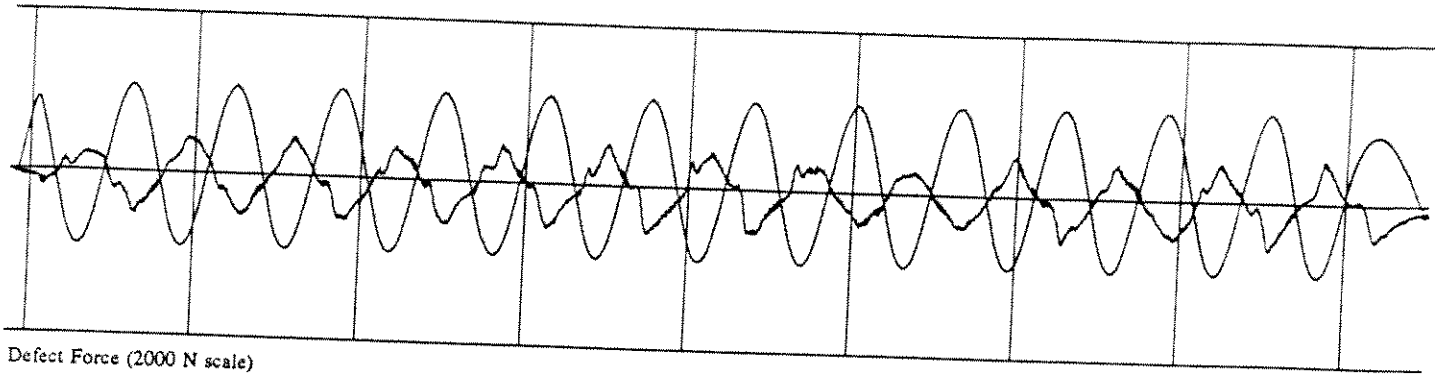

Defect Force (2000 N scale)

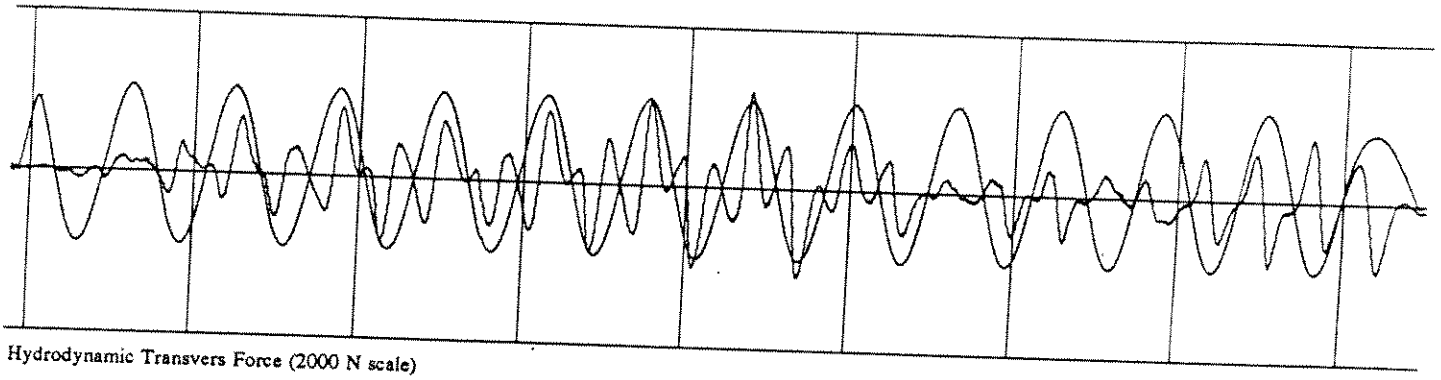

Hydrodynamic Transvers Force (2000 N scale)

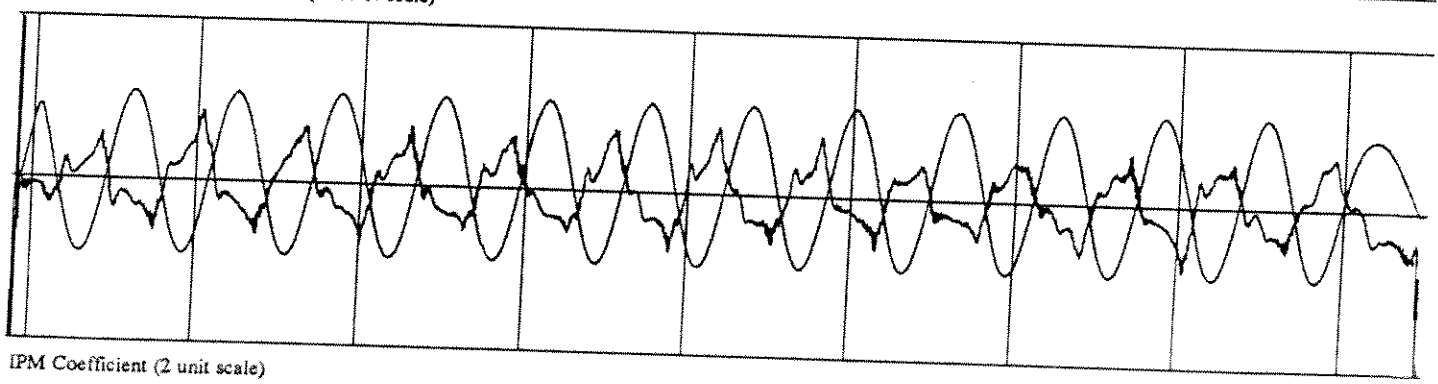

IPM Coefficient (2 unit scale)

PROCESSED DATA for RUN 365 points 880 to 9500

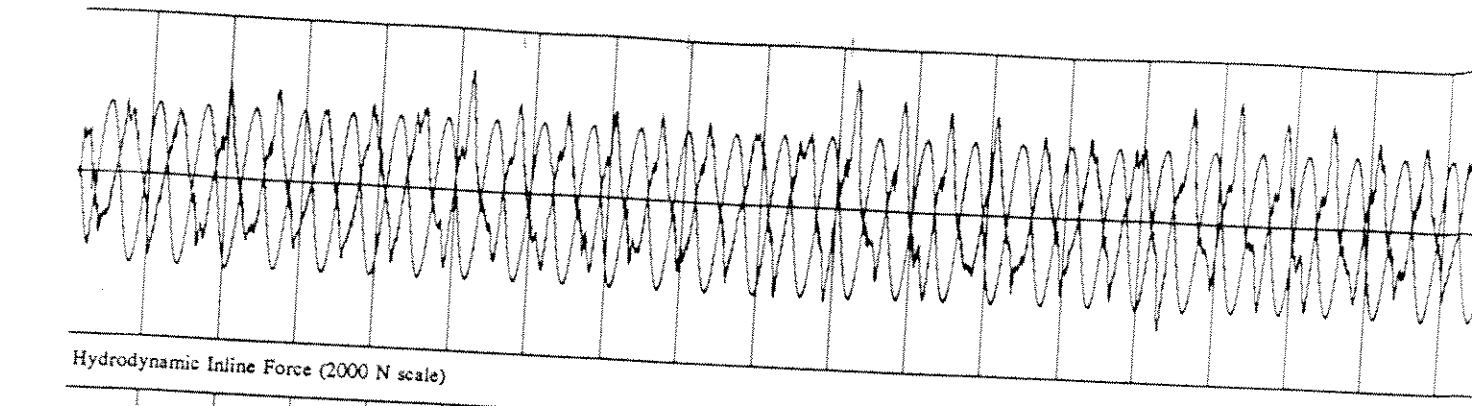

Hydrodynamic Inline Force (2000 N scale)

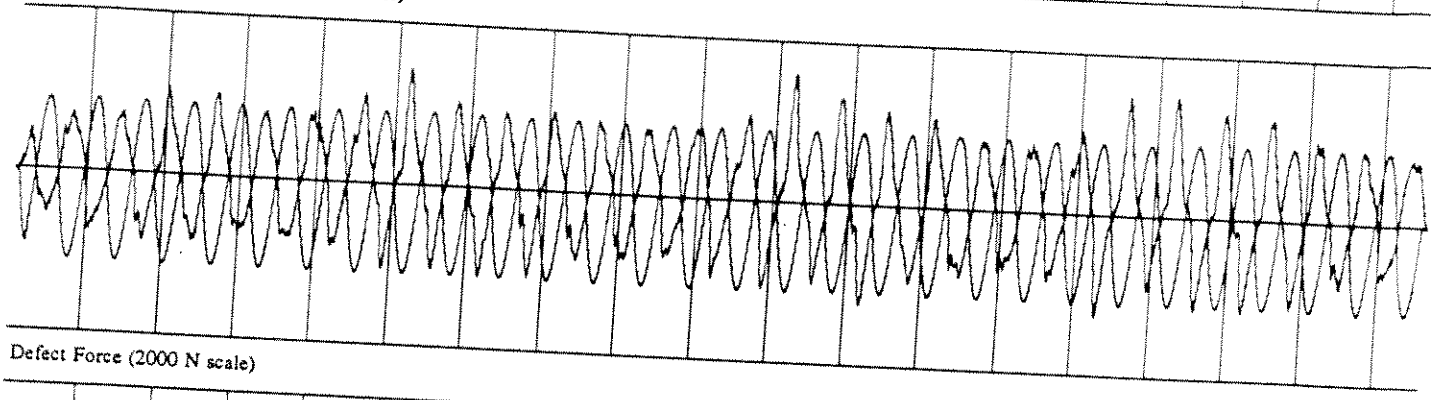

Defect Force (2000 N scale)

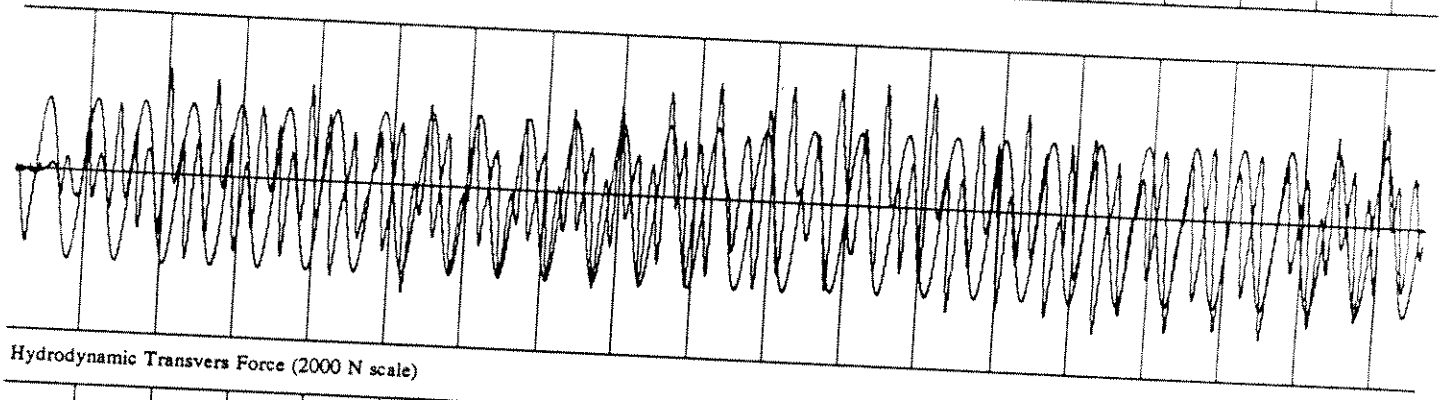

Hydrodynamic Transvers Force (2000 N scale)

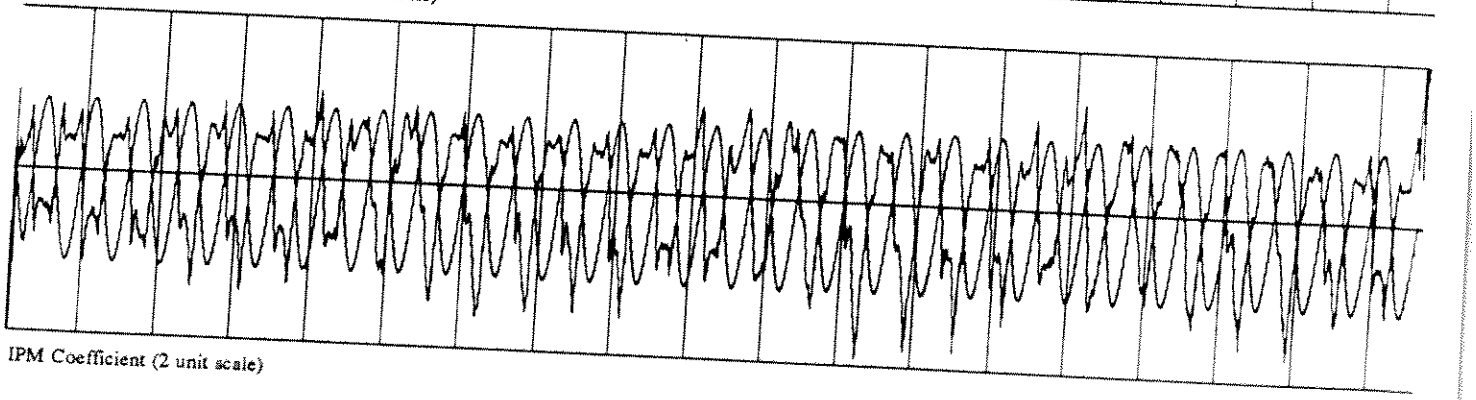

IPM Coefficient (2 unit scale)

PROCESSED DATA for RUN 107 points 1055 to 19600

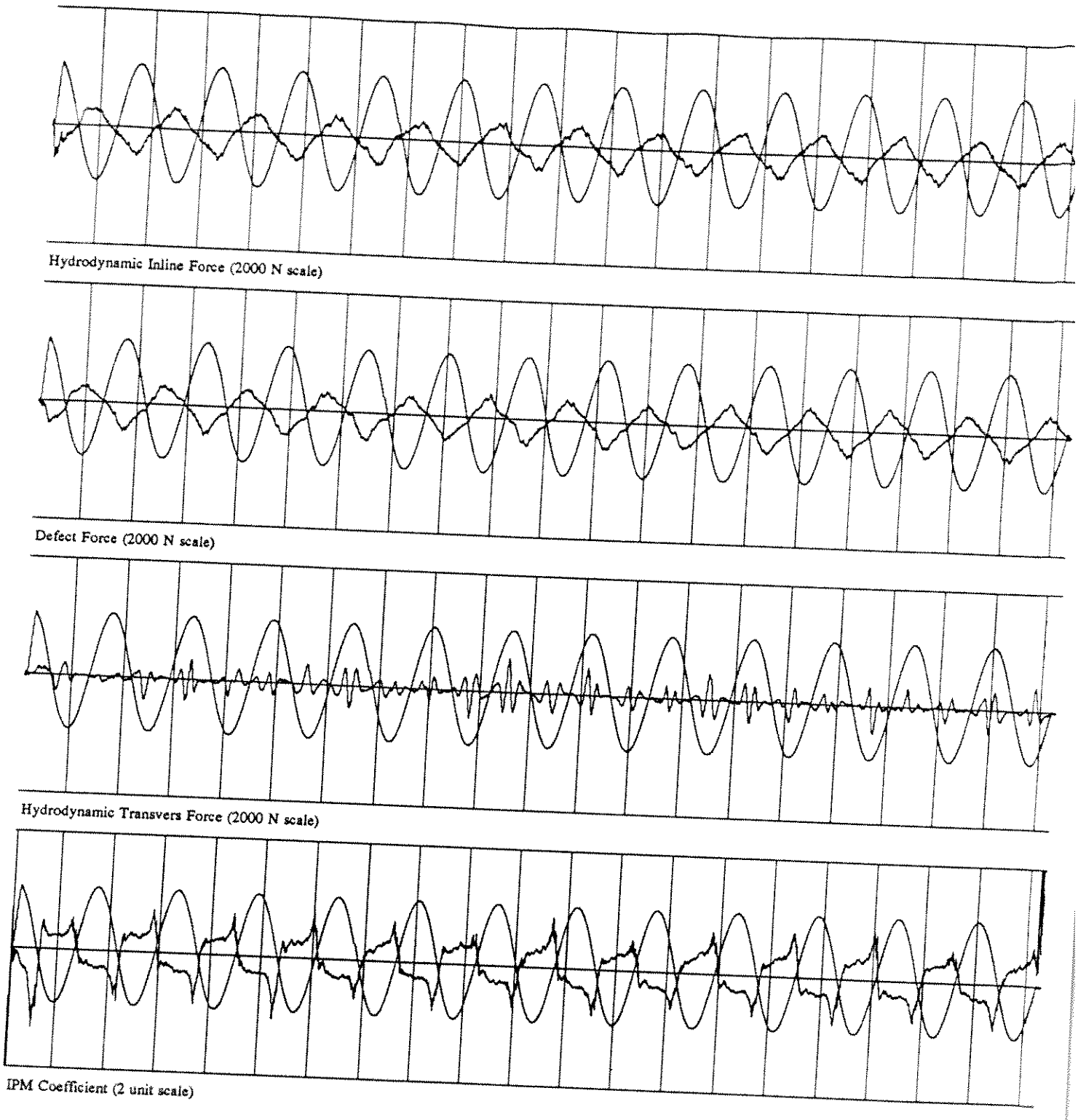

PROCESSED DATA for RUN 366 points 1080 to 21260

S-31-88-0-0.1

PROCESSED DATA for RUN 108 points 1120 to 18815

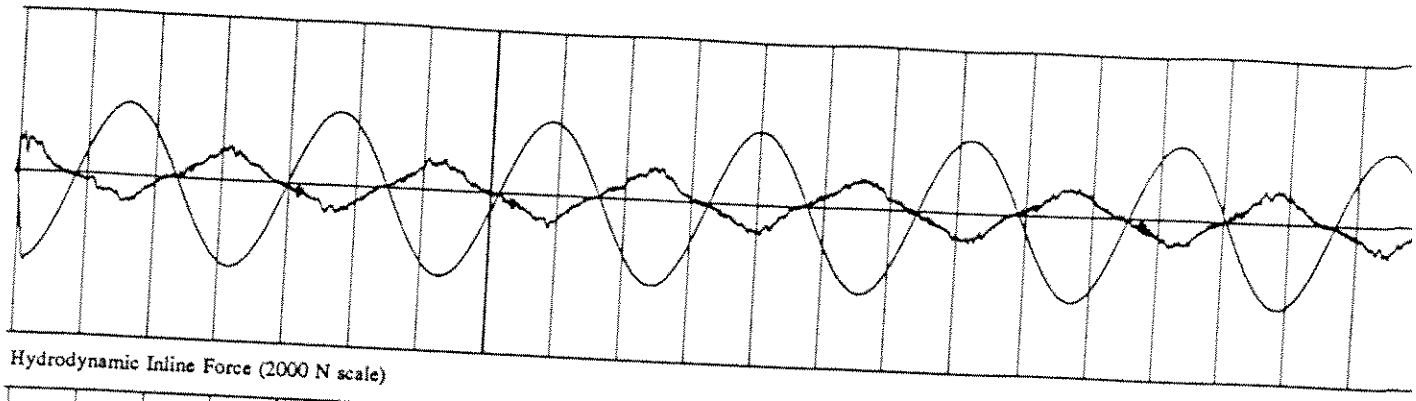

Hydrodynamic Inline Force (2000 N scale)

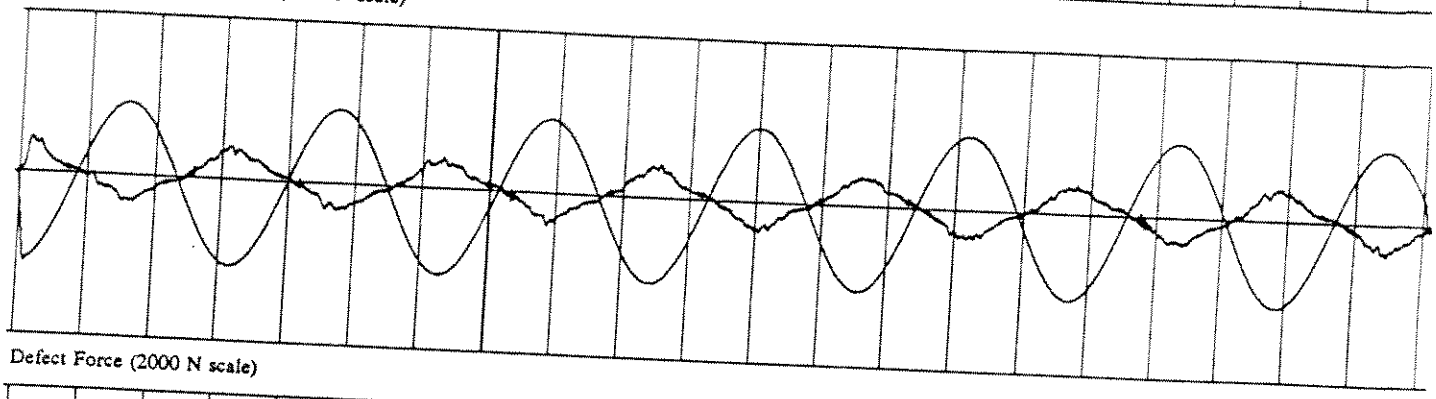

Defect Force (2000 N scale)

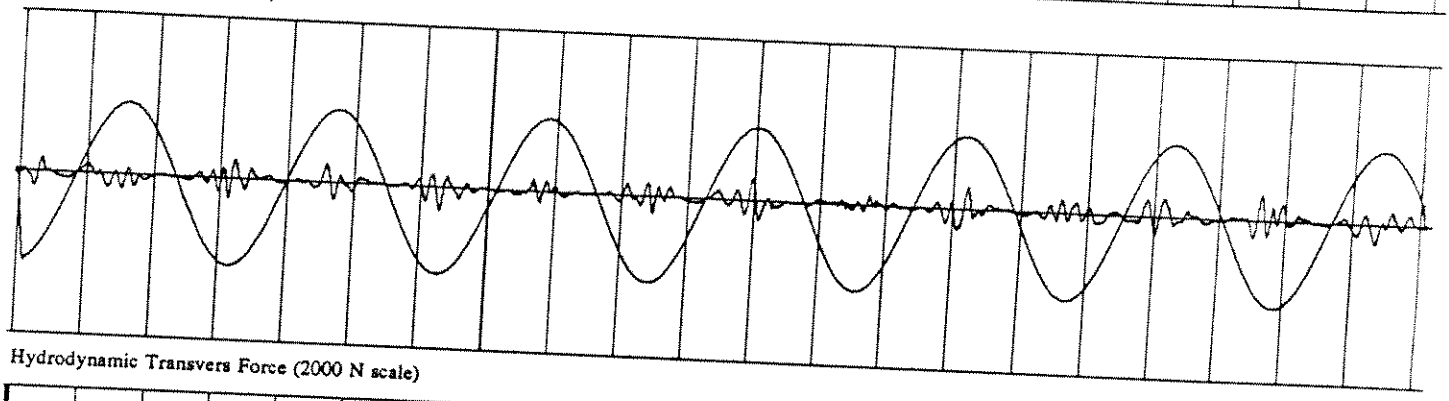

Hydrodynamic Transvers Force (2000 N scale)

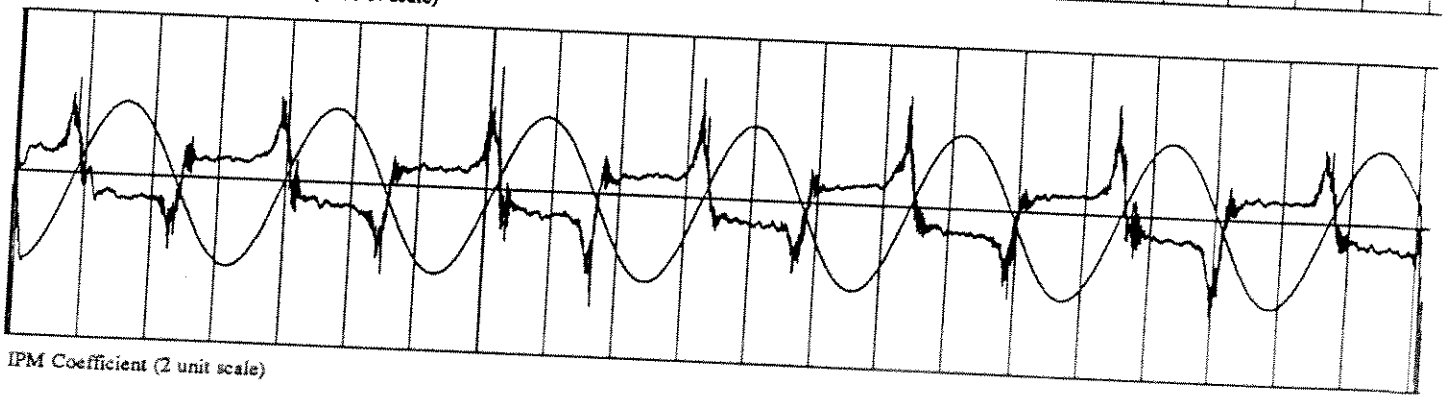

IPM Coefficient (2 unit scale)

PROCESSED DATA for RUN 367 points 920 to 22170

PROCESSED DATA for RUN 109 points 1220 to 22450

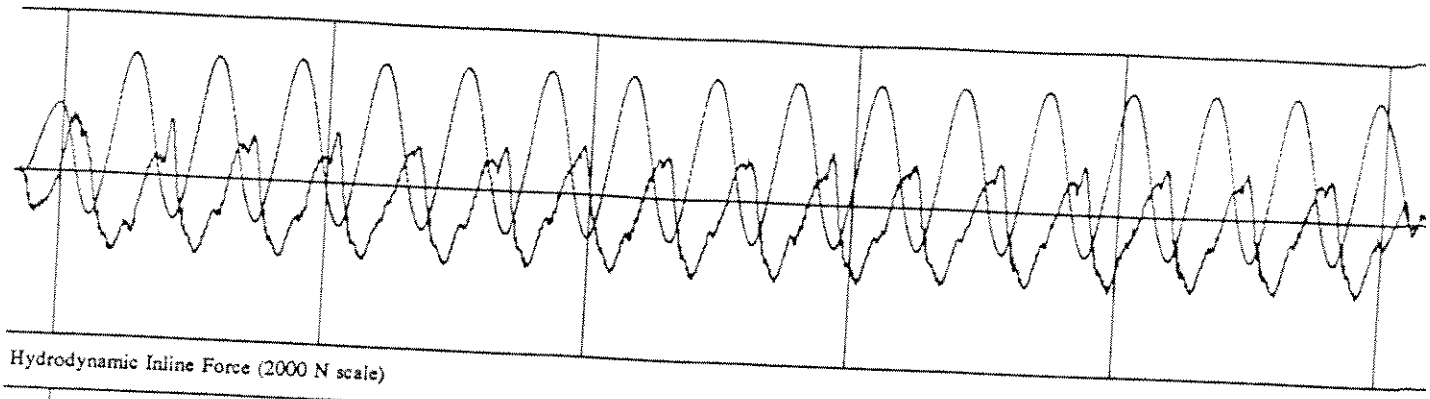

Hydrodynamic Inline Force (2000 N scale)

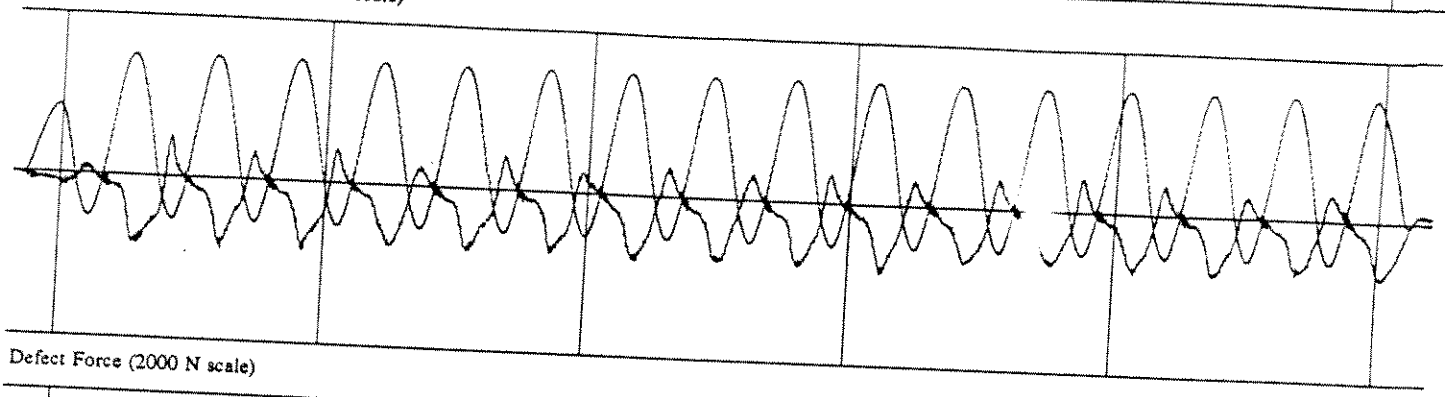

Defect Force (2000 N scale)

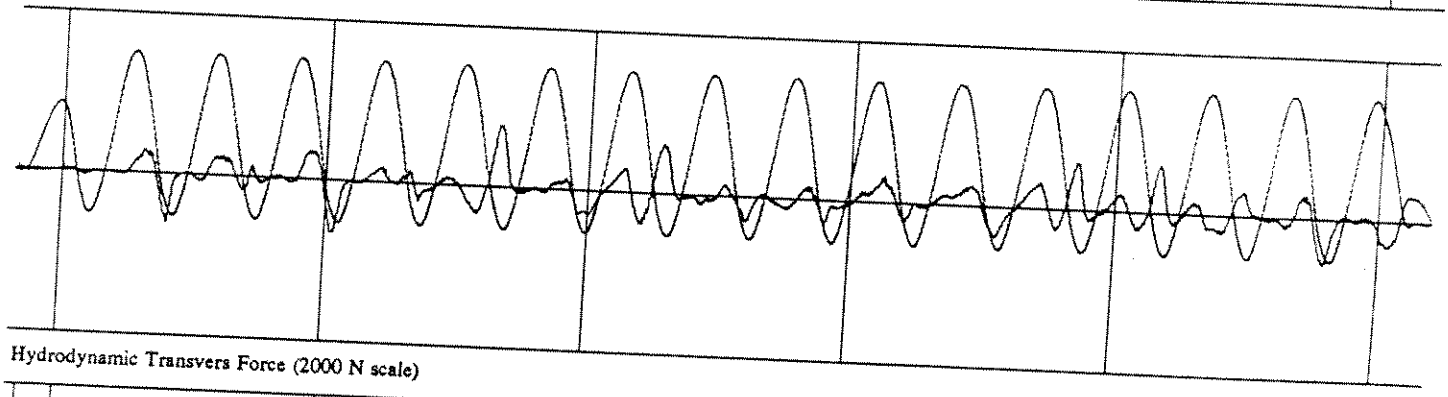

Hydrodynamic Transvers Force (2000 N scale)

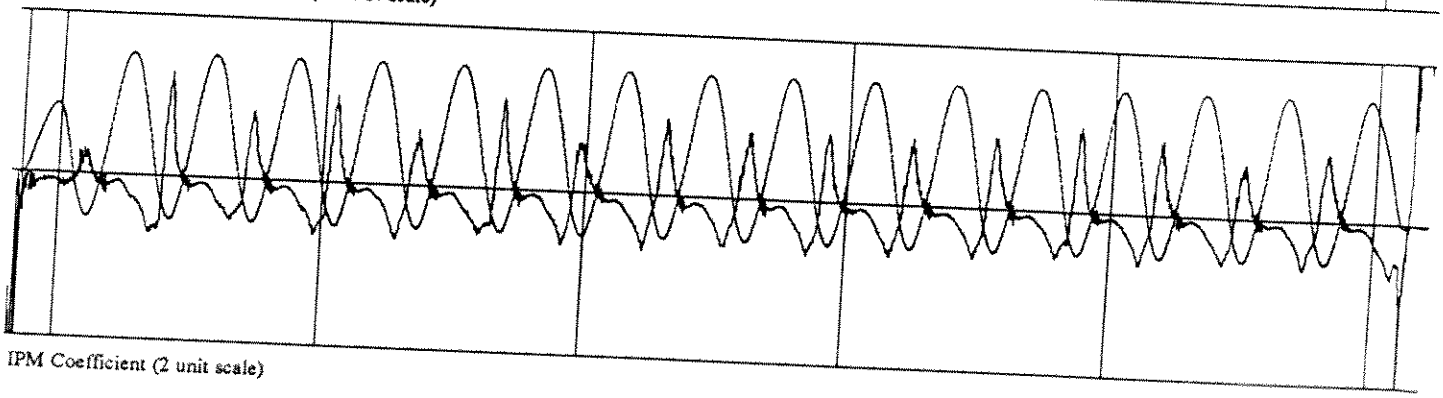

IPM Coefficient (2 unit scale)

PROCESSED DATA for RUN 368 points 820 to 6200

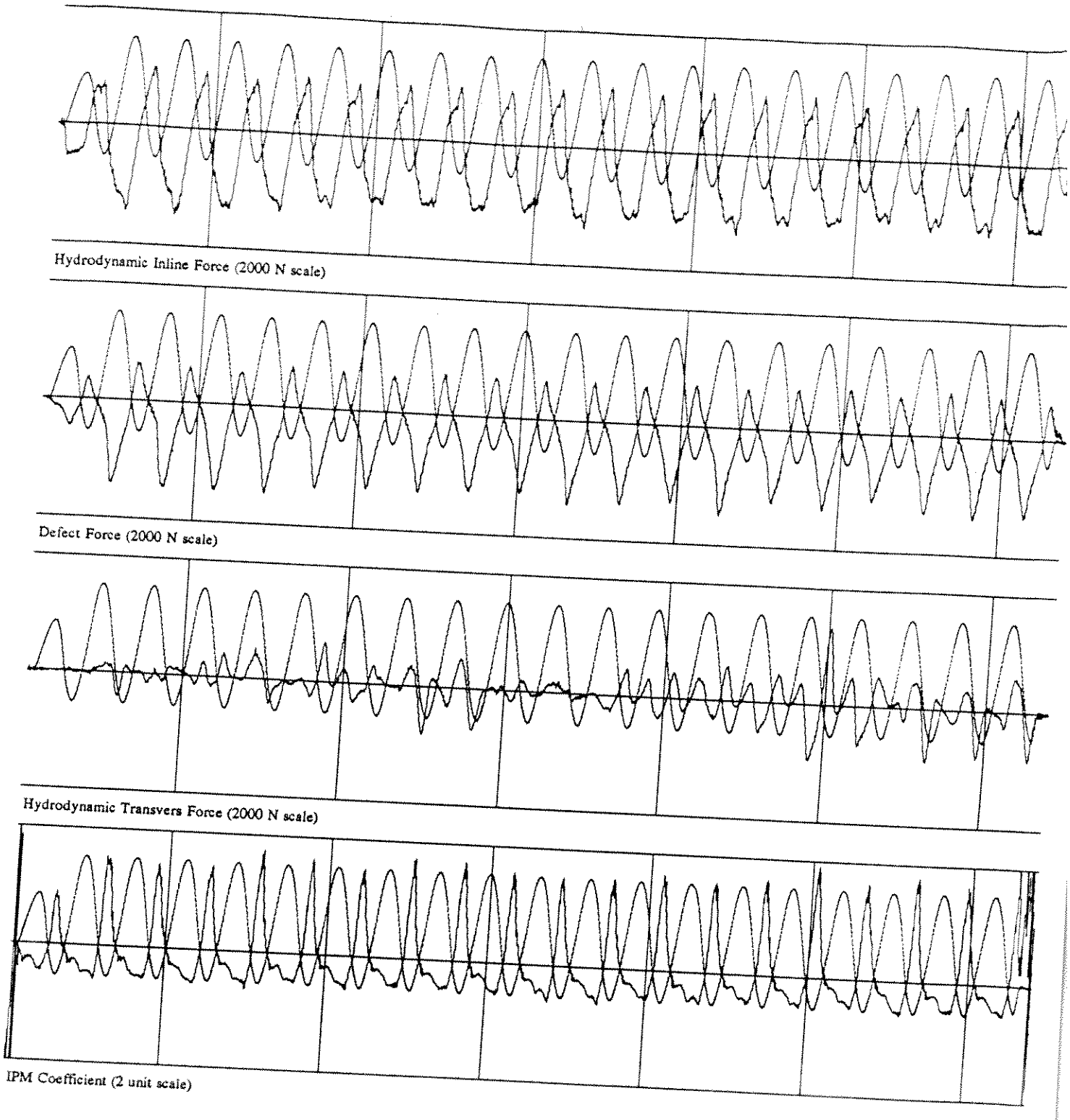

PROCESSED DATA for RUN 117 points 1045 to 7380

R-6-88-0-0.5+

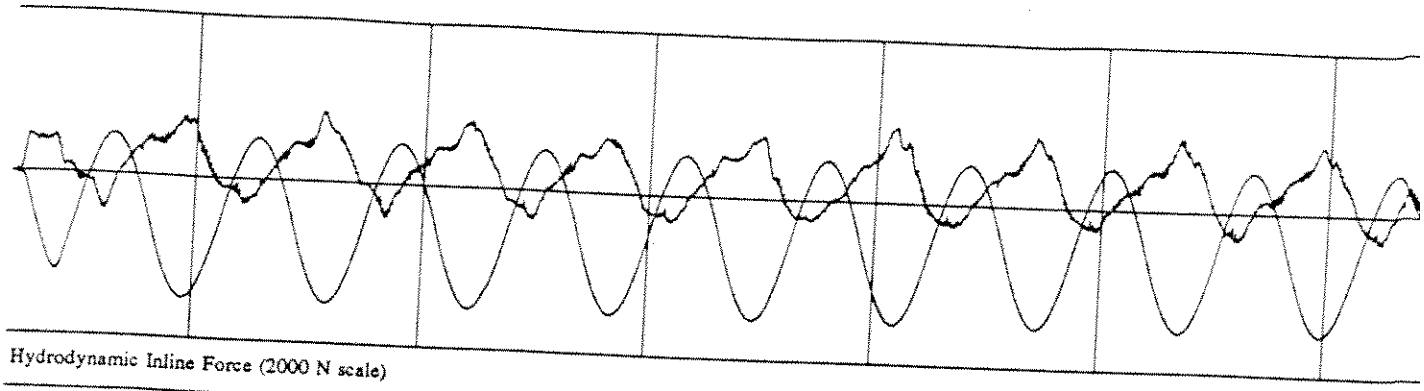

Hydrodynamic Inline Force (2000 N scale)

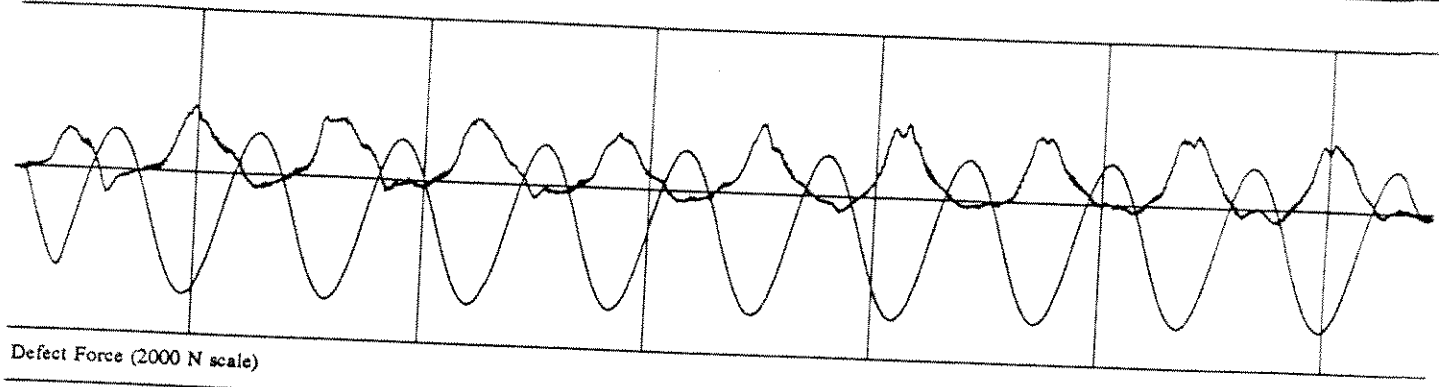

Defect Force (2000 N scale)

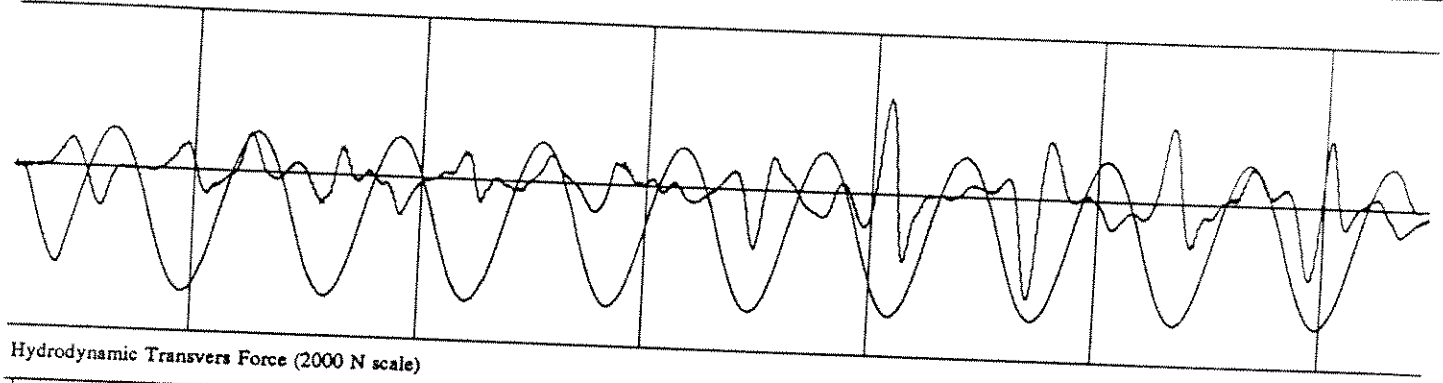

Hydrodynamic Transvers Force (2000 N scale)

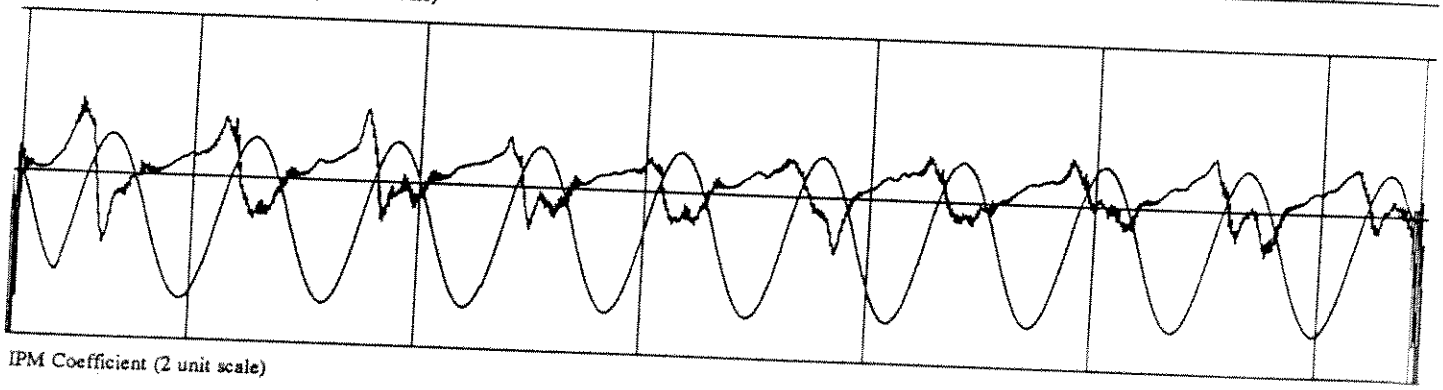

IPM Coefficient (2 unit scale)

PROCESSED DATA for RUN 369 points 1200 to 7460

S-12-88-0-0.5

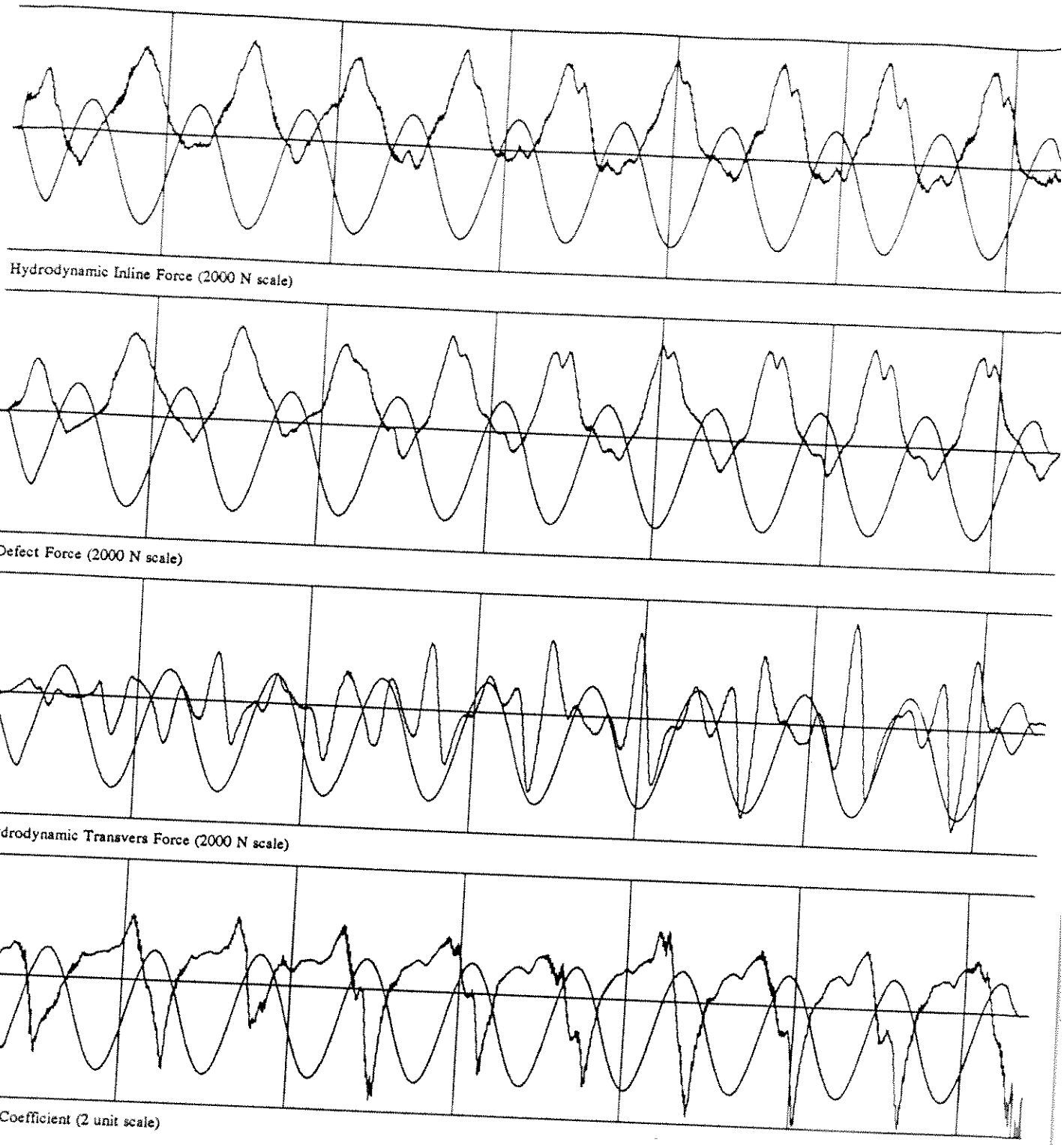

PROCESSED DATA for RUN 114 points 1110 to 7375

R-12-88-0-0.5

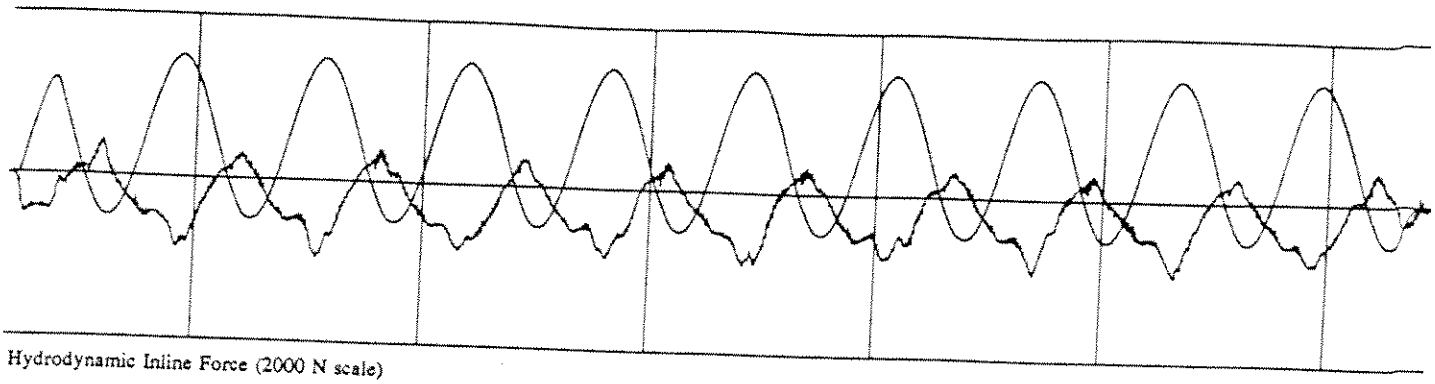

Hydrodynamic Inline Force (2000 N scale)

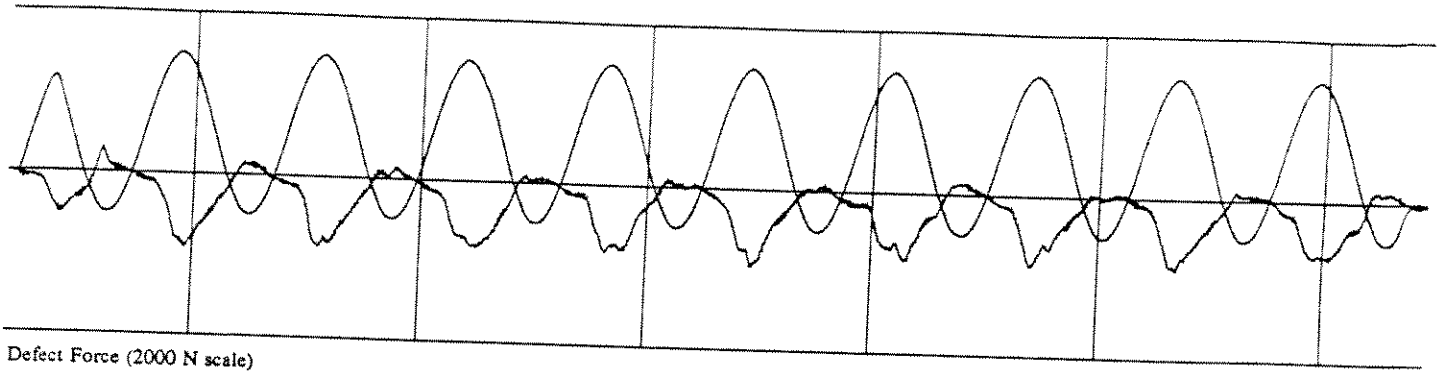

Defect Force (2000 N scale)

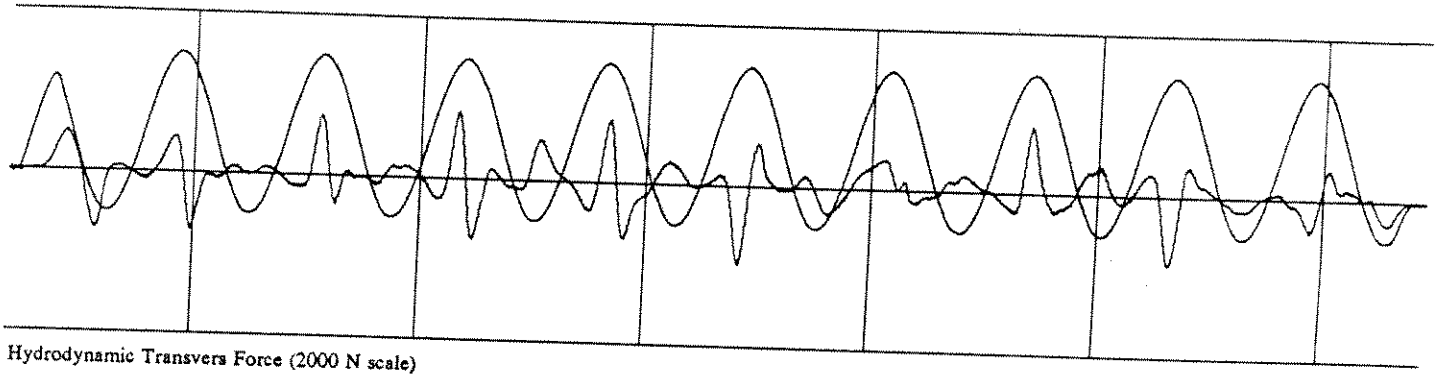

Hydrodynamic Transvers Force (2000 N scale)

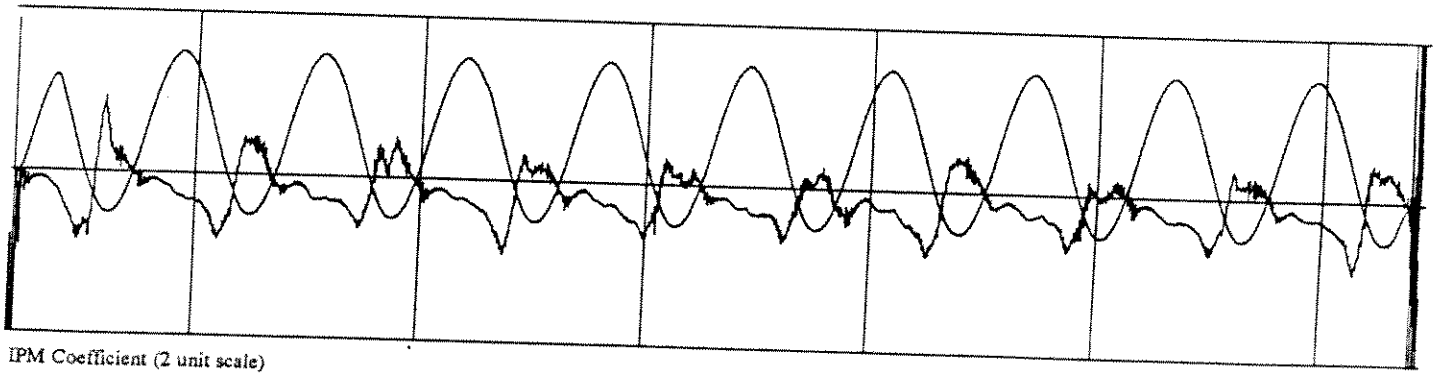

IPM Coefficient (2 unit scale)

PROCESSED DATA for RUN 370 points 1185 to 7450

S-12-88-0-0.5+

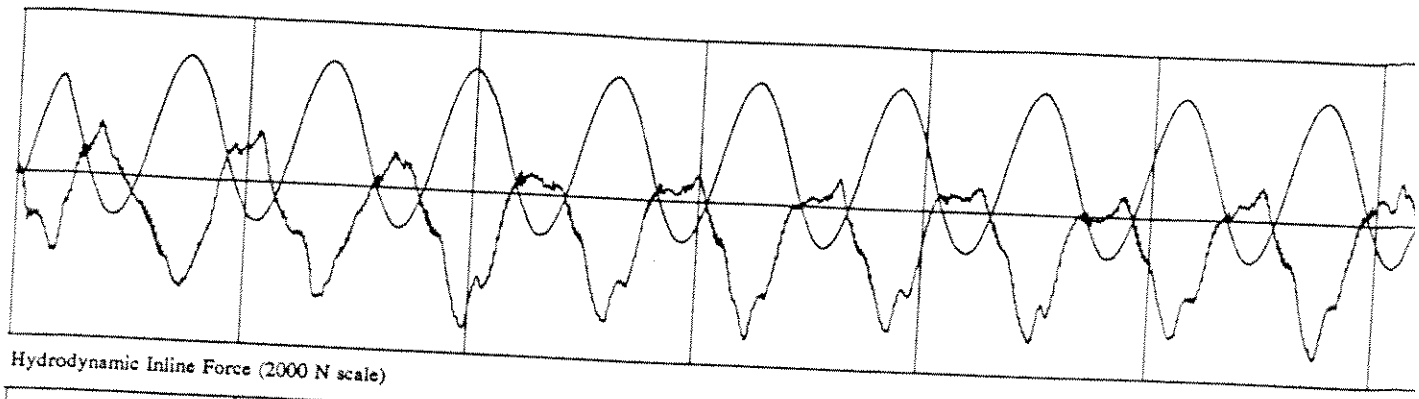

Hydrodynamic Inline Force (2000 N scale)

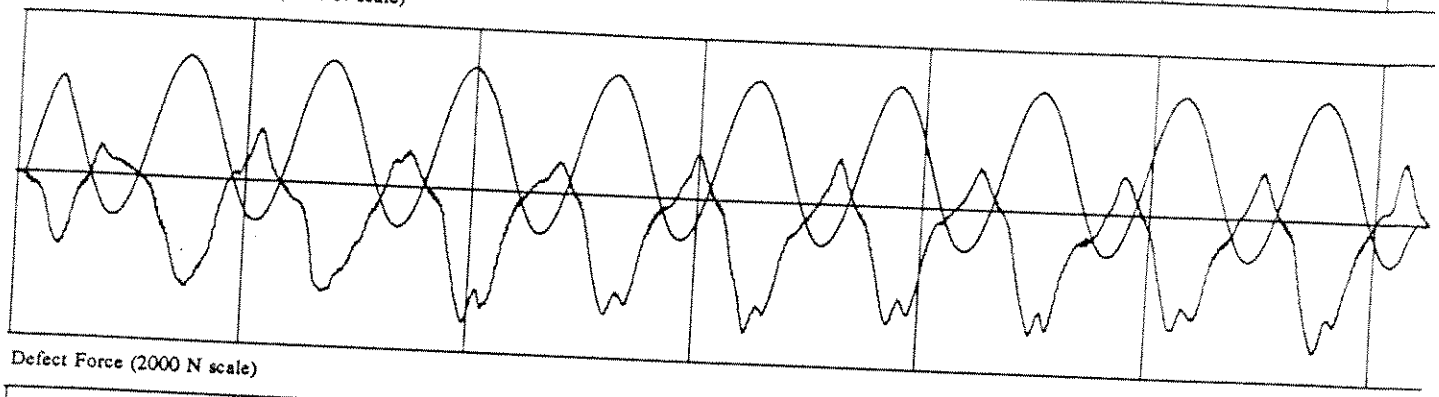

Defect Force (2000 N scale)

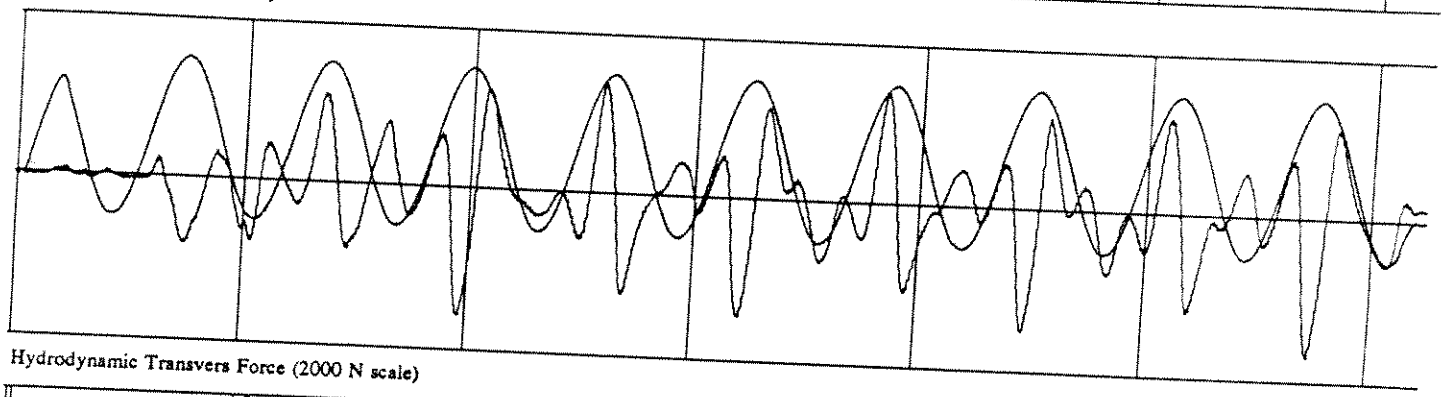

Hydrodynamic Transvers Force (2000 N scale)

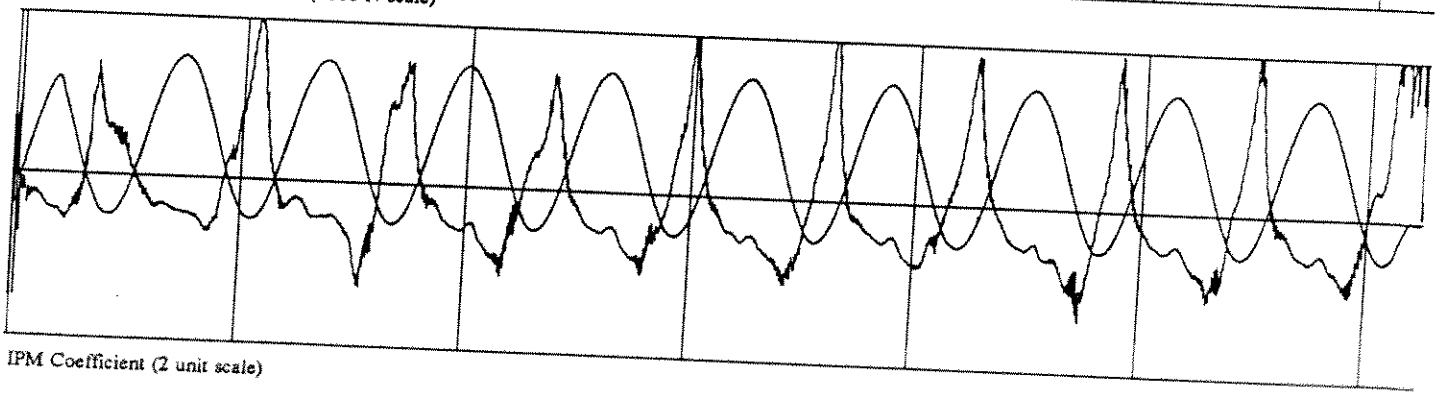

IPM Coefficient (2 unit scale)

PROCESSED DATA for RUN 115 points 987 to 7236

R-12-88-0-0.5+

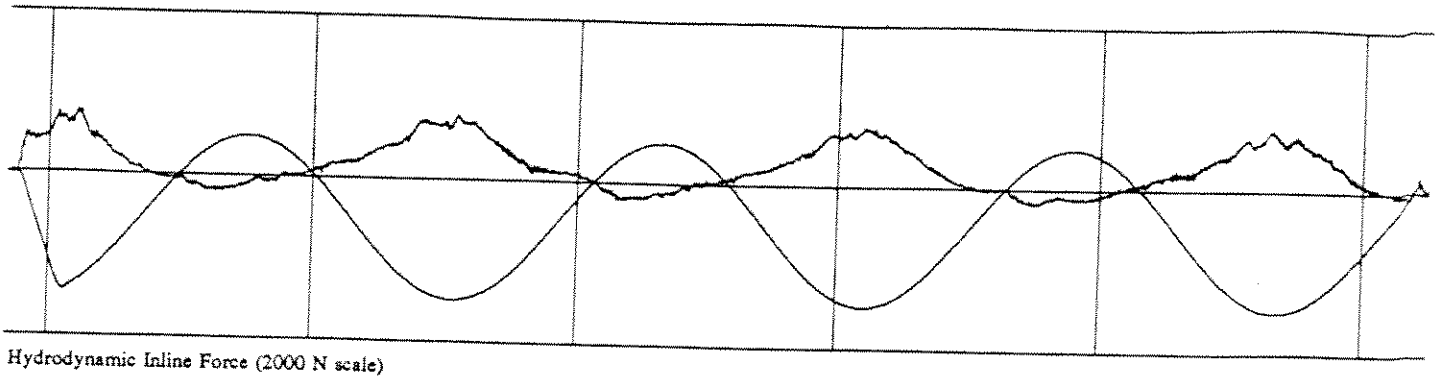

Hydrodynamic Inline Force (2000 N scale)

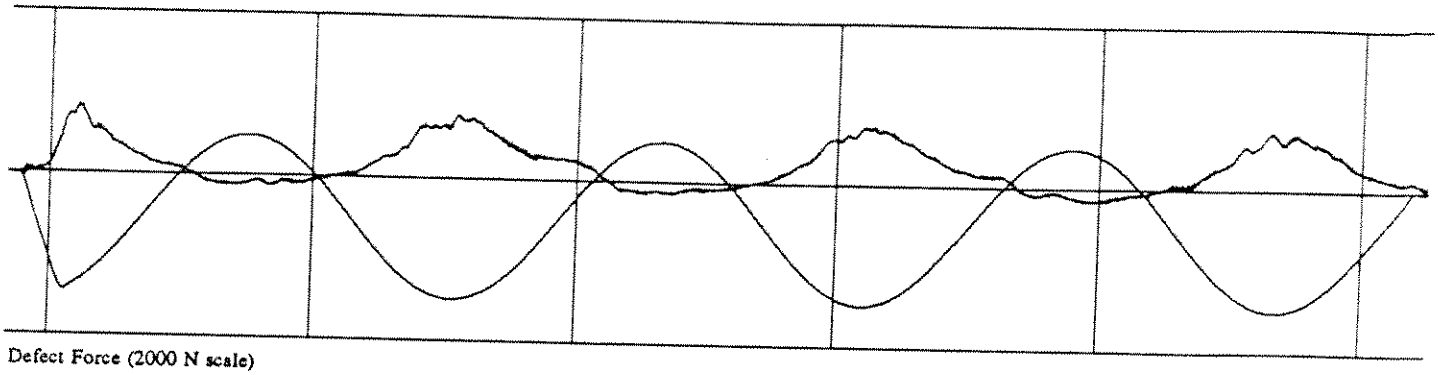

Defect Force (2000 N scale)

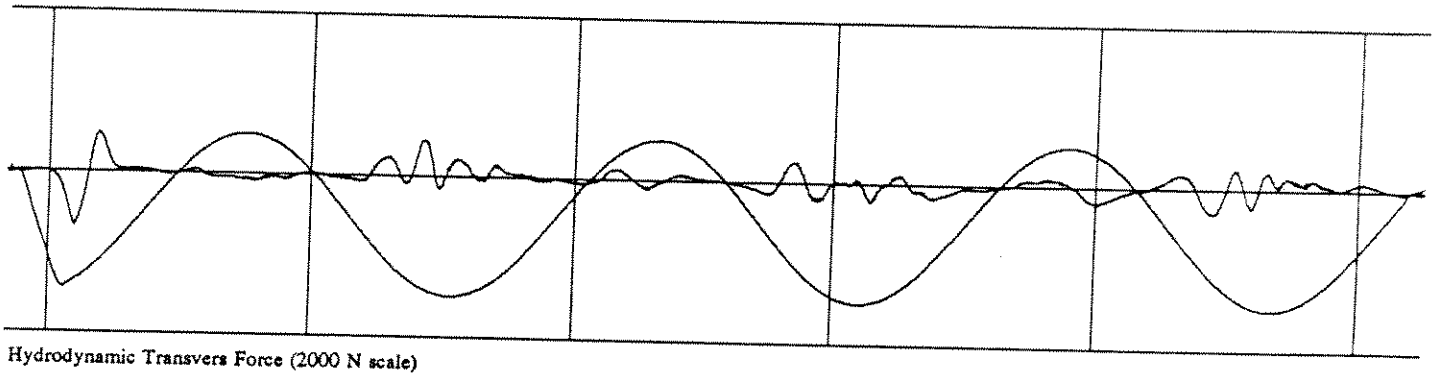

Hydrodynamic Transvers Force (2000 N scale)

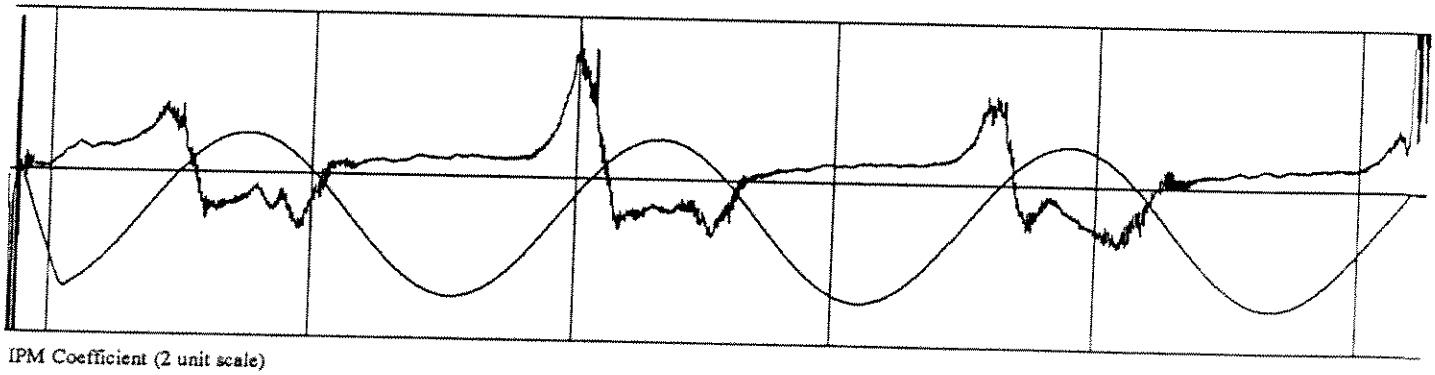

IPM Coefficient (2 unit scale)

PROCESSED DATA for RUN 371 points 840 to 6250

S-31-88-0-0.5

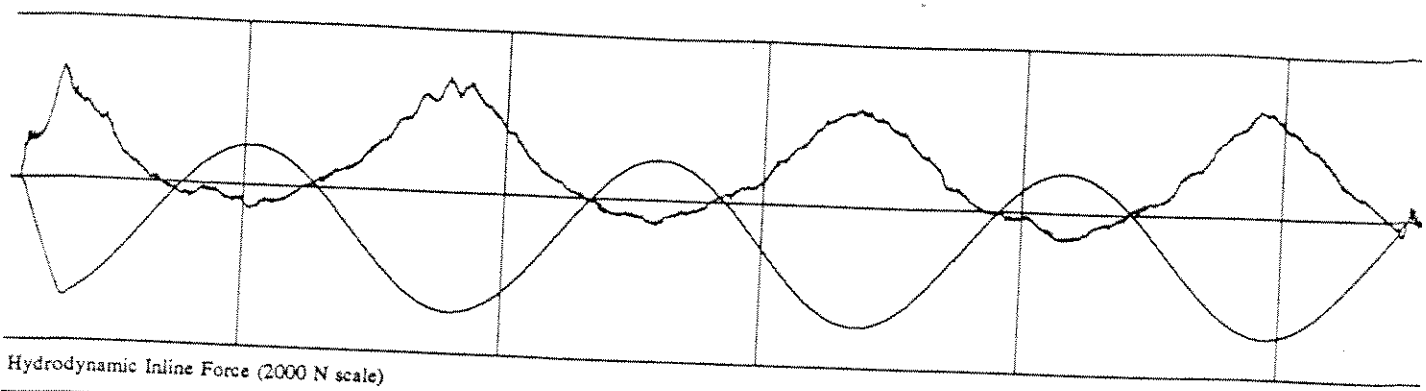

Hydrodynamic Inline Force (2000 N scale)

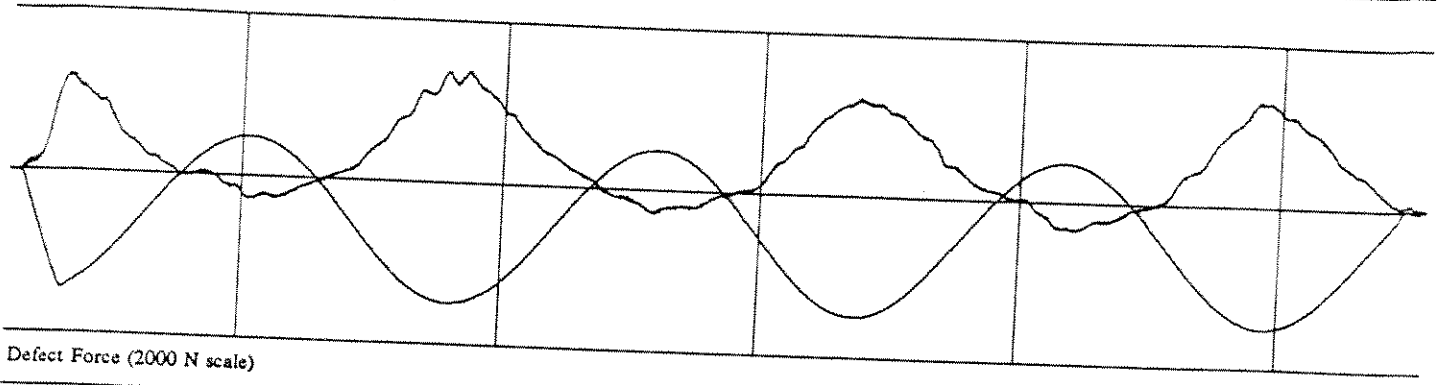

Defect Force (2000 N scale)

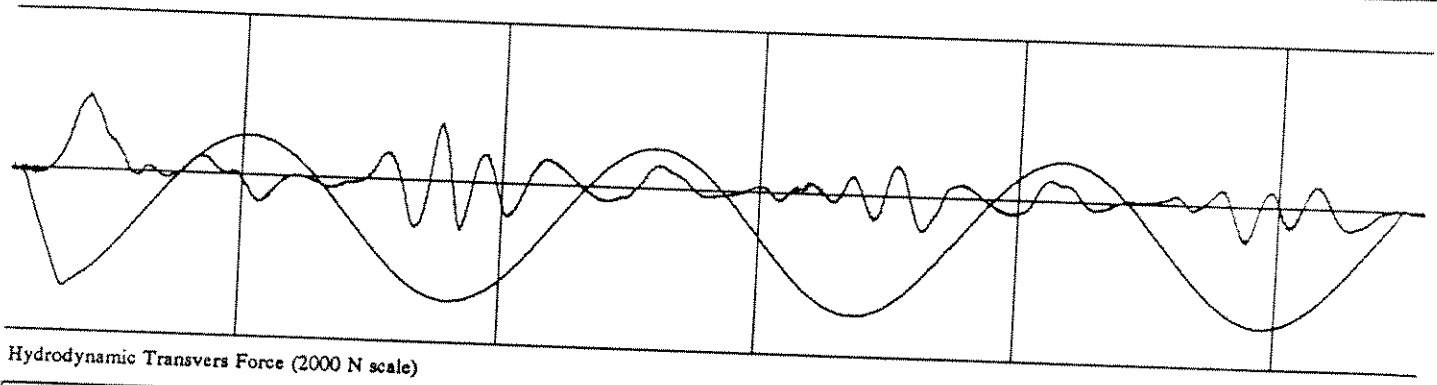

Hydrodynamic Transvers Force (2000 N scale)

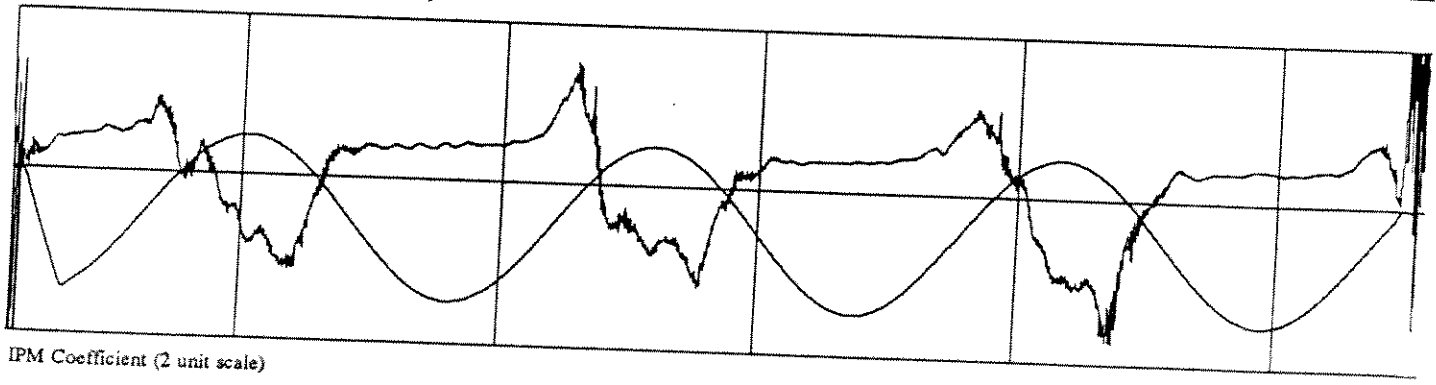

IPM Coefficient (2 unit scale)

PROCESSED DATA for RUN 110 points 1120 to 6550

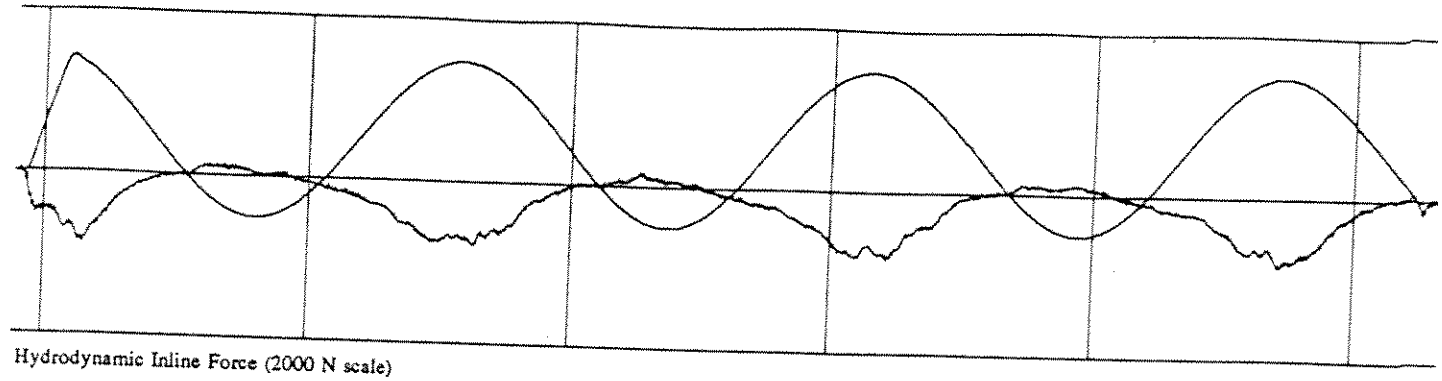

Hydrodynamic Inline Force (2000 N scale)

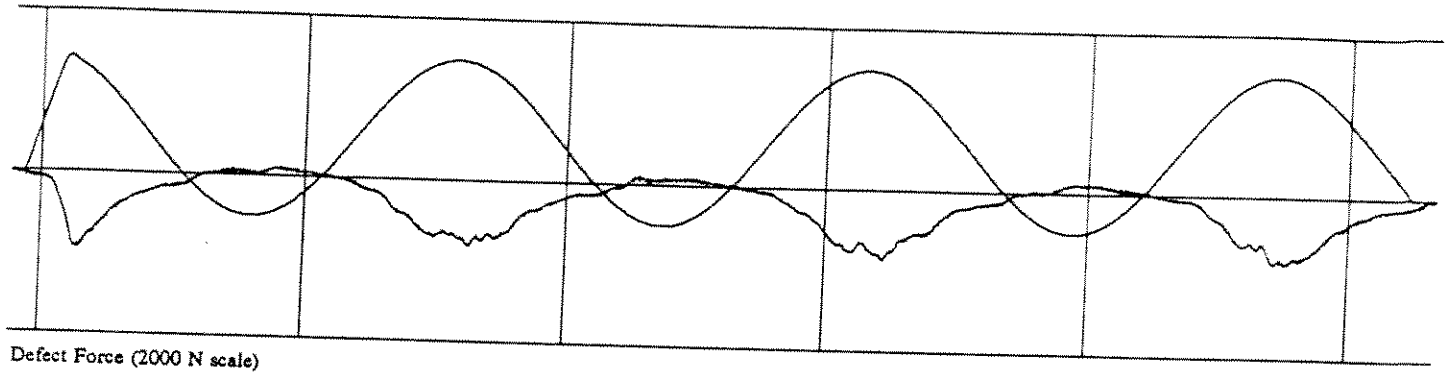

Defect Force (2000 N scale)

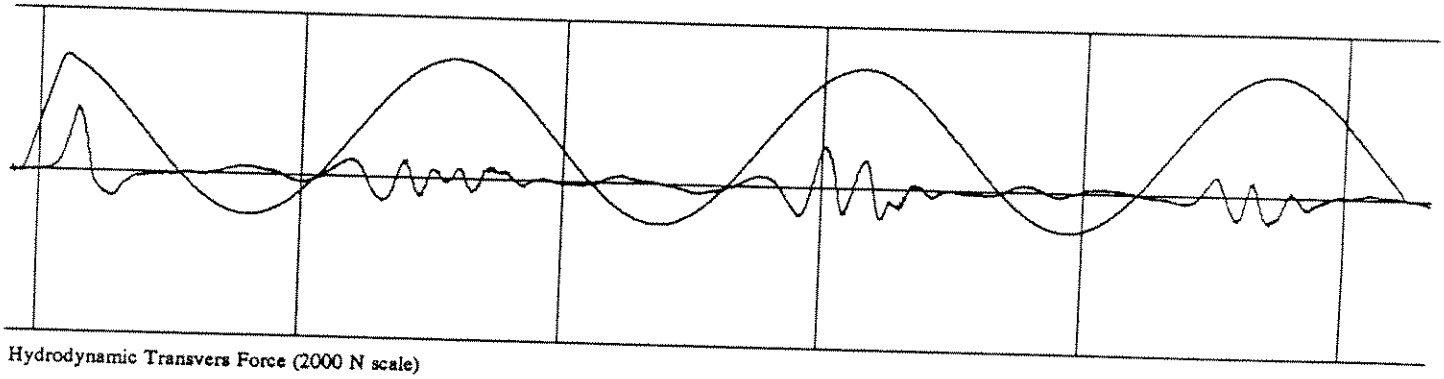

Hydrodynamic Transvers Force (2000 N scale)

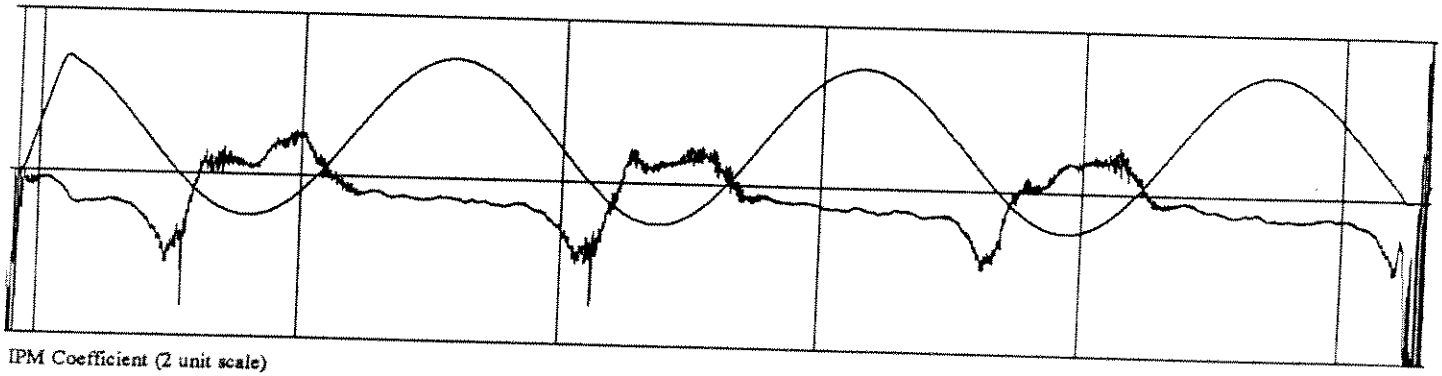

IPM Coefficient (2 unit scale)

PROCESSED DATA for RUN 372 points 890 to 6330

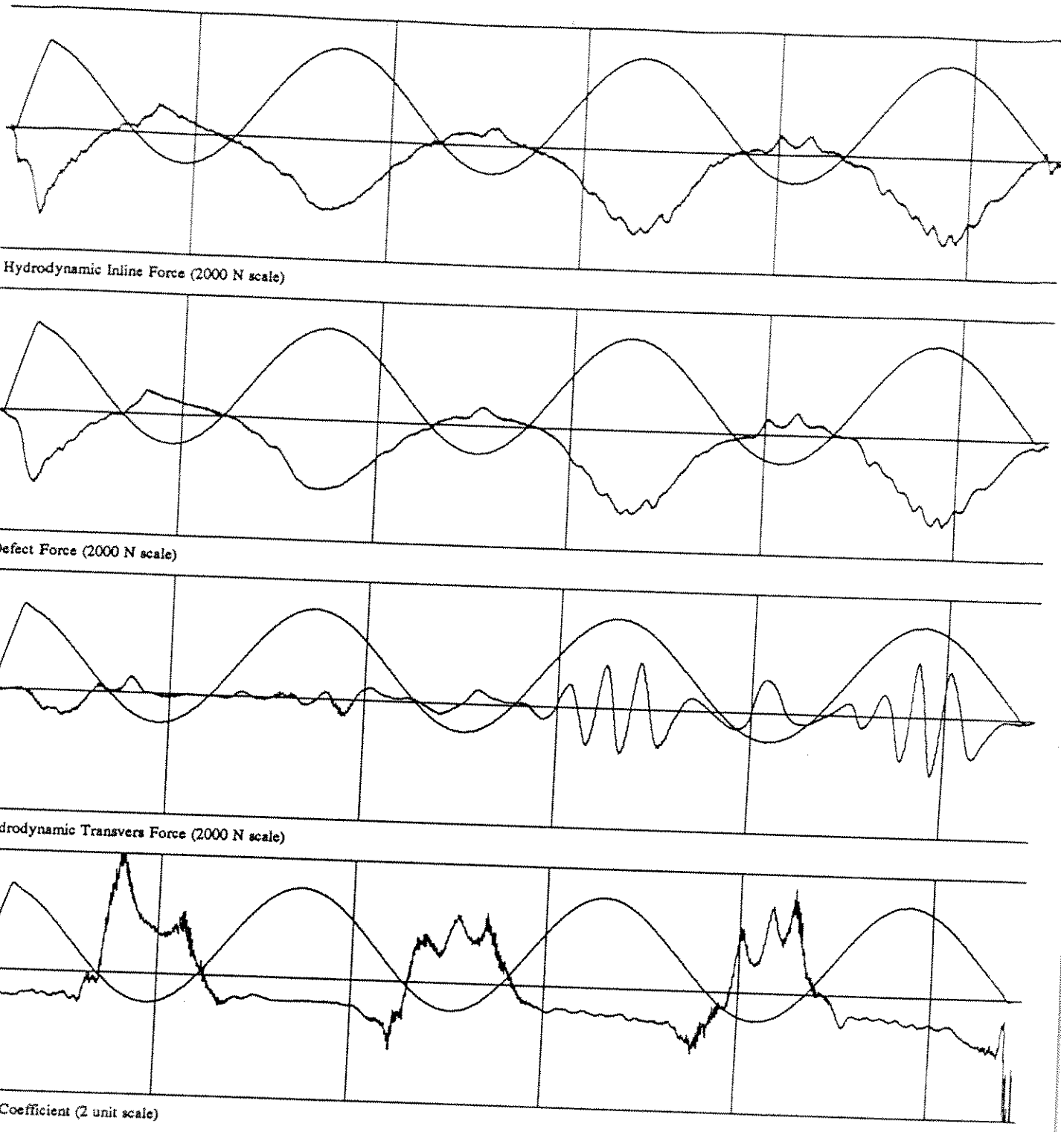

PROCESSED DATA for RUN 111 points 1040 to 6460

R-31-88-0-0.5+

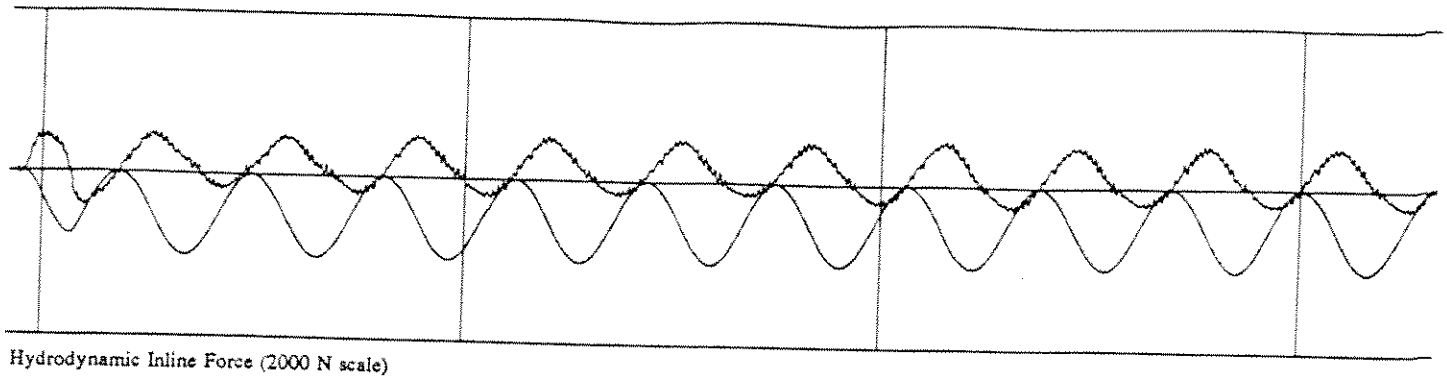

Hydrodynamic Inline Force (2000 N scale)

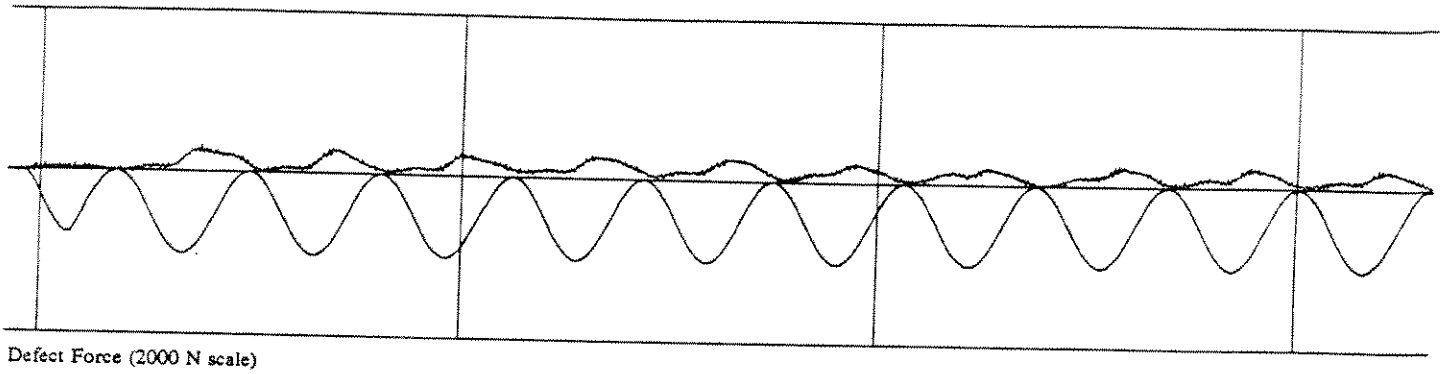

Defect Force (2000 N scale)

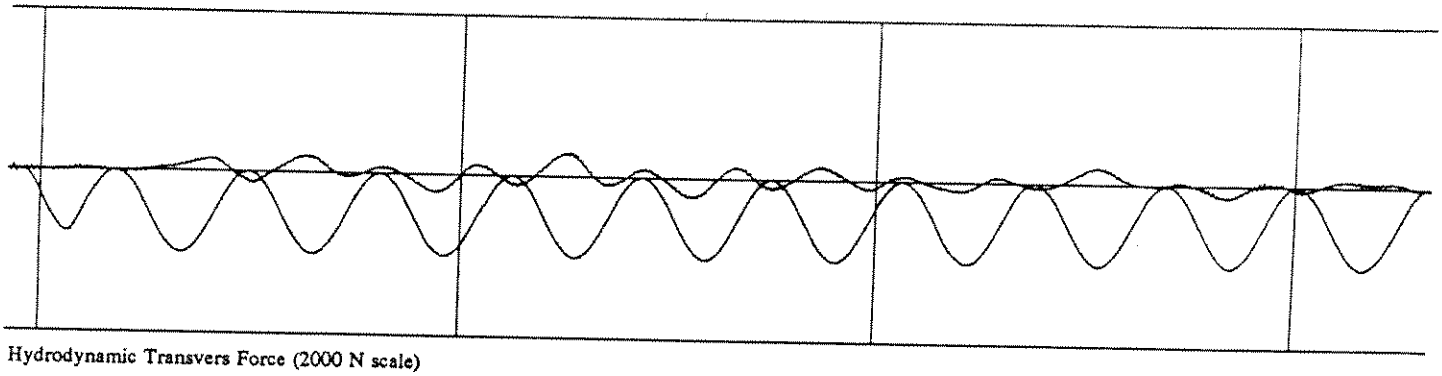

Hydrodynamic Transvers Force (2000 N scale)

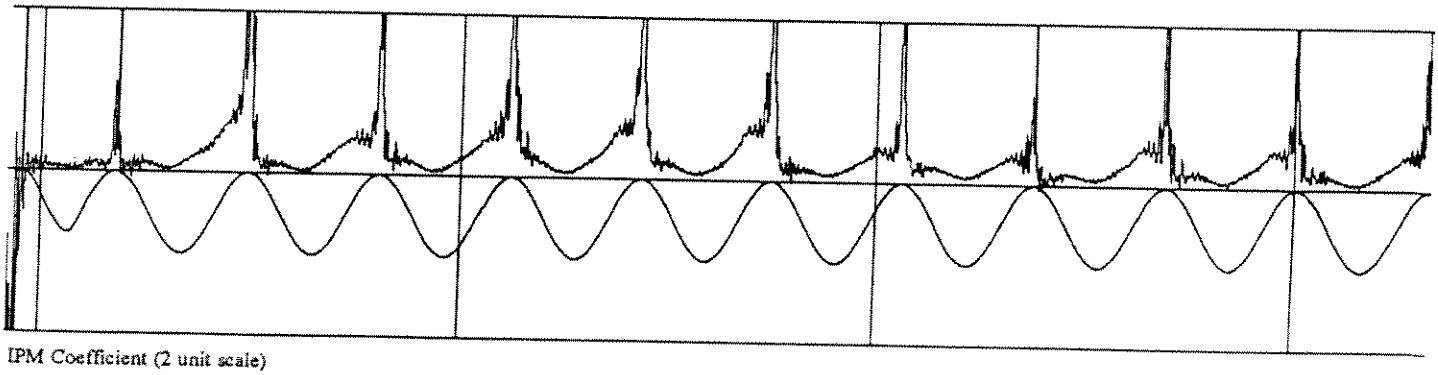

IPM Coefficient (2 unit scale)

PROCESSED DATA for RUN 373 points 920 to 4320

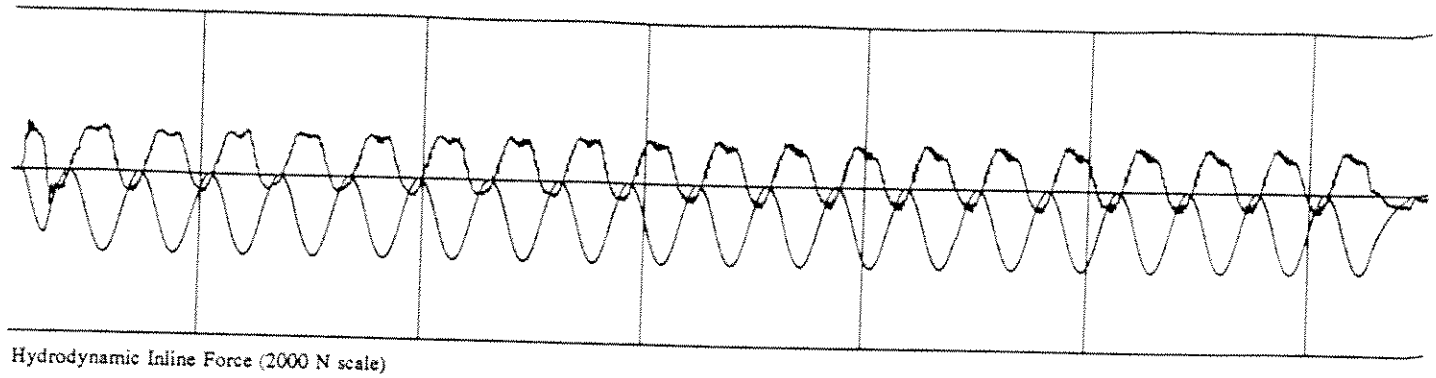

Hydrodynamic Inline Force (2000 N scale)

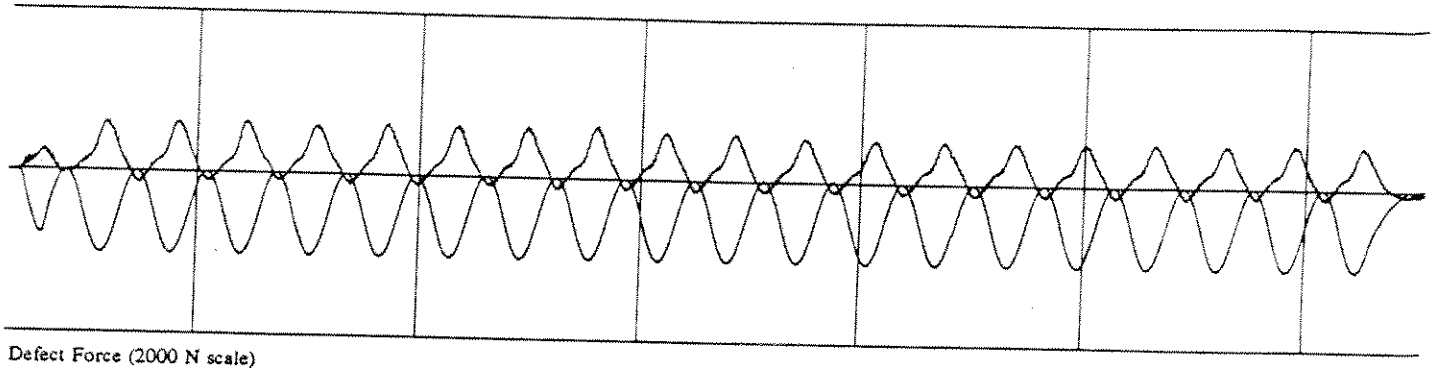

Defect Force (2000 N scale)

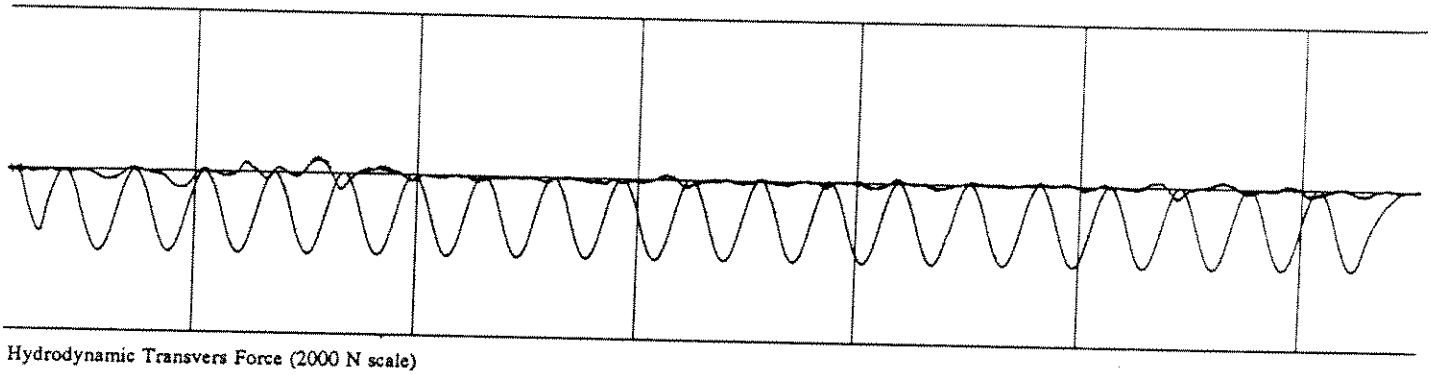

Hydrodynamic Transvers Force (2000 N scale)

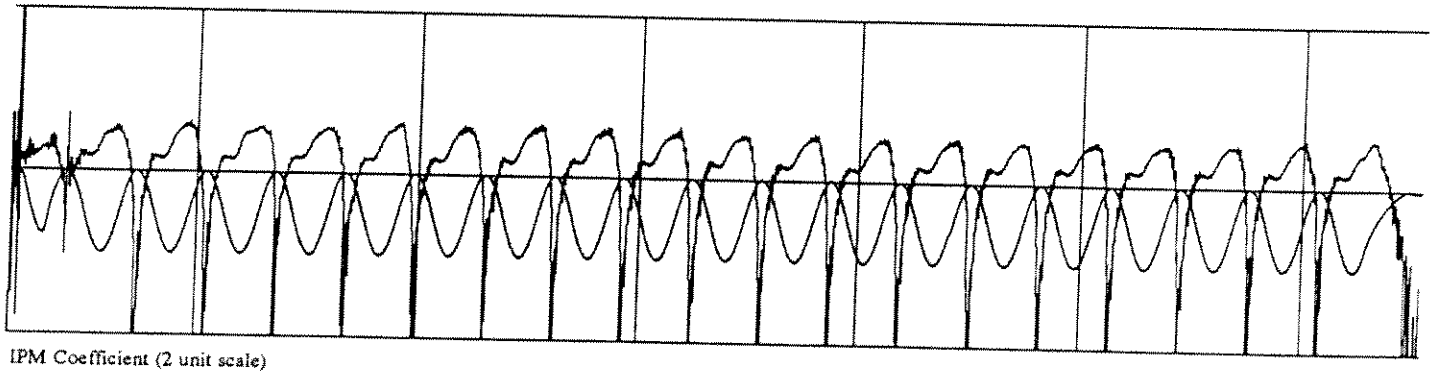

IPM Coefficient (2 unit scale)

PROCESSED DATA for RUN 116 points 1160 to 7535

R-3-44-0-1.0

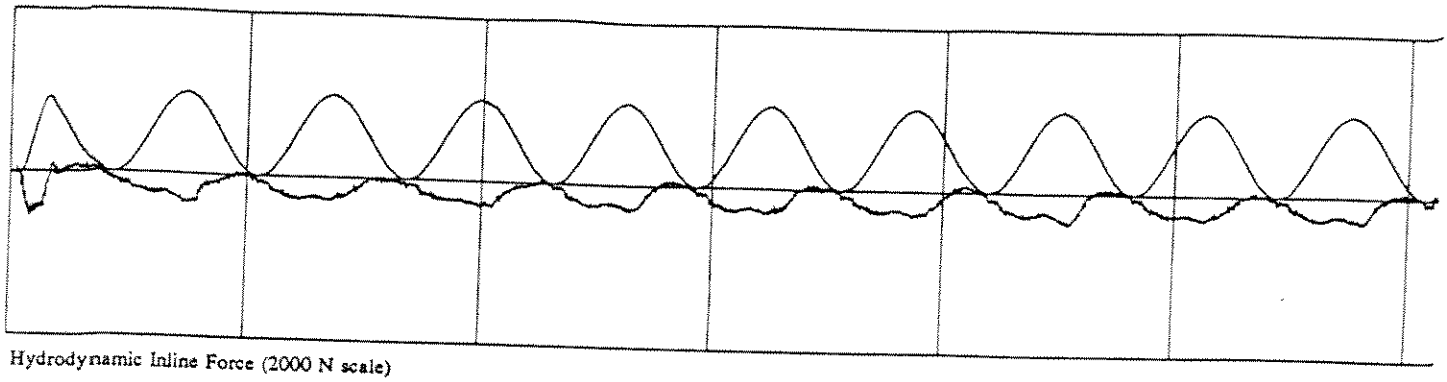

Hydrodynamic Inline Force (2000 N scale)

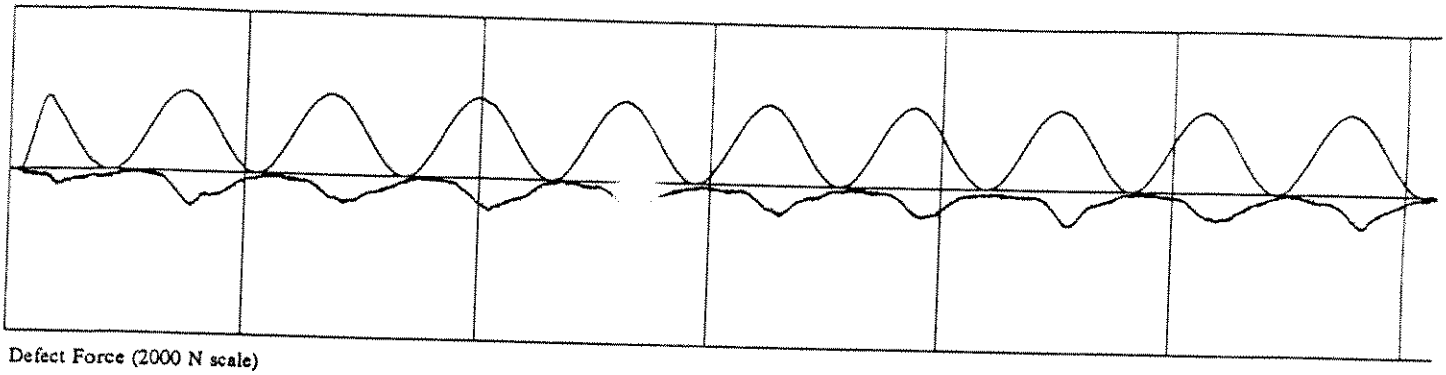

Defect Force (2000 N scale)

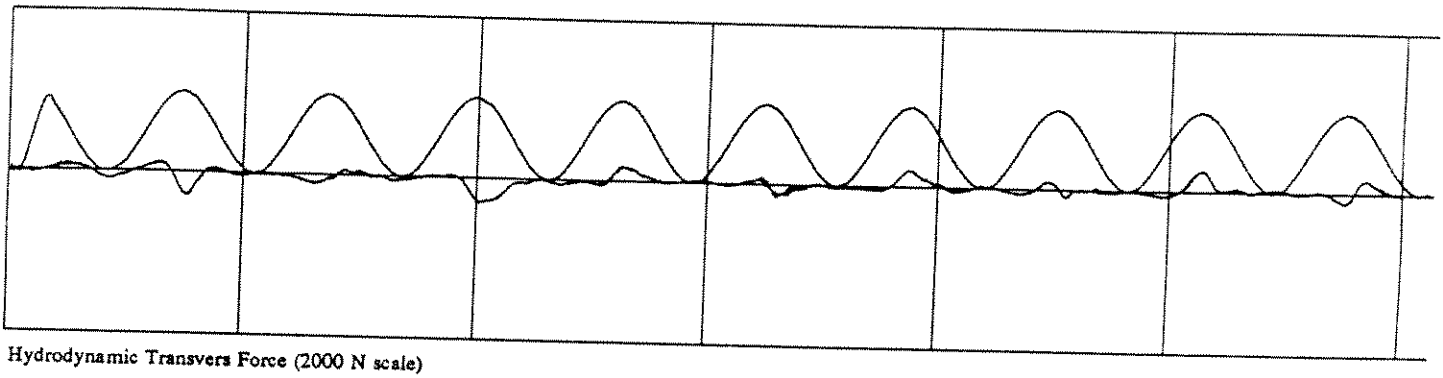

Hydrodynamic Transvers Force (2000 N scale)

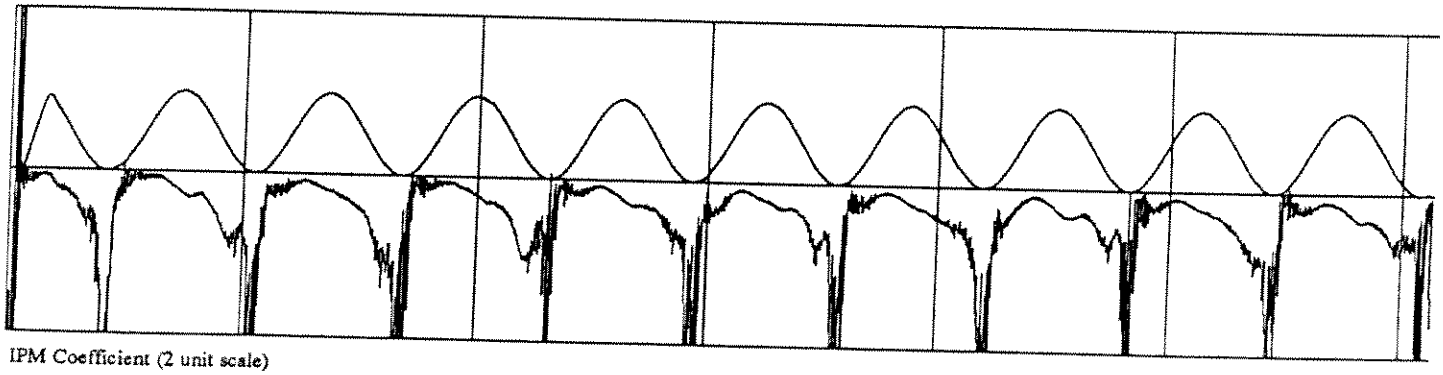

IPM Coefficient (2 unit scale)

PROCESSED DATA for RUN 374 points 1000 to 7127

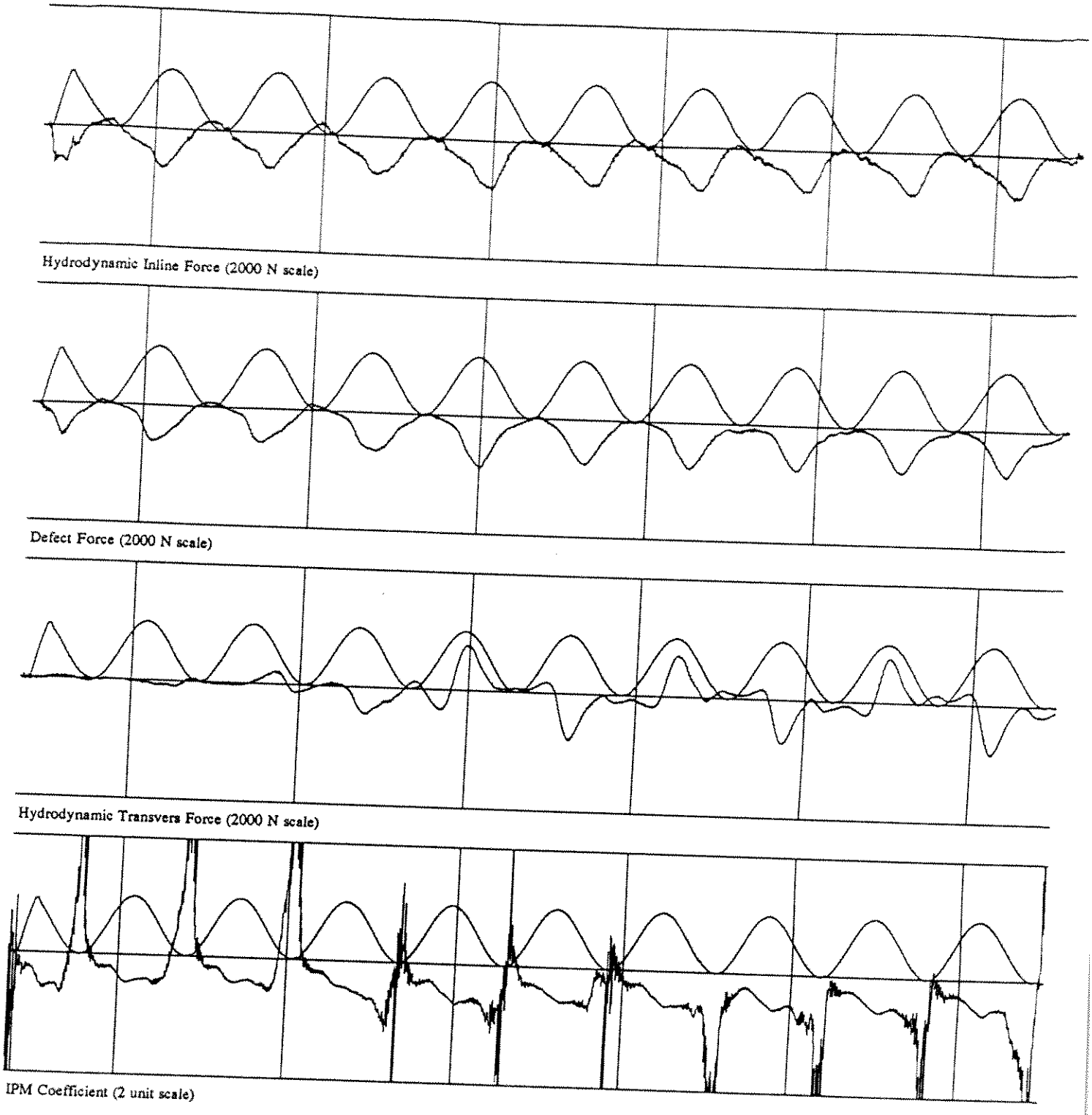

PROCESSED DATA for RUN 113 points 1357 to 7490

R-6-44-0-1.0+

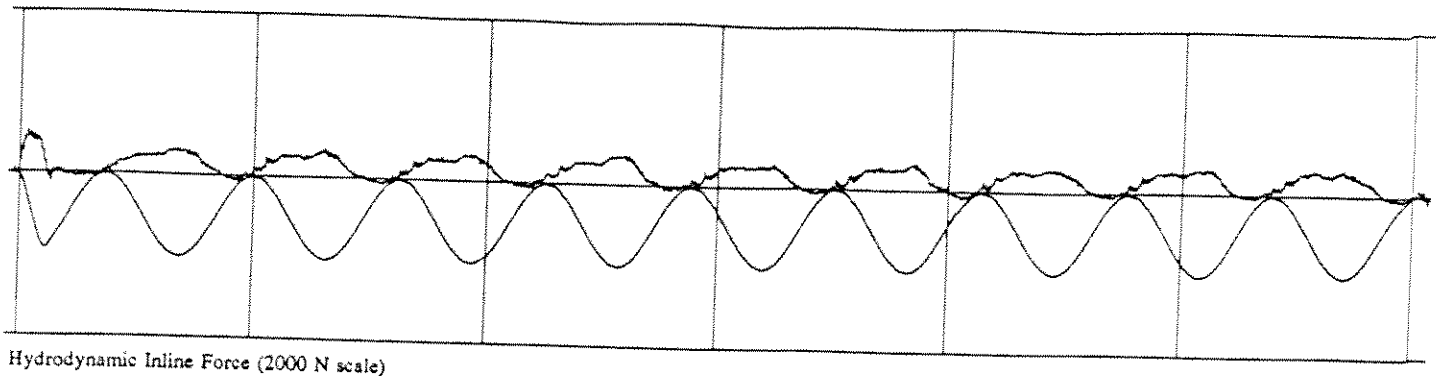

Hydrodynamic Inline Force (2000 N scale)

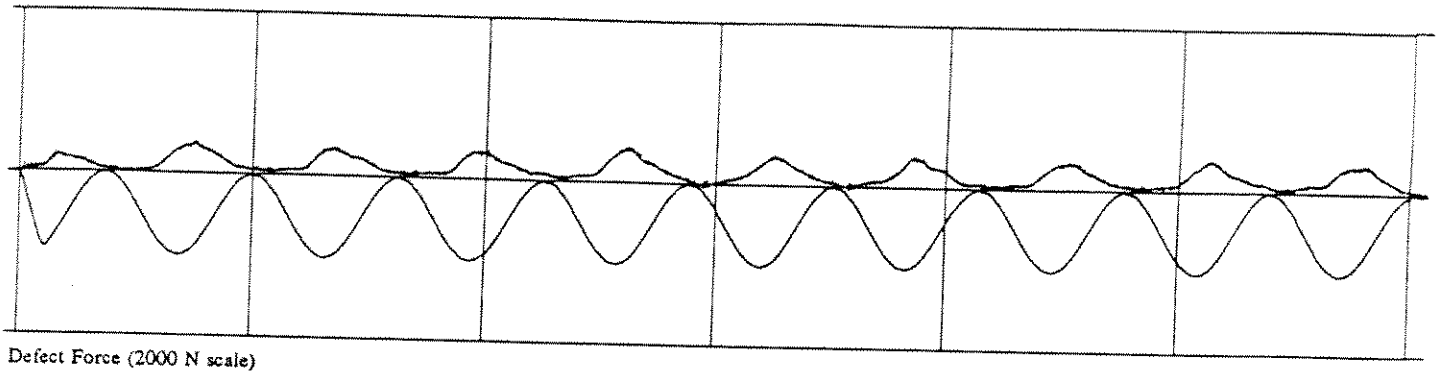

Defect Force (2000 N scale)

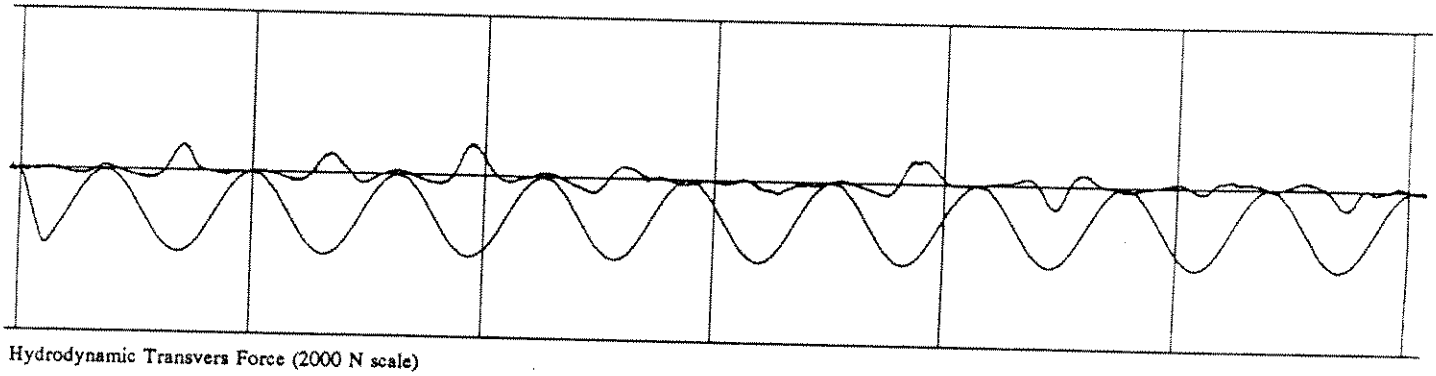

Hydrodynamic Transvers Force (2000 N scale)

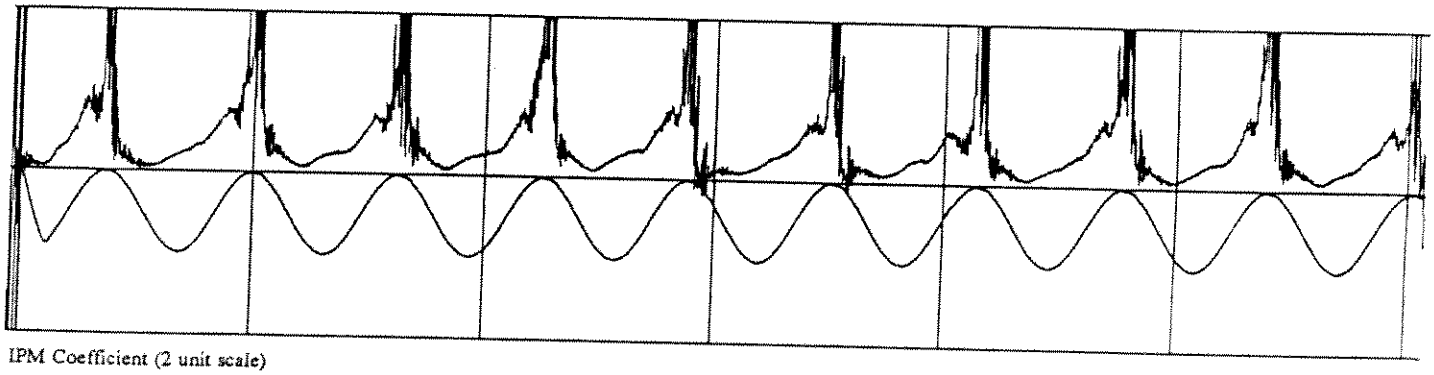

IPM Coefficient (2 unit scale)

PROCESSED DATA for RUN 375 points 950 to 7077

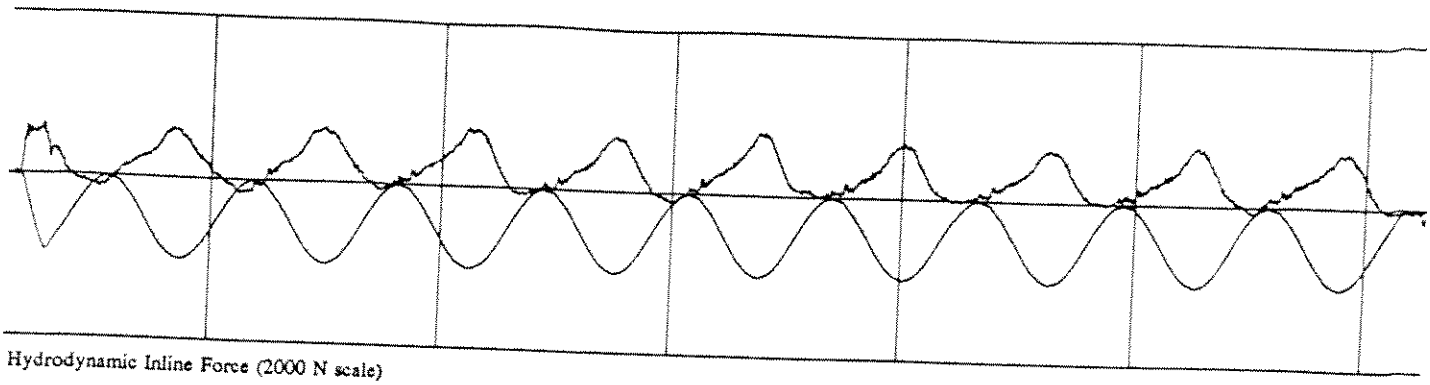

Hydrodynamic Inline Force (2000 N scale)

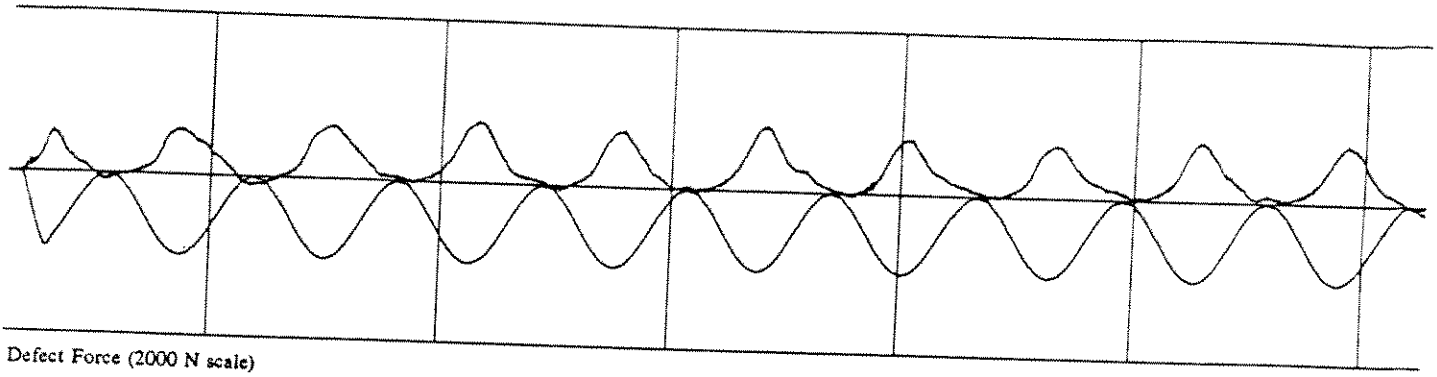

Defect Force (2000 N scale)

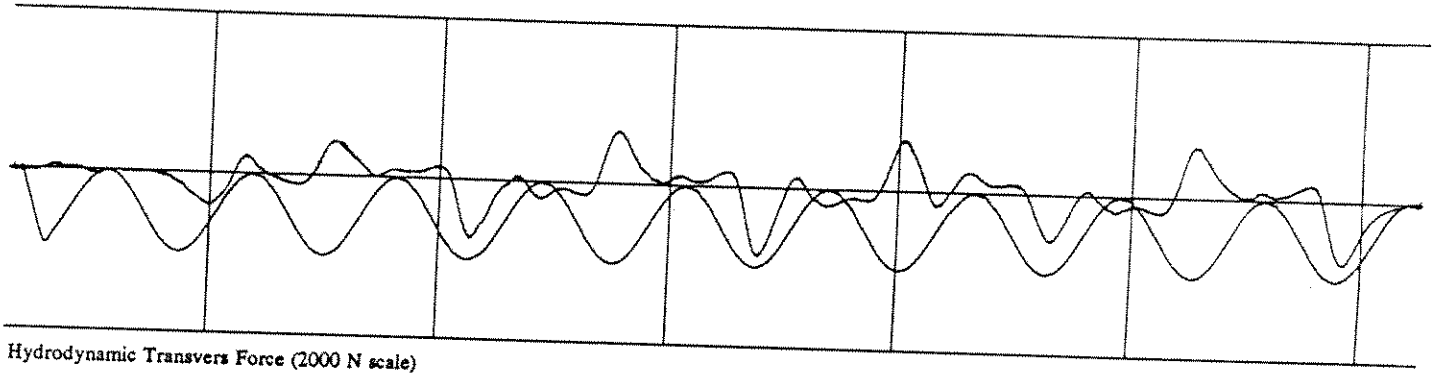

Hydrodynamic Transvers Force (2000 N scale)

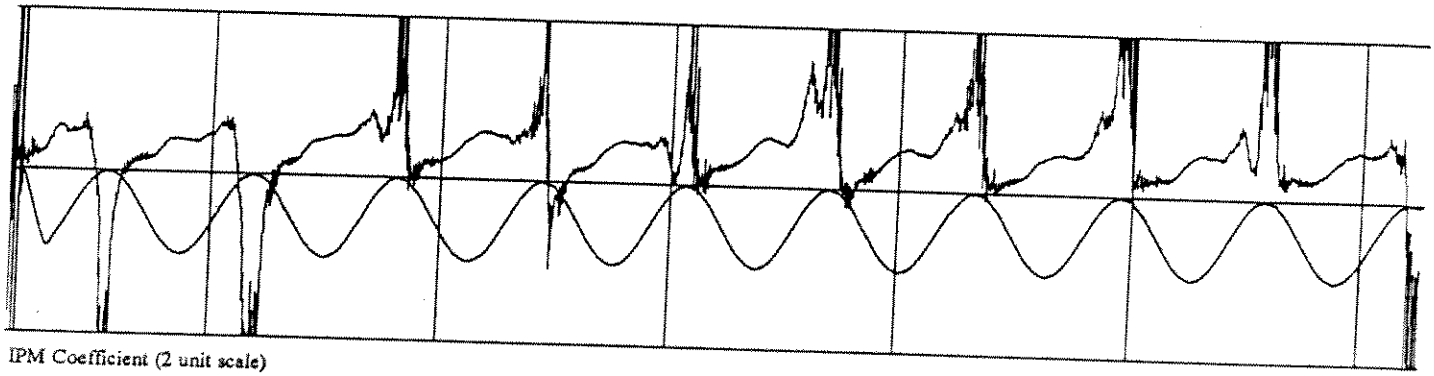

IPM Coefficient (2 unit scale)

PROCESSED DATA for RUN 112 points 1135 to 7260

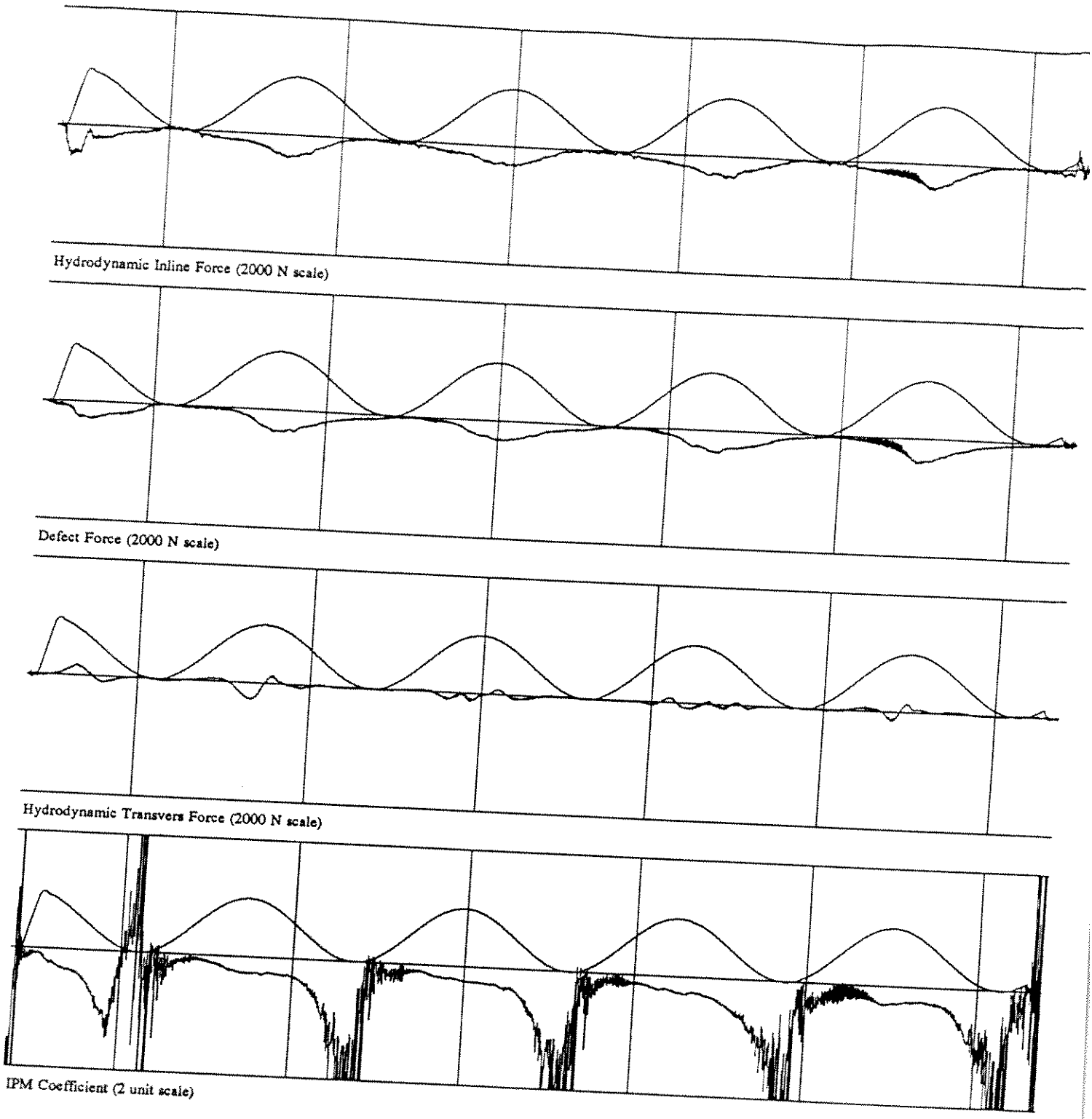

PROCESSED DATA for RUN 376 points 1360 to 7370

S-12-44-0-1.0+

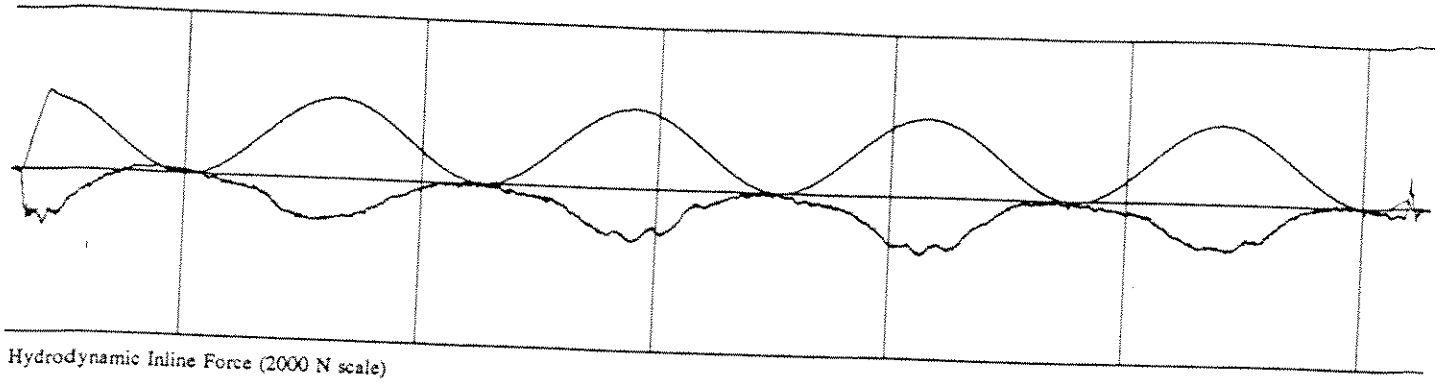

Hydrodynamic Inline Force (2000 N scale)

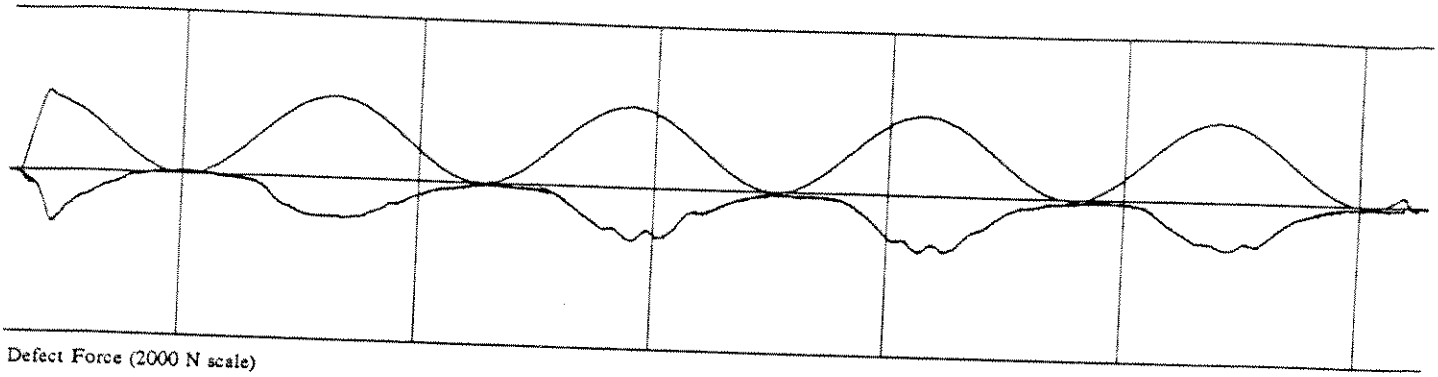

Defect Force (2000 N scale)

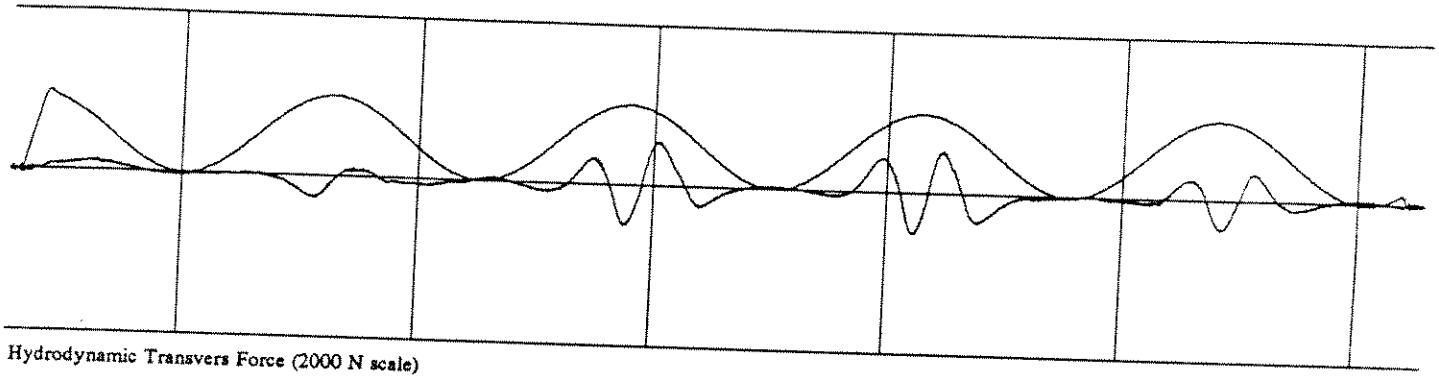

Hydrodynamic Transvers Force (2000 N scale)

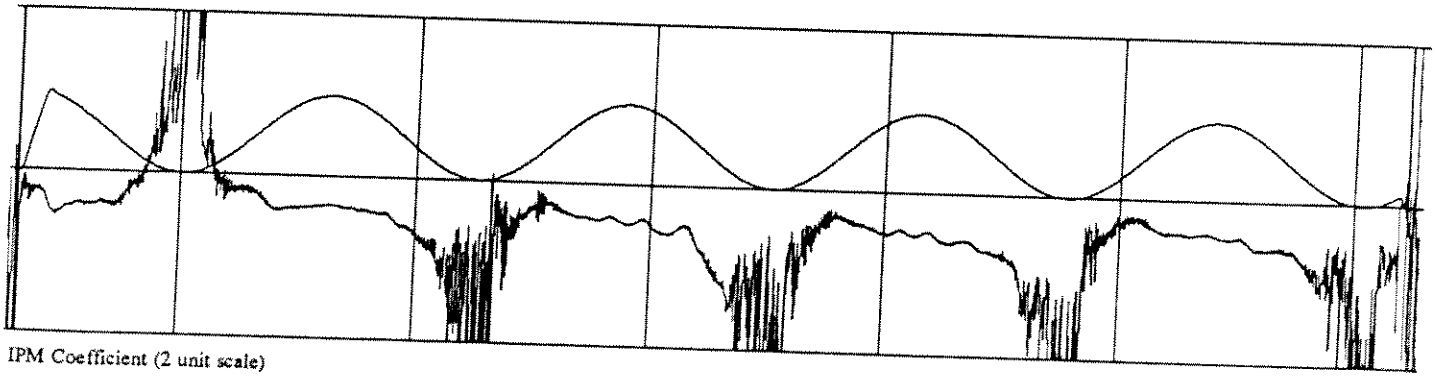

IPM Coefficient (2 unit scale)

PROCESSED DATA for RUN 129 points 1280 to 7280

R-12-44-0-1.0+

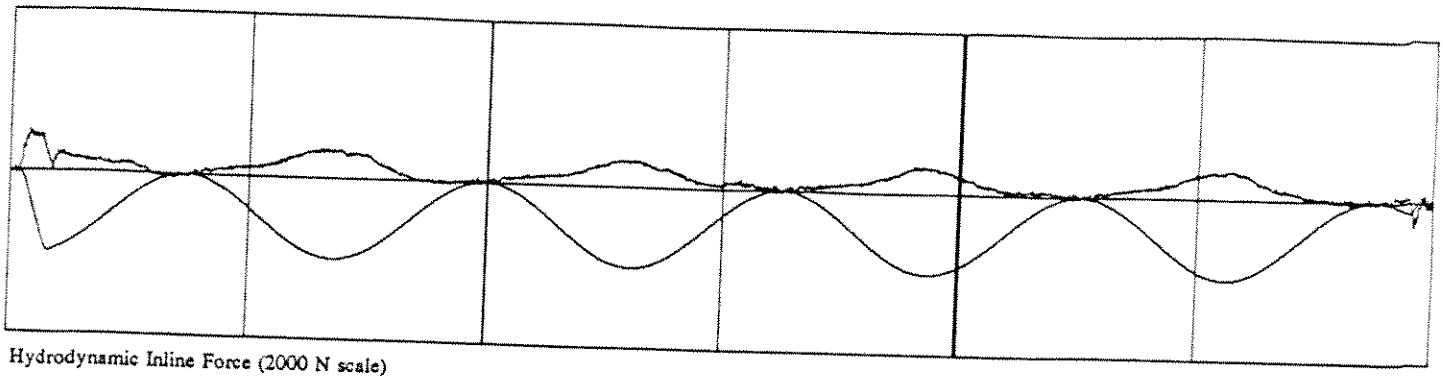

Hydrodynamic Inline Force (2000 N scale)

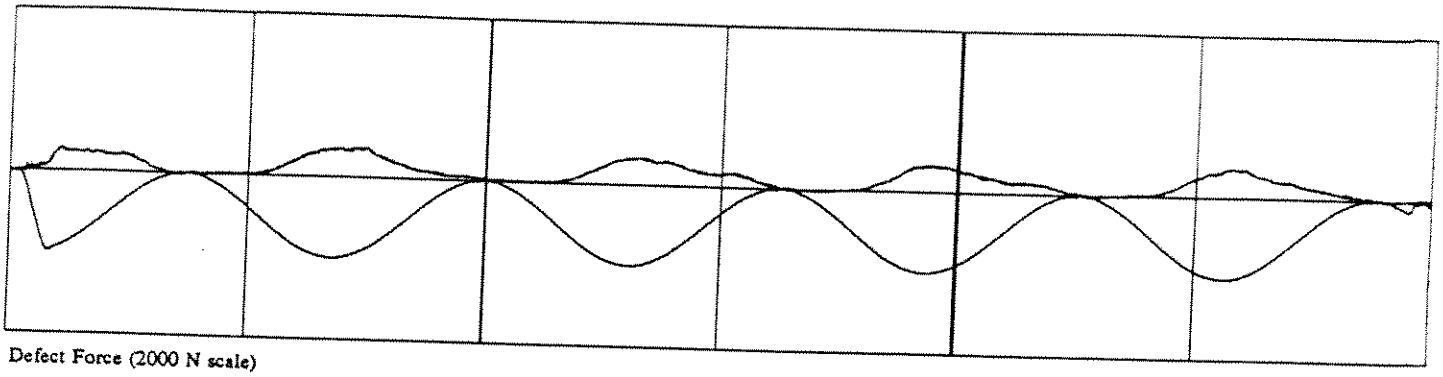

Defect Force (2000 N scale)

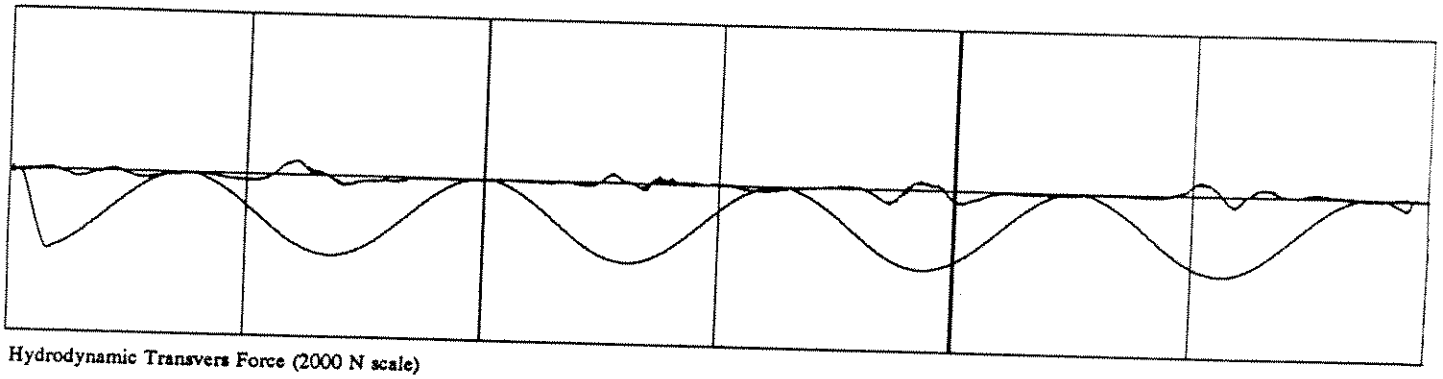

Hydrodynamic Transvers Force (2000 N scale)

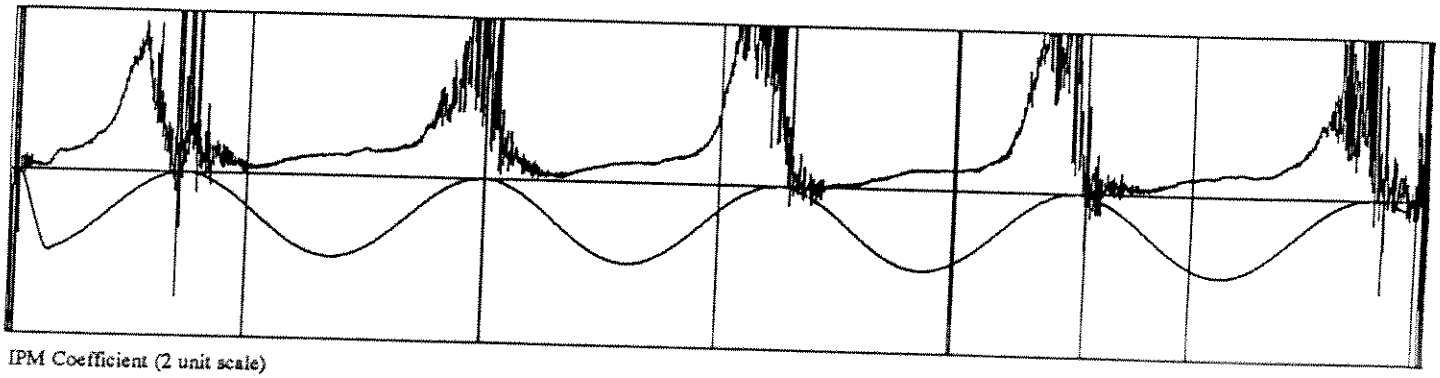

IPM Coefficient (2 unit scale)

PROCESSED DATA for RUN 377 points 1000 to 7000

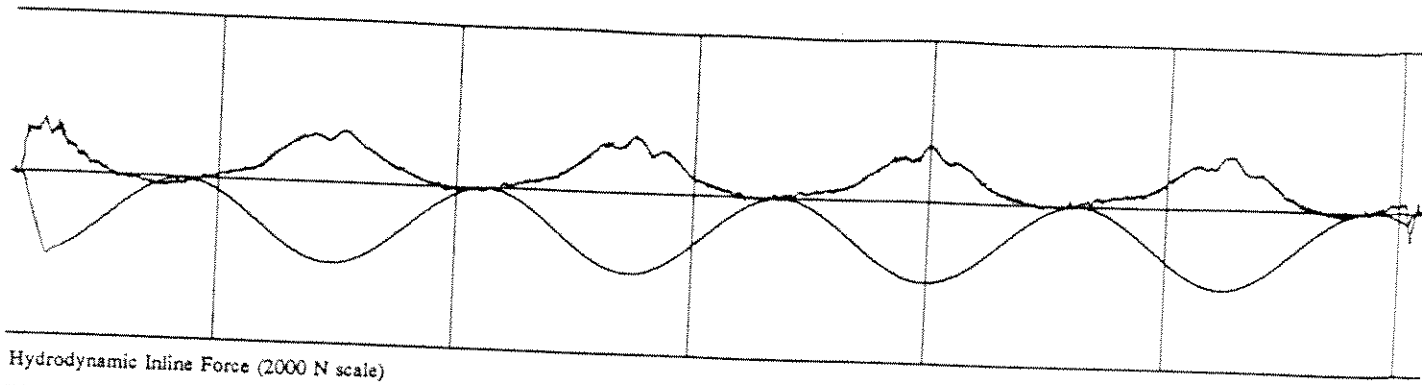

Hydrodynamic Inline Force (2000 N scale)

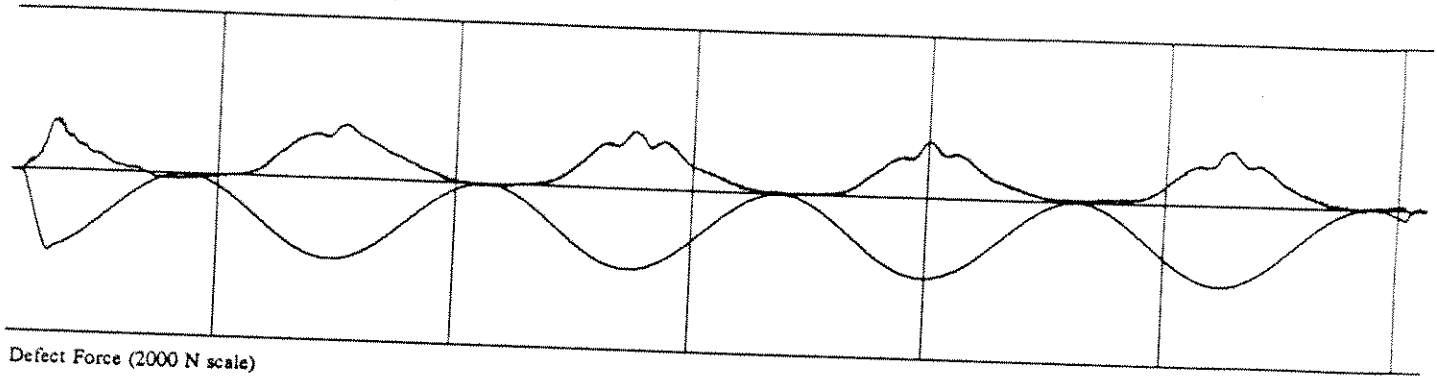

Defect Force (2000 N scale)

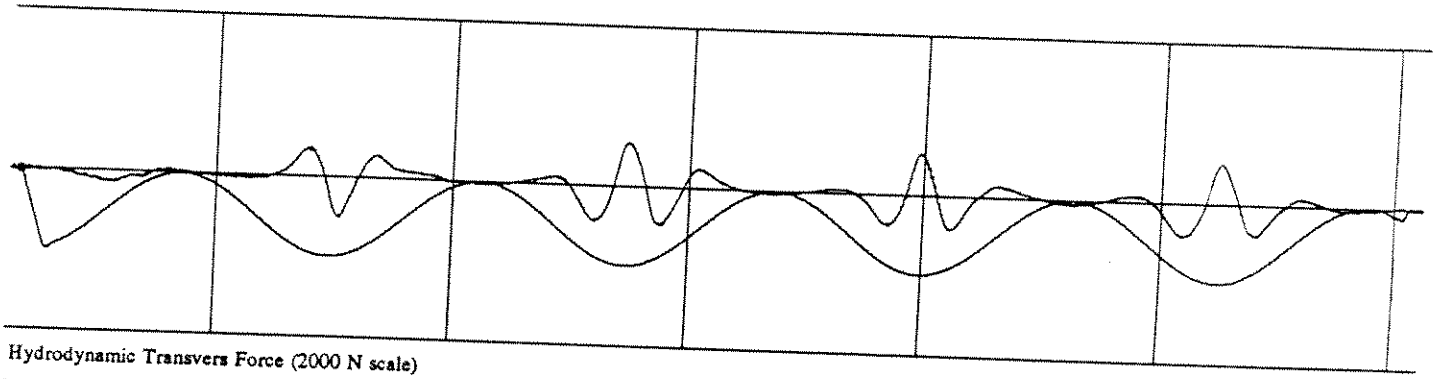

Hydrodynamic Transvers Force (2000 N scale)

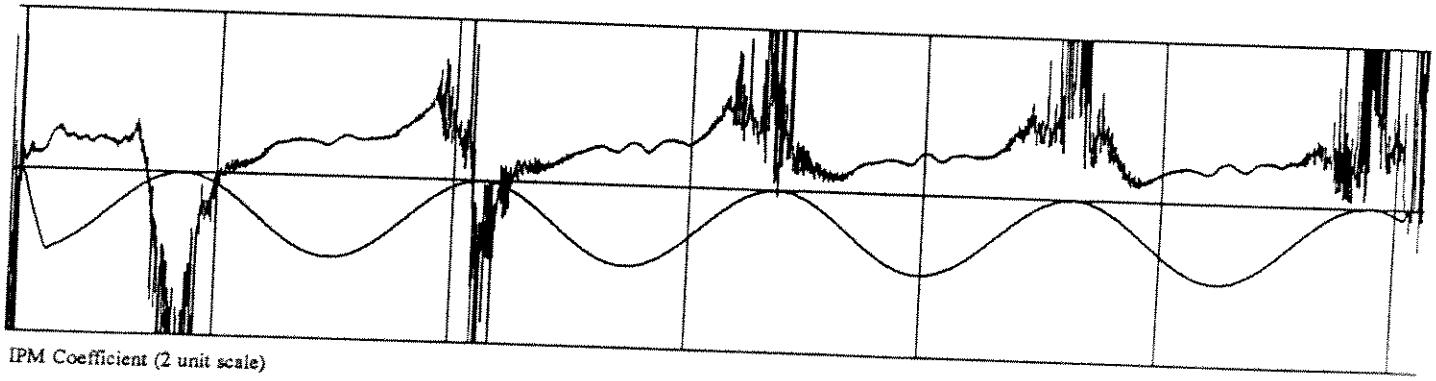

IPM Coefficient (2 unit scale)

PROCESSED DATA for RUN 128 points 1130 to 7115

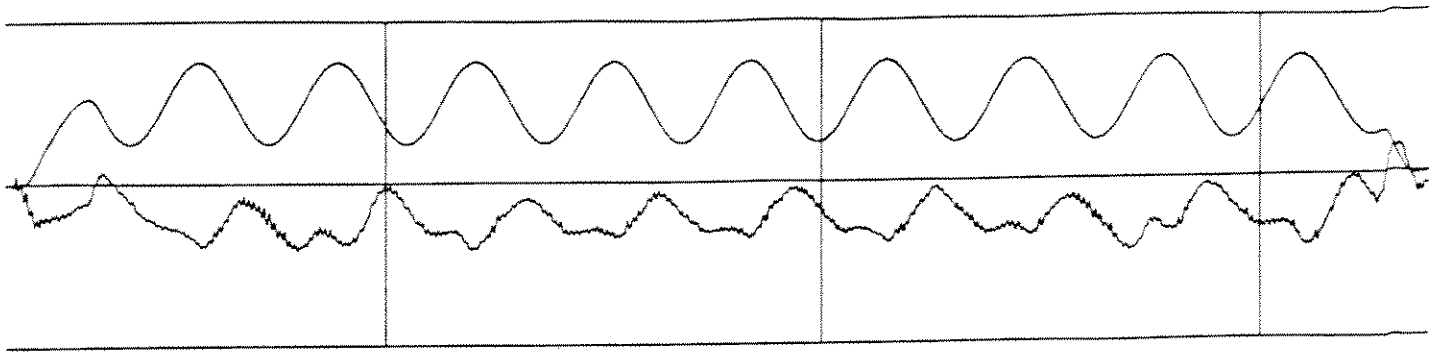

Hydrodynamic Inline Force (2000 N scale)

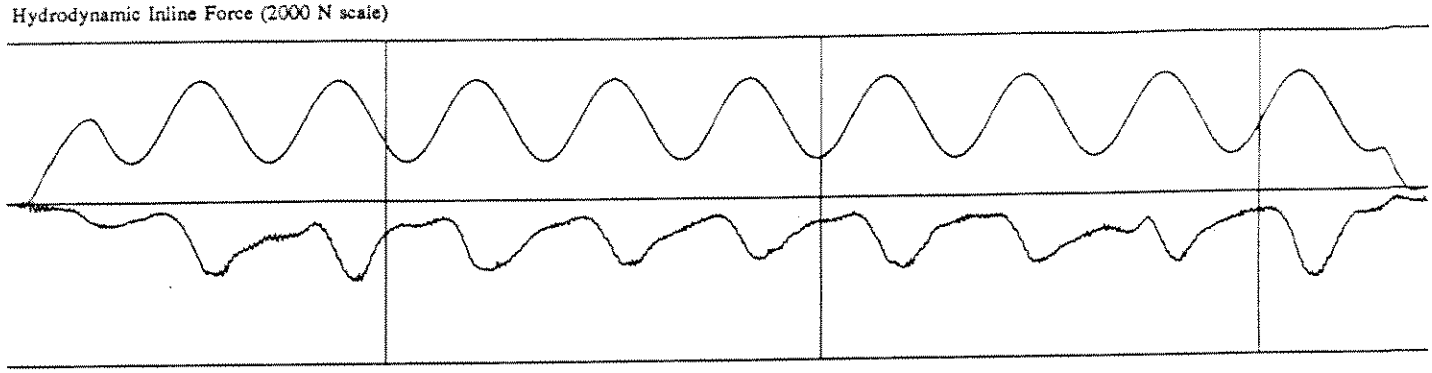

Defect Force (2000 N scale)

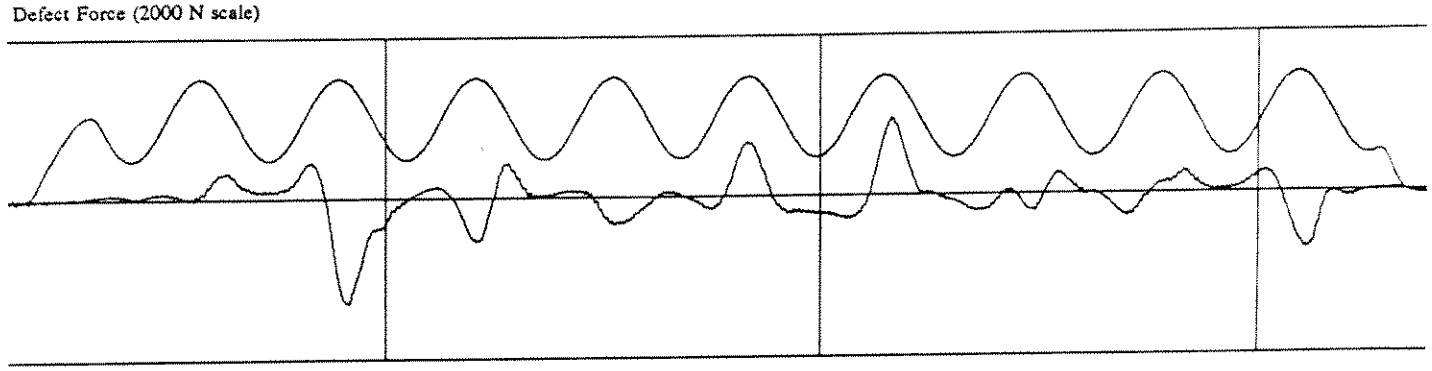

Hydrodynamic Transvers Force (2000 N scale)

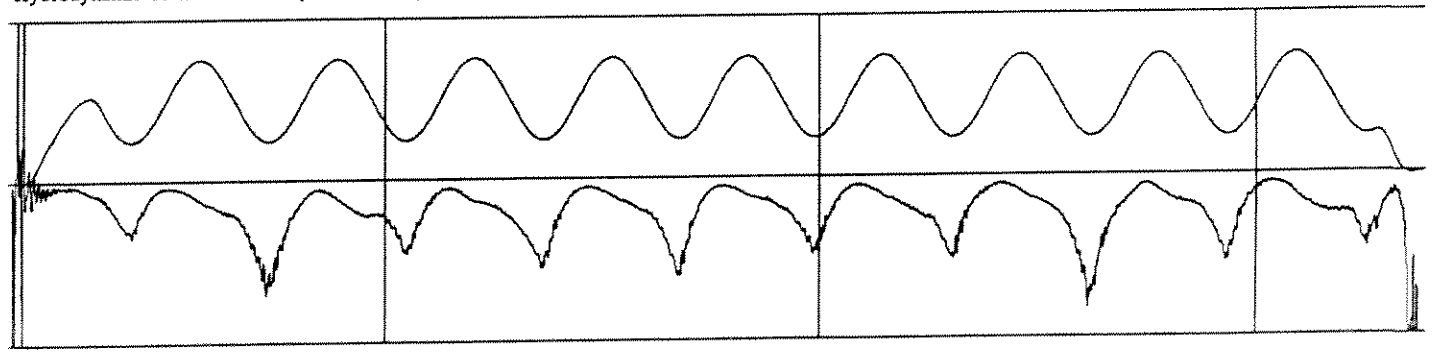

IPM Coefficient (2 unit scale)

PROCESSED DATA for RUN 378 points 1140 to 4380

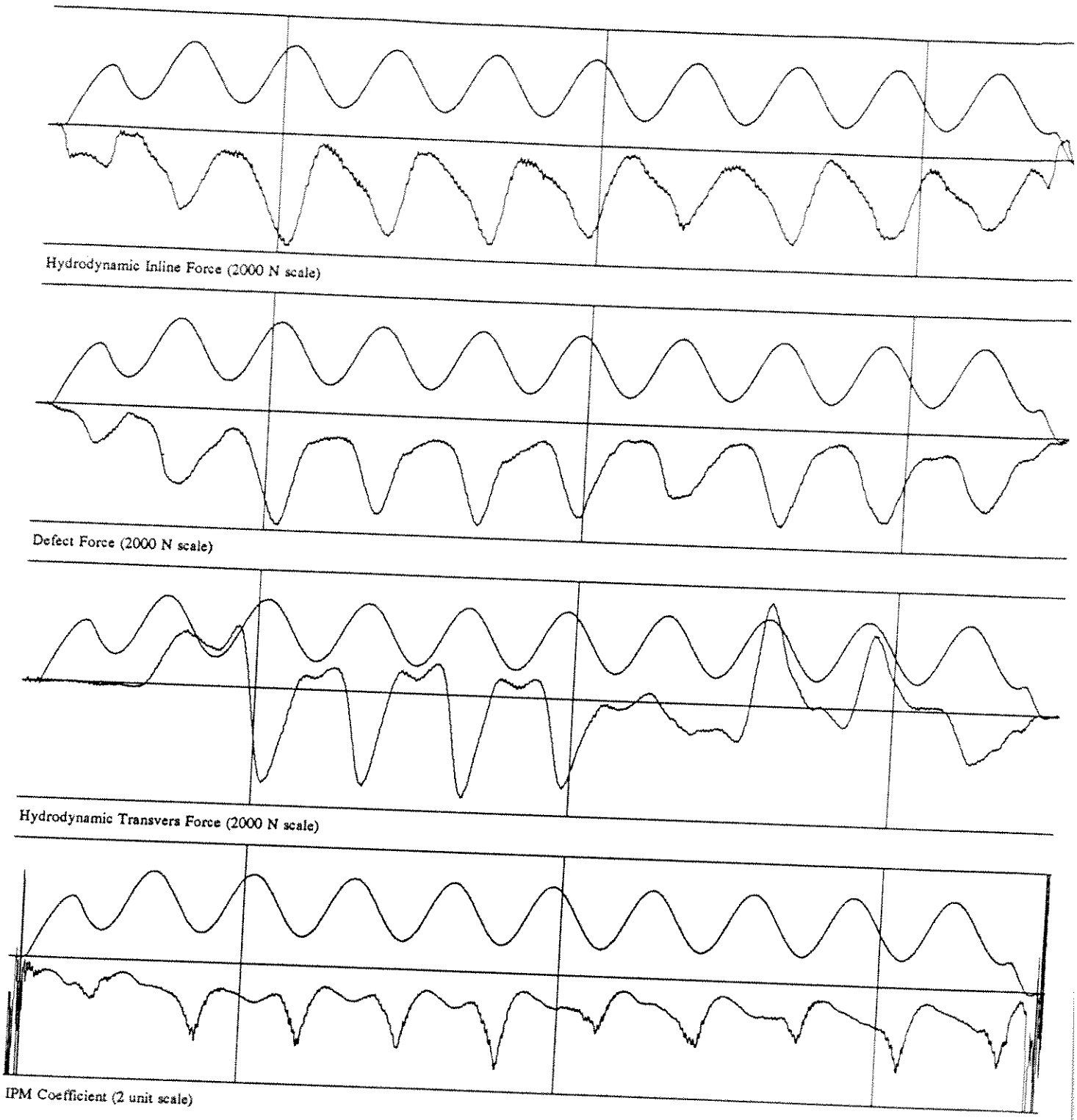

PROCESSED DATA for RUN 131 points 1270 to 4520

R-3-44-0-2.0+

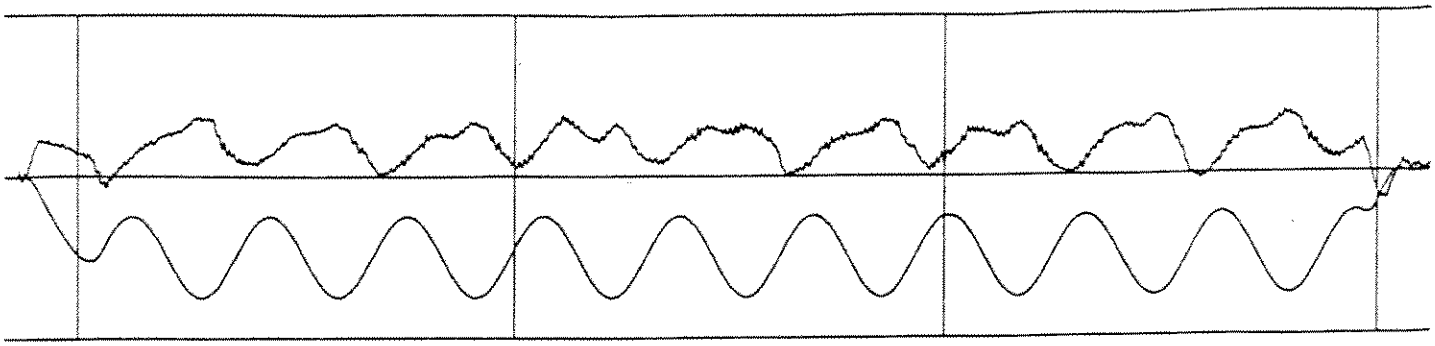

Hydrodynamic Inline Force (2000 N scale)

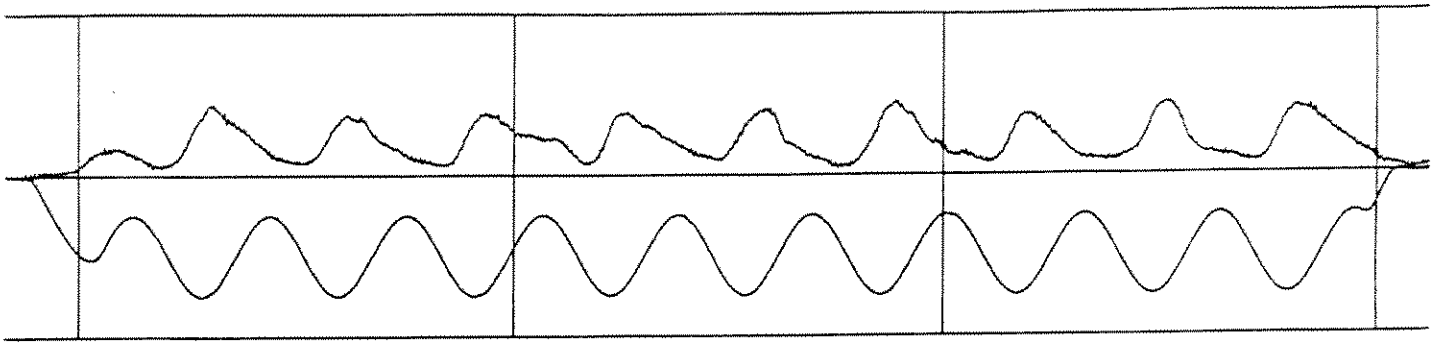

Defect Force (2000 N scale)

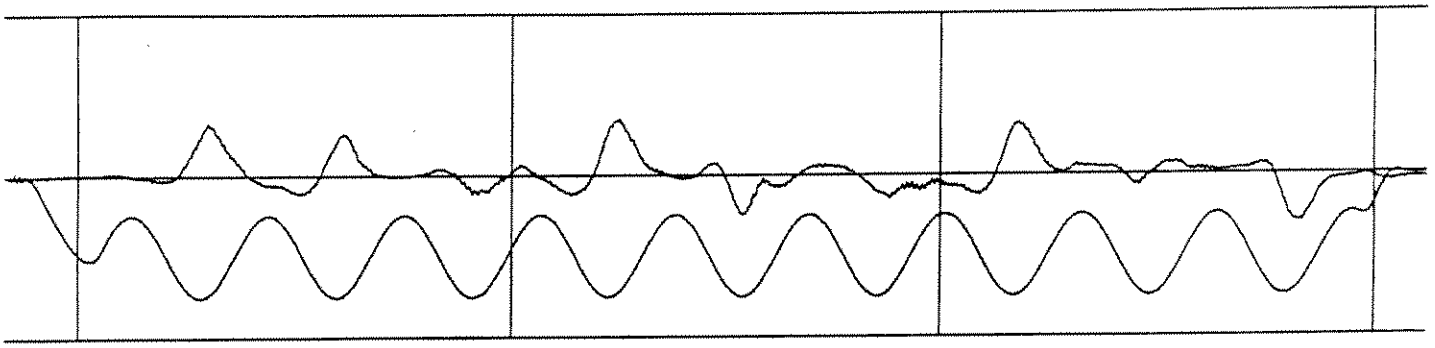

Hydrodynamic Transvers Force (2000 N scale)

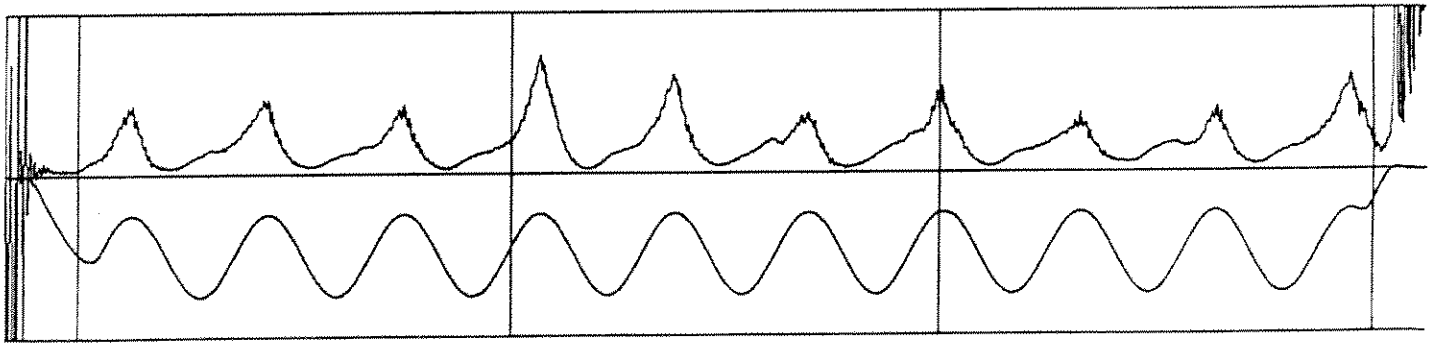

IPM Coefficient (2 unit scale)

PROCESSED DATA for RUN 379 points 830 to 4120

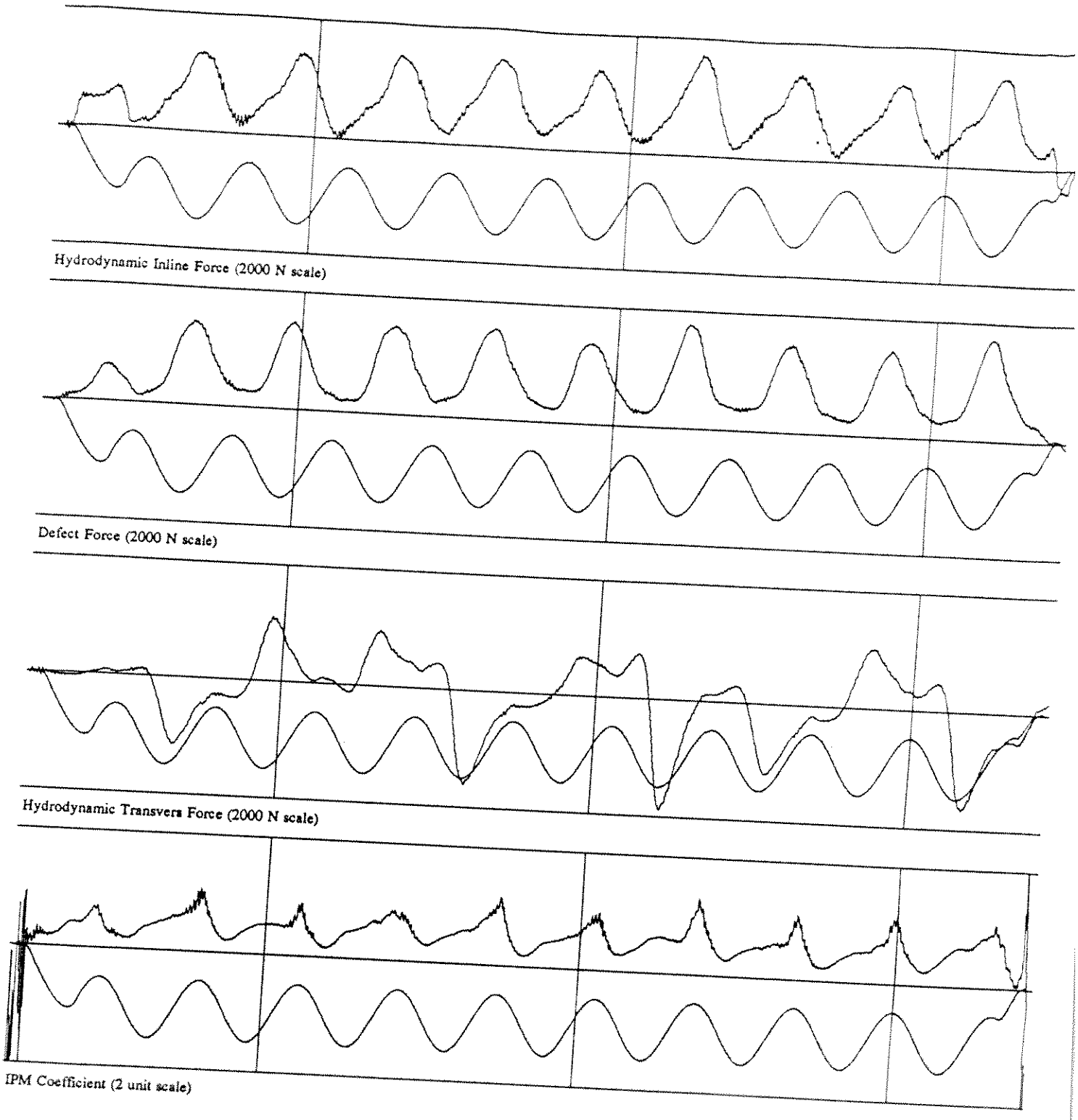

PROCESSED DATA for RUN 130 points 1200 to 4430

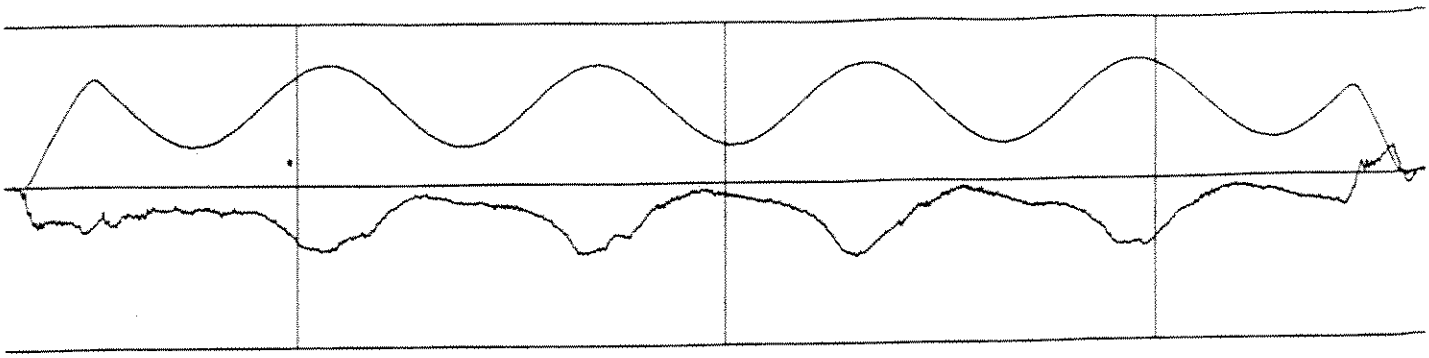

Hydrodynamic Inline Force (2000 N scale)

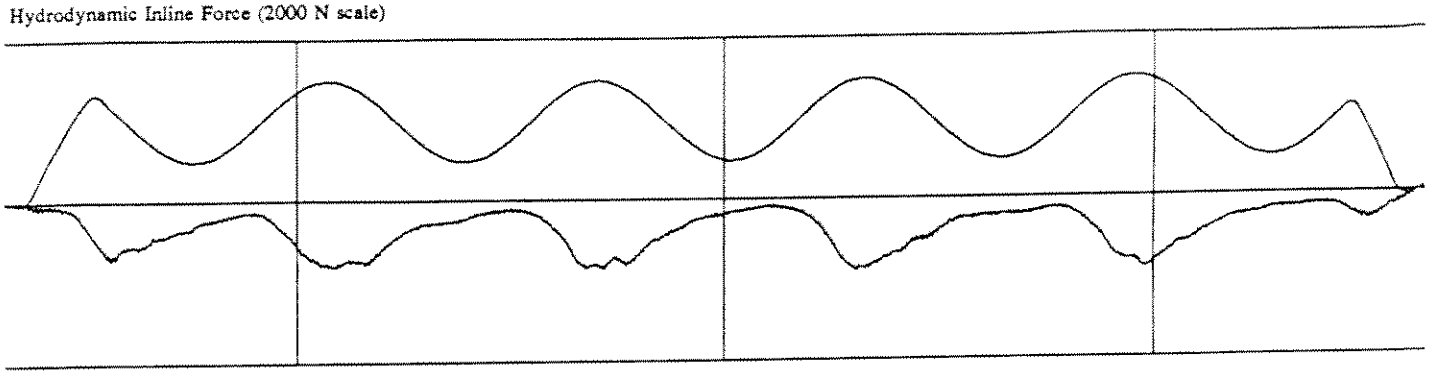

Defect Force (2000 N scale)

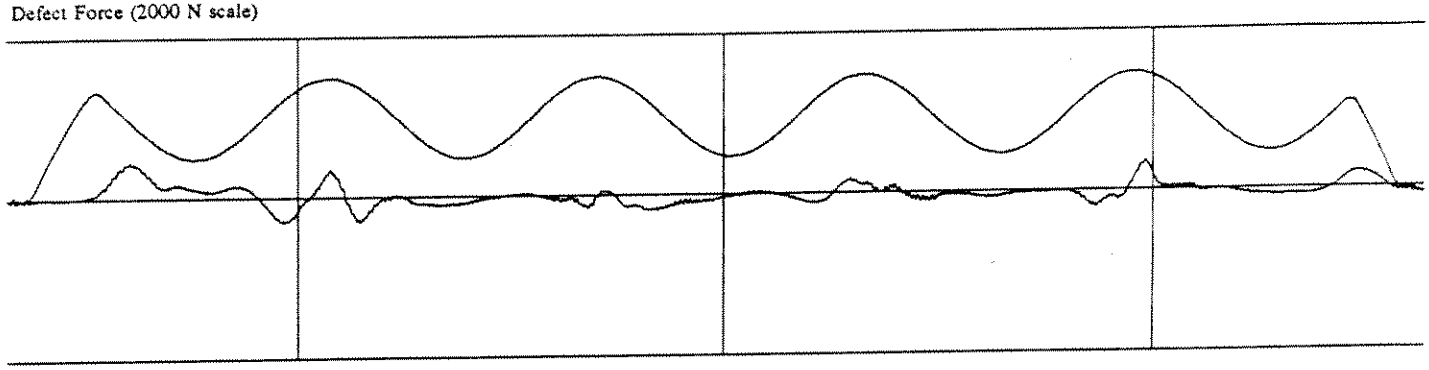

Hydrodynamic Transvers Force (2000 N scale)

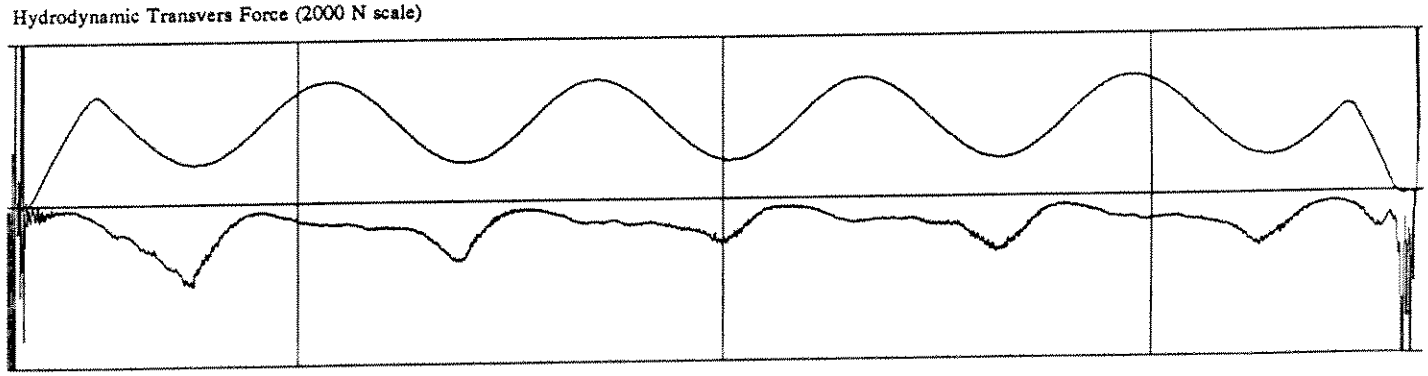

IPM Coefficient (2 unit scale)

PROCESSED DATA for RUN 380 points 1320 to 4635

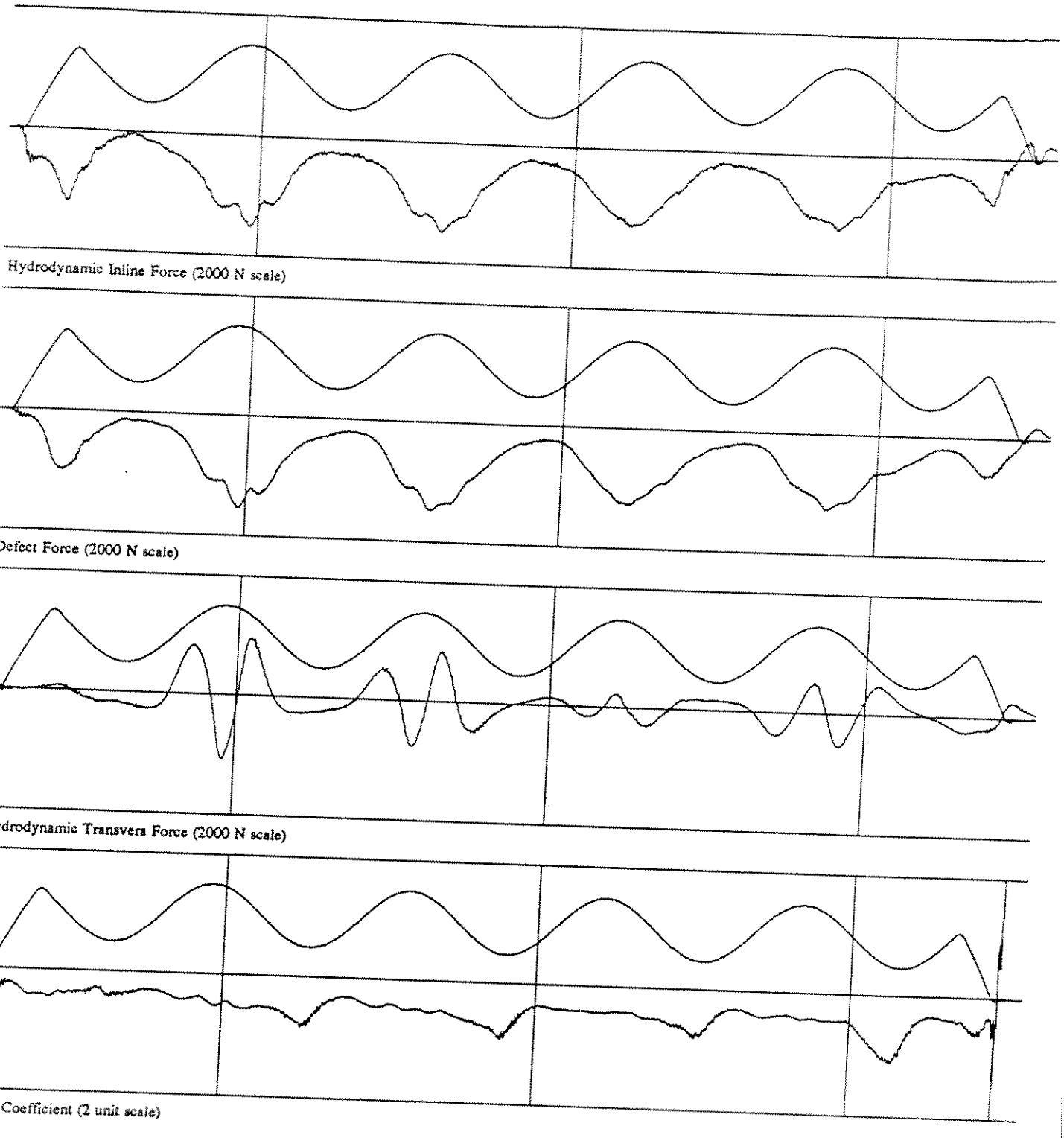

PROCESSED DATA for RUN 133 points 1205 to 4545

R-6-44-0-2.0+

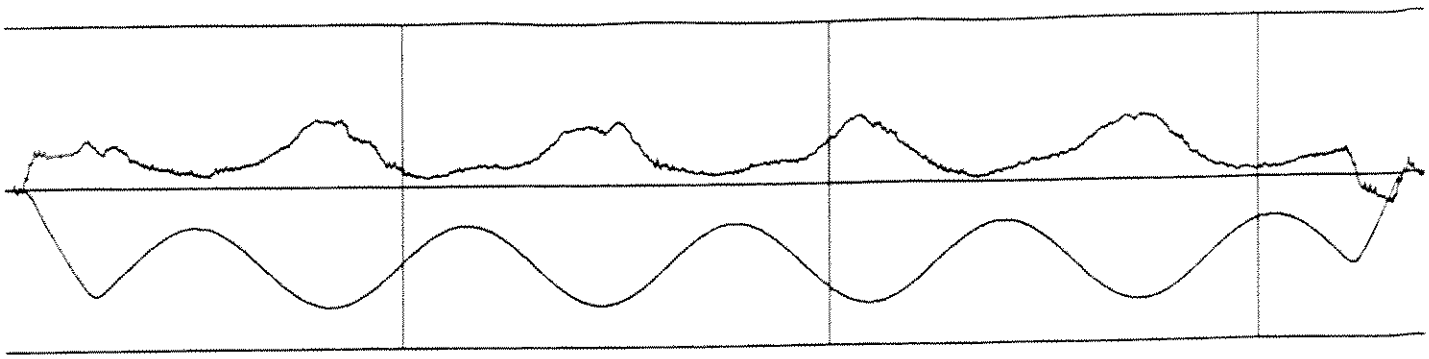

Hydrodynamic Inline Force (2000 N scale)

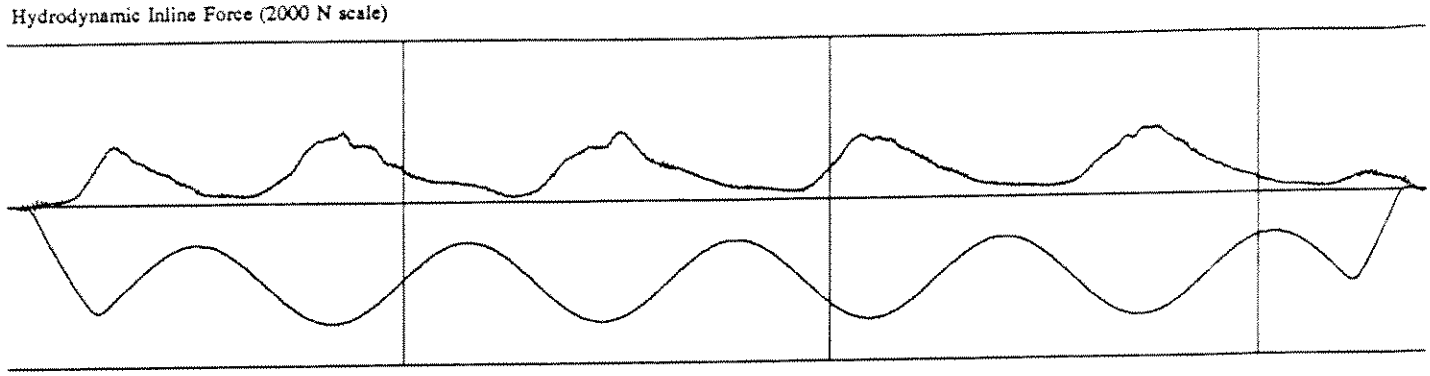

Defect Force (2000 N scale)

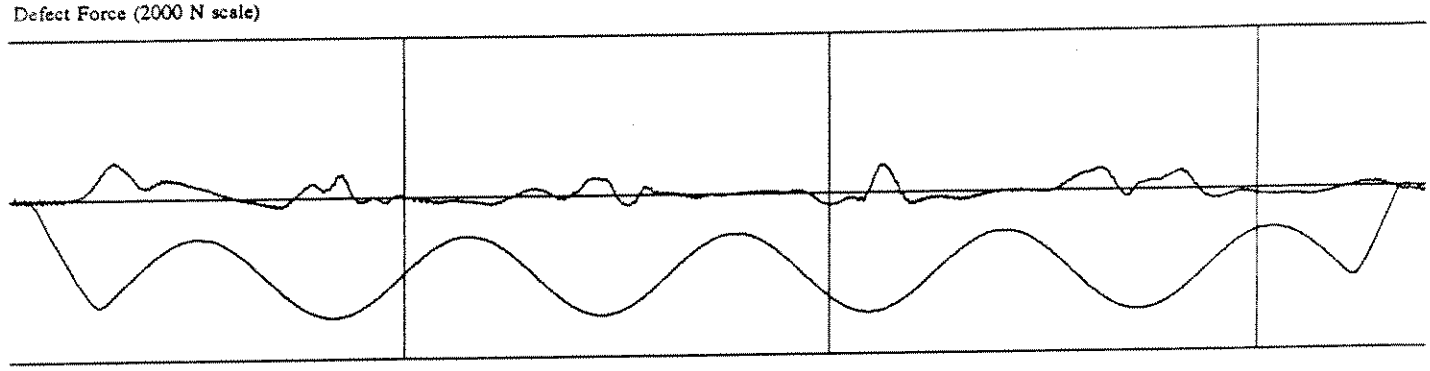

Hydrodynamic Transvers Force (2000 N scale)

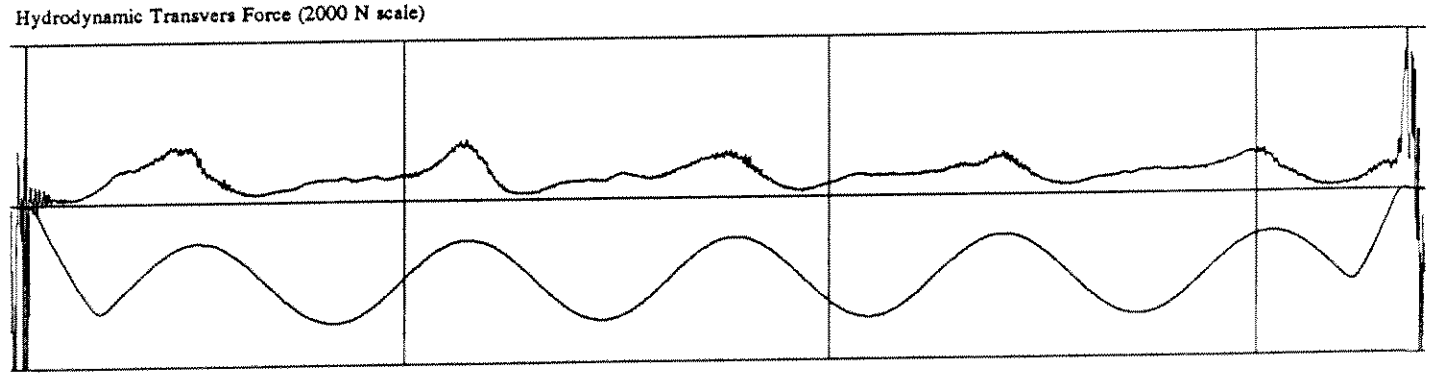

IPM Coefficient (2 unit scale)

PROCESSED DATA for RUN 381 points 1080 to 4390

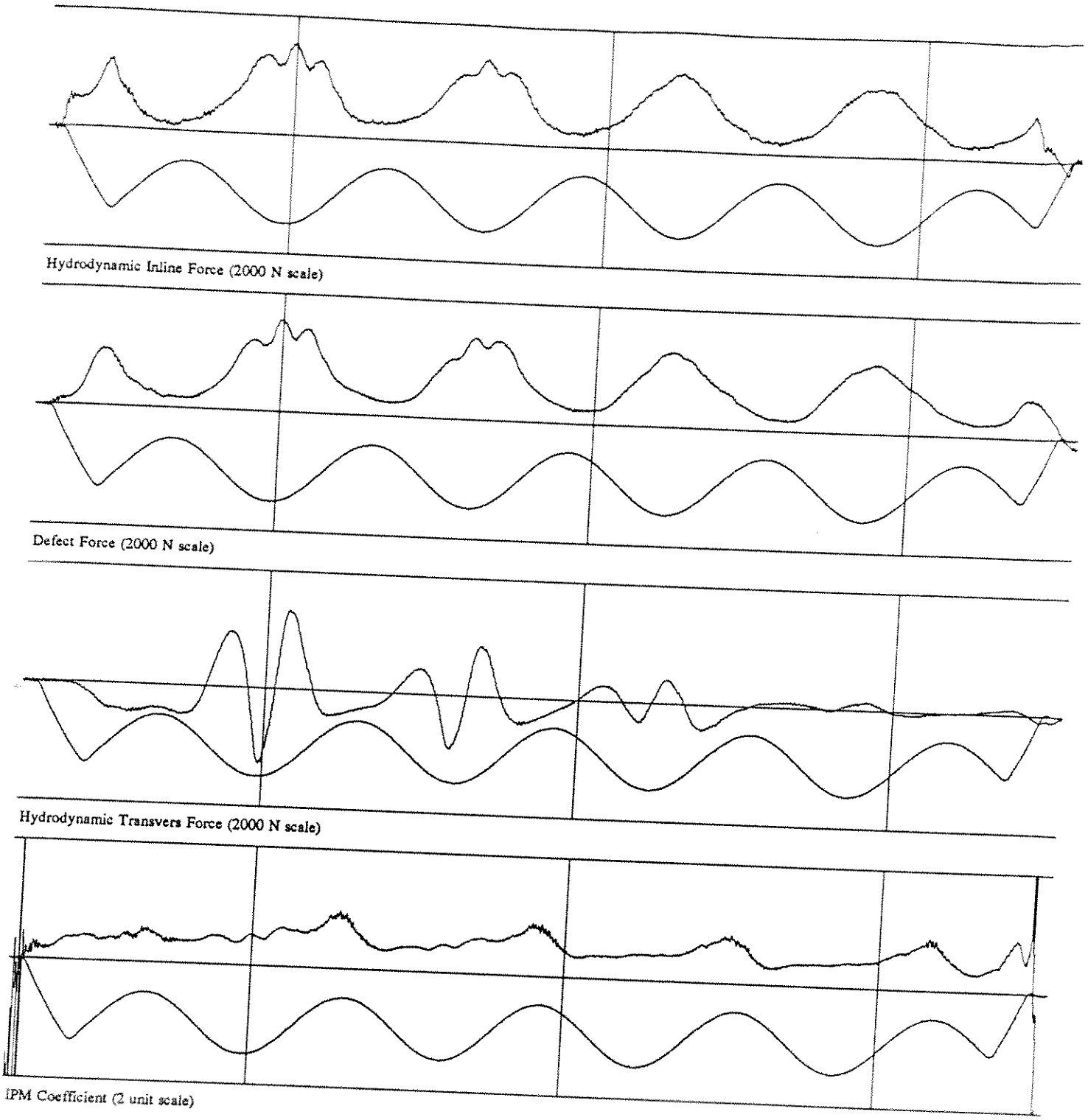

PROCESSED DATA for RUN 132 points 1230 to 4535

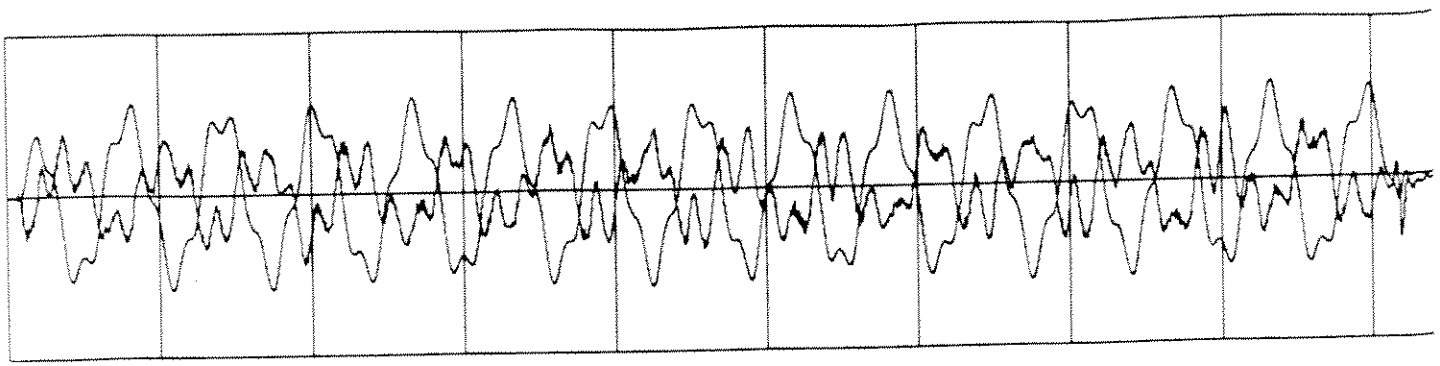

Hydrodynamic Inline Force (2000 N scale)

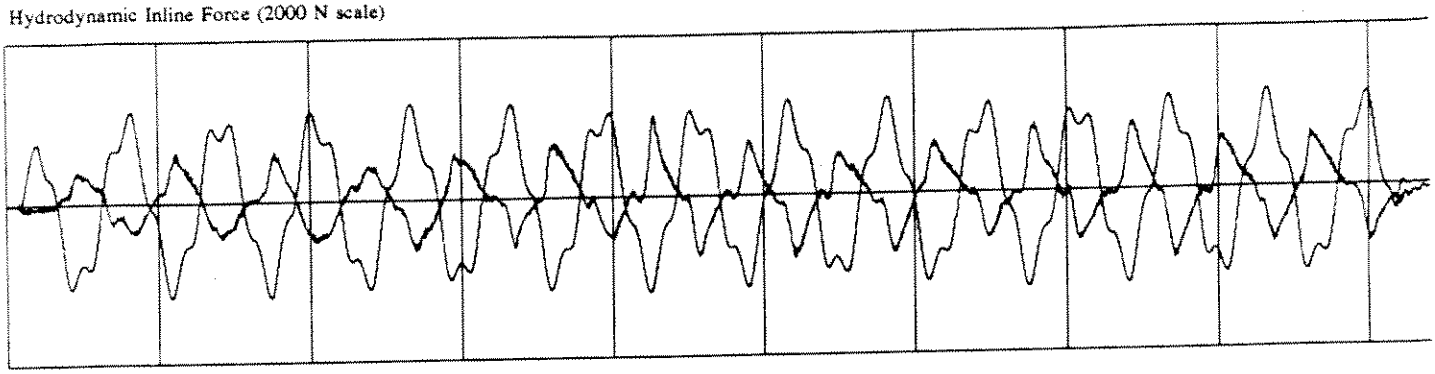

Defect Force (2000 N scale)

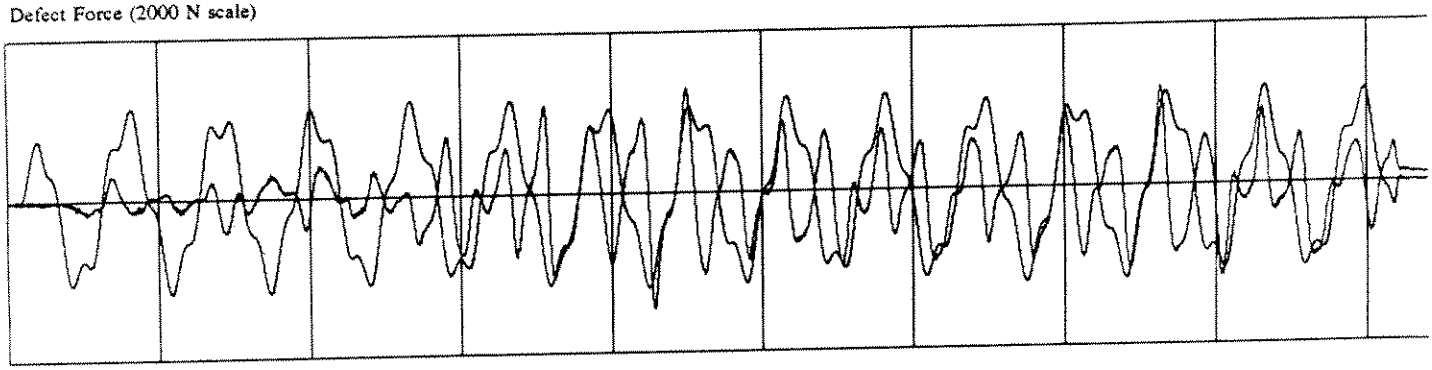

Hydrodynamic Transvers Force (2000 N scale)

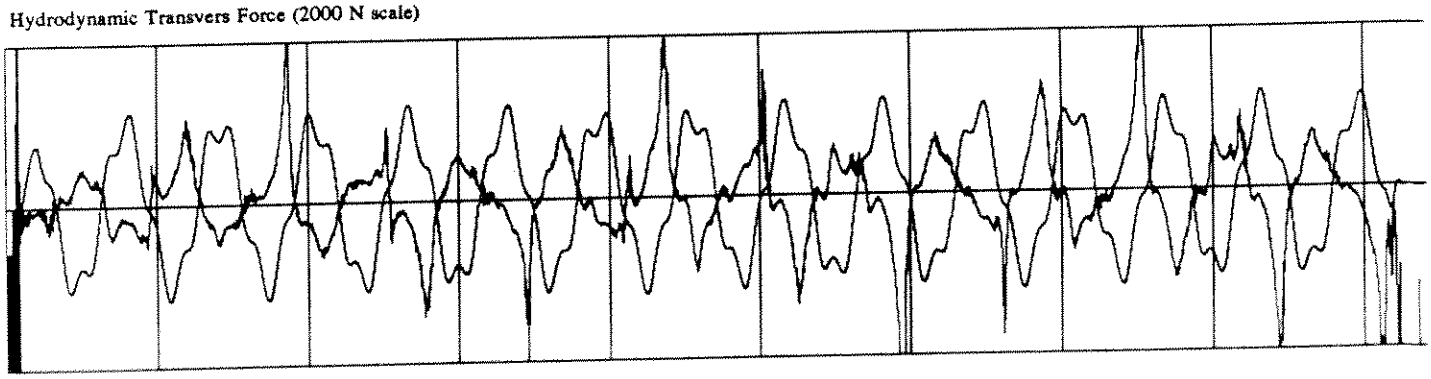

IPM Coefficient (2 unit scale)

PROCESSED DATA for RUN 437 points 1000 to 10400

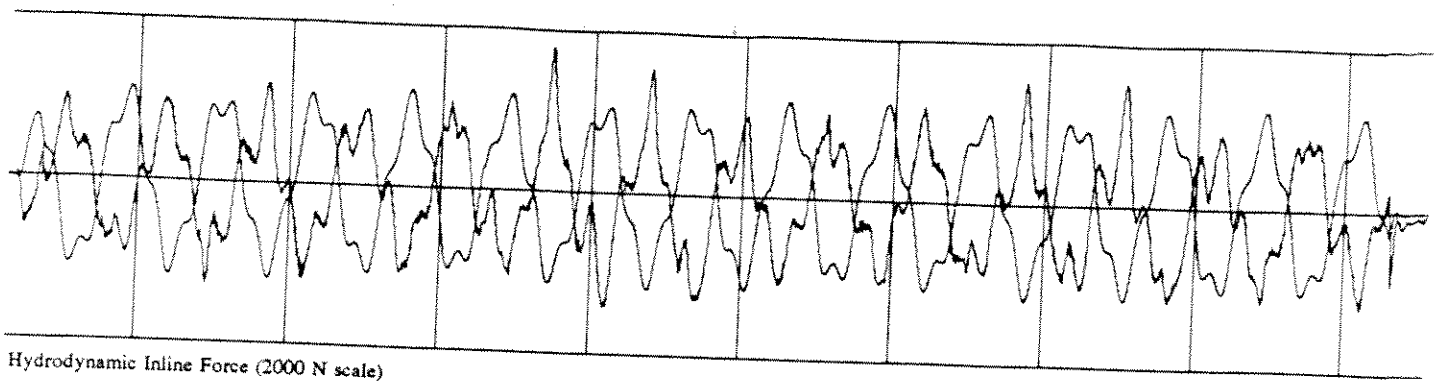

Hydrodynamic Inline Force (2000 N scale)

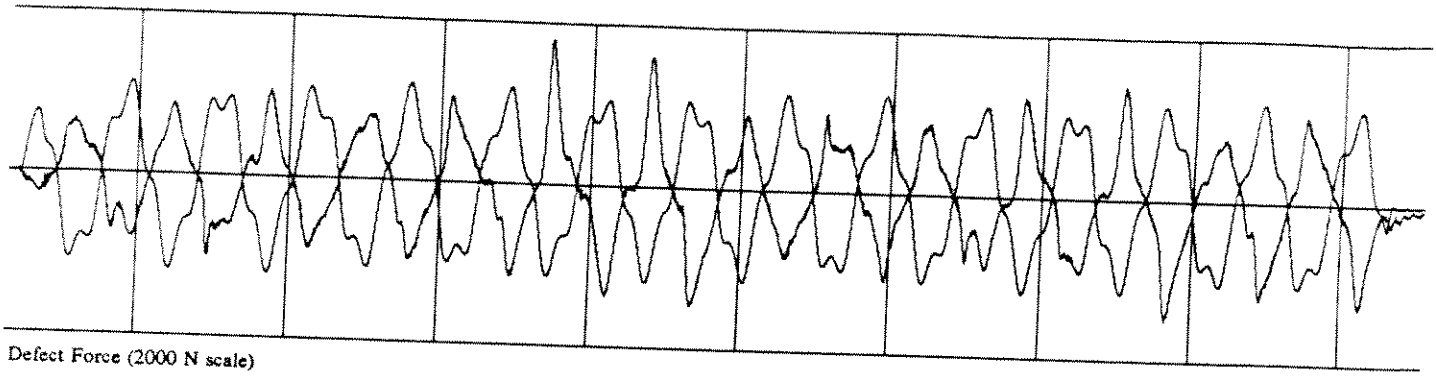

Defect Force (2000 N scale)

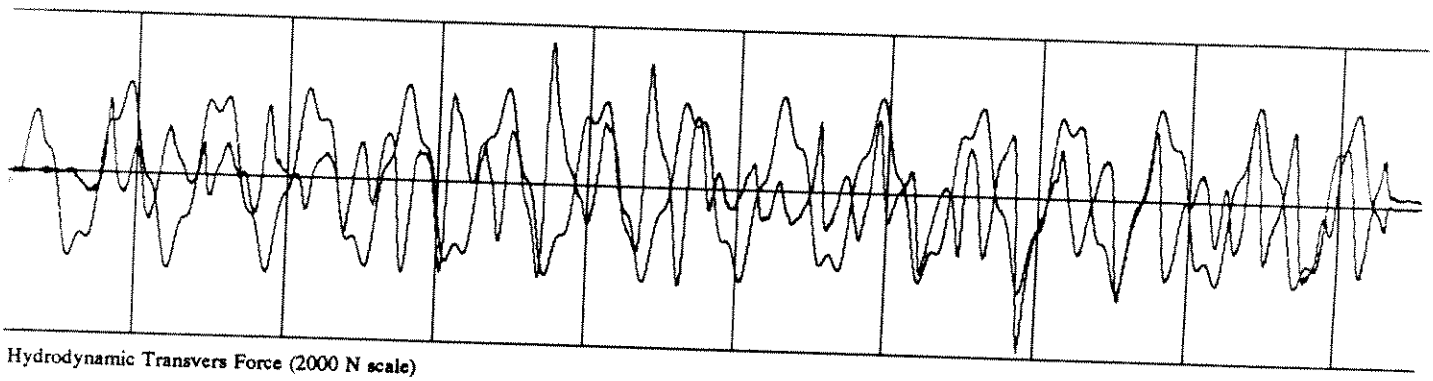

Hydrodynamic Transvers Force (2000 N scale)

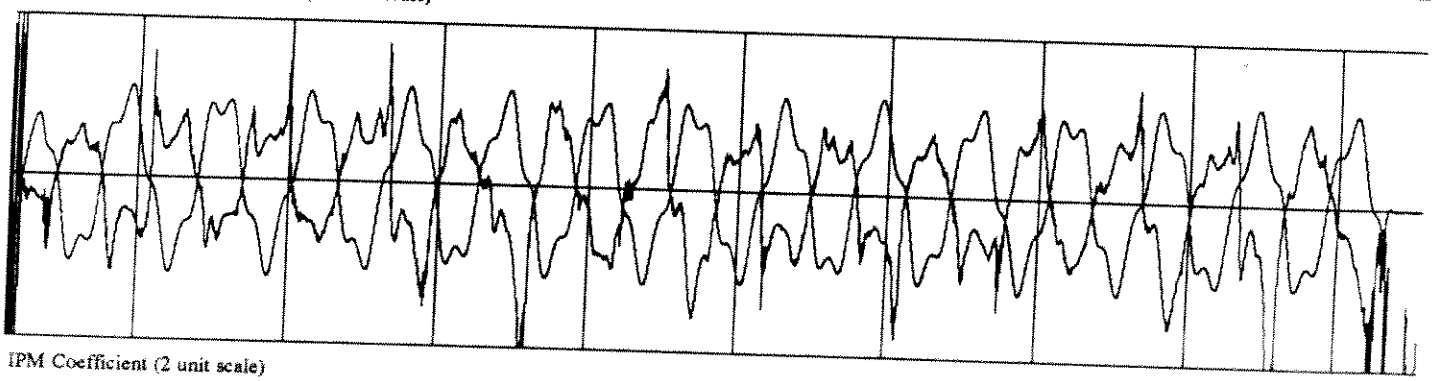

IPM Coefficient (2 unit scale)

PROCESSED DATA for RUN 192 points 1150 to 10550

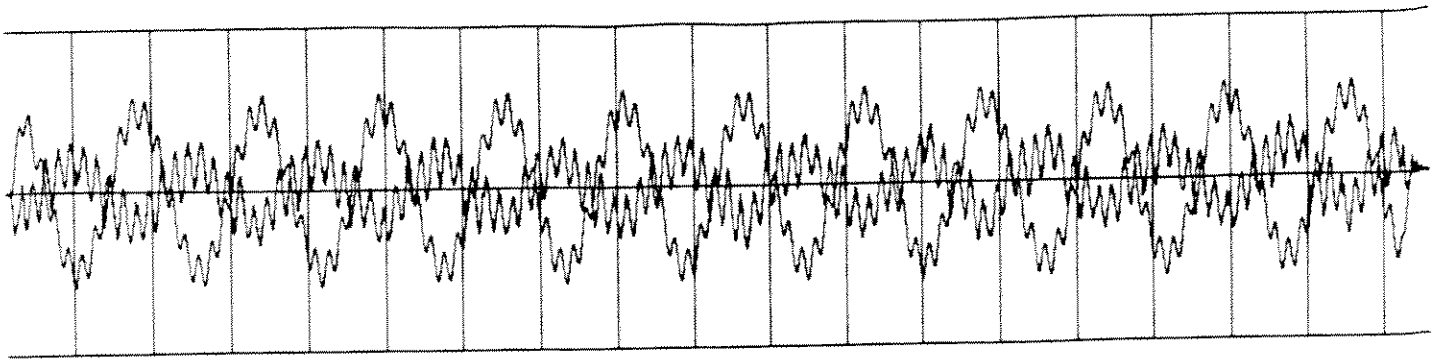

Hydrodynamic Inline Force (2000 N scale)

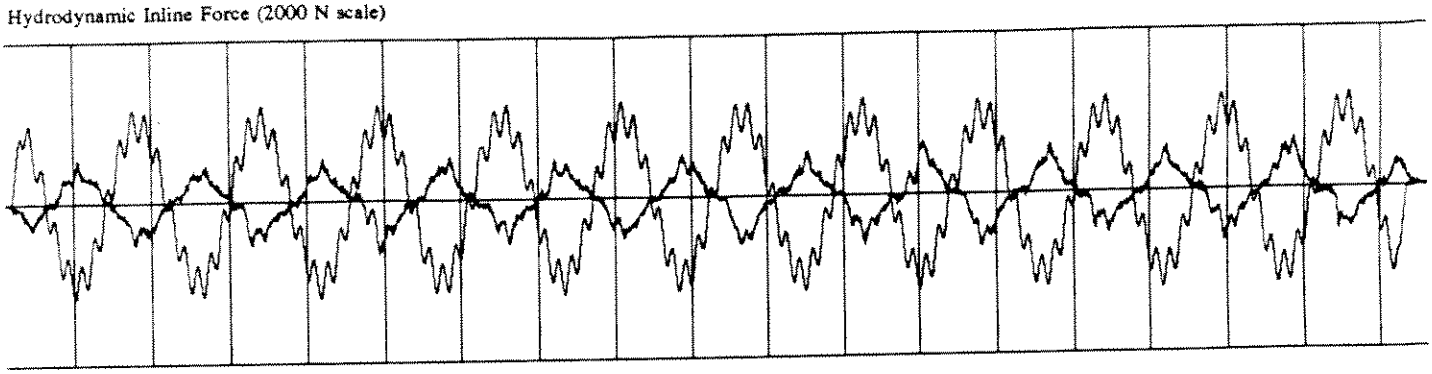

Defect Force (2000 N scale)

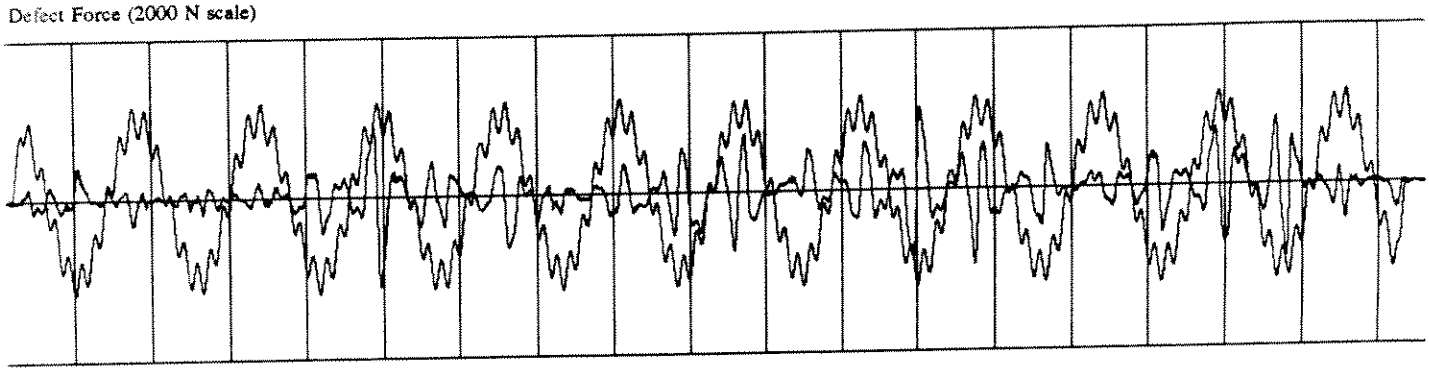

Hydrodynamic Transvers Force (2000 N scale)

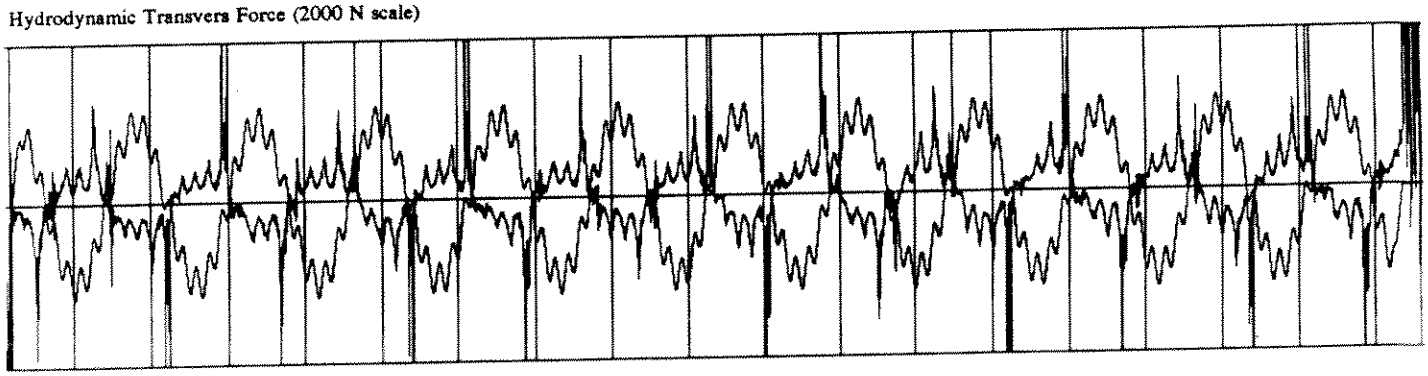

IPM Coefficient (2 unit scale)

PROCESSED DATA for RUN 438 points 1100 to 19600

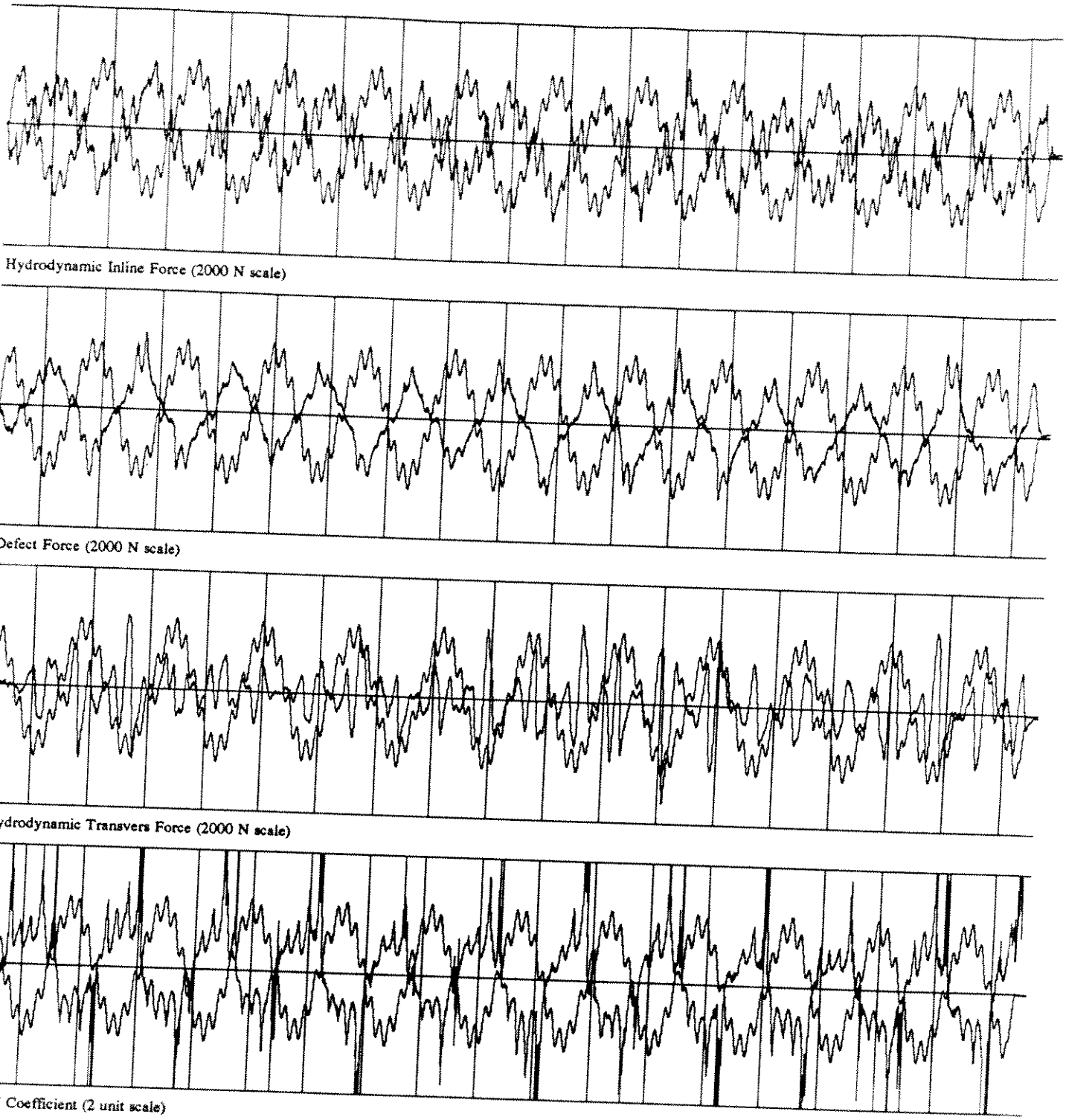

PROCESSED DATA for RUN 193 points 1200 to 19600

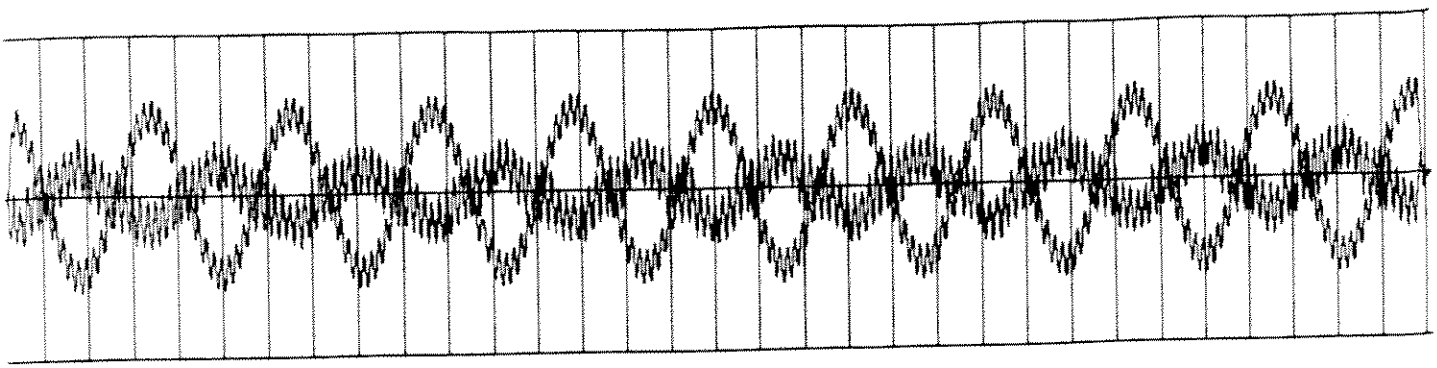

Hydrodynamic Inline Force (2000 N scale)

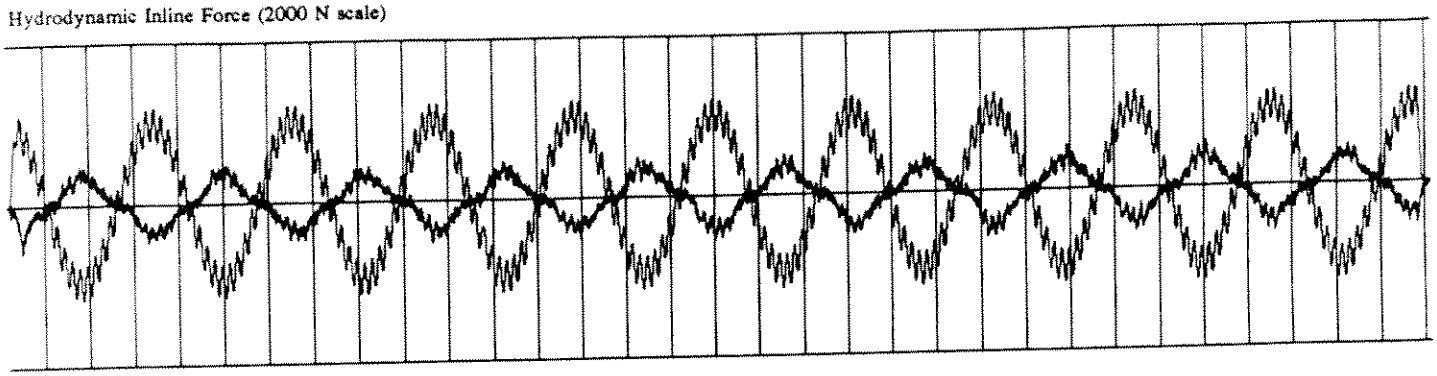

Defect Force (2000 N scale)

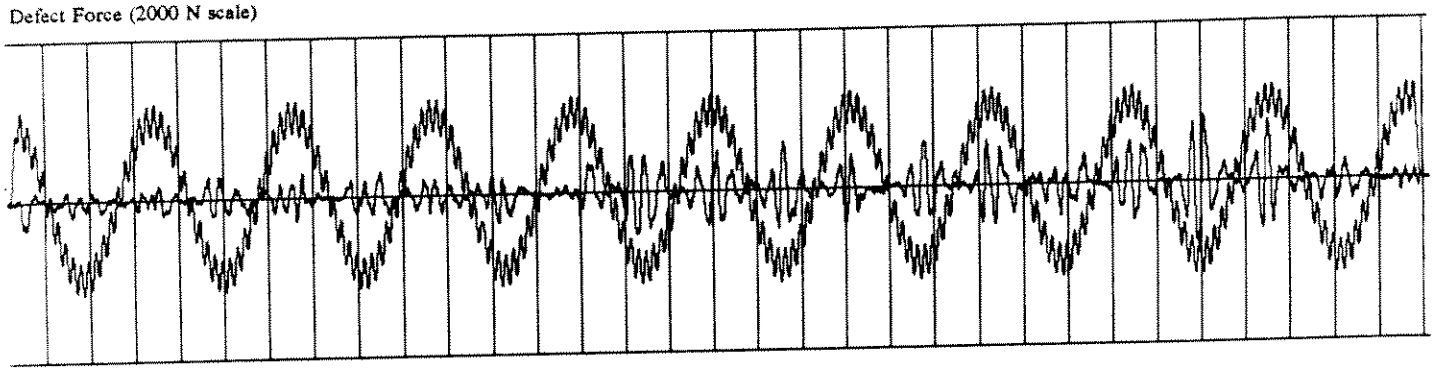

Hydrodynamic Transvers Force (2000 N scale)

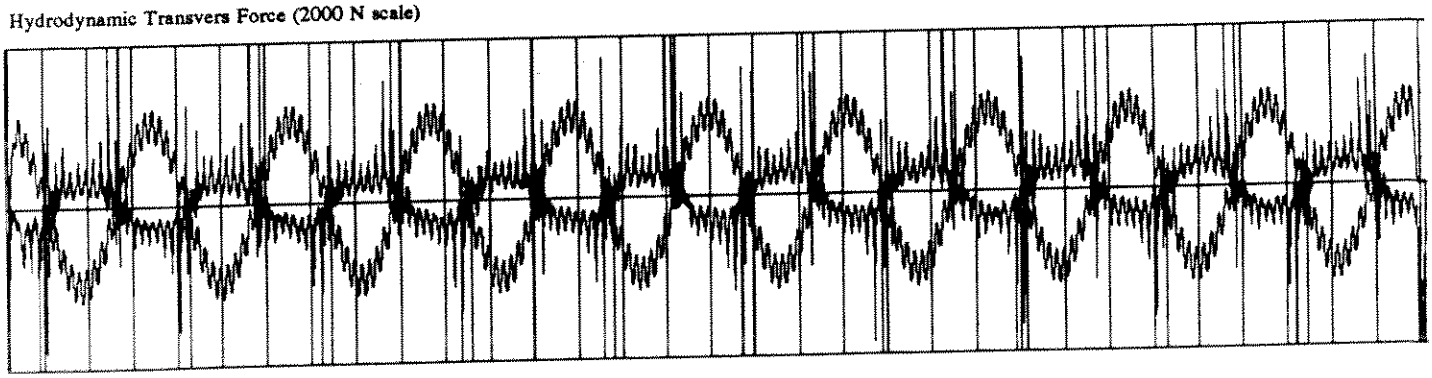

IPM Coefficient (2 unit scale)

PROCESSED DATA for RUN 439 points 150 to 32100

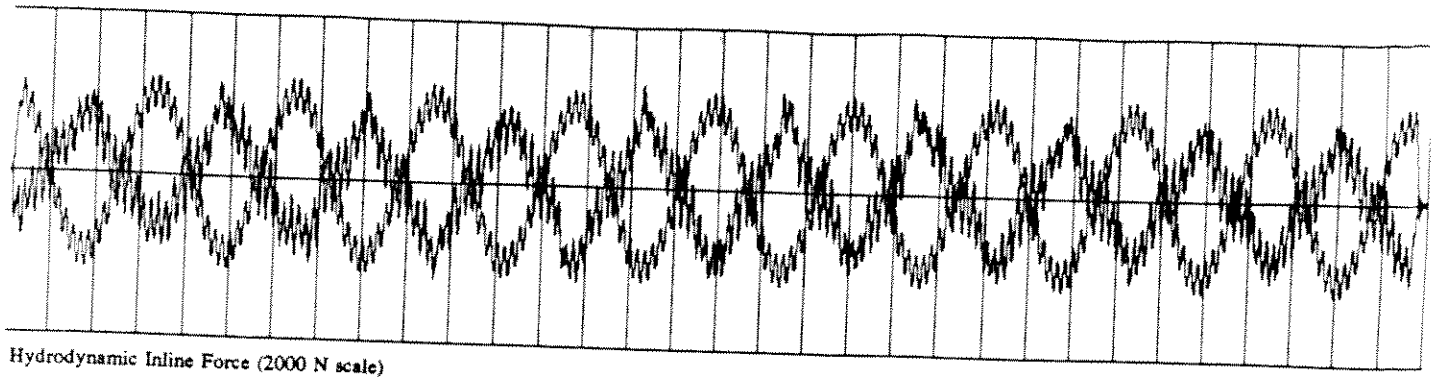

Hydrodynamic Inline Force (2000 N scale)

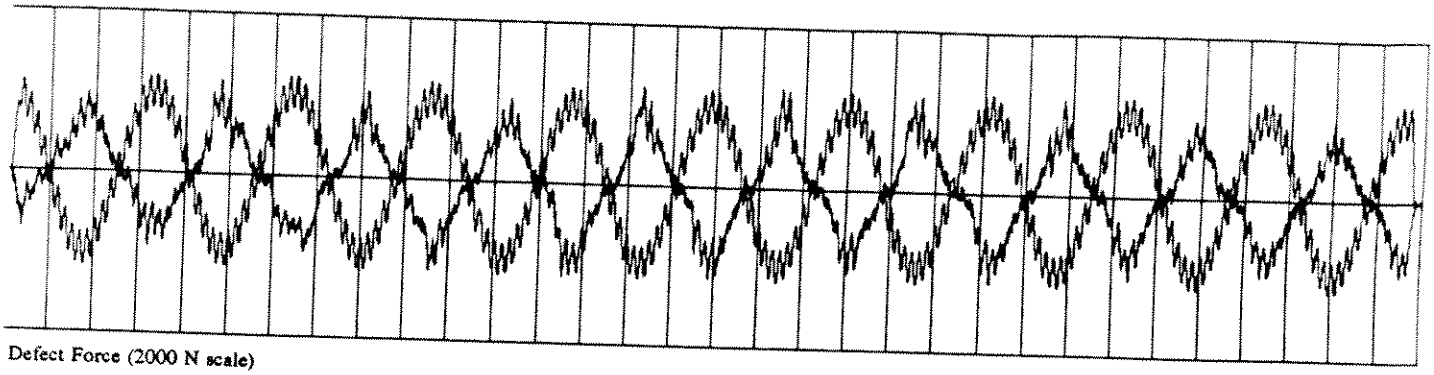

Defect Force (2000 N scale)

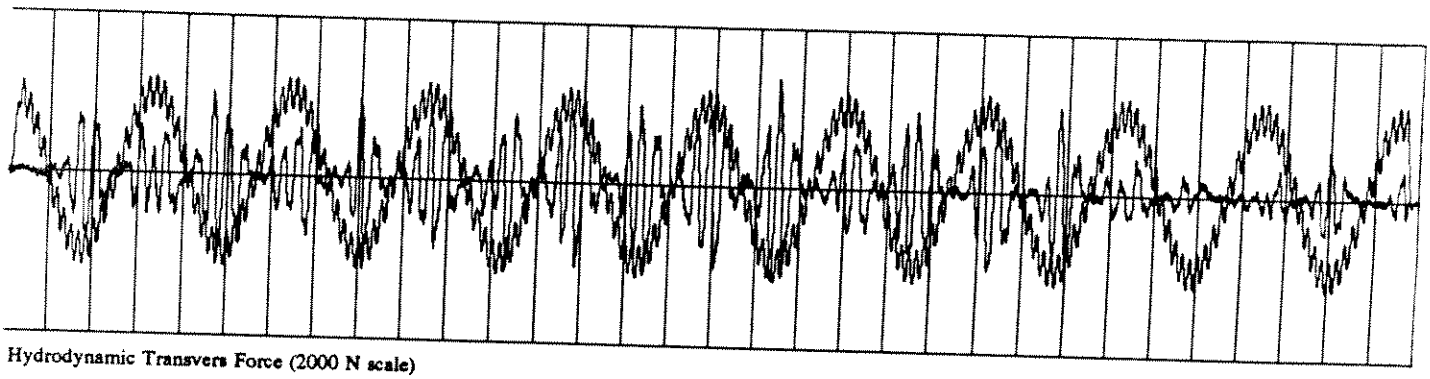

Hydrodynamic Transvers Force (2000 N scale)

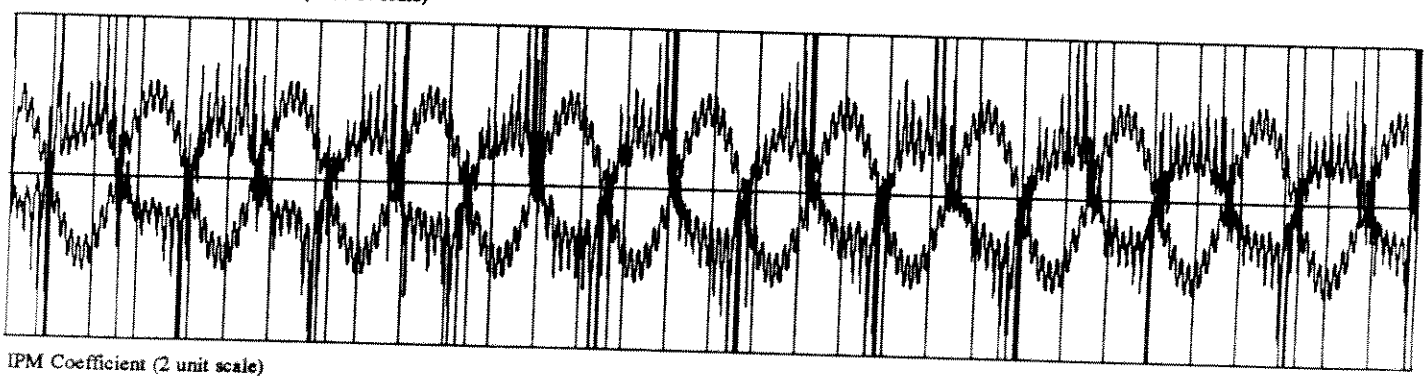

IPM Coefficient (2 unit scale)

PROCESSED DATA for RUN 194 points 50 to 32000

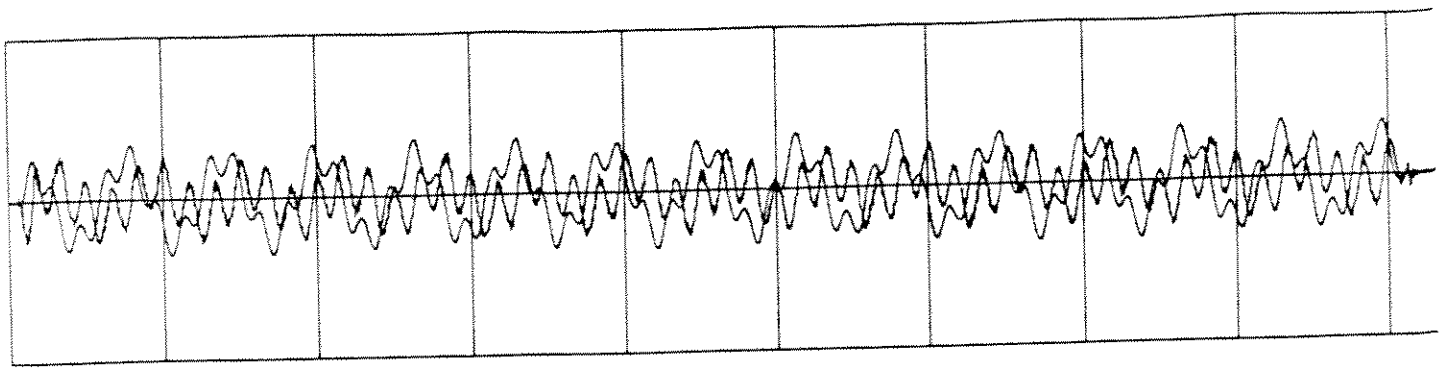

Hydrodynamic Inline Force (2000 N scale)

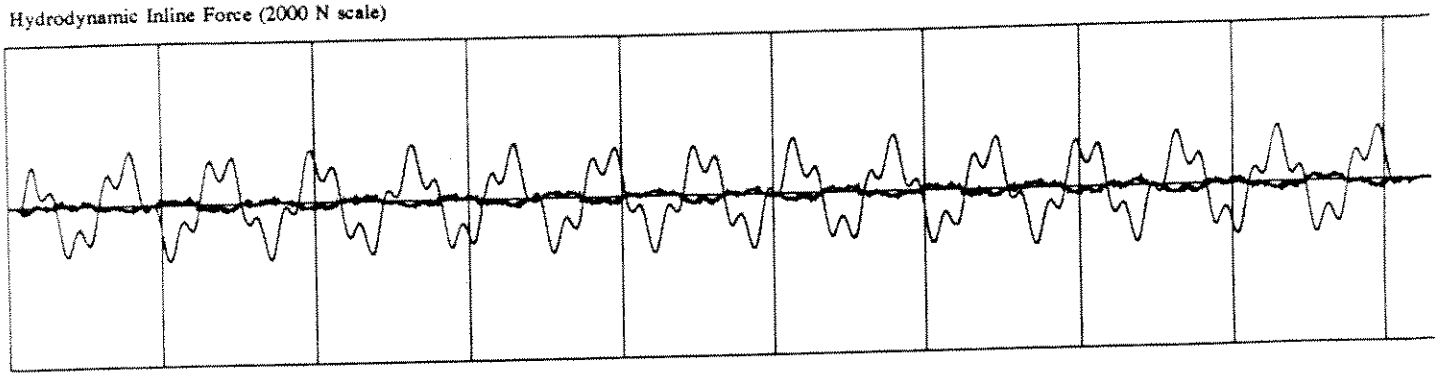

Defect Force (2000 N scale)

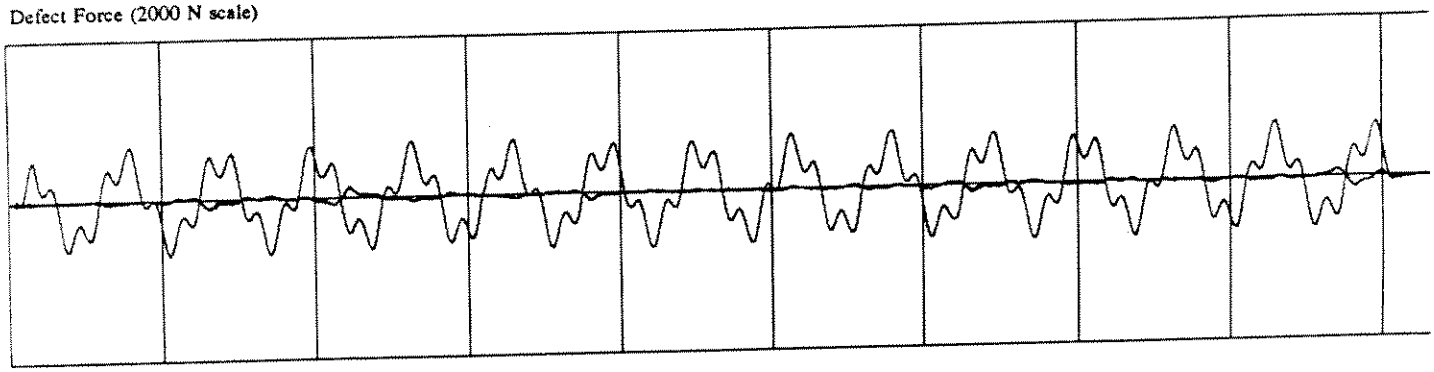

Hydrodynamic Transvers Force (2000 N scale)

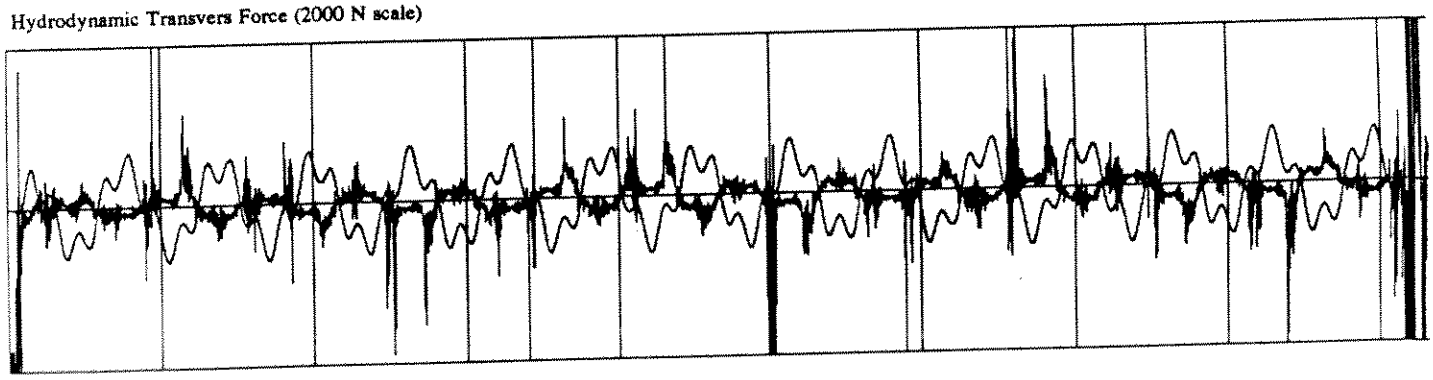

IPM Coefficient (2 unit scale)

PROCESSED DATA for RUN 440 points 1000 to 10300

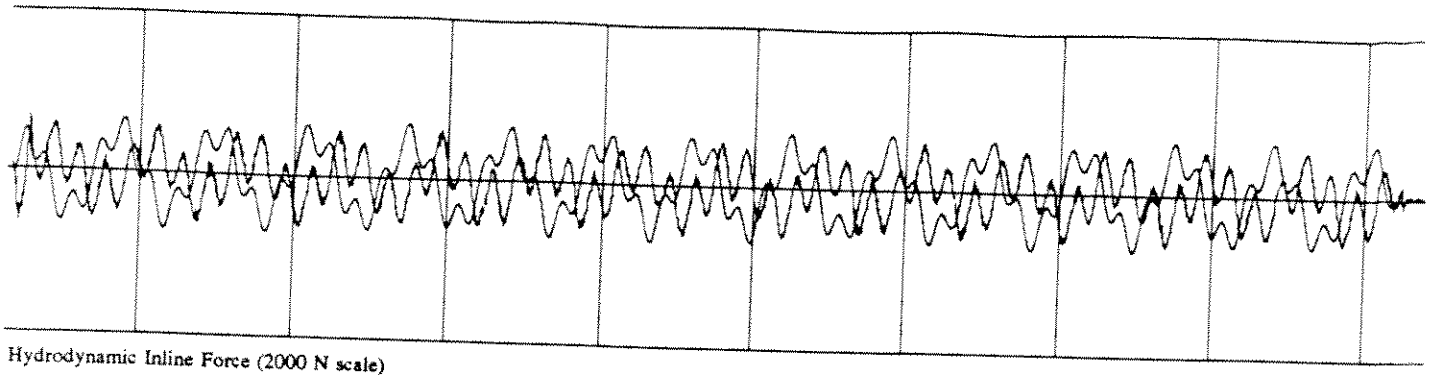

Hydrodynamic Inline Force (2000 N scale)

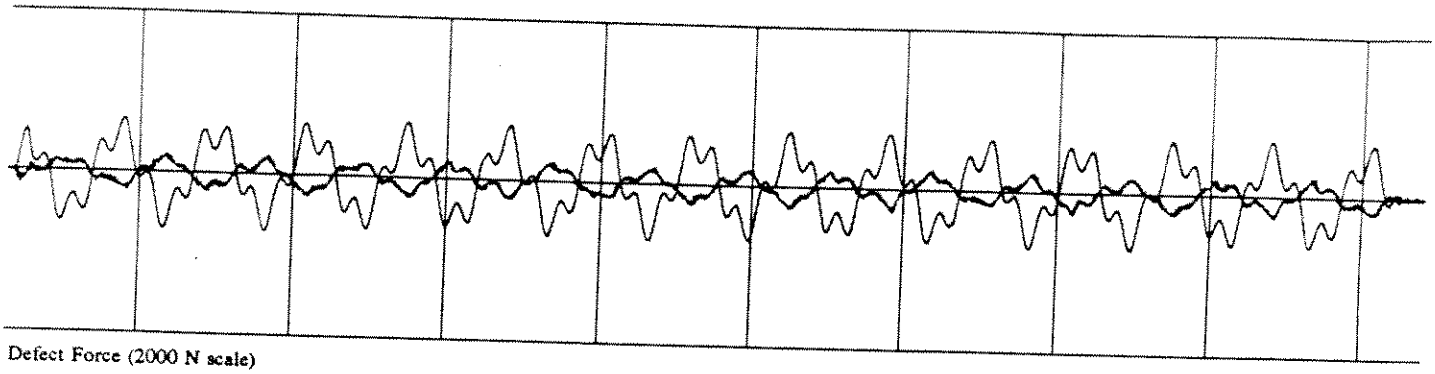

Defect Force (2000 N scale)

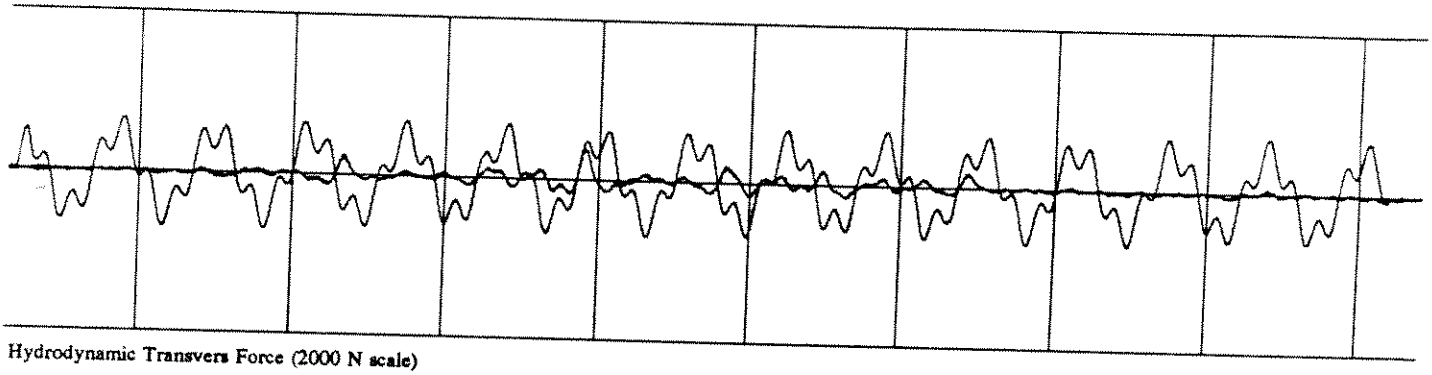

Hydrodynamic Transvers Force (2000 N scale)

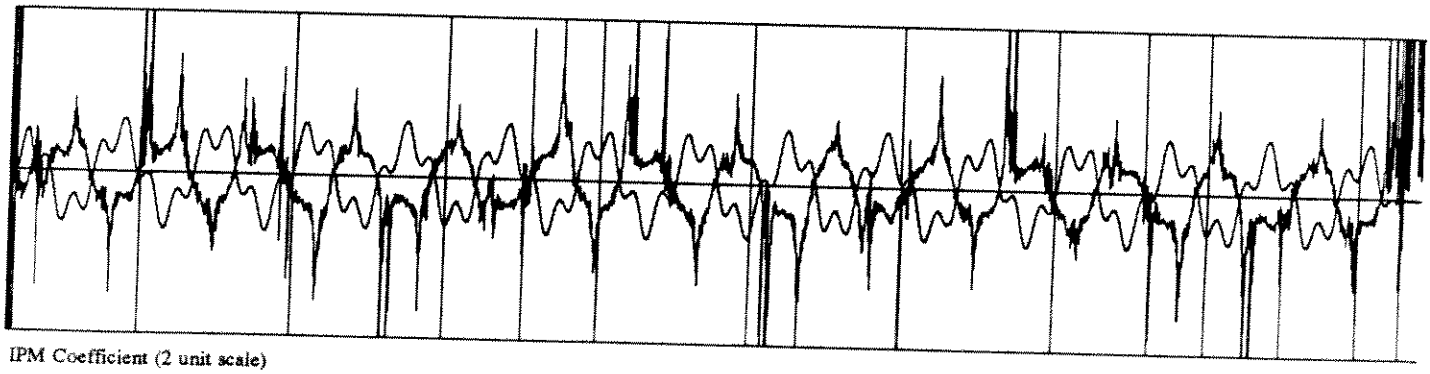

IPM Coefficient (2 unit scale)

PROCESSED DATA for RUN 195 points 1150 to 10400

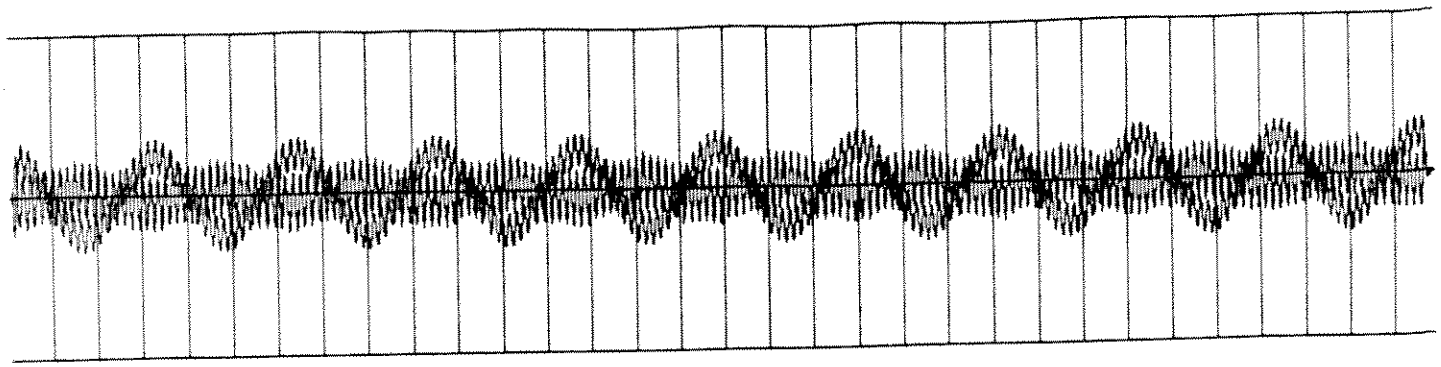

Hydrodynamic Inline Force (2000 N scale)

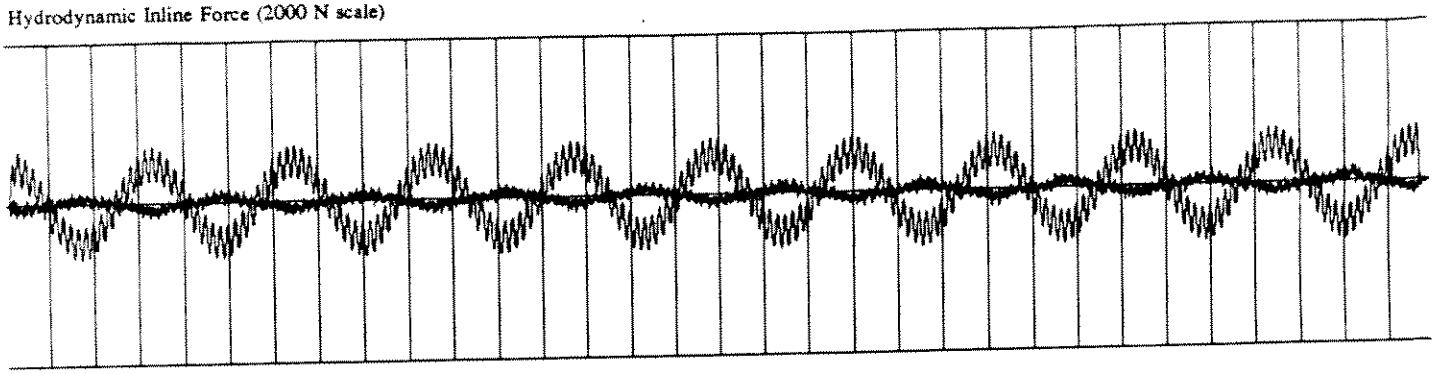

Defect Force (2000 N scale)

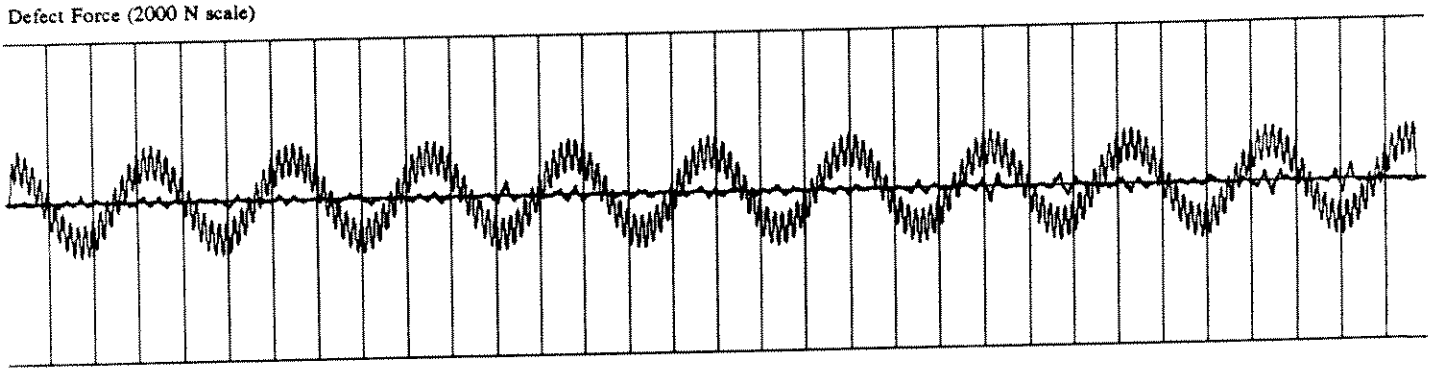

Hydrodynamic Transvers Force (2000 N scale)

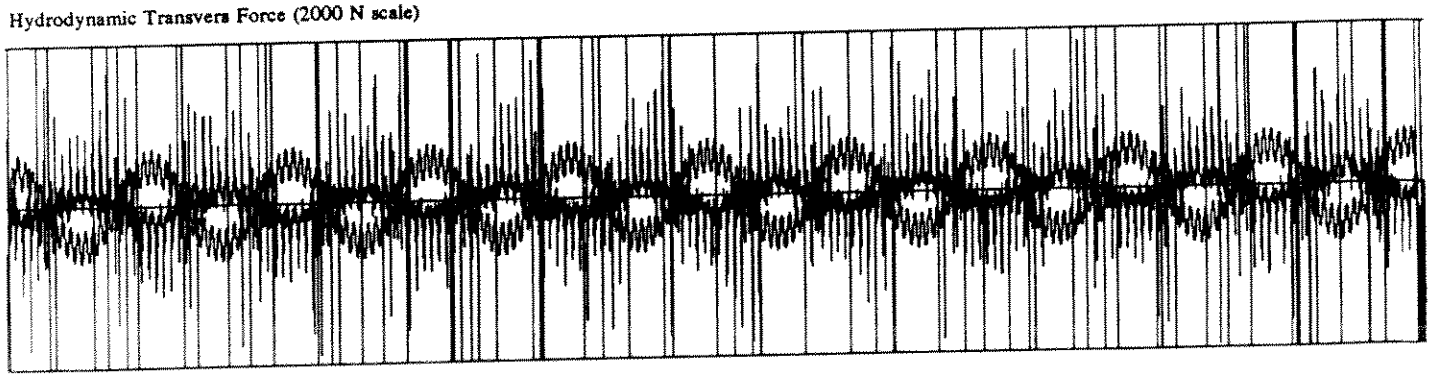

IPM Coefficient (2 unit scale)

PROCESSED DATA for RUN 441 points 30 to 31900

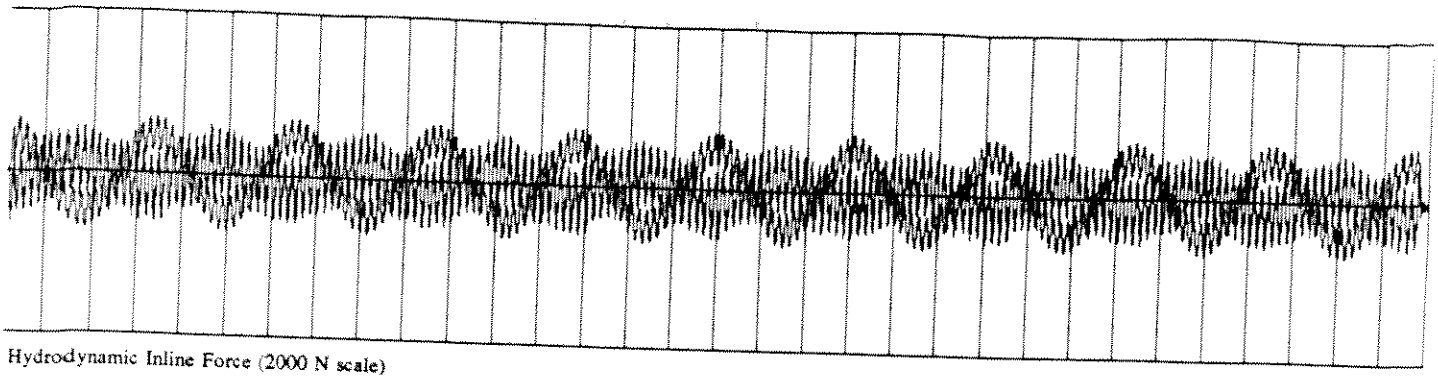

Hydrodynamic Inline Force (2000 N scale)

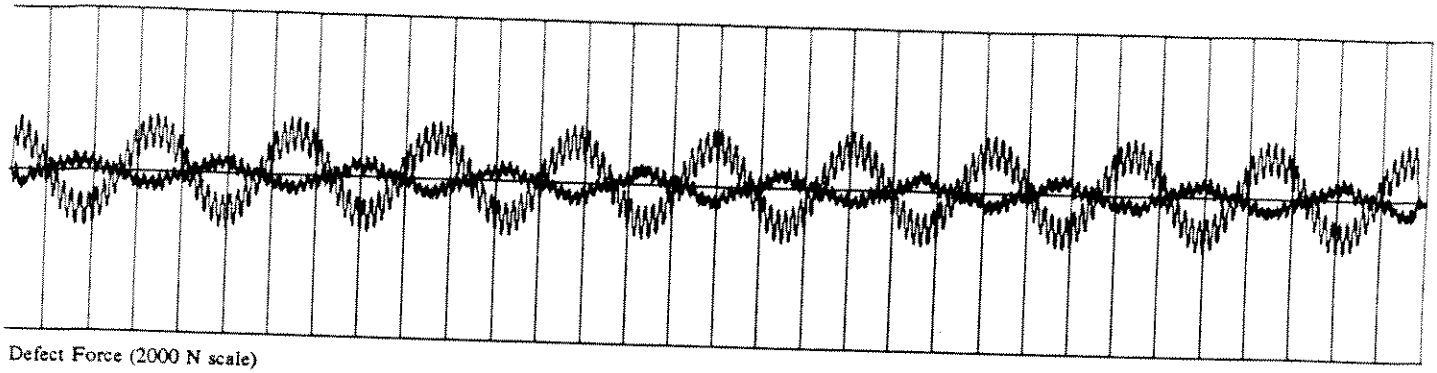

Defect Force (2000 N scale)

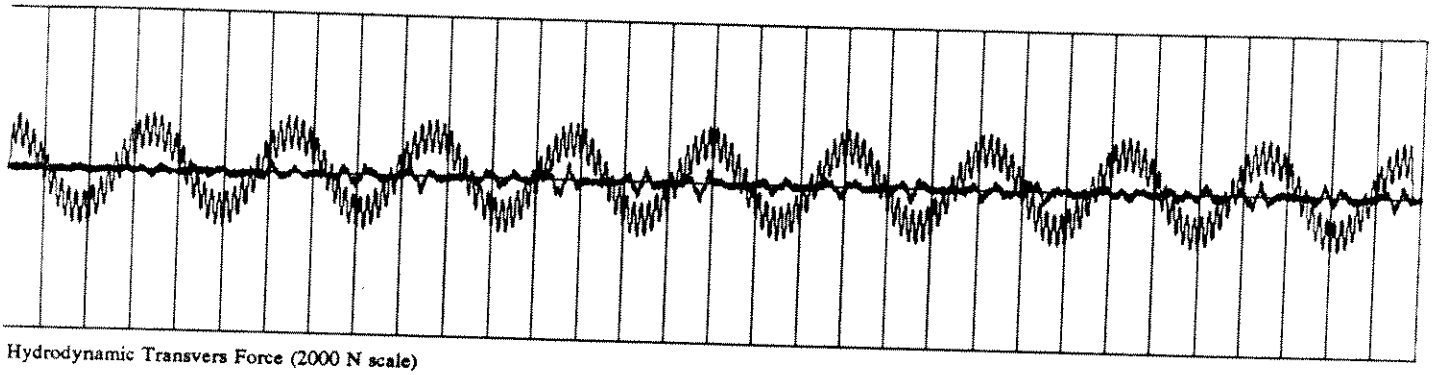

Hydrodynamic Transvers Force (2000 N scale)

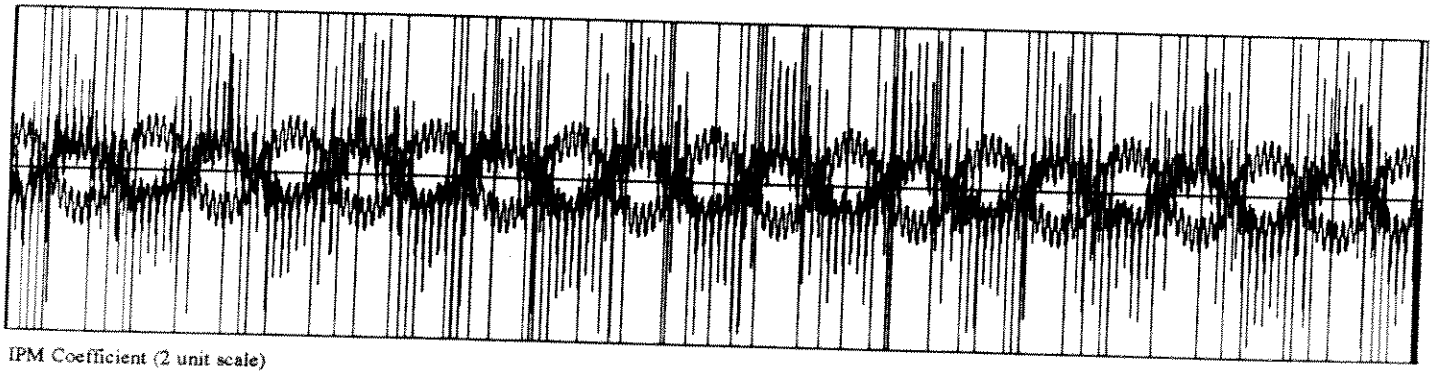

IPM Coefficient (2 unit scale)

PROCESSED DATA for RUN 196 points 150 to 32000

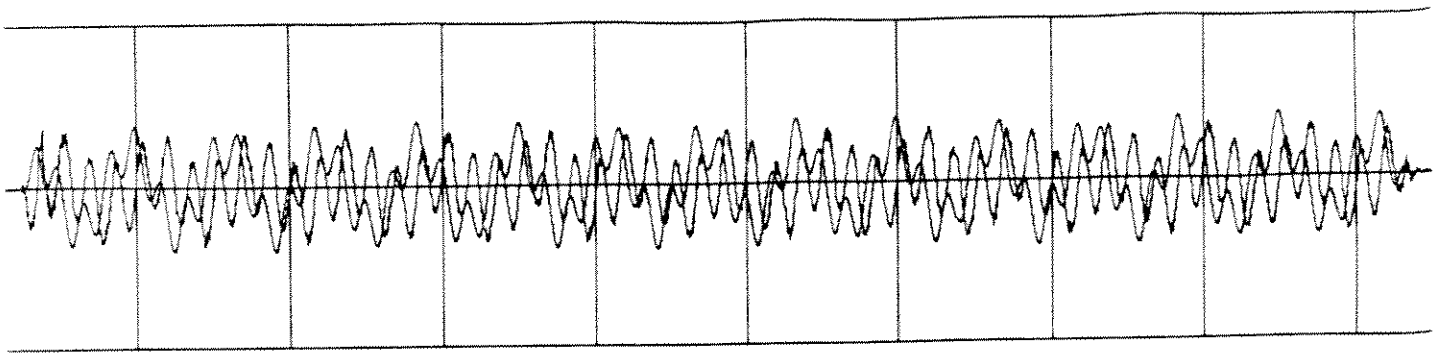

Hydrodynamic Inline Force (2000 N scale)

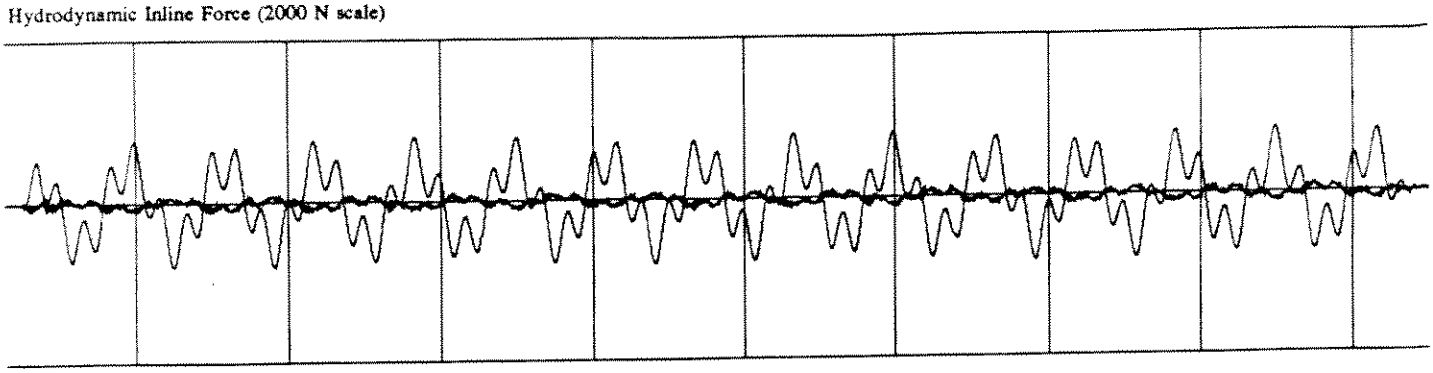

Defect Force (2000 N scale)

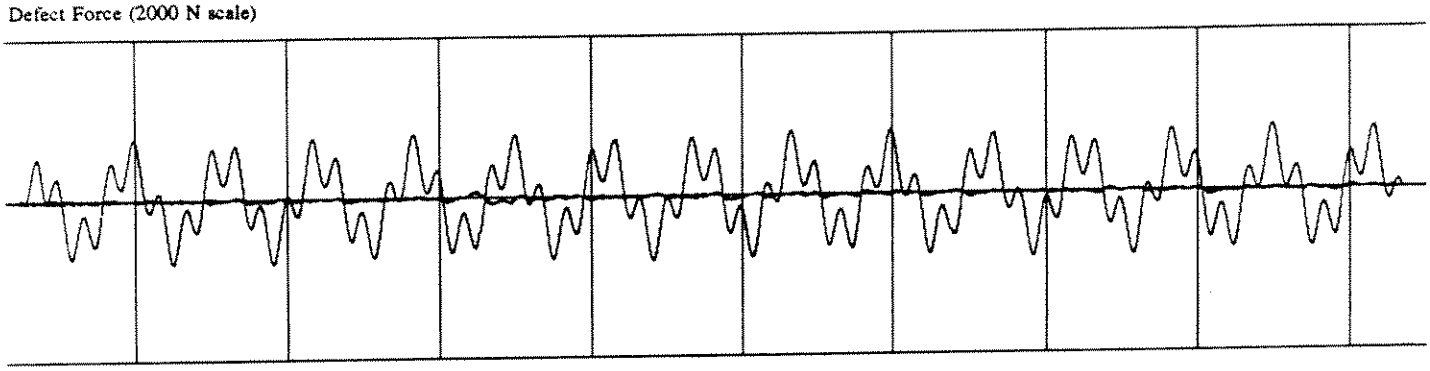

Hydrodynamic Transvers Force (2000 N scale)

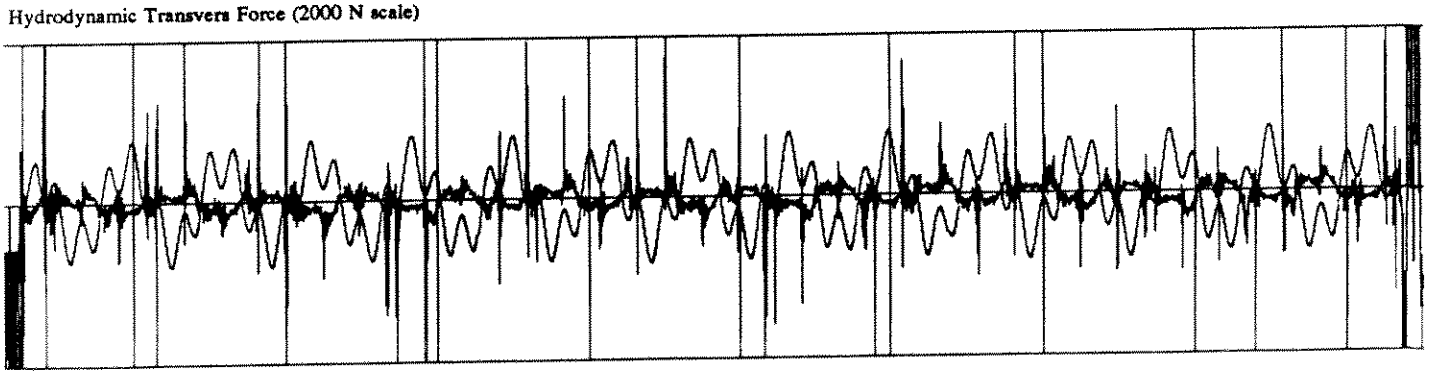

IPM Coefficient (2 unit scale)

PROCESSED DATA for RUN 443 points 1150 to 10500

PROCESSED DATA for RUN 197 points 1200 to 10400

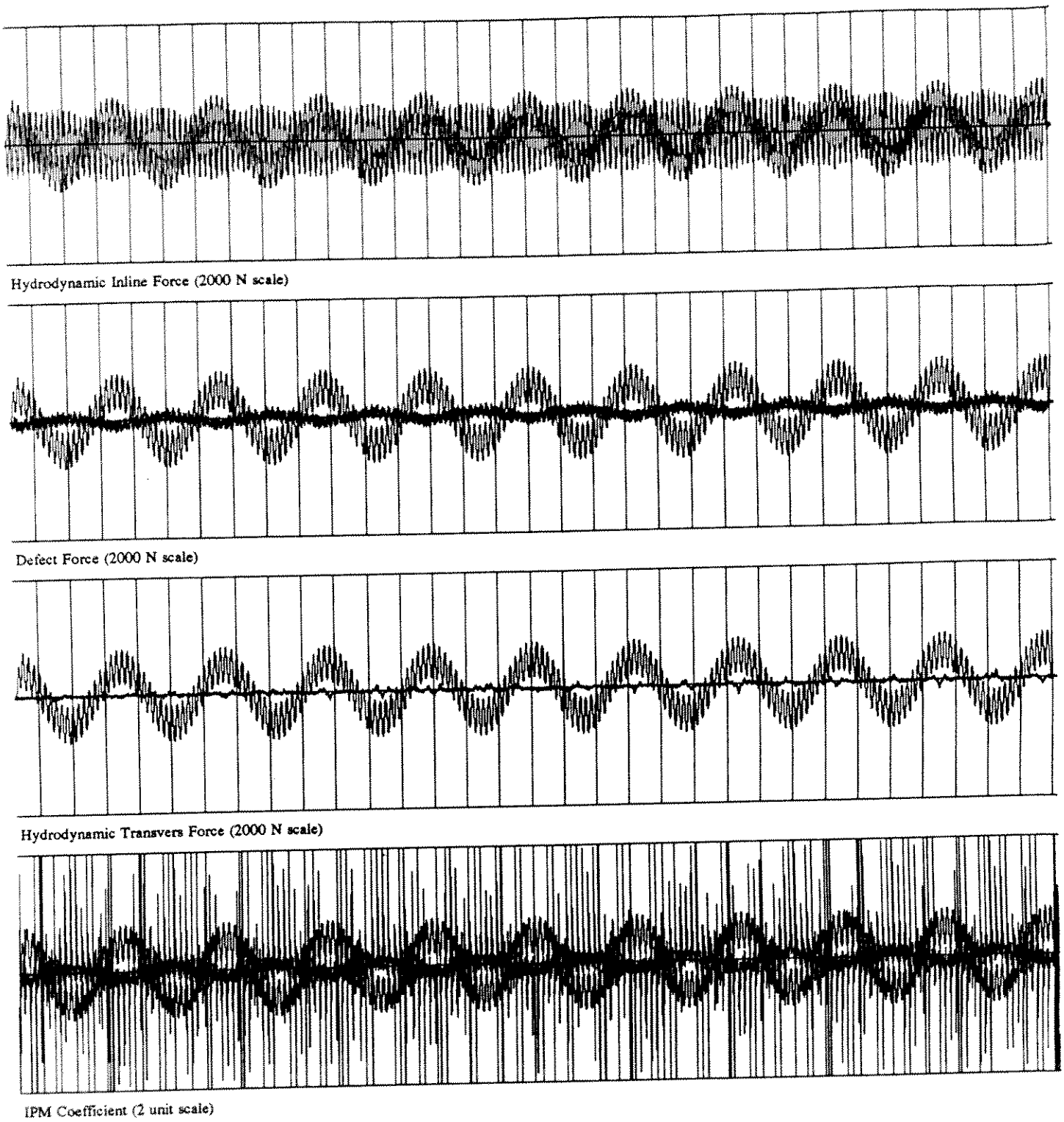

PROCESSED DATA for RUN 442 points 250 to 32100

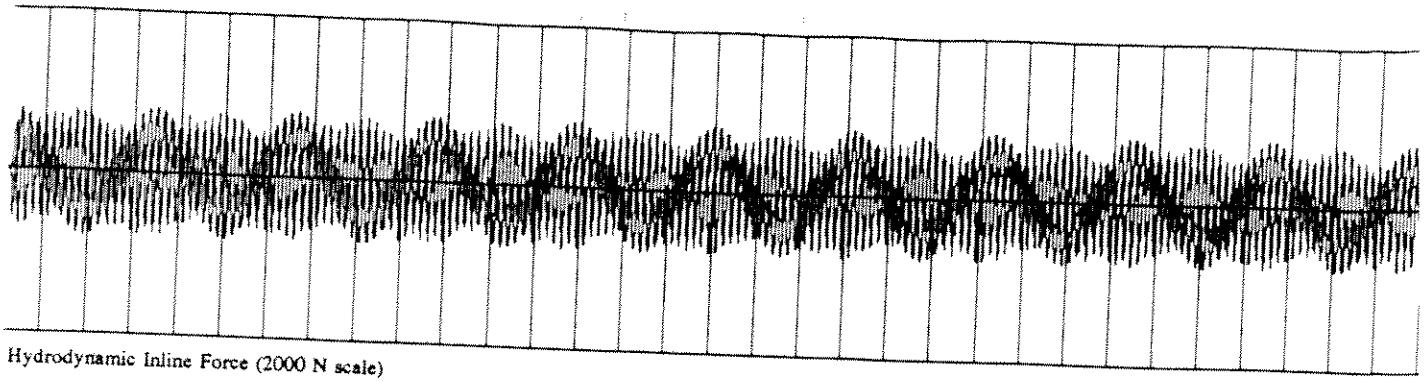

Hydrodynamic Inline Force (2000 N scale)

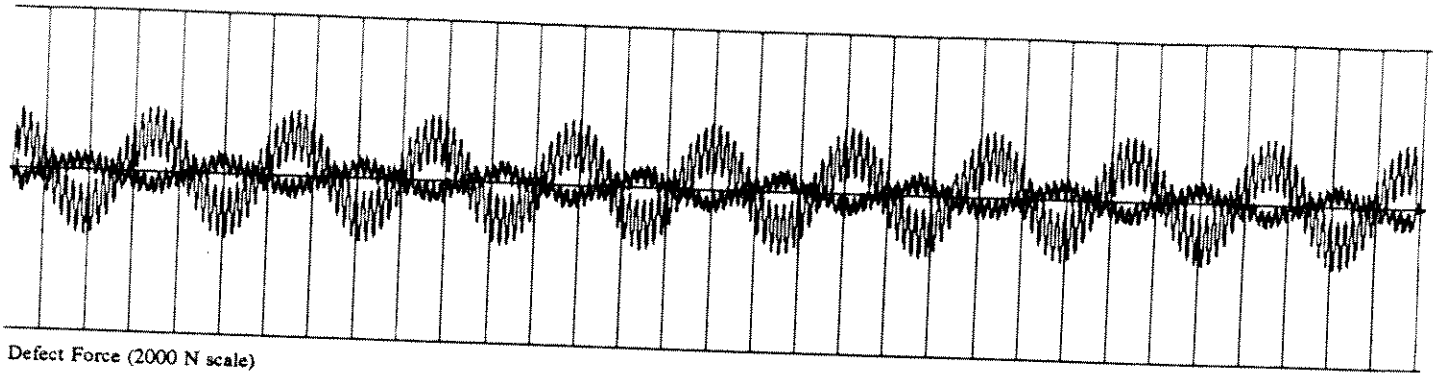

Defect Force (2000 N scale)

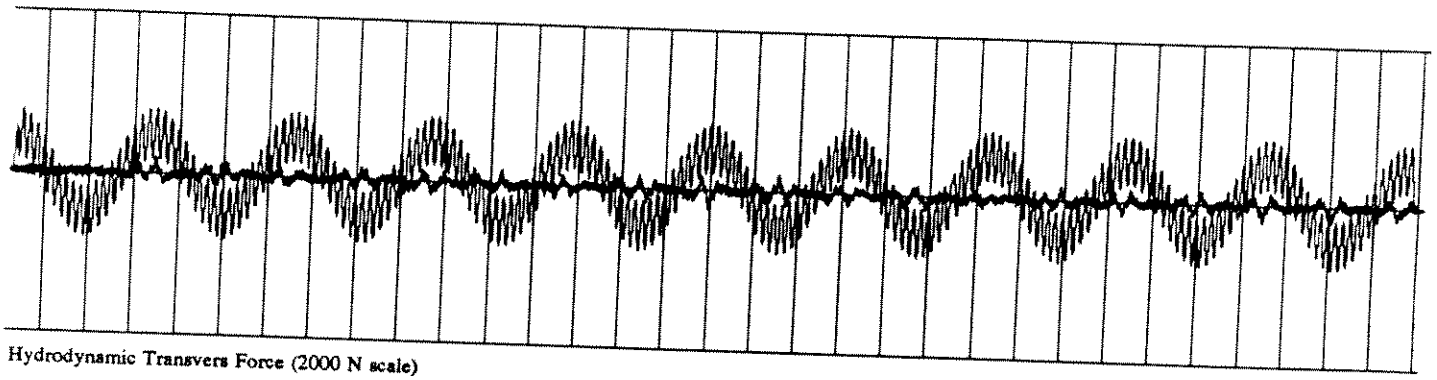

Hydrodynamic Transvers Force (2000 N scale)

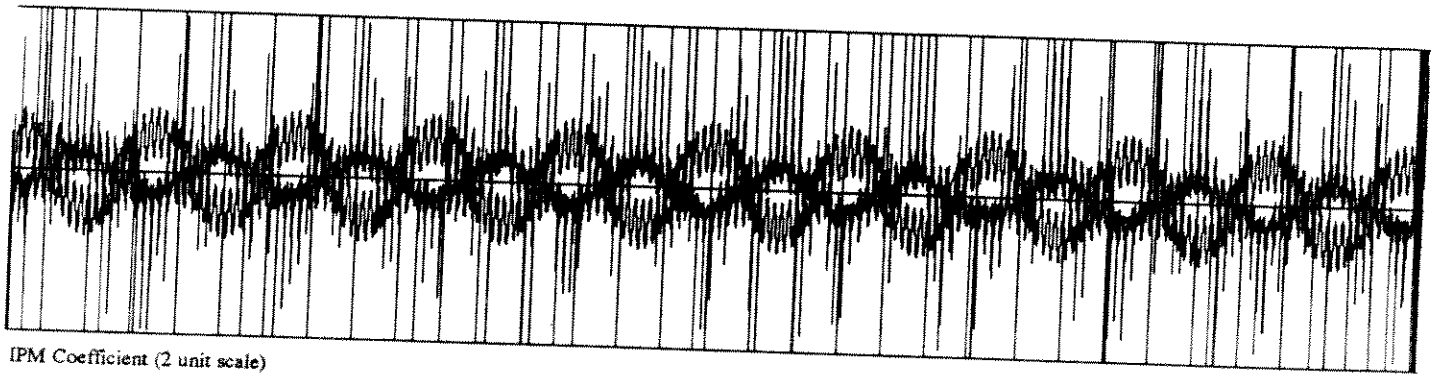

IPM Coefficient (2 unit scale)

PROCESSED DATA for RUN 198 points 200 to 32100

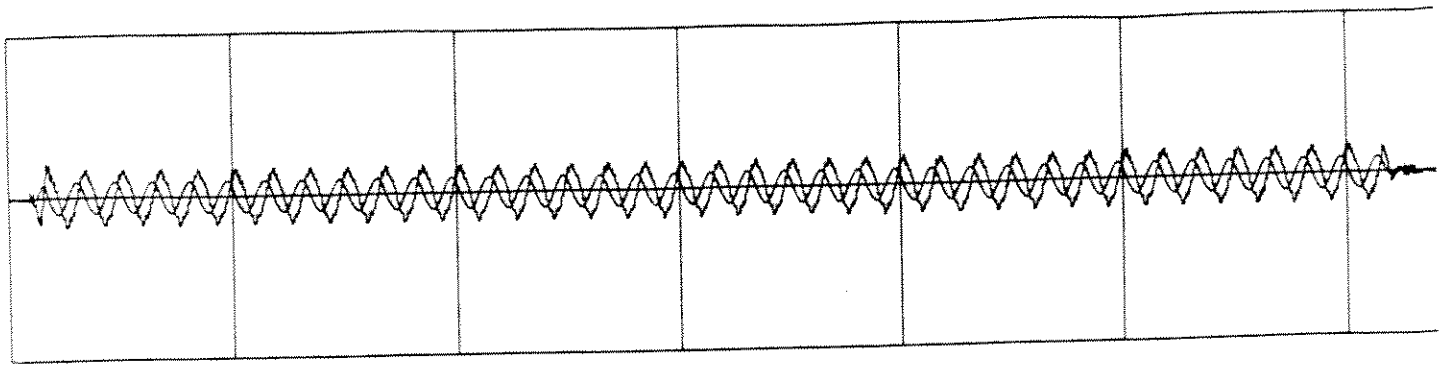

Hydrodynamic Inline Force (2000 N scale)

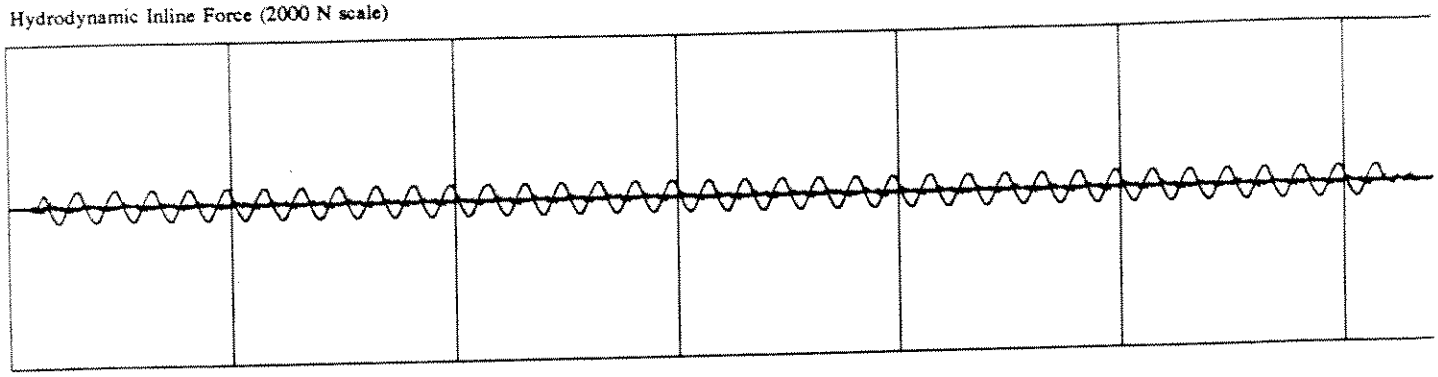

Defect Force (2000 N scale)

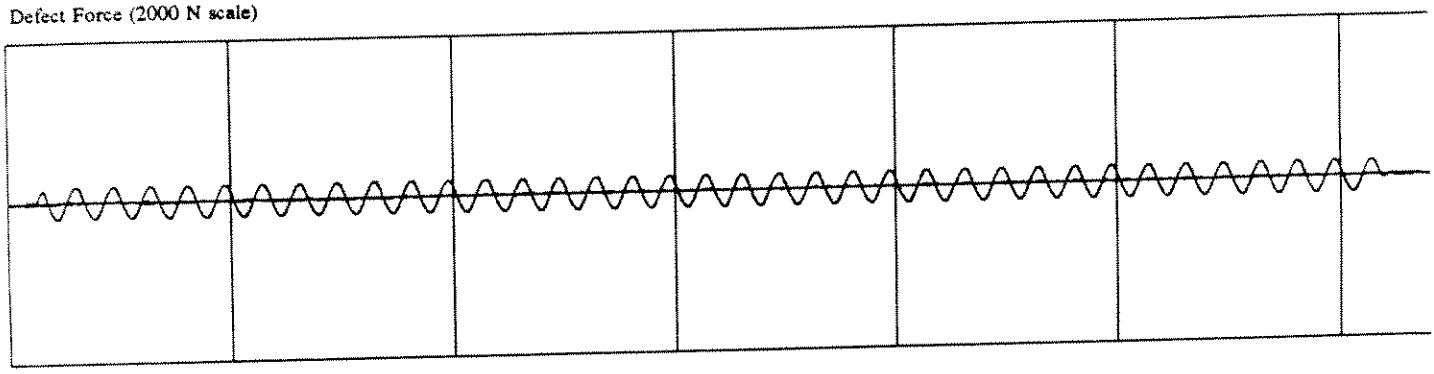

Hydrodynamic Transvers Force (2000 N scale)

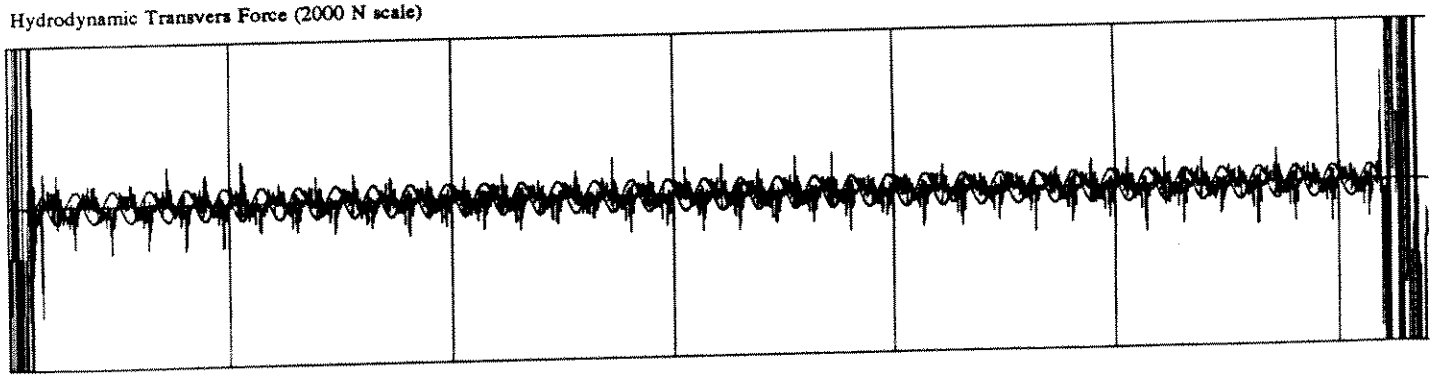

IPM Coefficient (2 unit scale)

PROCESSED DATA for RUN 445 points 1000 to 7400

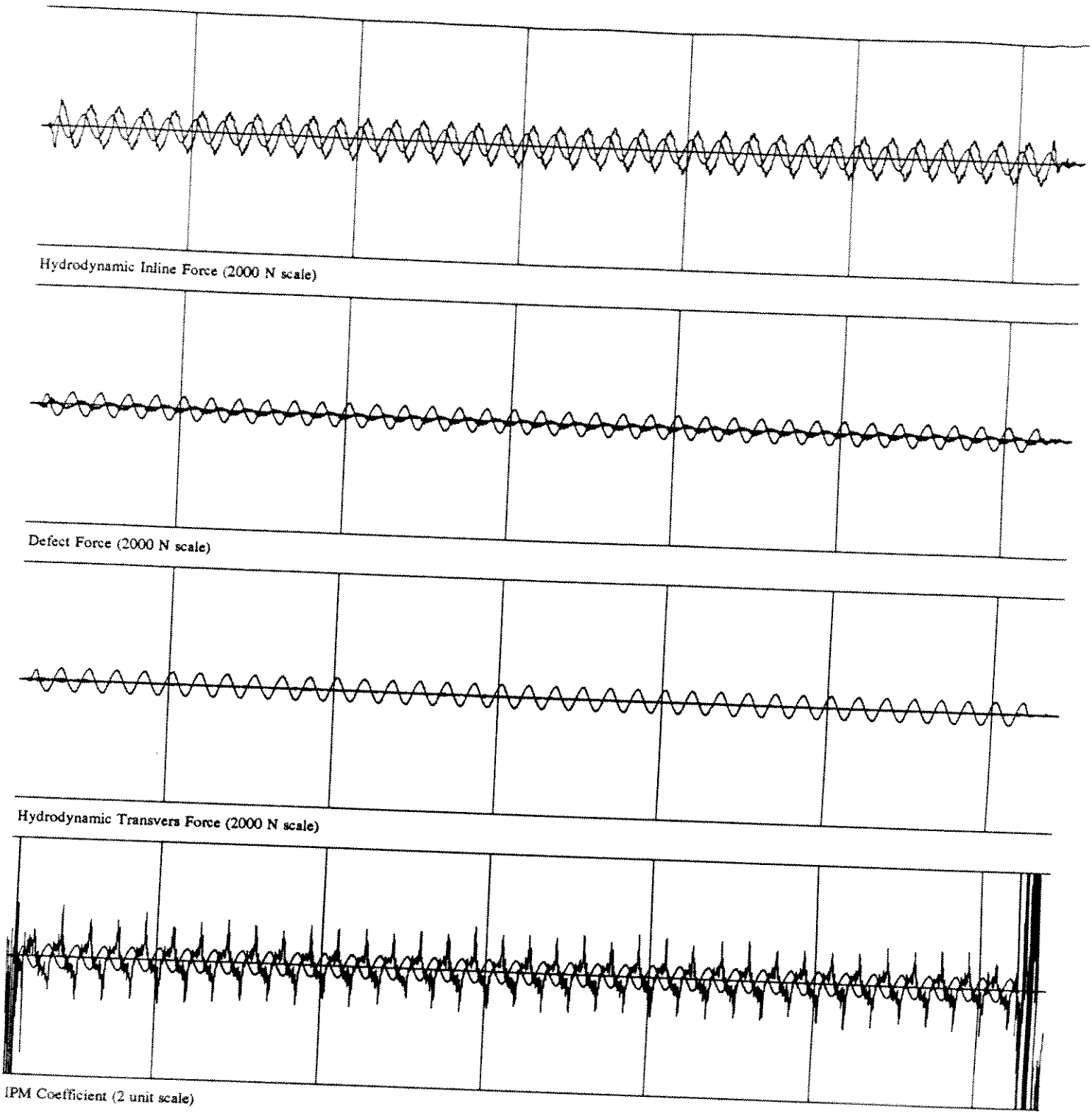

PROCESSED DATA for RUN 199 points 1100 to 7400

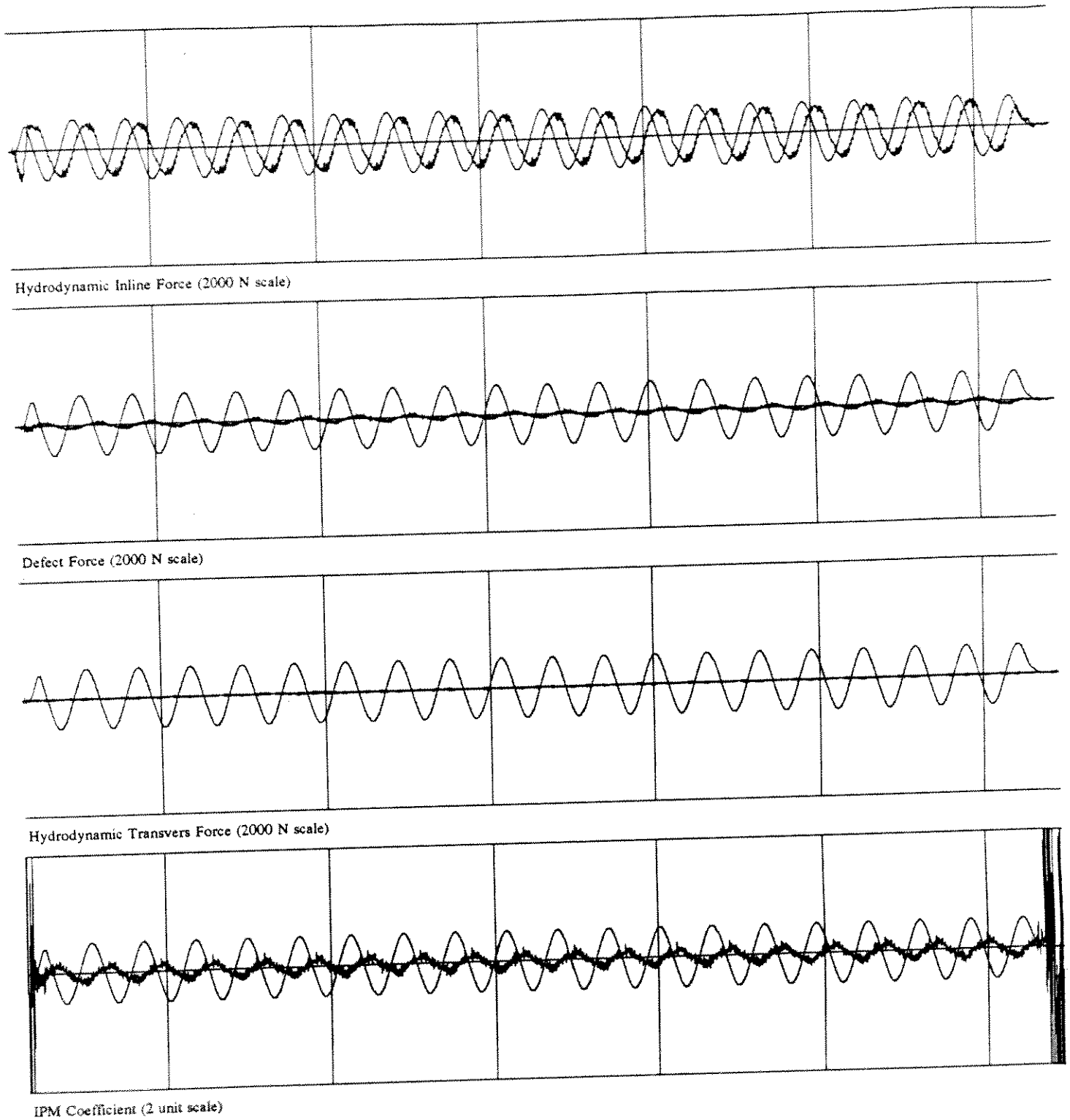

PROCESSED DATA for RUN 351 points 1160 to 7450

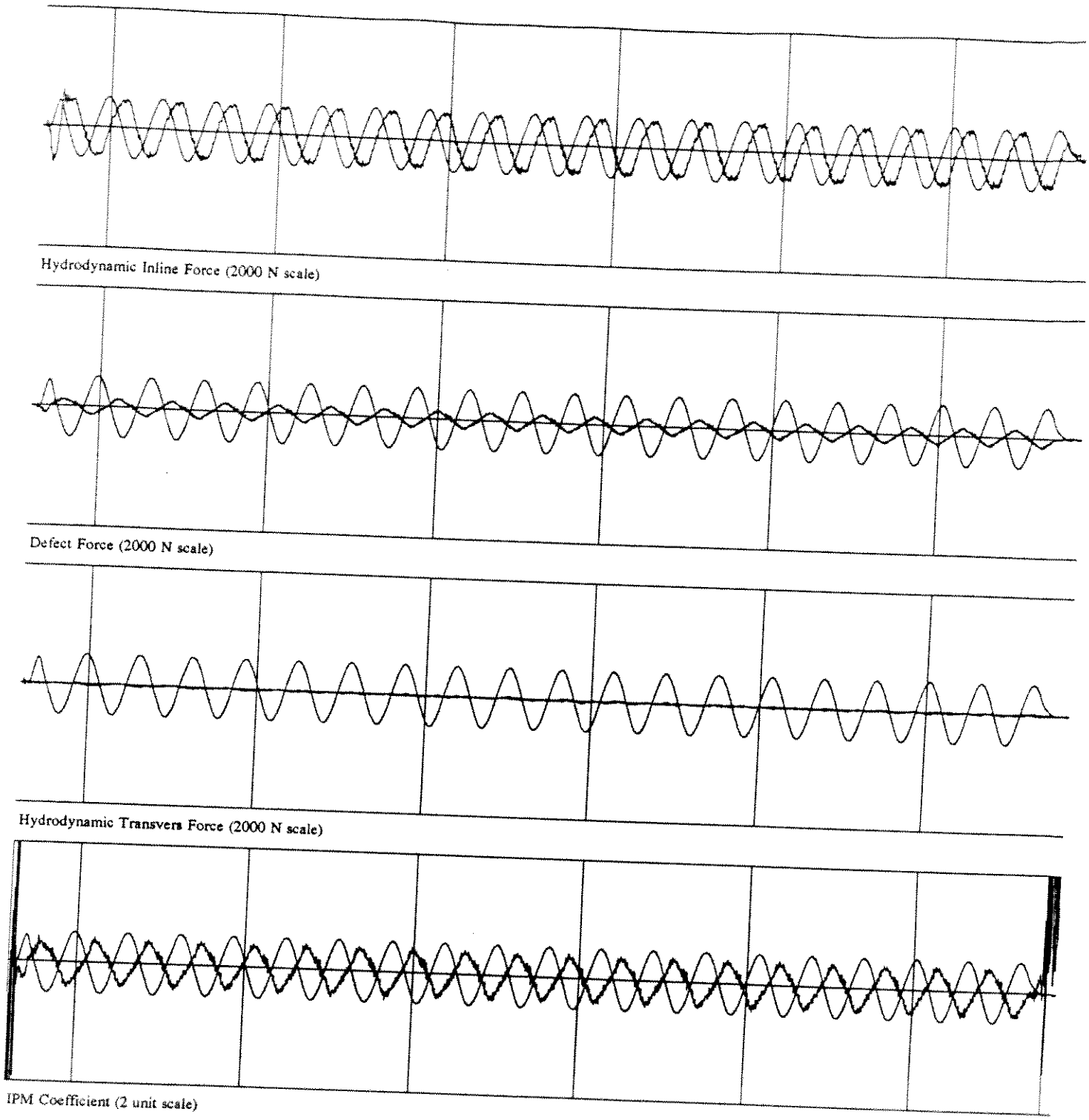

PROCESSED DATA for RUN 95 points 1600 to 7850

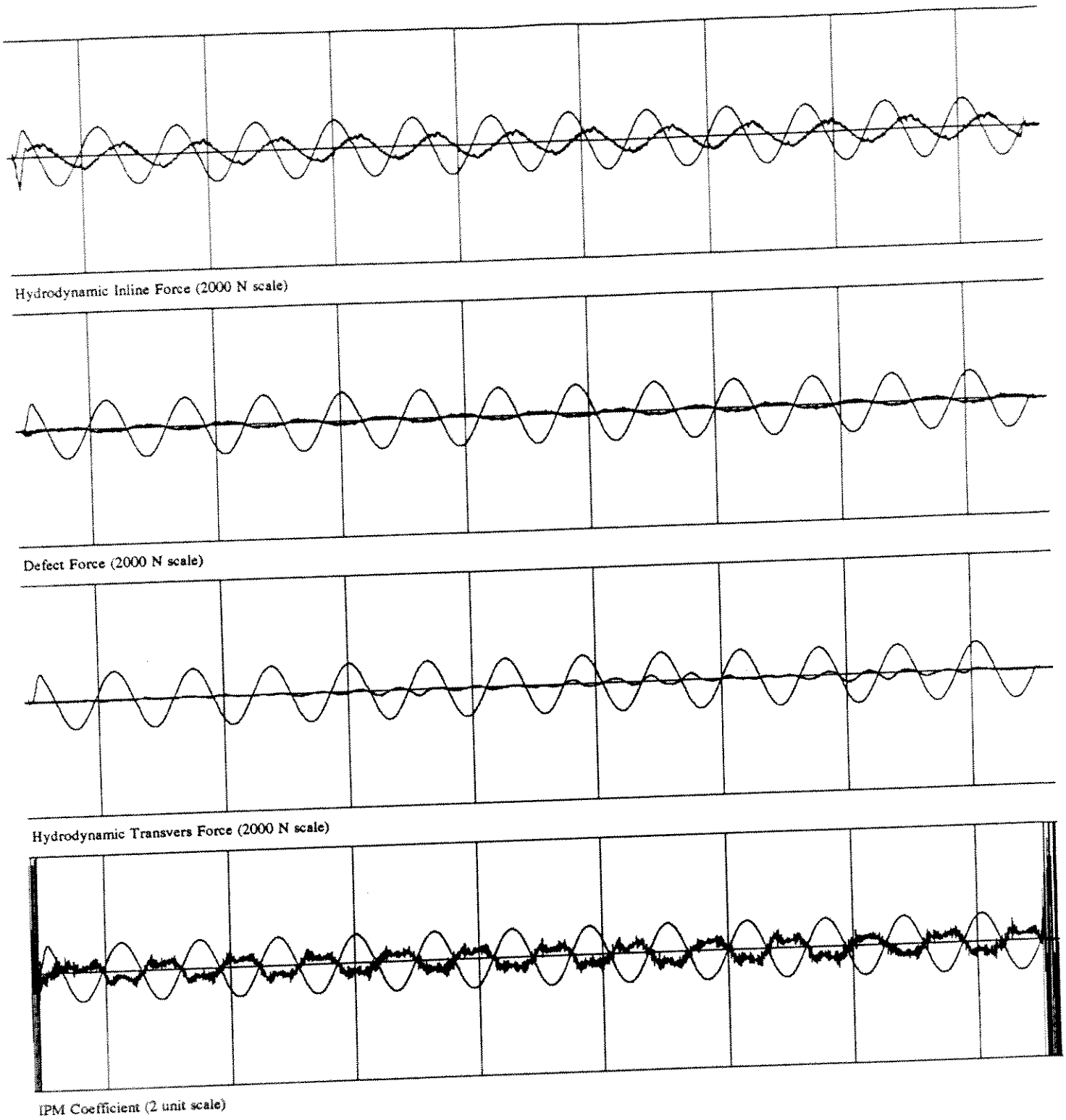

PROCESSED DATA for RUN 352 points 1400 to 9650

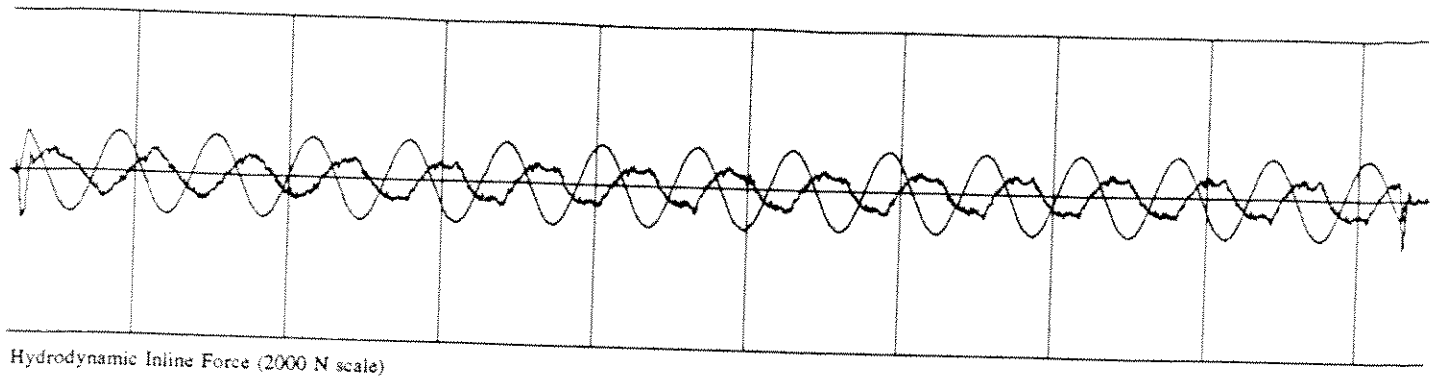

Hydrodynamic Inline Force (2000 N scale)

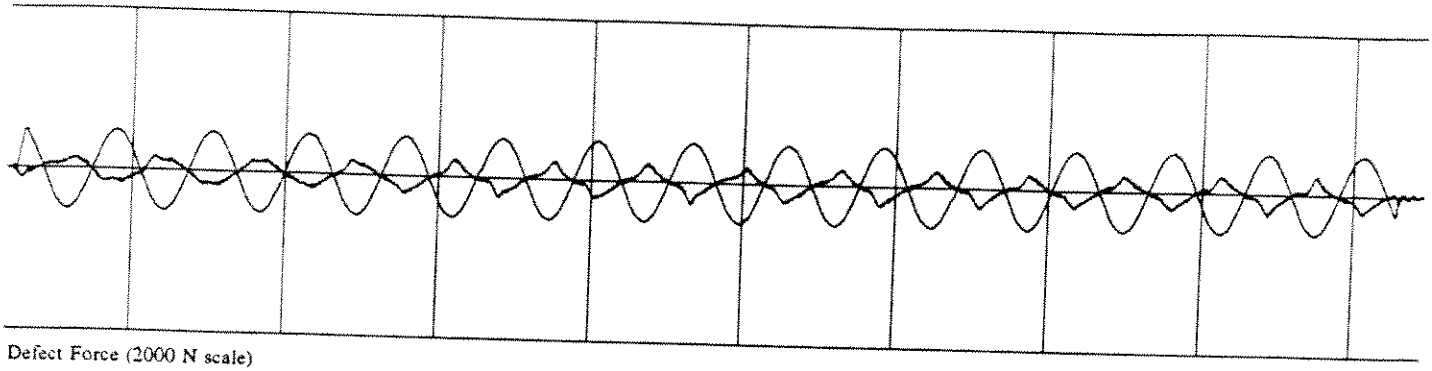

Defect Force (2000 N scale)

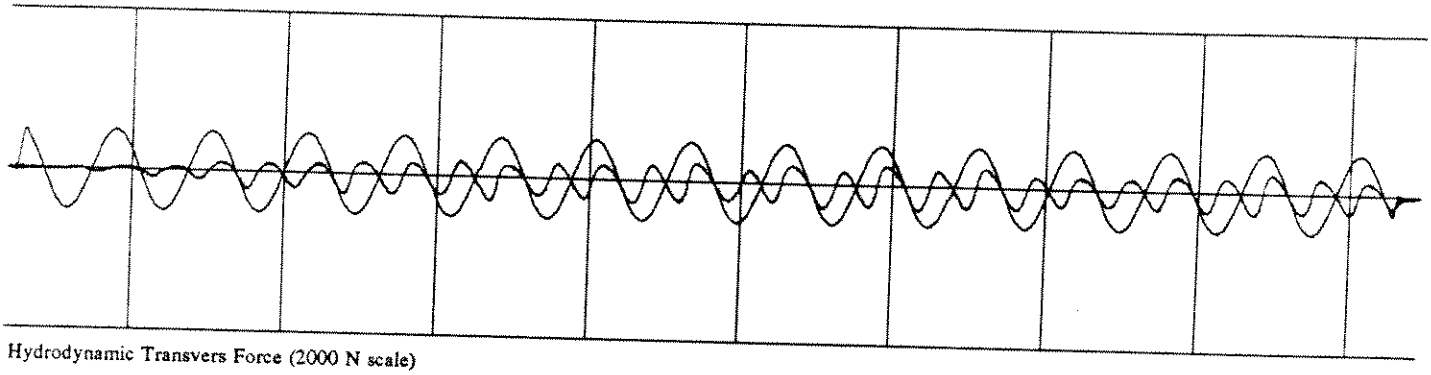

Hydrodynamic Transvers Force (2000 N scale)

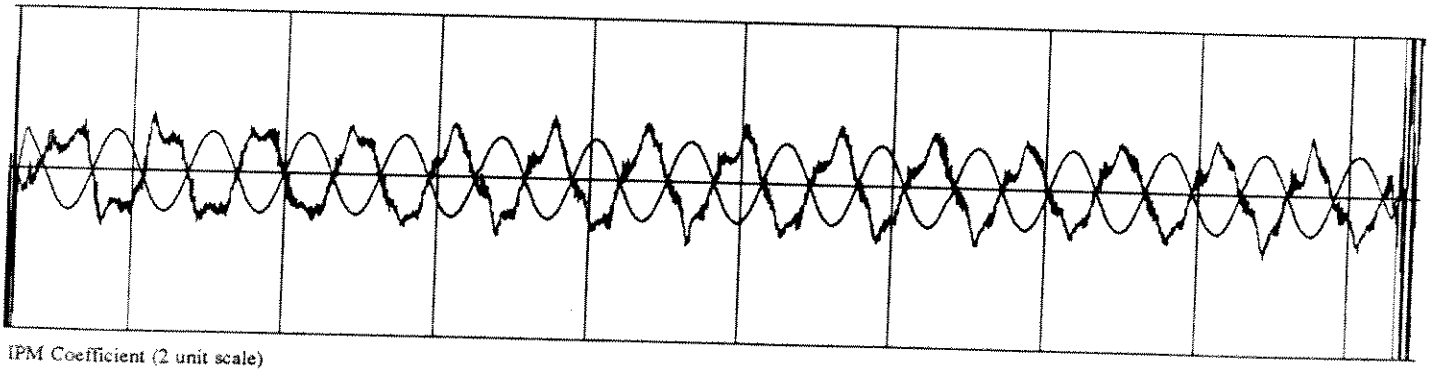

IPM Coefficient (2 unit scale)

PROCESSED DATA for RUN 96 points 1180 to 10450

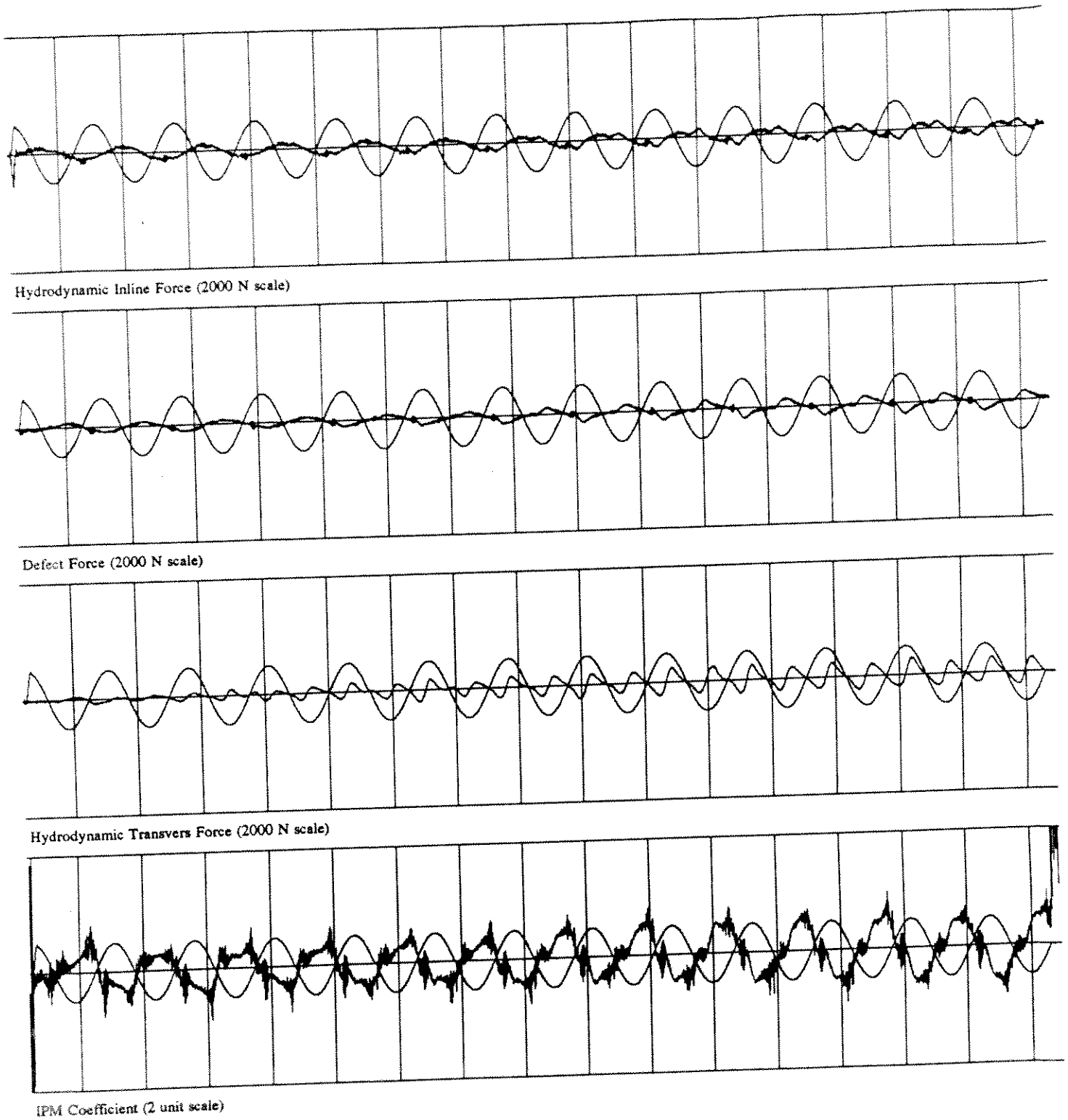

PROCESSED DATA for RUN 353 points 1200 to 17450

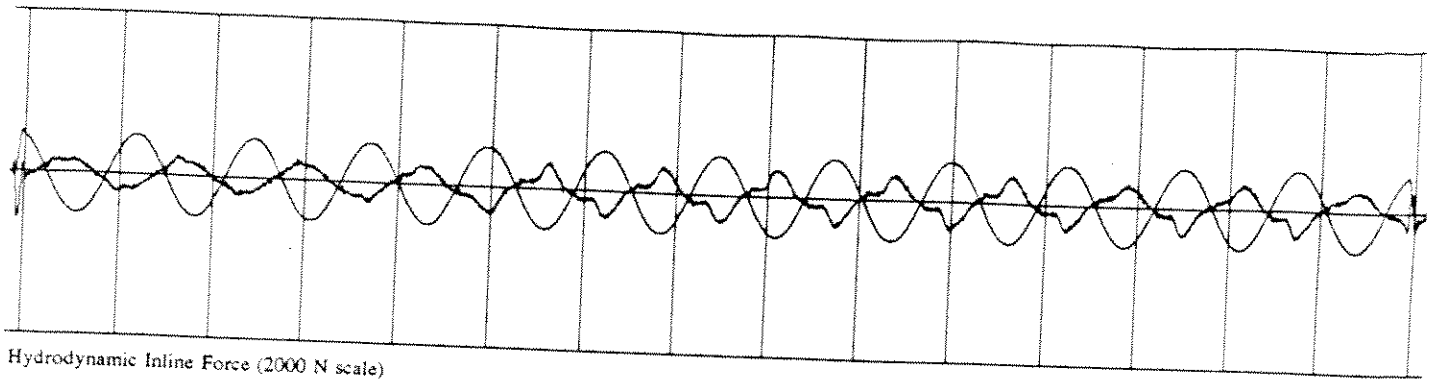

Hydrodynamic Inline Force (2000 N scale)

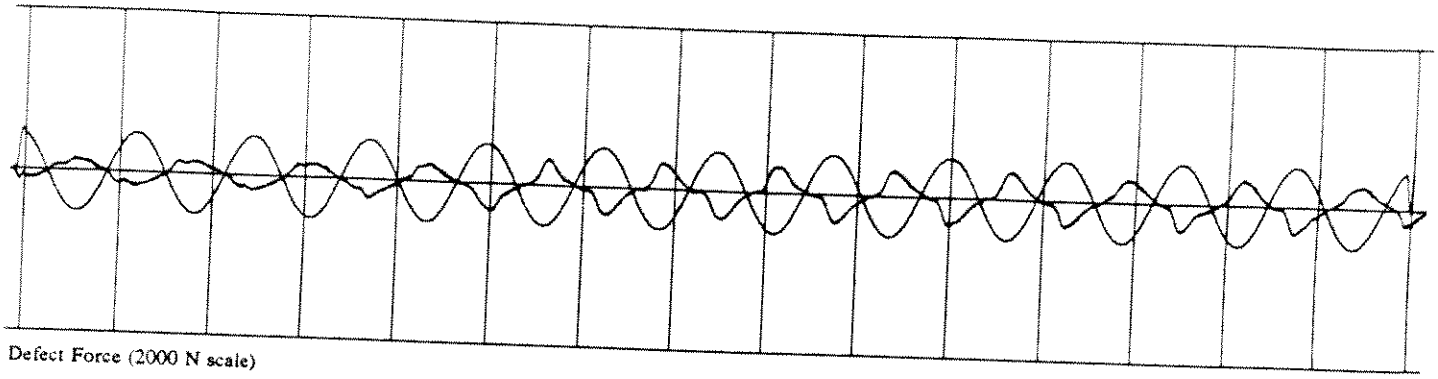

Defect Force (2000 N scale)

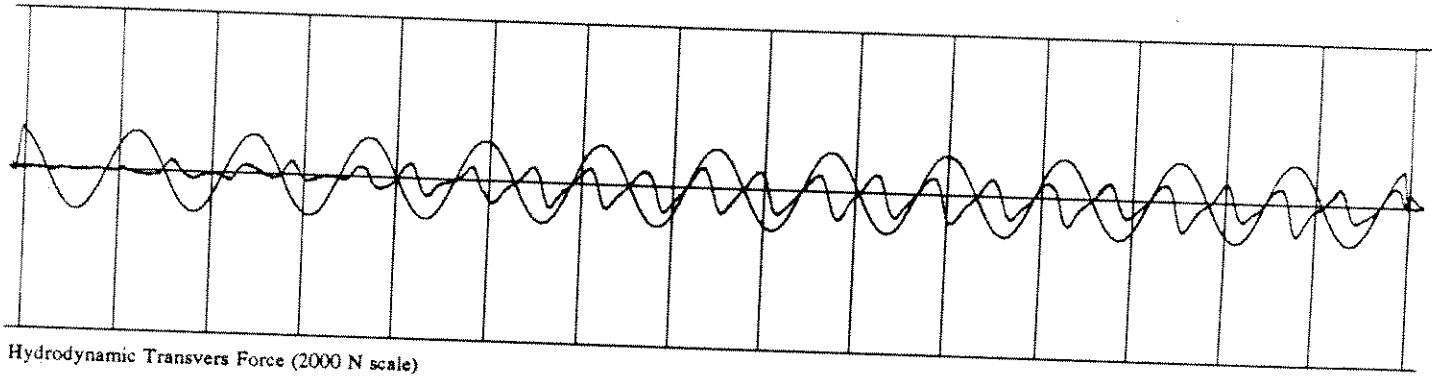

Hydrodynamic Transvers Force (2000 N scale)

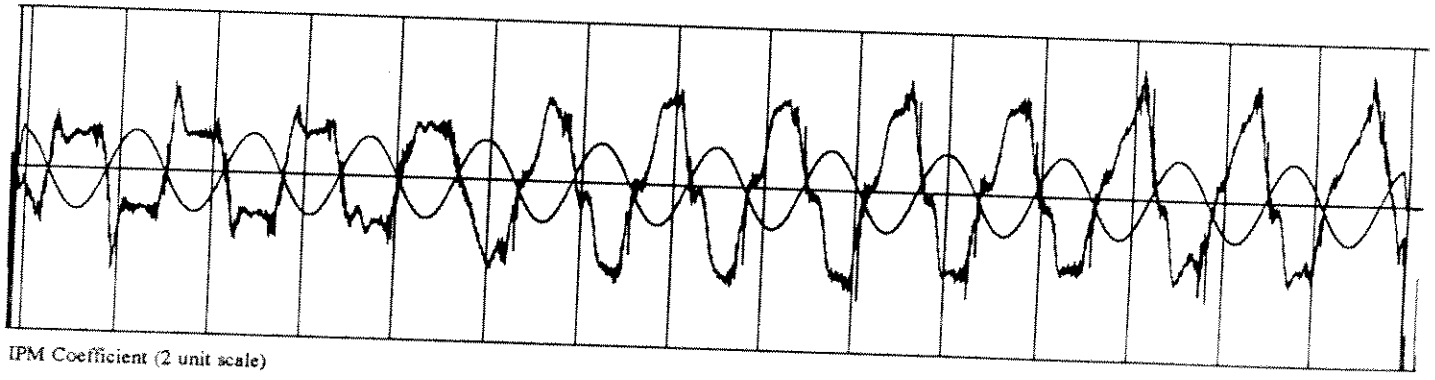

IPM Coefficient (2 unit scale)

PROCESSED DATA for RUN 97 points 1830 to 17150

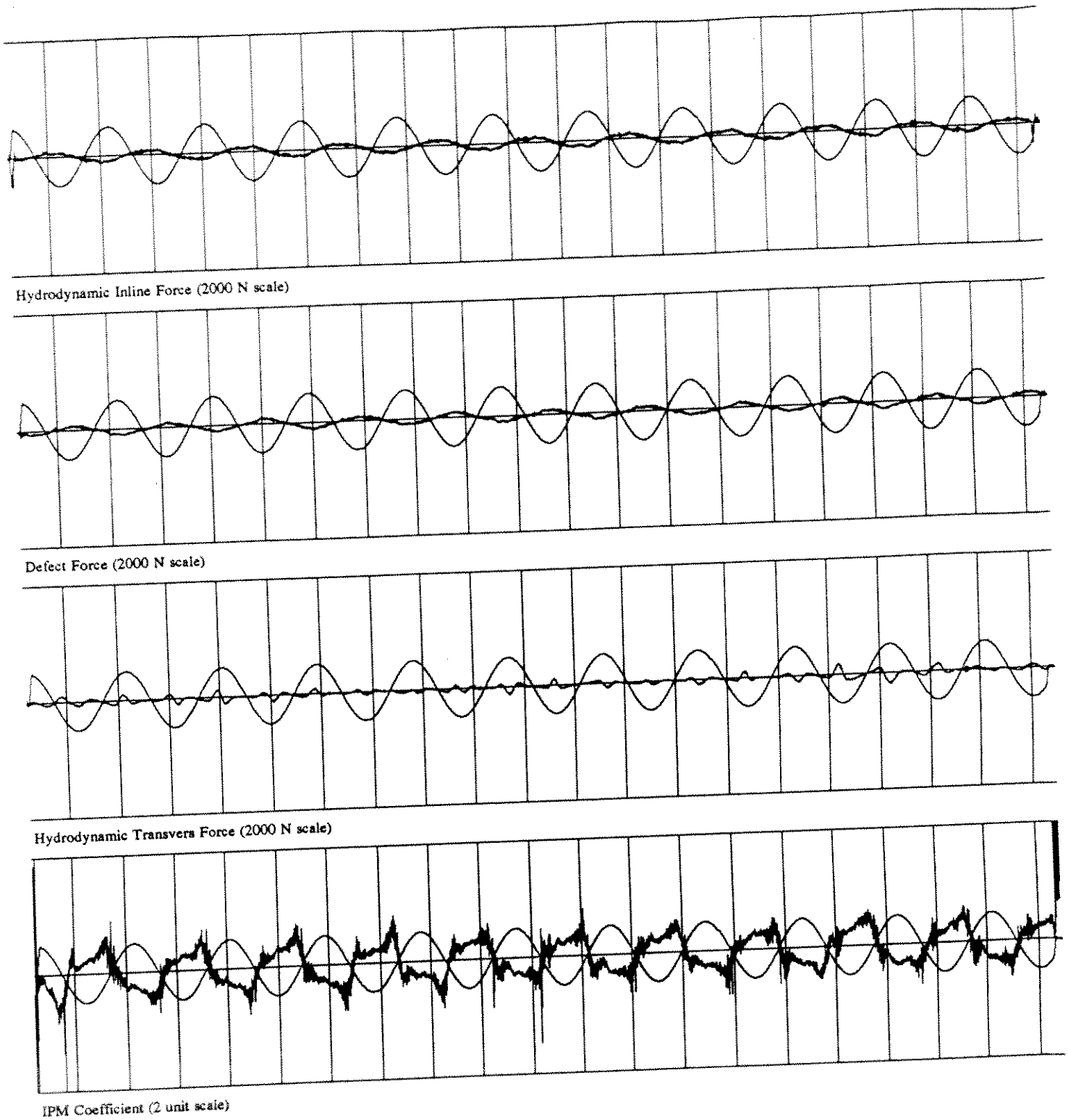

PROCESSED DATA for RUN 356 points 1200 to 21450

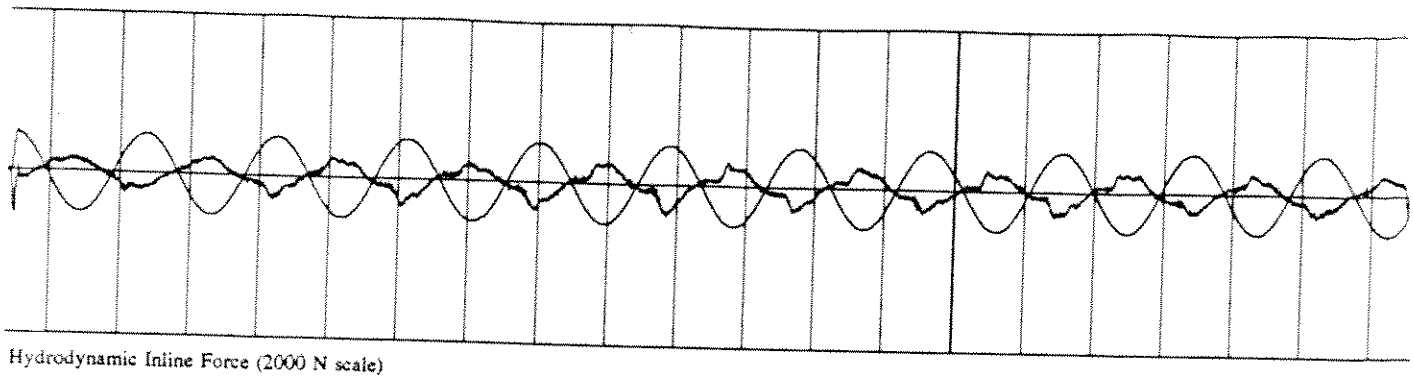

Hydrodynamic Inline Force (2000 N scale)

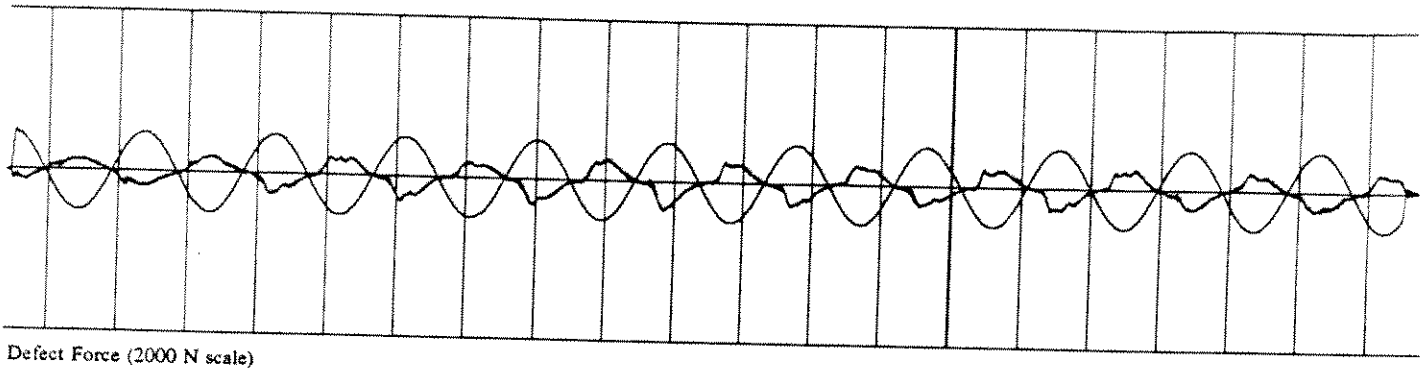

Defect Force (2000 N scale)

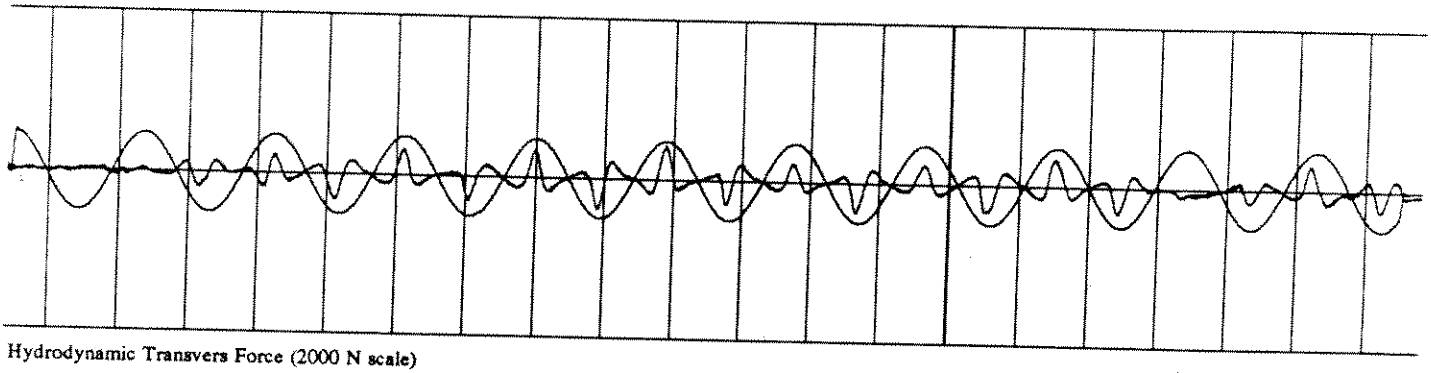

Hydrodynamic Transvers Force (2000 N scale)

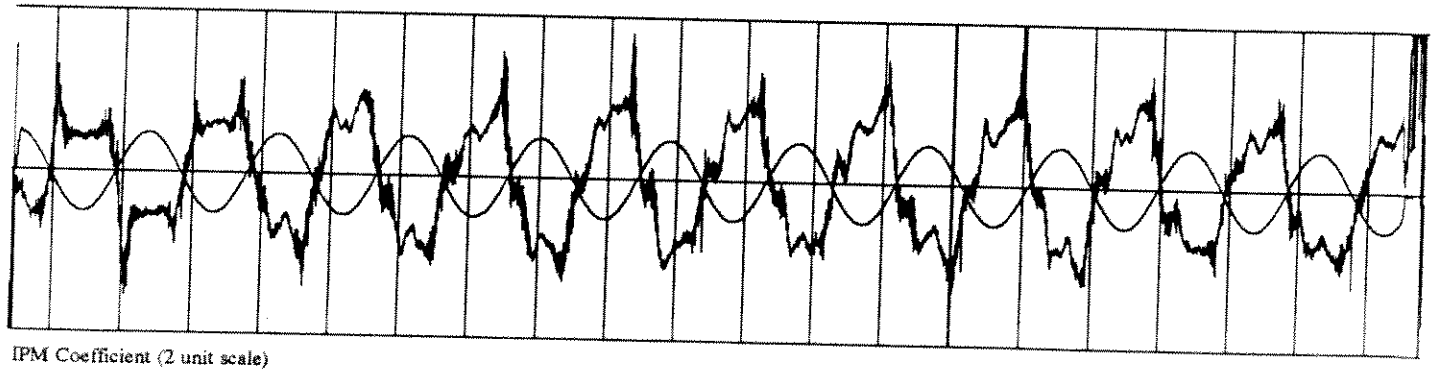

IPM Coefficient (2 unit scale)

PROCESSED DATA for RUN 295 points 1400 to 21800

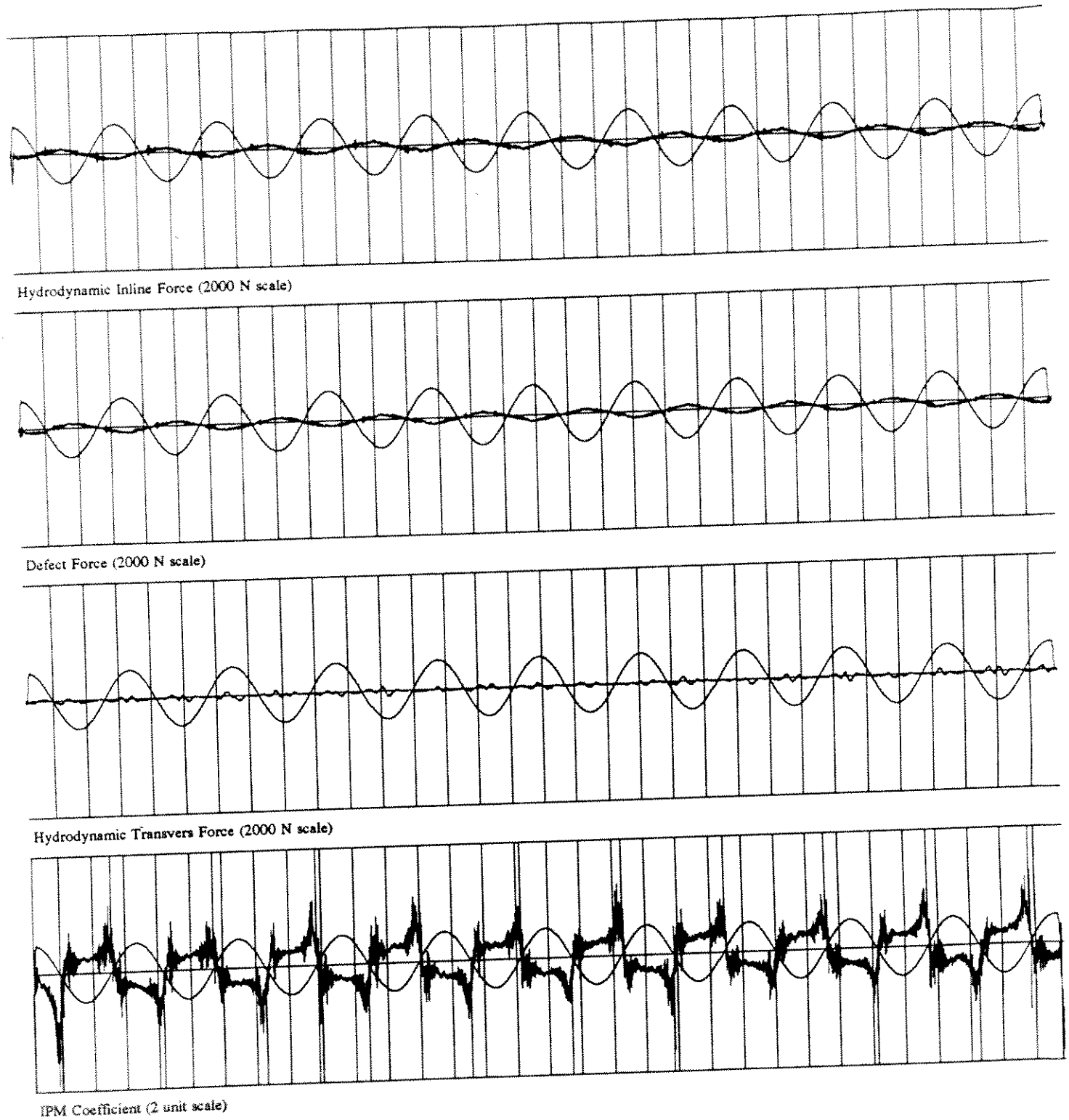

PROCESSED DATA for RUN 354 points 140 to 31850

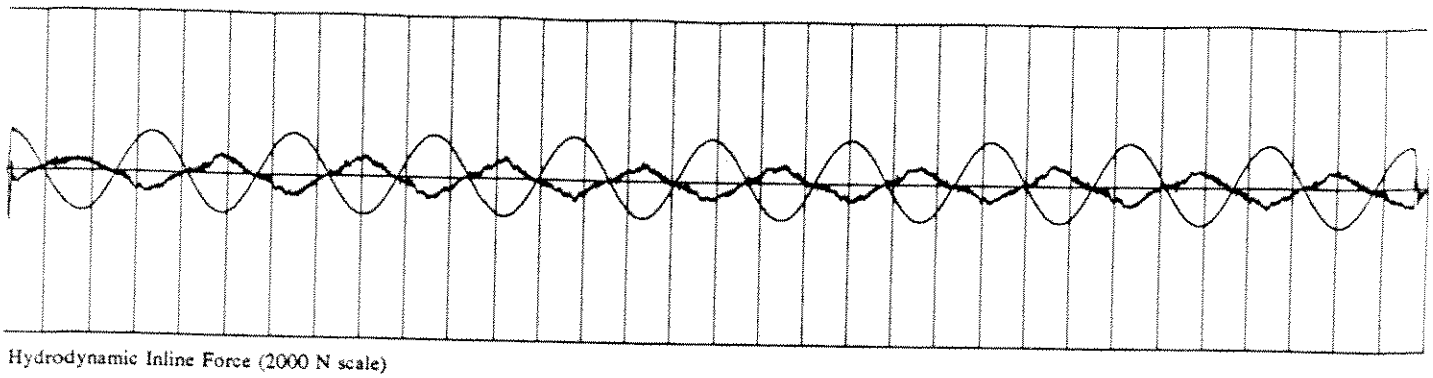

Hydrodynamic Inline Force (2000 N scale)

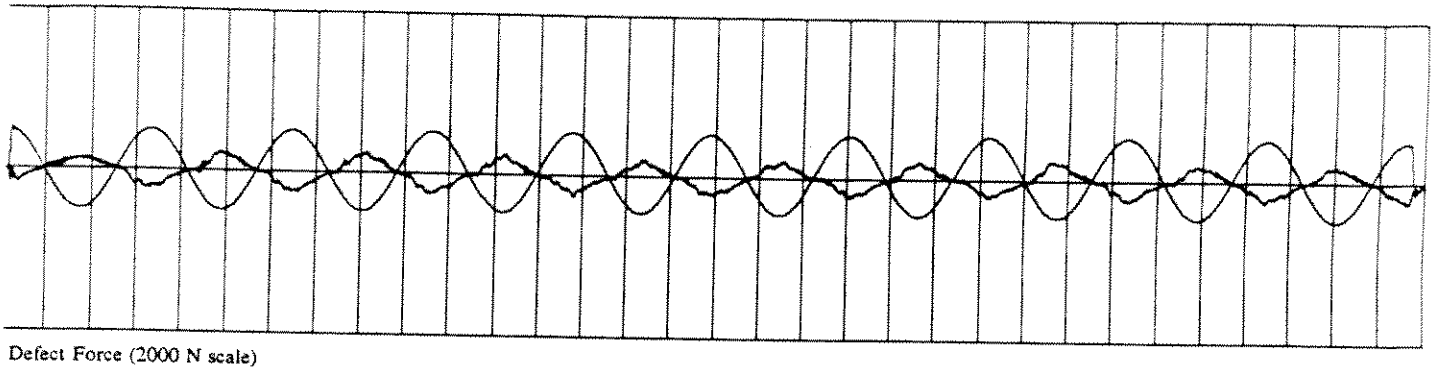

Defect Force (2000 N scale)

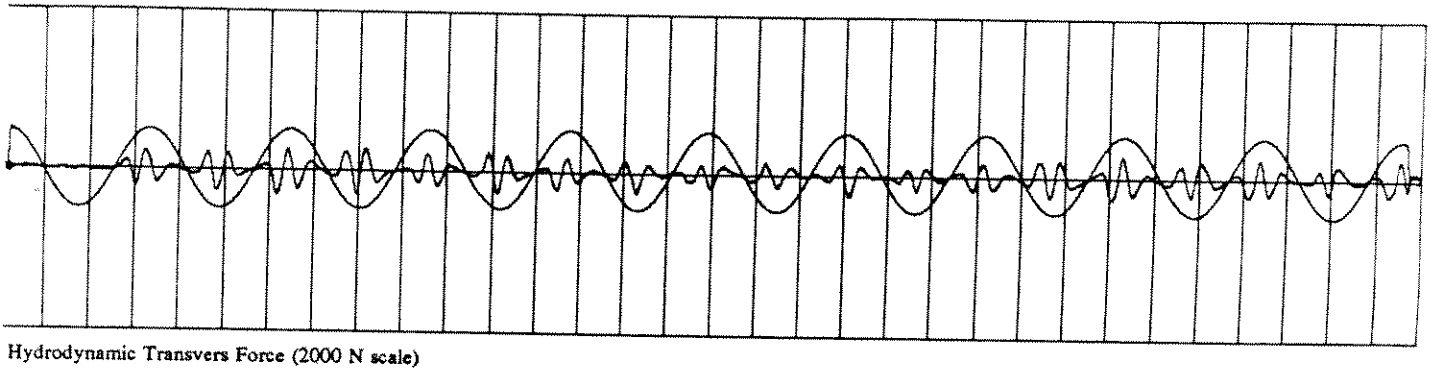

Hydrodynamic Transvers Force (2000 N scale)

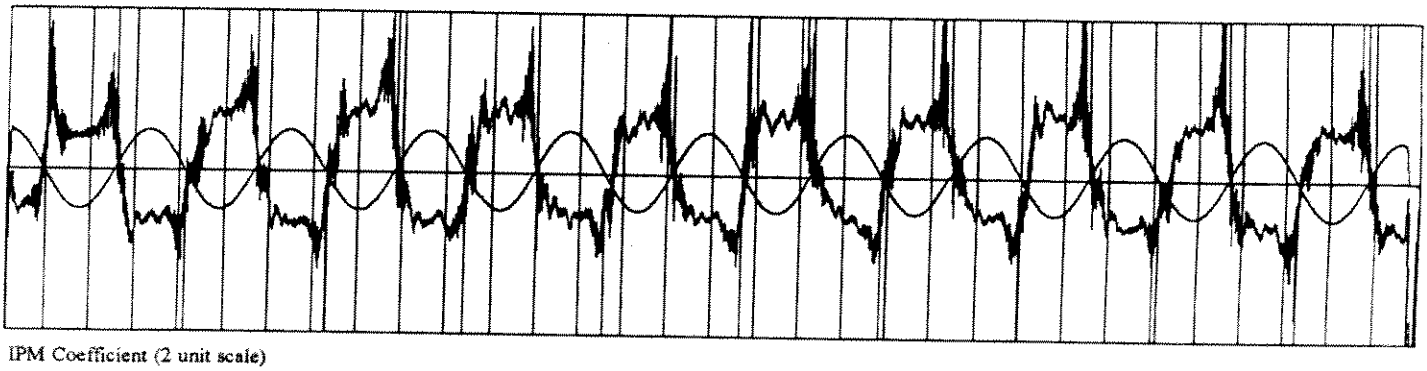

IPM Coefficient (2 unit scale)

PROCESSED DATA for RUN 98 points 120 to 32000

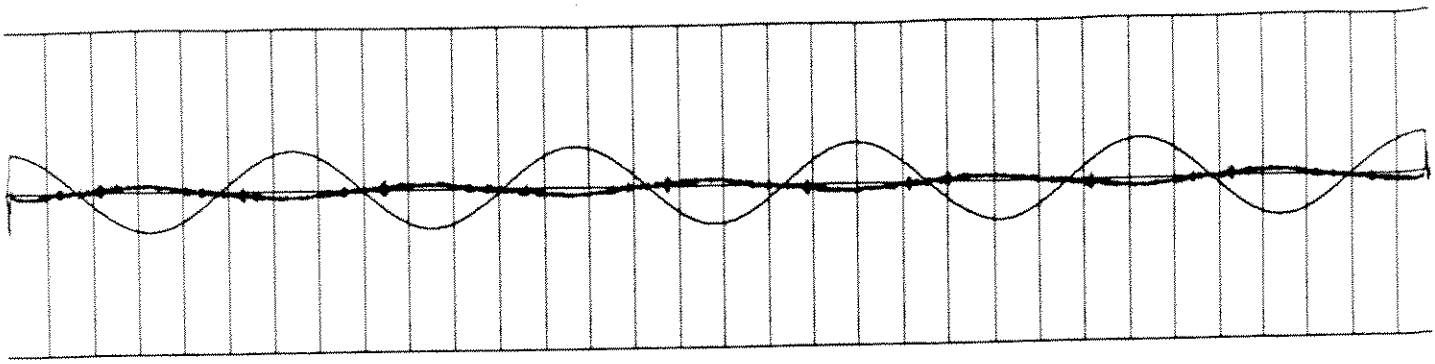

Hydrodynamic Inline Force (2000 N scale)

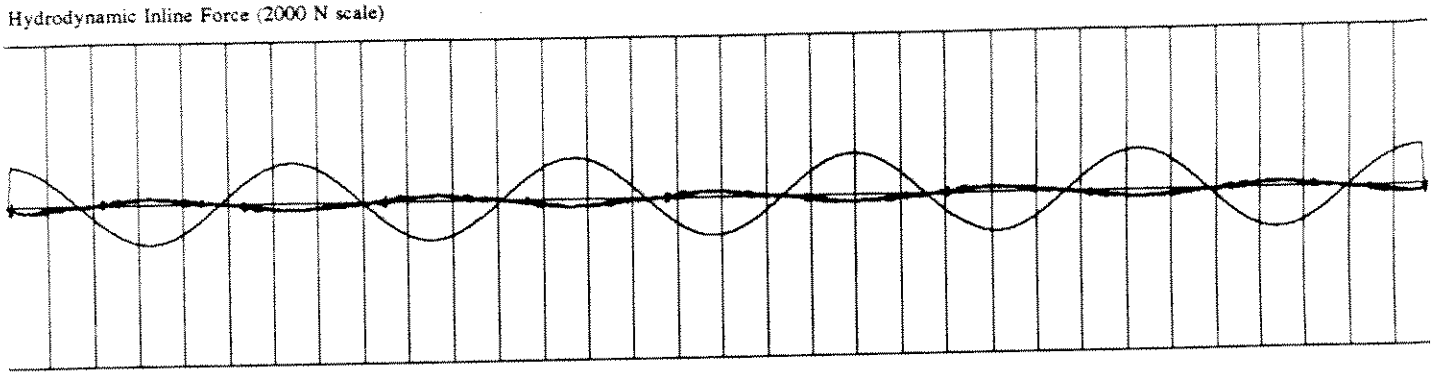

Defect Force (2000 N scale)

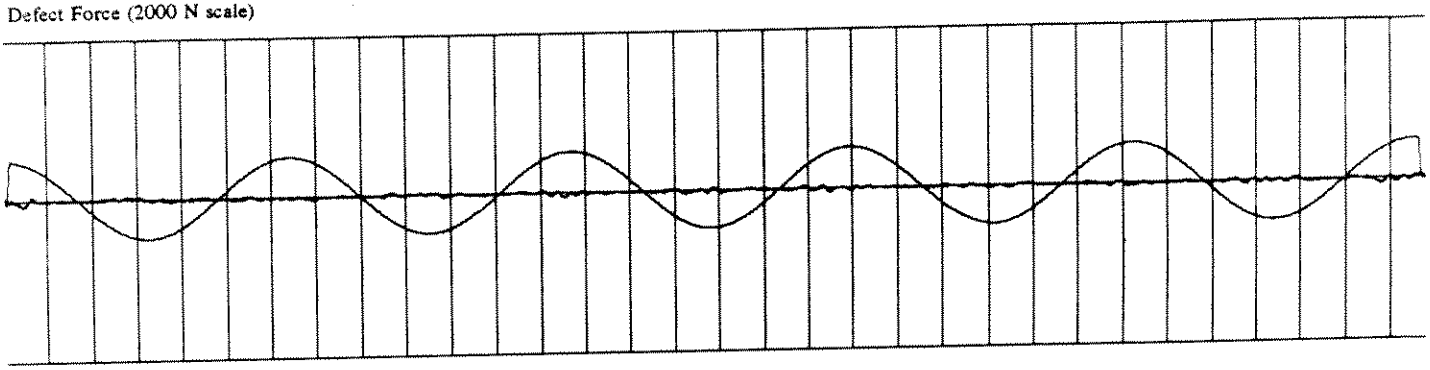

Hydrodynamic Transvers Force (2000 N scale)

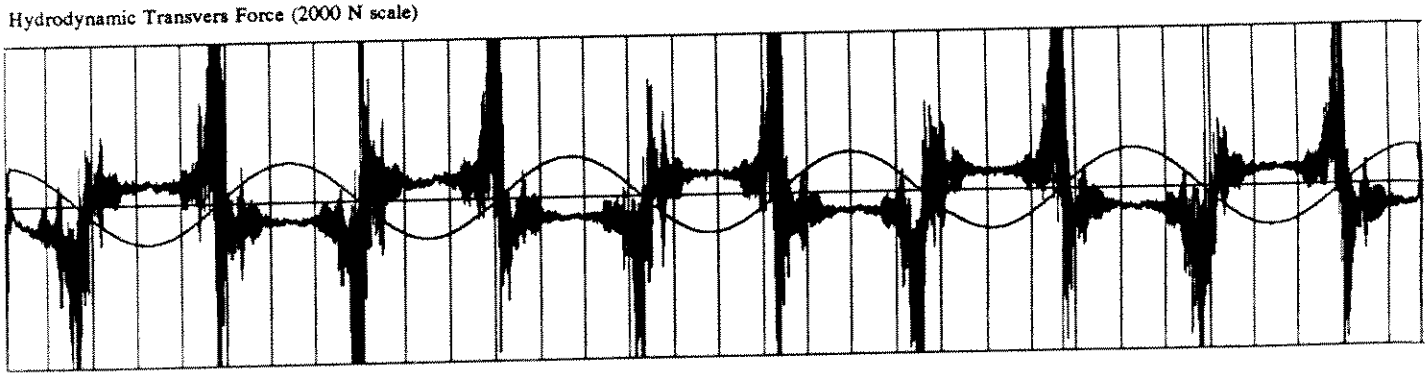

IPM Coefficient (2 unit scale)

PROCESSED DATA for RUN 357 points 60 to 31750

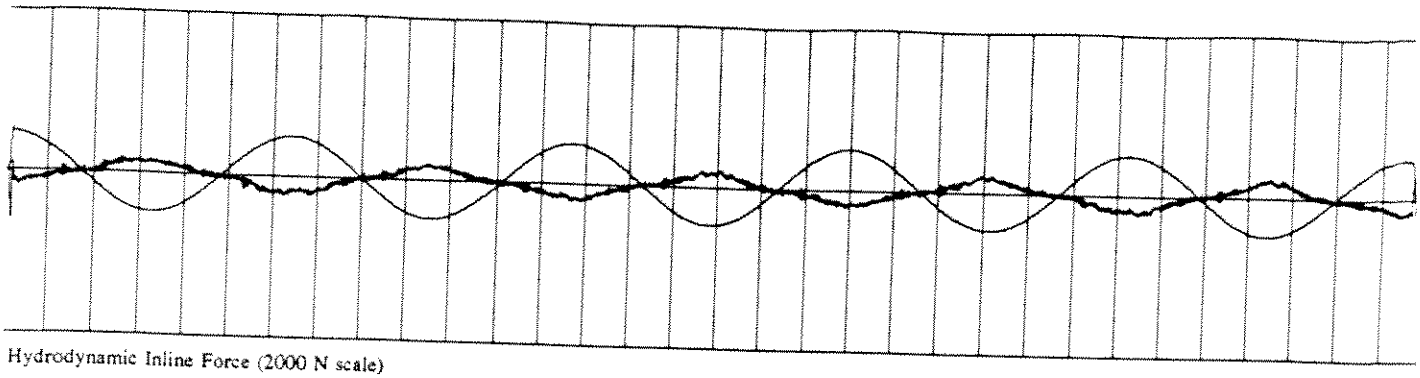

Hydrodynamic Inline Force (2000 N scale)

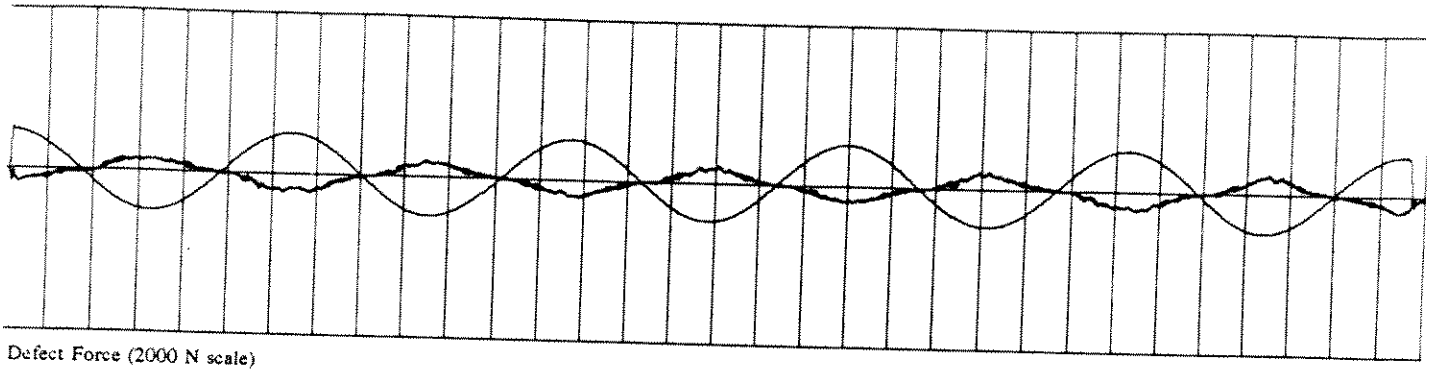

Defect Force (2000 N scale)

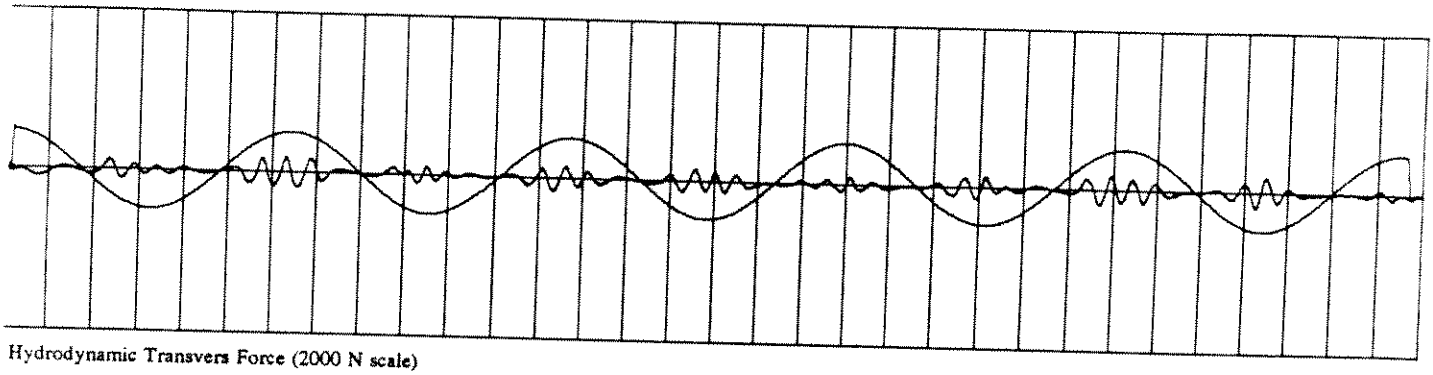

Hydrodynamic Transvers Force (2000 N scale)

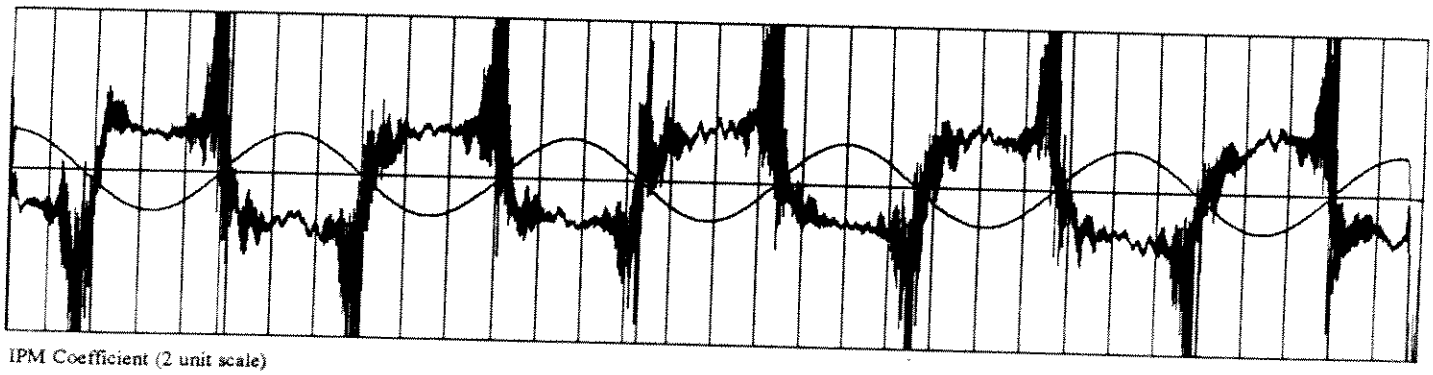

IPM Coefficient (2 unit scale)

PROCESSED DATA for RUN 100 points 80 to 32000

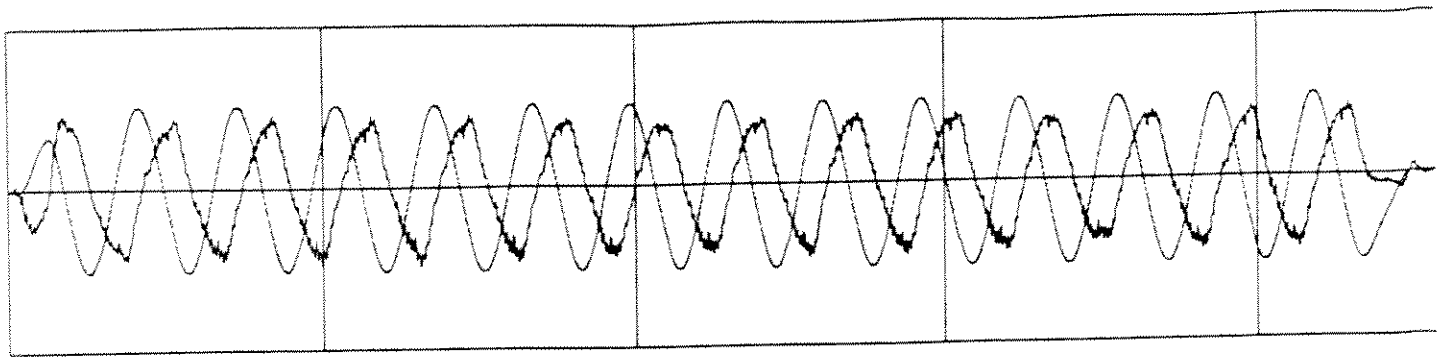

Hydrodynamic Inline Force (2000 N scale)

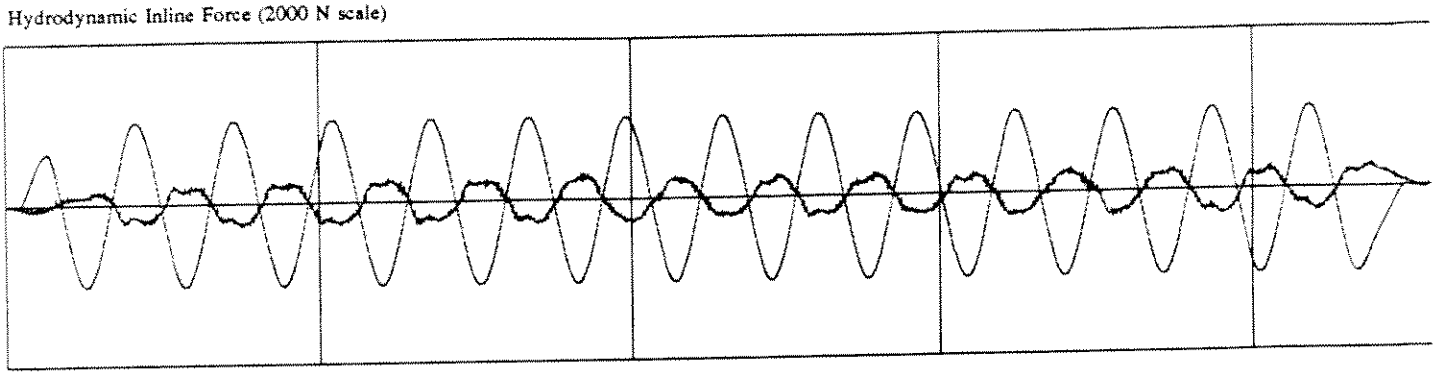

Defect Force (2000 N scale)

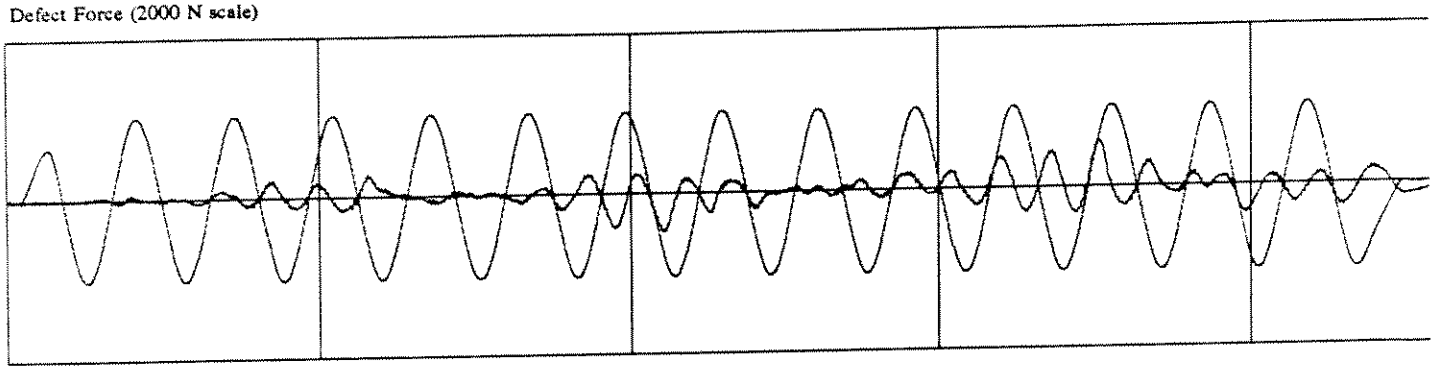

Hydrodynamic Transvers Force (2000 N scale)

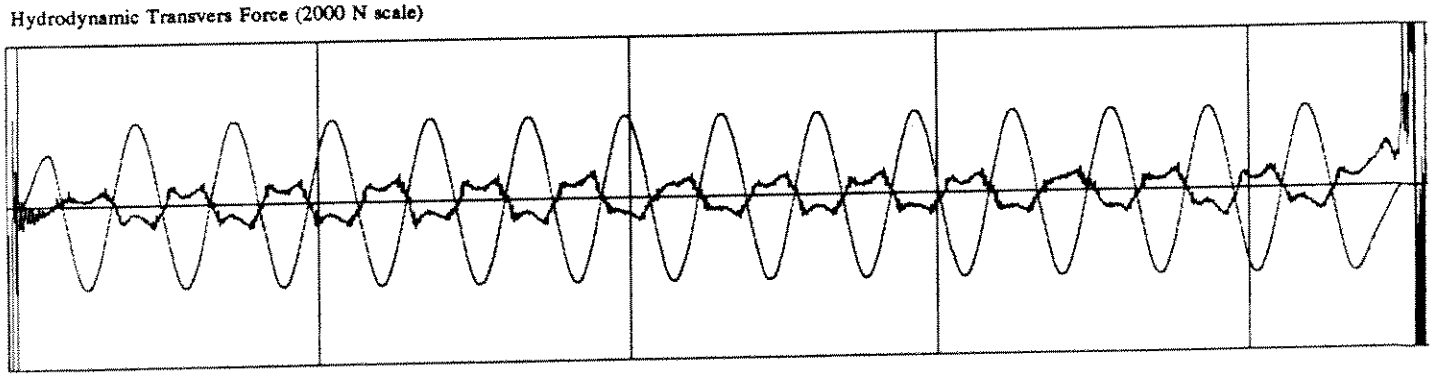

IPM Coefficient (2 unit scale)

PROCESSED DATA for RUN 358 points 1000 to 5570

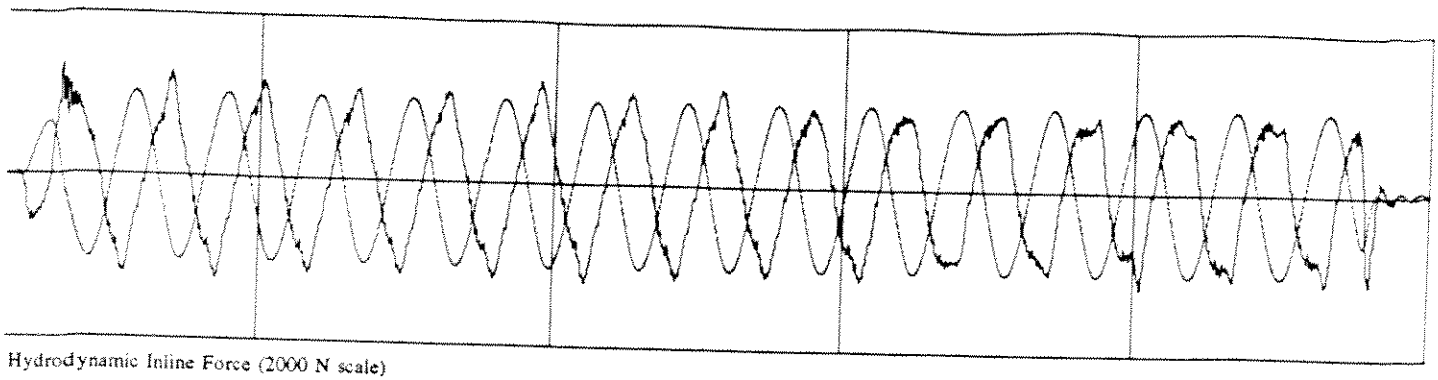

Hydrodynamic Inline Force (2000 N scale)

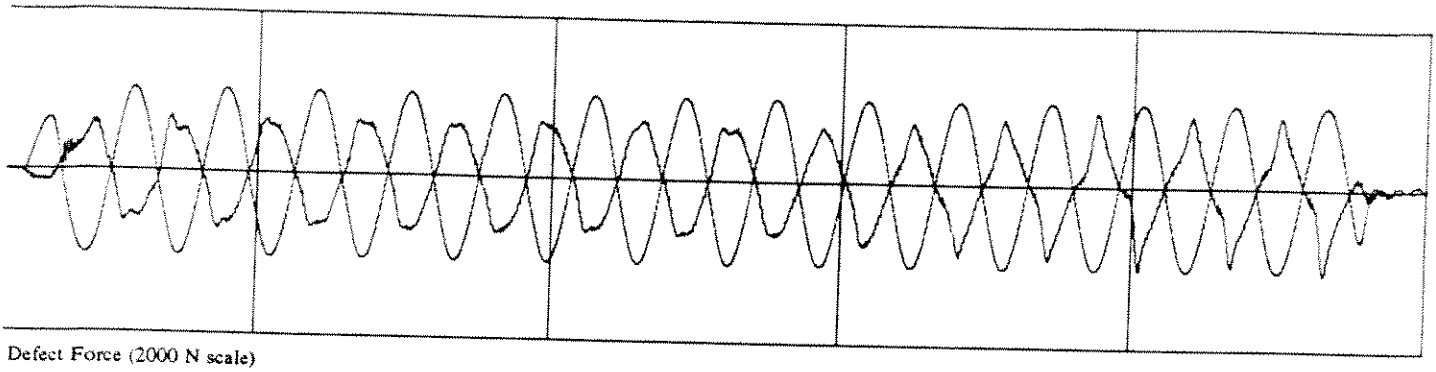

Defect Force (2000 N scale)

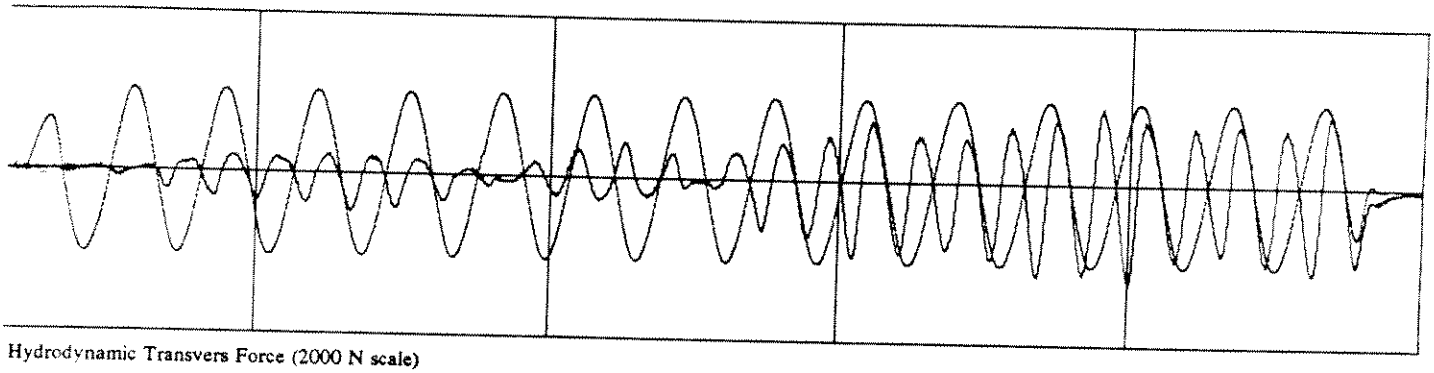

Hydrodynamic Transvers Force (2000 N scale)

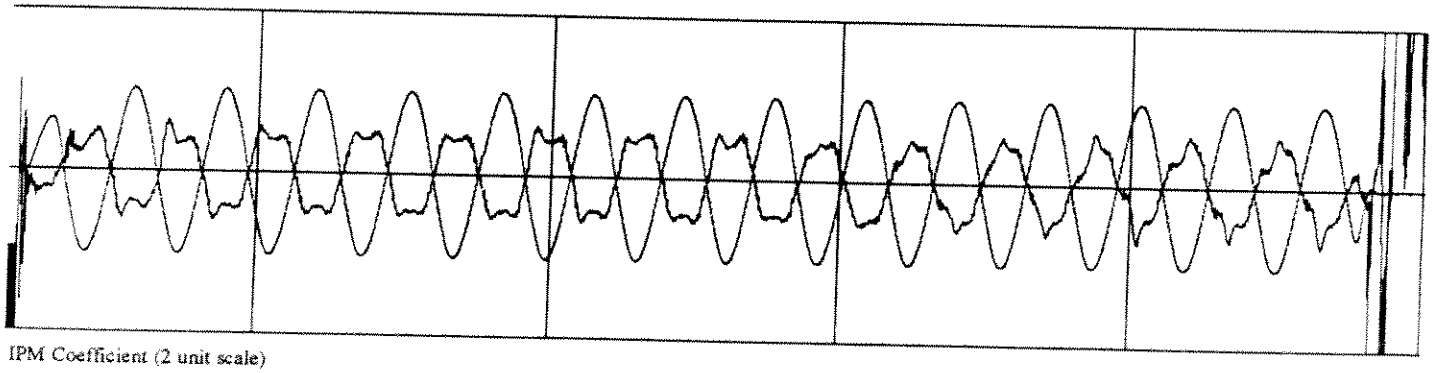

IPM Coefficient (2 unit scale)

PROCESSED DATA for RUN 101 points 1150 to 6000

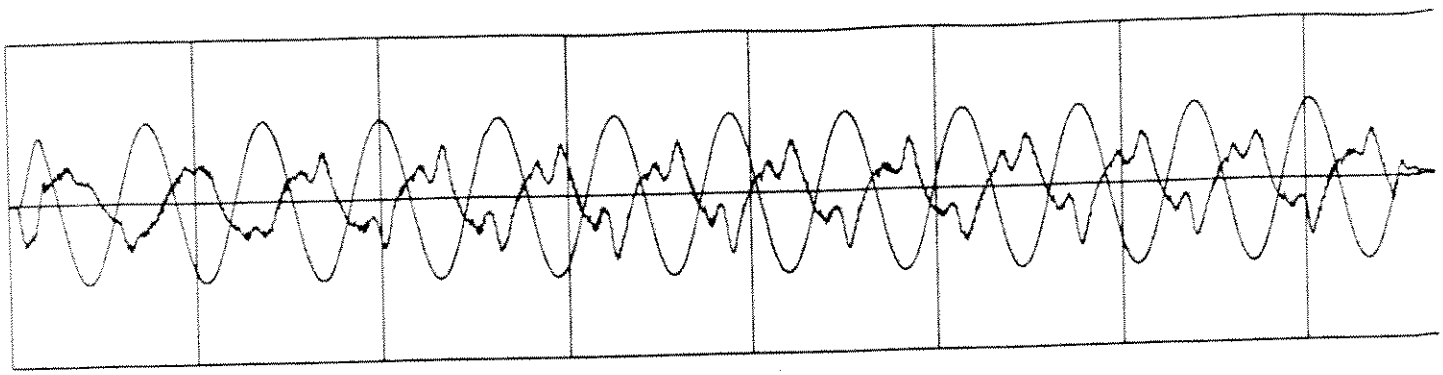

Hydrodynamic Inline Force (2000 N scale)

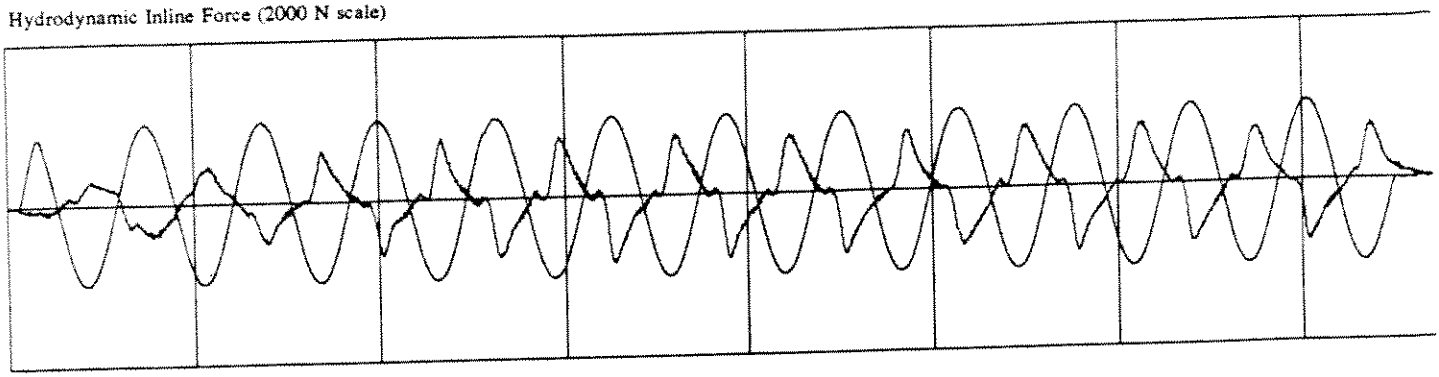

Defect Force (2000 N scale)

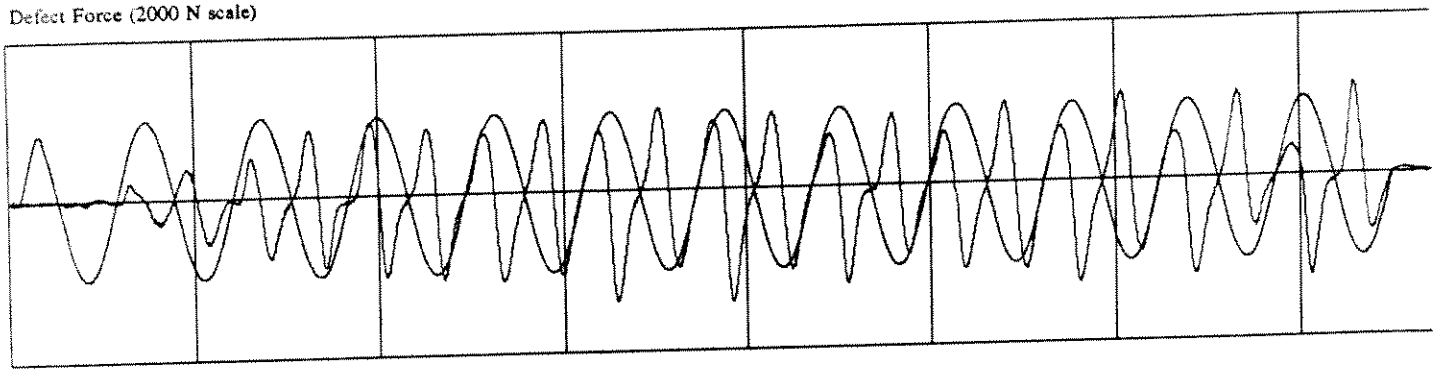

Hydrodynamic Transvers Force (2000 N scale)

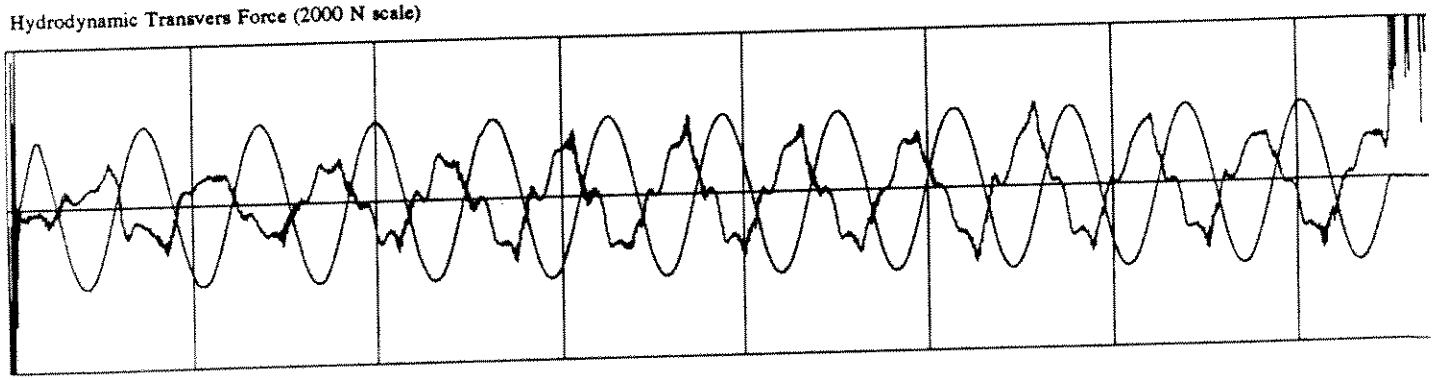

IPM Coefficient (2 unit scale)

PROCESSED DATA for RUN 359 points 1000 to 8700

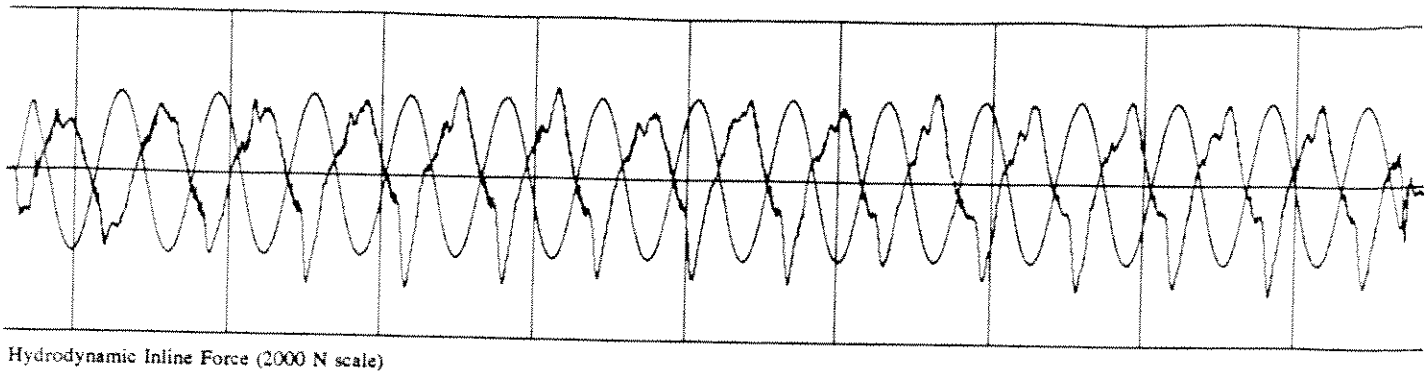

Hydrodynamic Inline Force (2000 N scale)

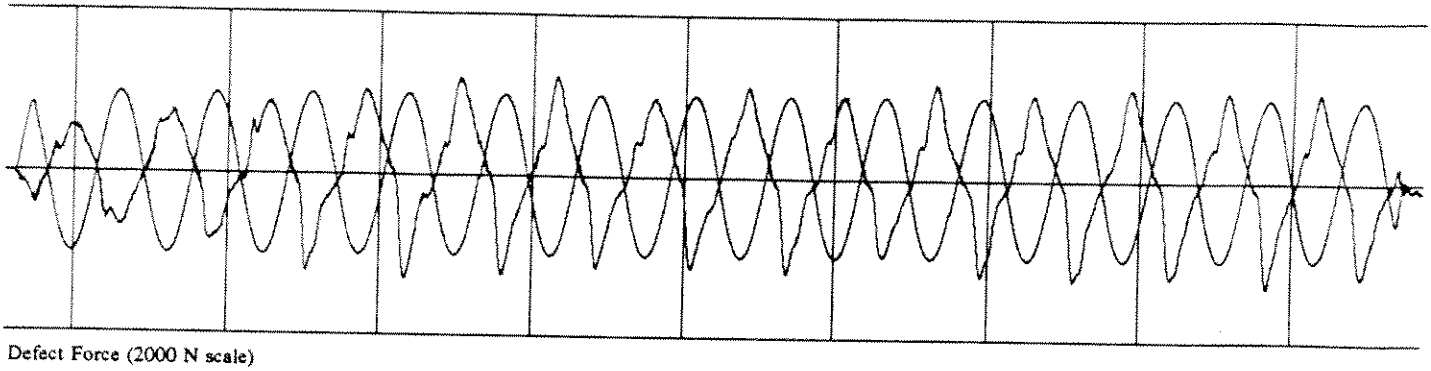

Defect Force (2000 N scale)

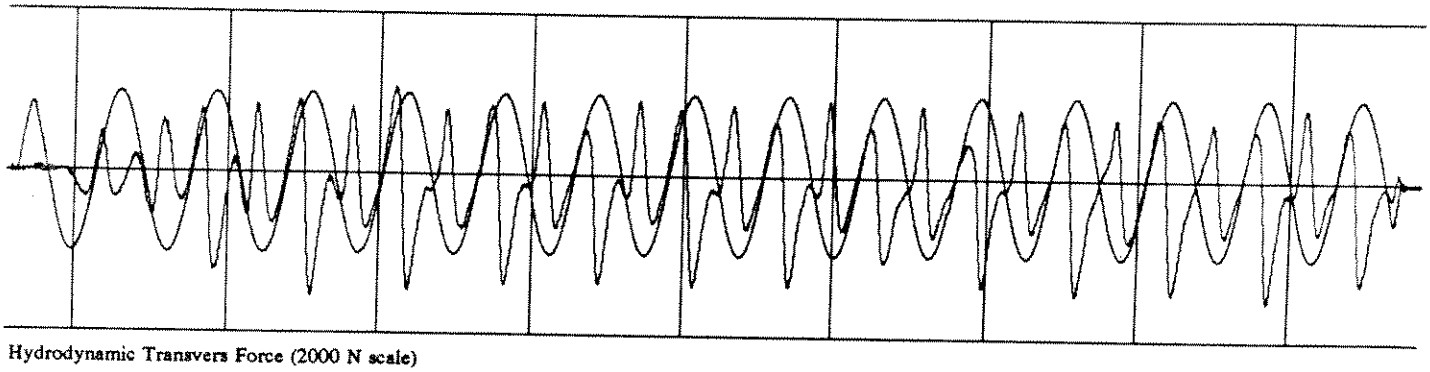

Hydrodynamic Transvers Force (2000 N scale)

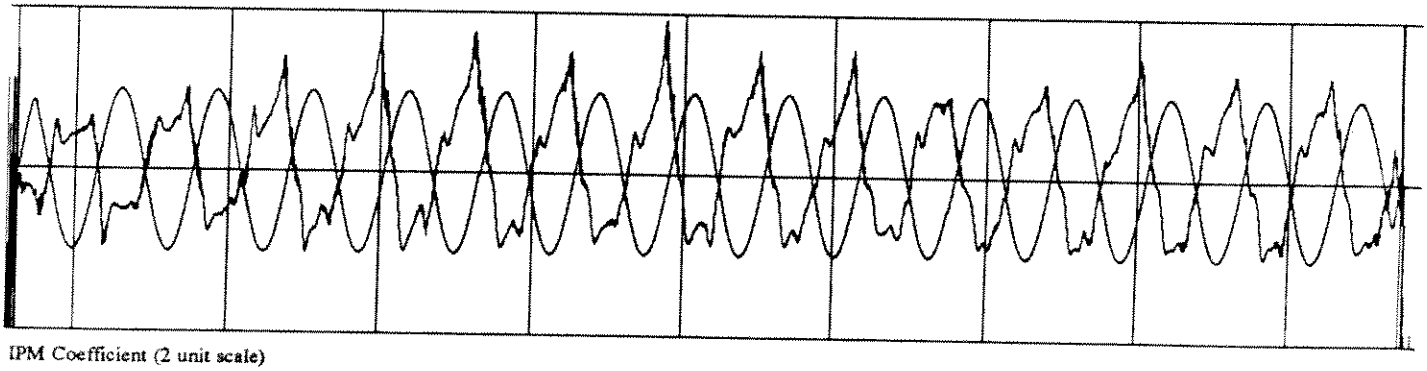

IPM Coefficient (2 unit scale)

PROCESSED DATA for RUN 102 points 1550 to 10850

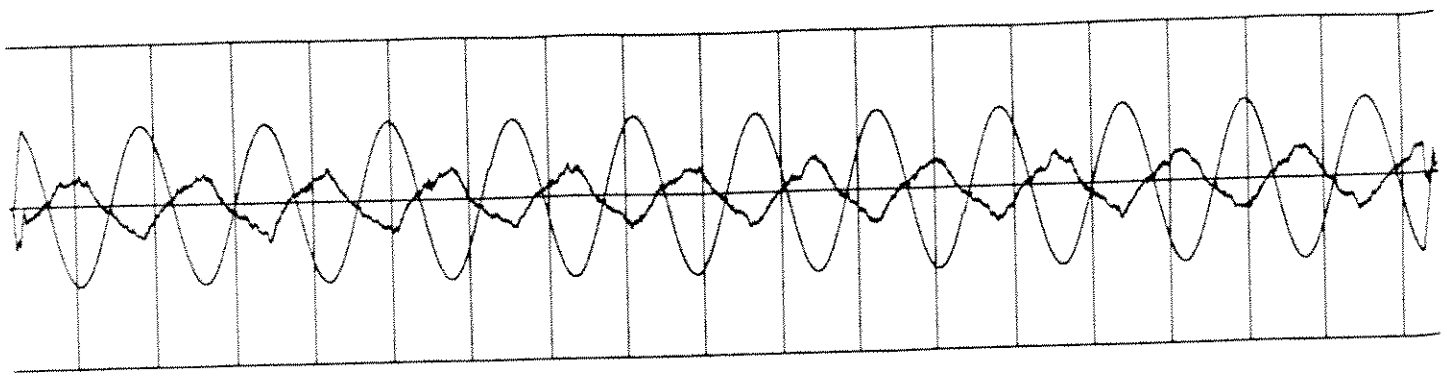

Hydrodynamic Inline Force (2000 N scale)

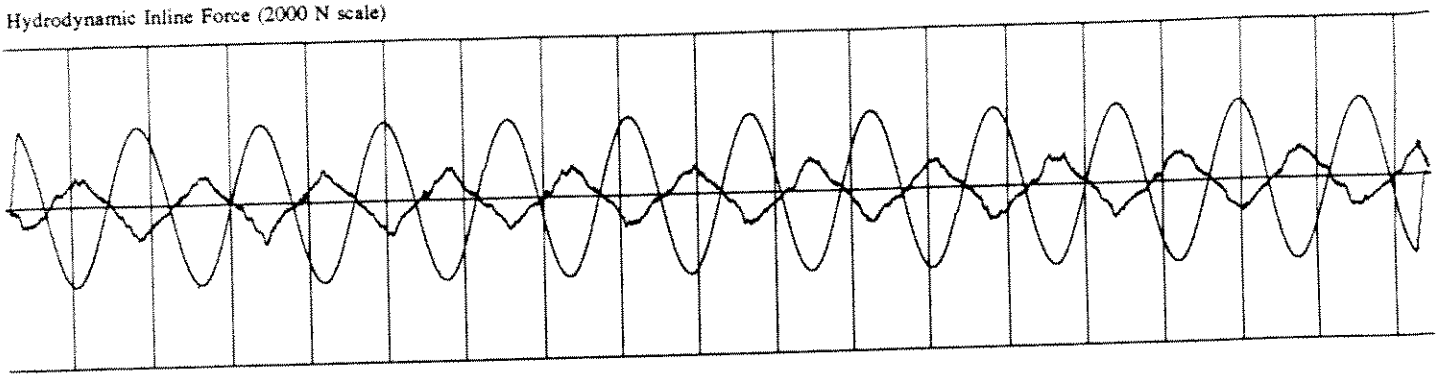

Defect Force (2000 N scale)

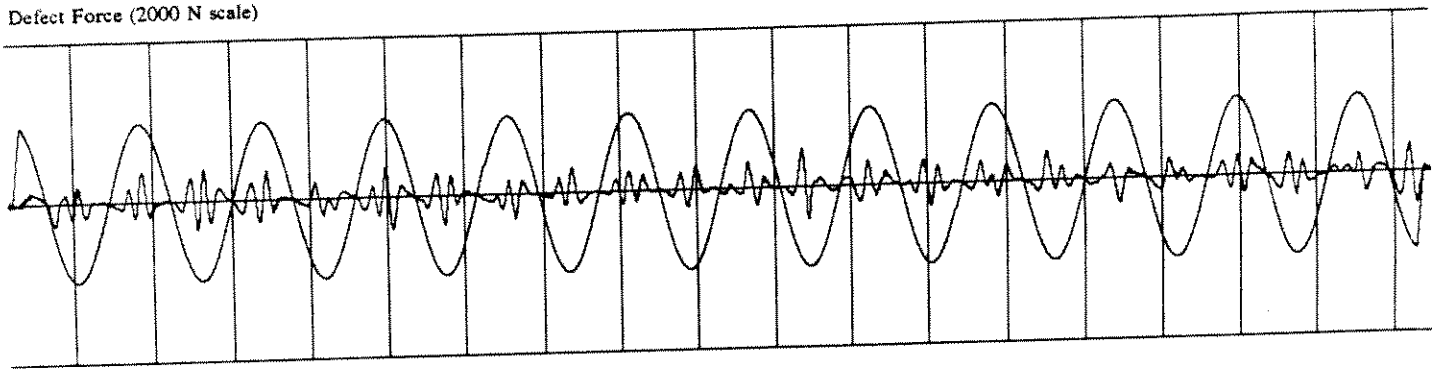

Hydrodynamic Transvers Force (2000 N scale)

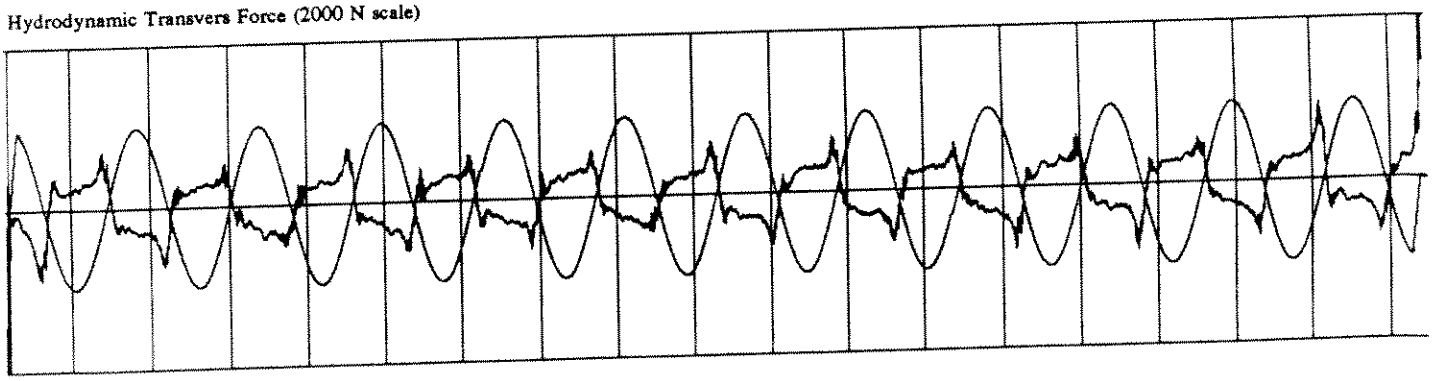

IPM Coefficient (2 unit scale)

PROCESSED DATA for RUN 360 points 1150 to 19450

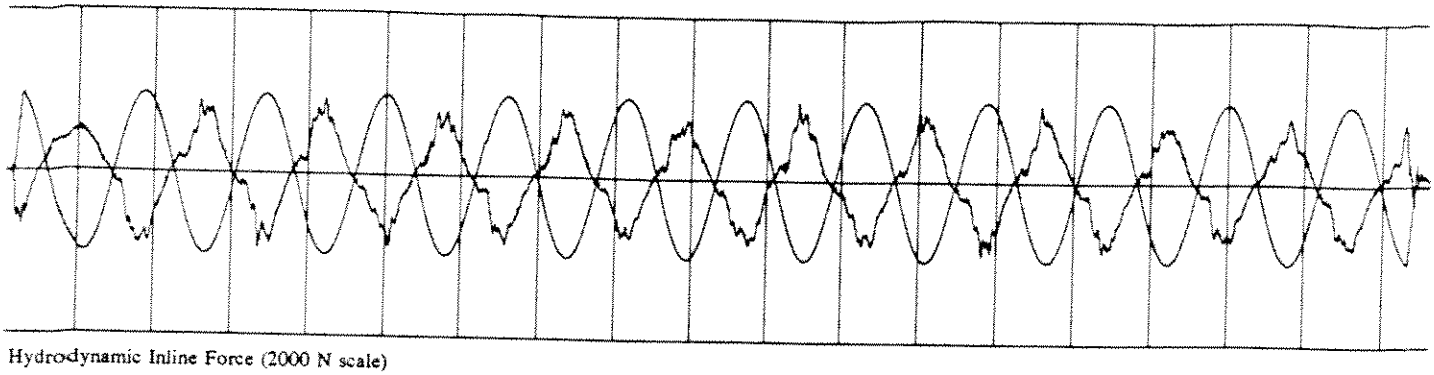

Hydrodynamic Inline Force (2000 N scale)

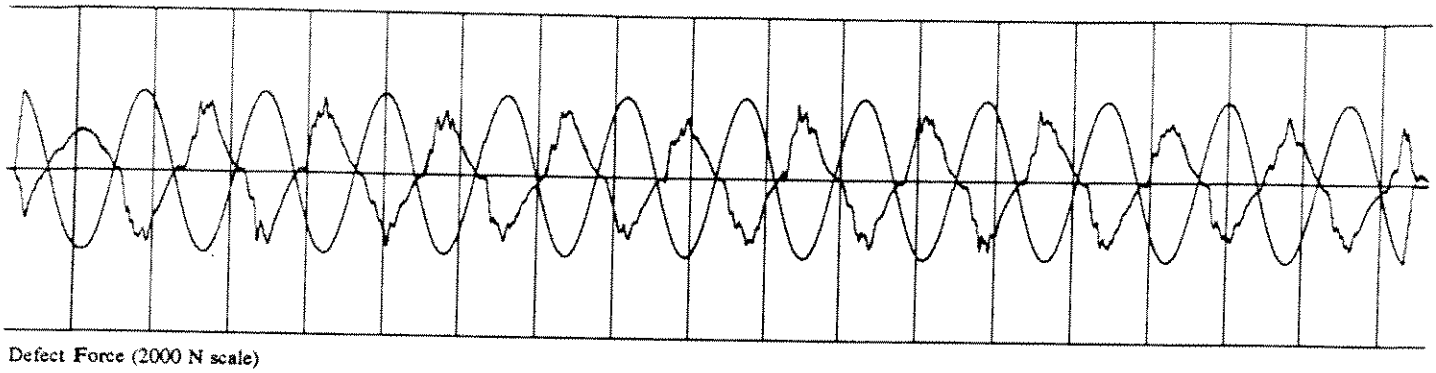

Defect Force (2000 N scale)

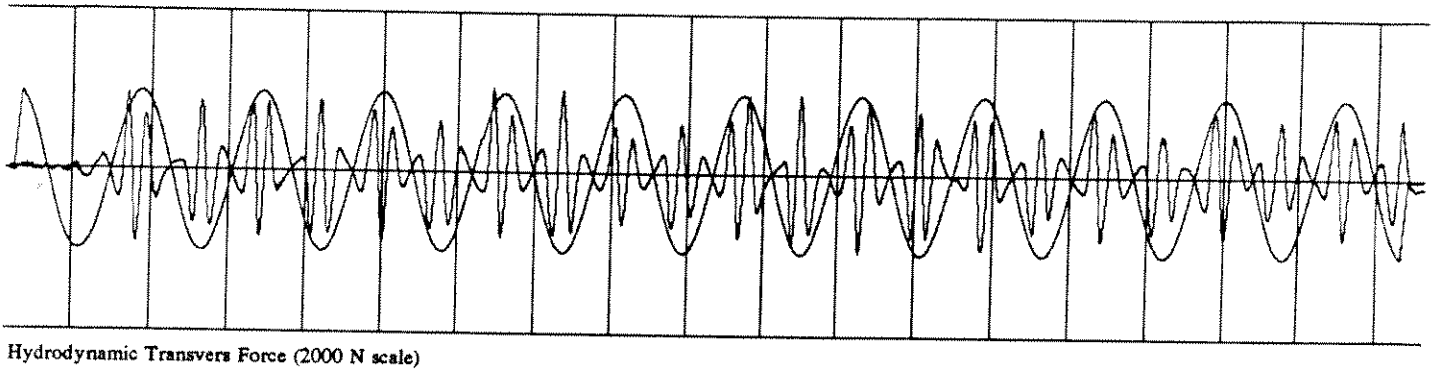

Hydrodynamic Transvers Force (2000 N scale)

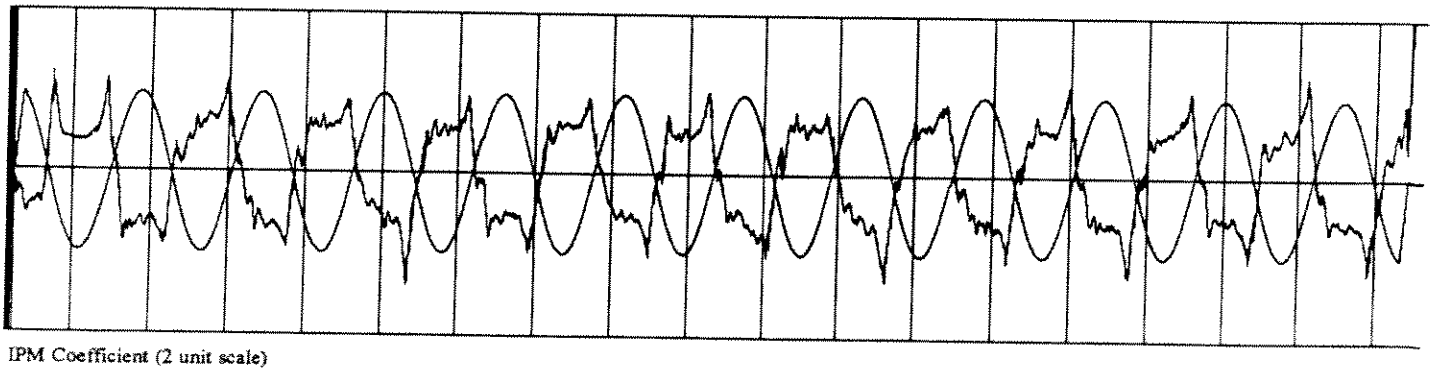

IPM Coefficient (2 unit scale)

PROCESSED DATA for RUN 103 points 1150 to 19600

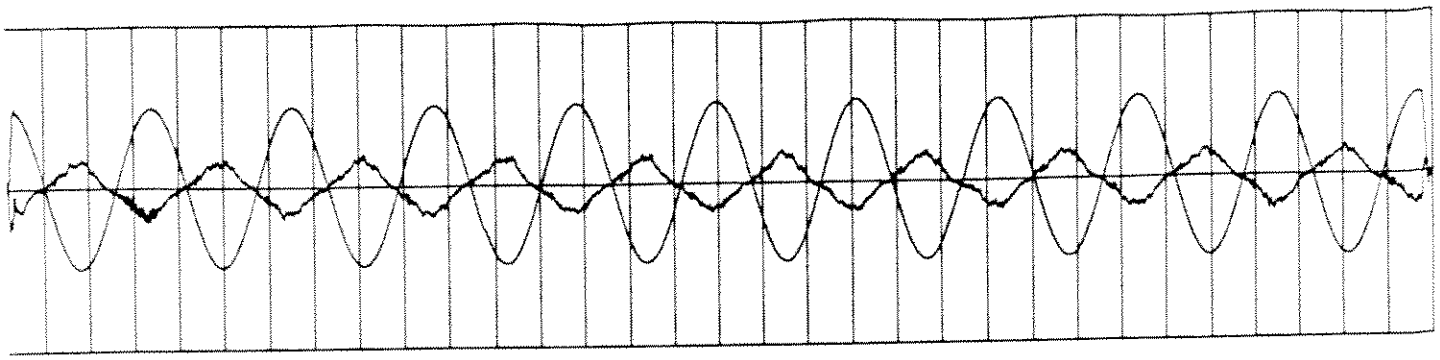

Hydrodynamic Inline Force (2000 N scale)

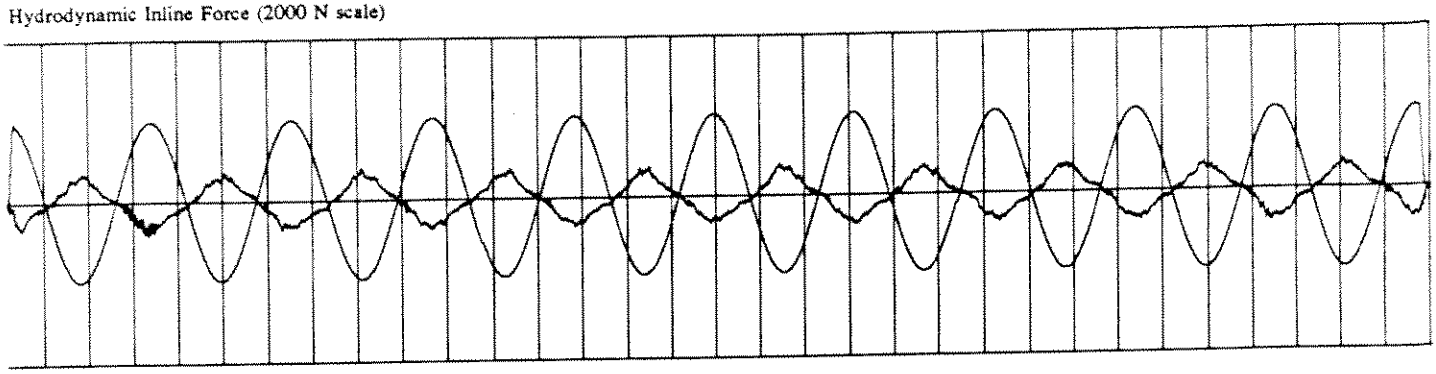

Defect Force (2000 N scale)

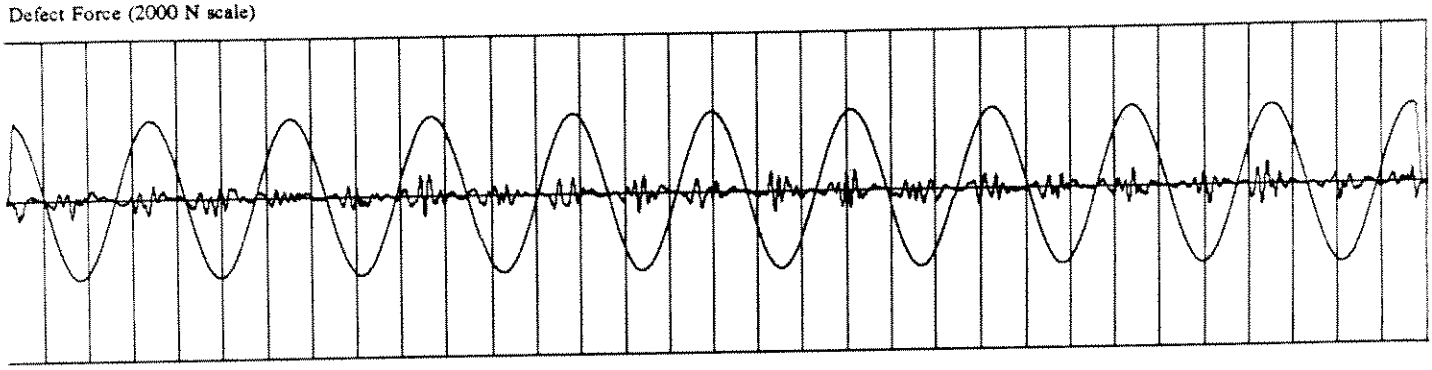

Hydrodynamic Transvers Force (2000 N scale)

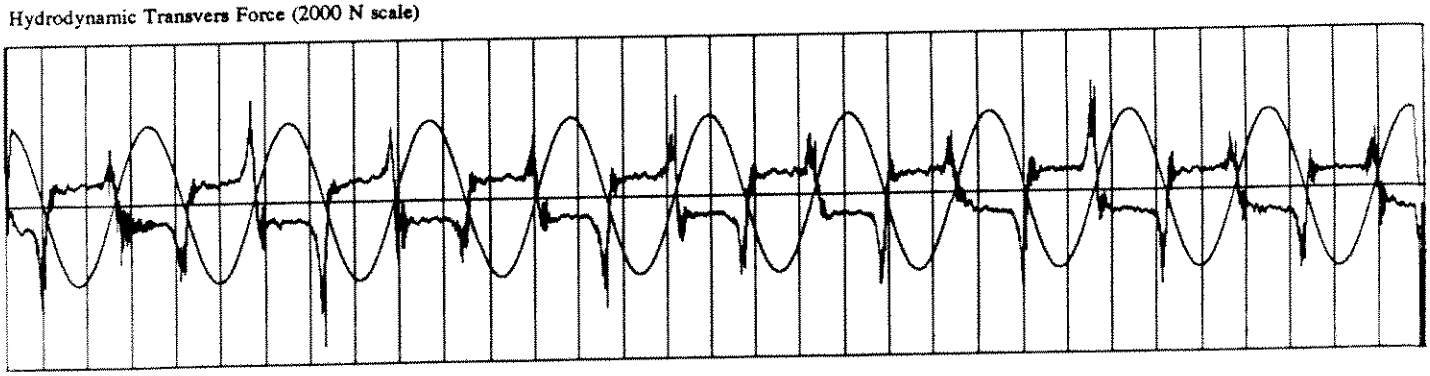

IPM Coefficient (2 unit scale)

PROCESSED DATA for RUN 361 points 160 to 32000

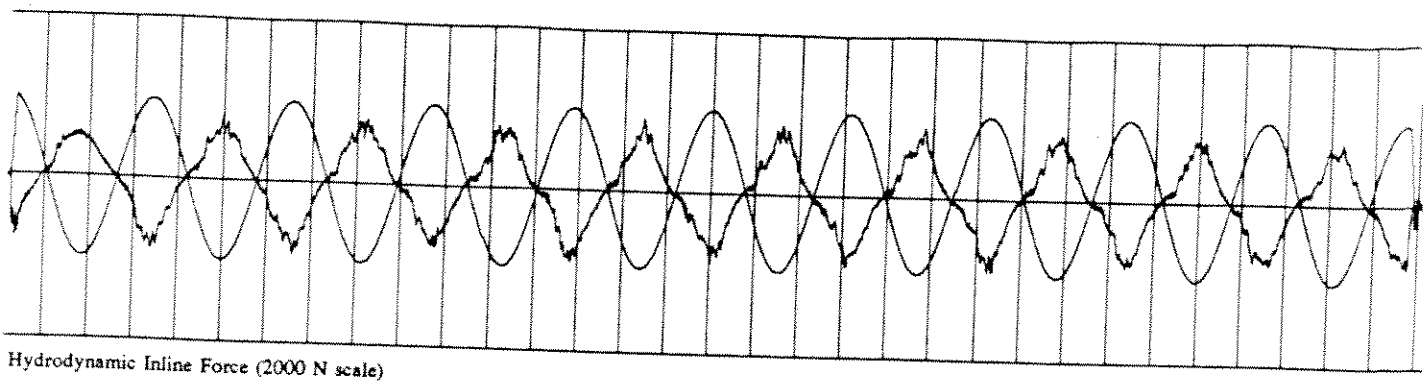

Hydrodynamic Inline Force (2000 N scale)

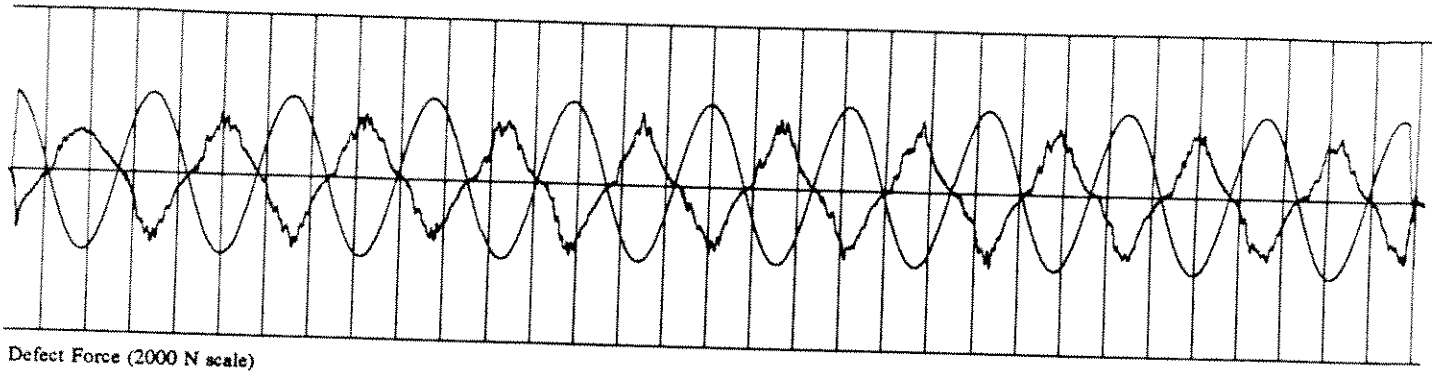

Defect Force (2000 N scale)

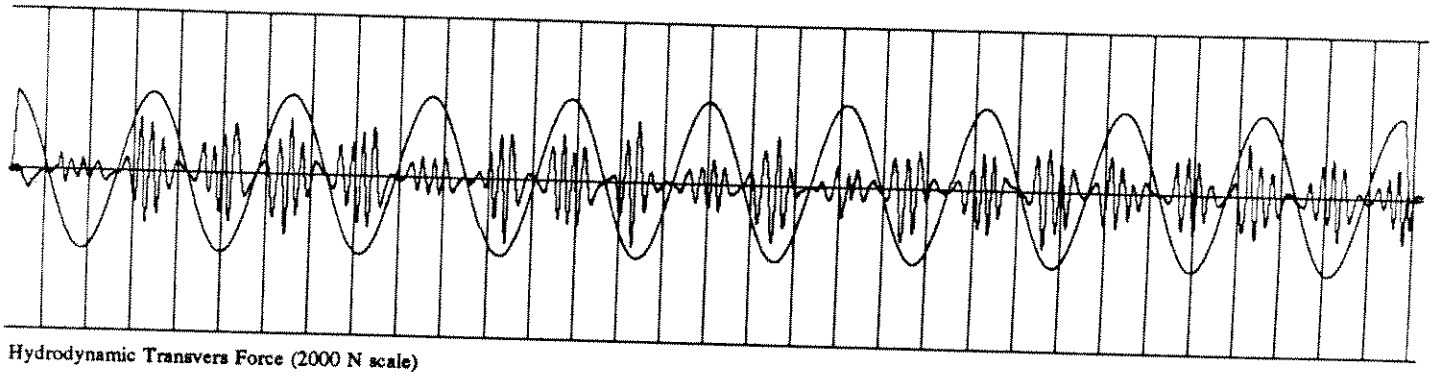

Hydrodynamic Transvers Force (2000 N scale)

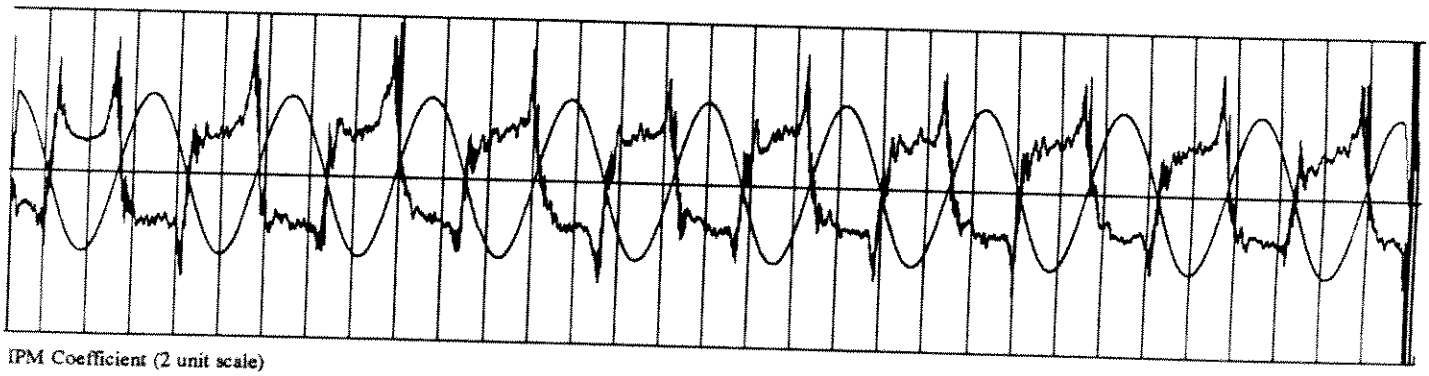

IPM Coefficient (2 unit scale)

PROCESSED DATA for RUN 104 points 170 to 32200

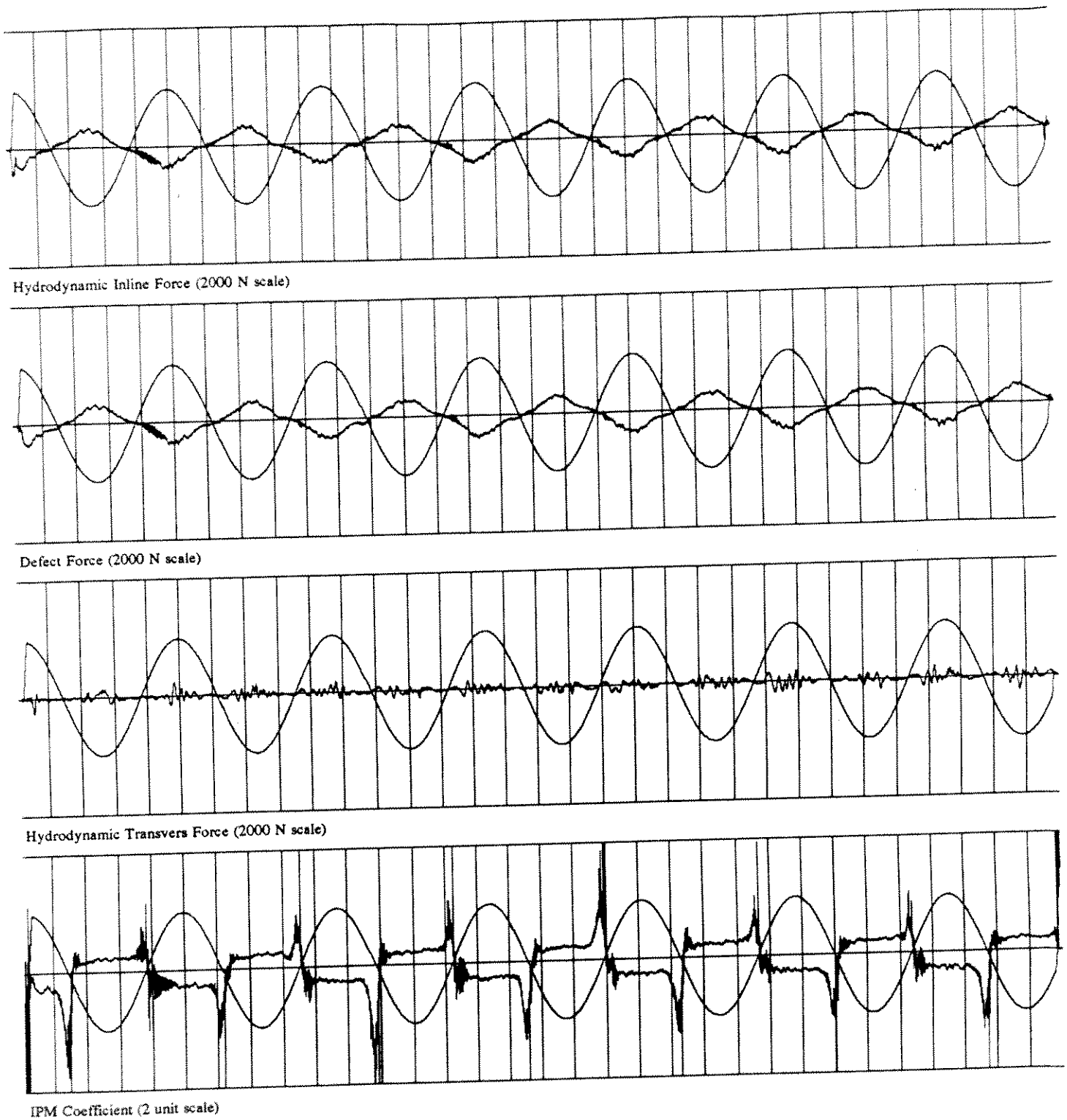

PROCESSED DATA for RUN 362 points 80 to 31950

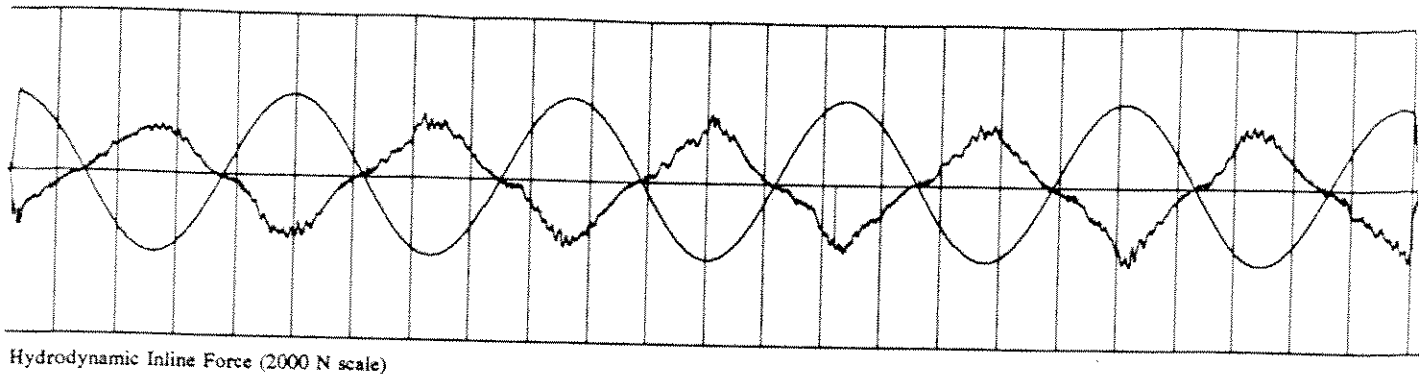

Hydrodynamic Inline Force (2000 N scale)

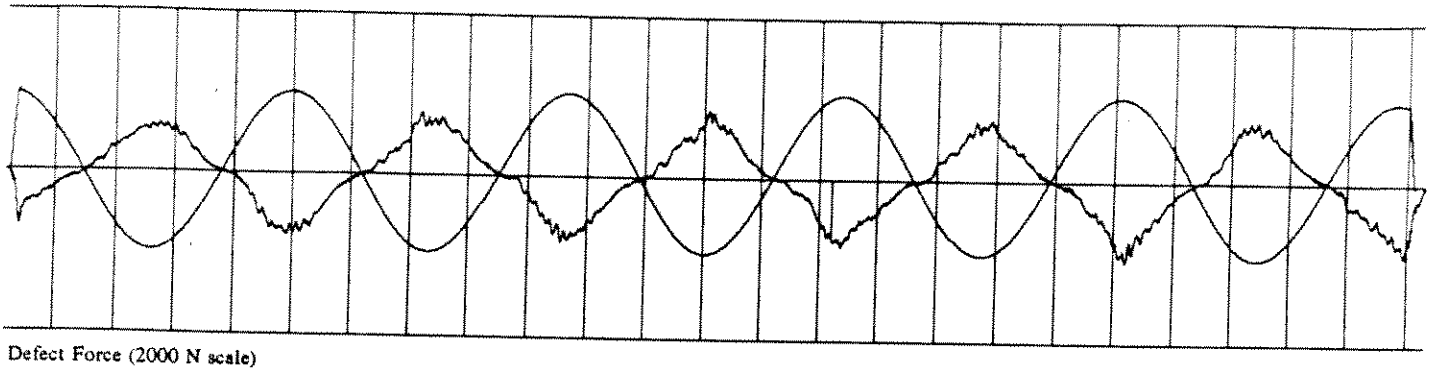

Defect Force (2000 N scale)

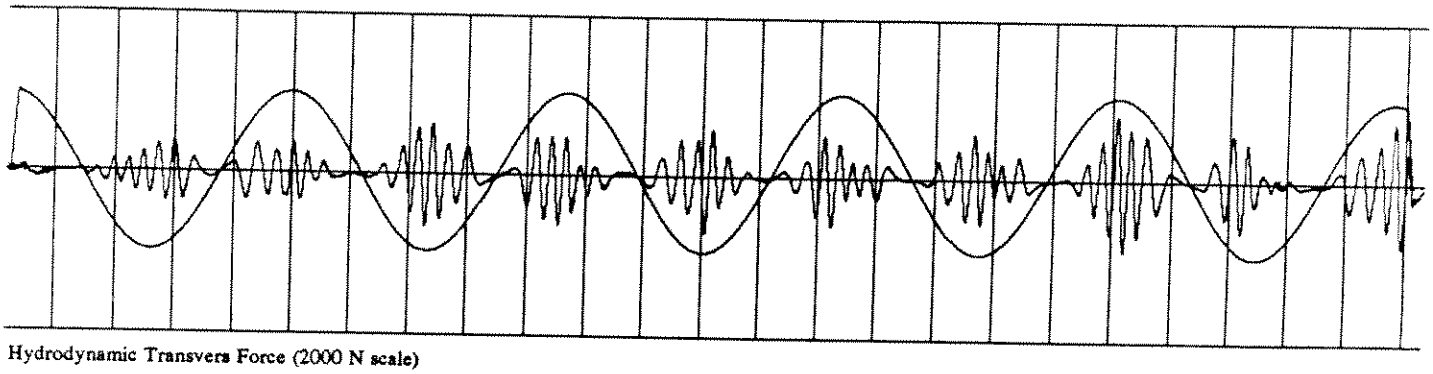

Hydrodynamic Transvers Force (2000 N scale)

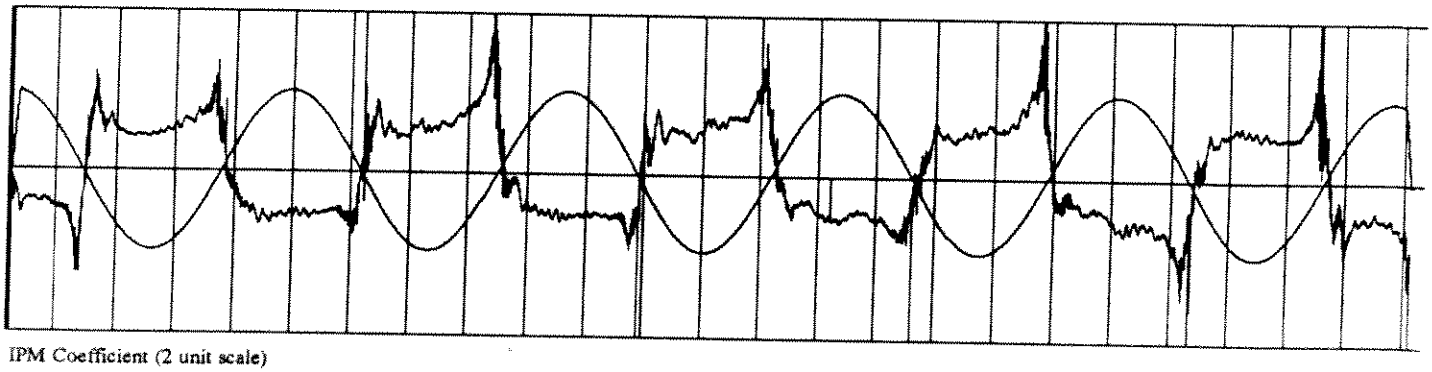

IPM Coefficient (2 unit scale)

PROCESSED DATA for RUN 105 points 1180 to 25300

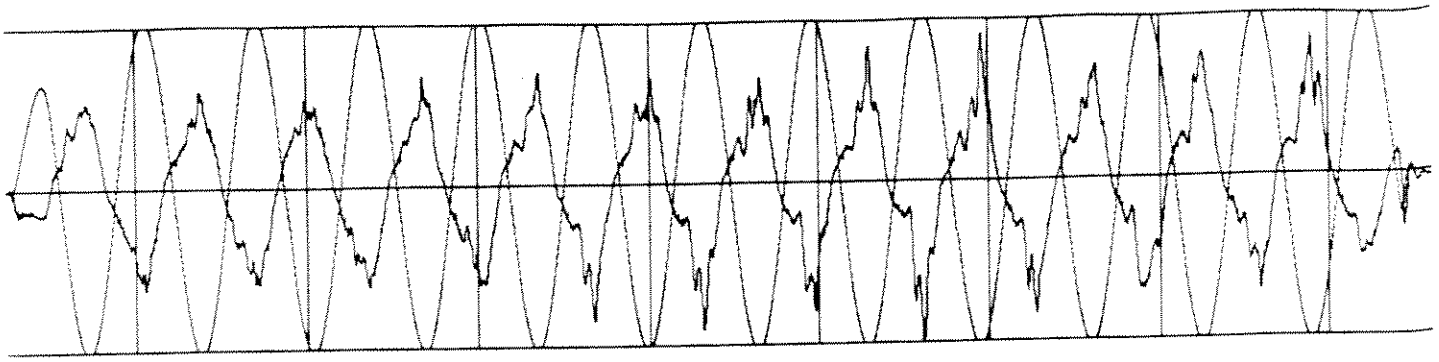

Hydrodynamic Inline Force (3270 N scale)

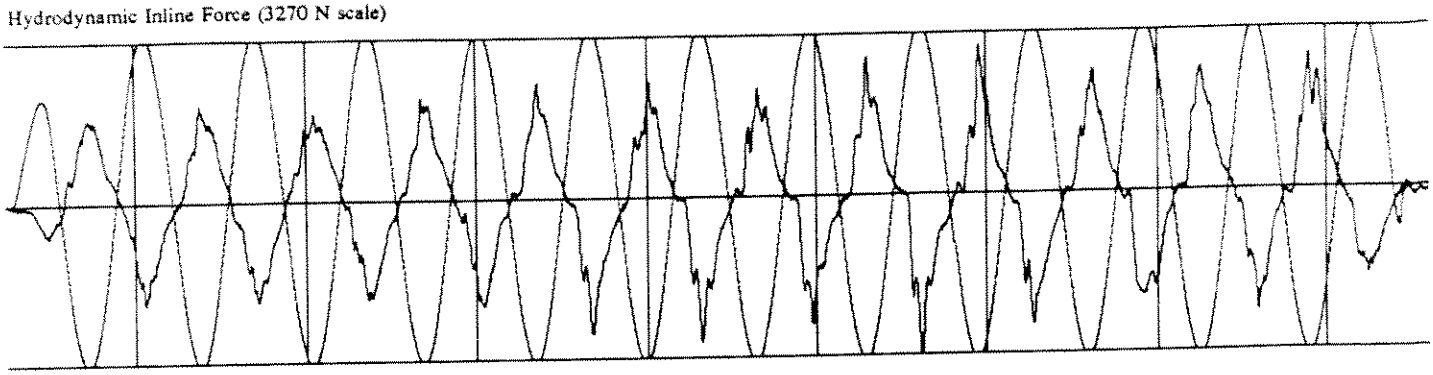

Defect Force (3270 N scale)

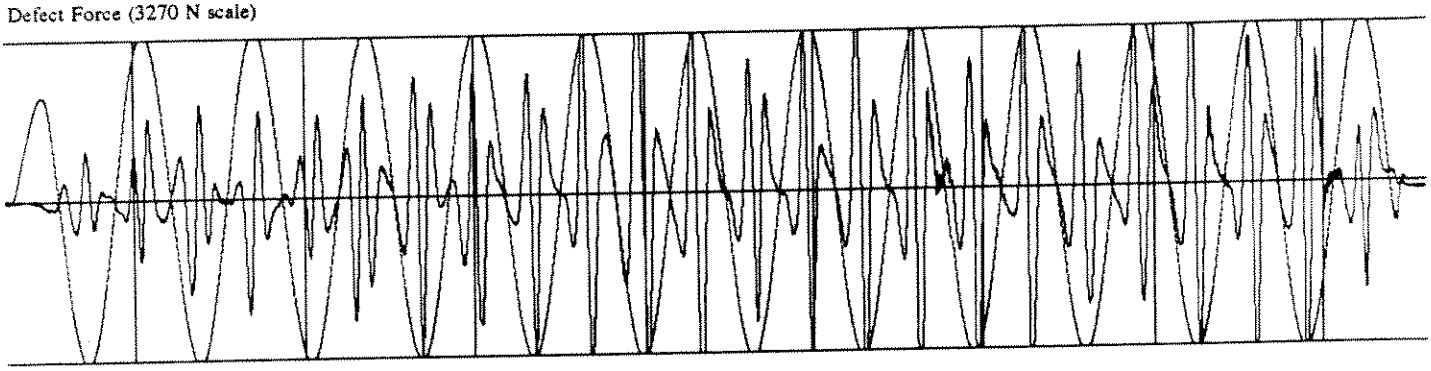

Hydrodynamic Transvers Force (3270 N scale)

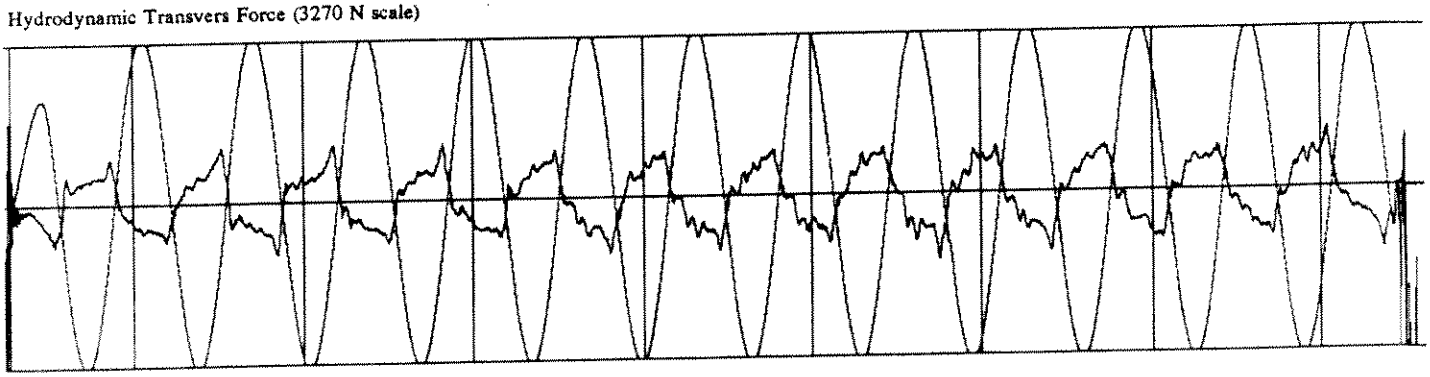

IPM Coefficient (2 unit scale)

PROCESSED DATA for RUN 363 points 1250 to 9600

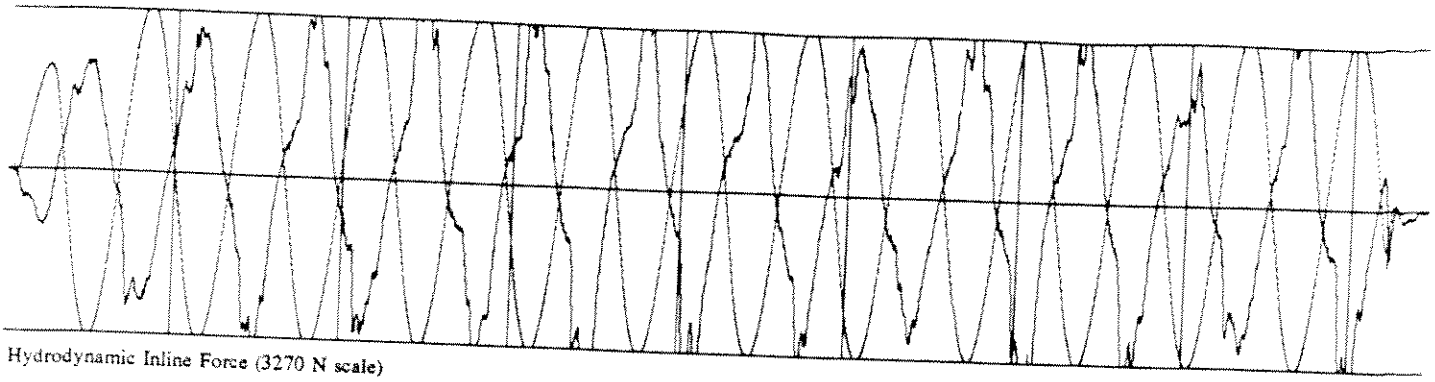

Hydrodynamic Inline Force (3270 N scale)

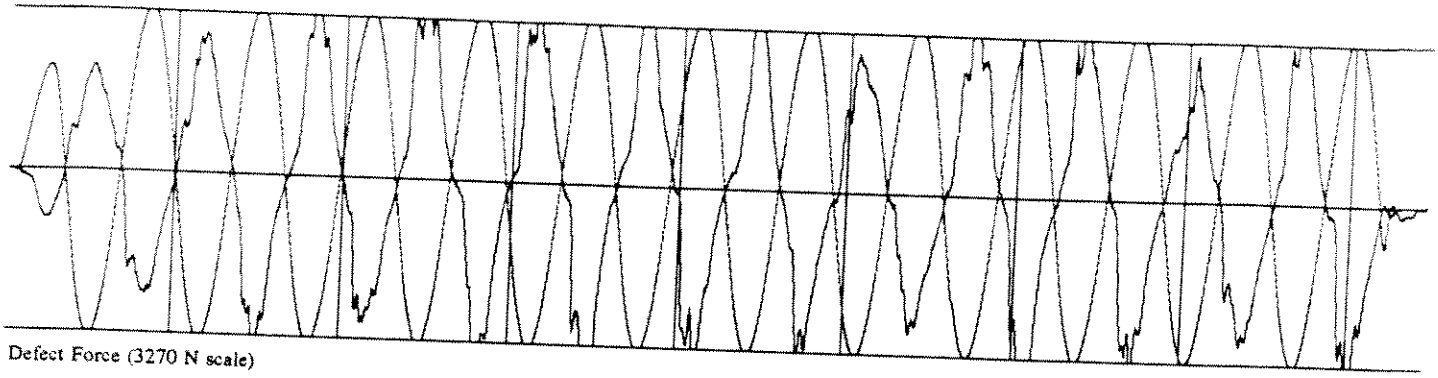

Defect Force (3270 N scale)

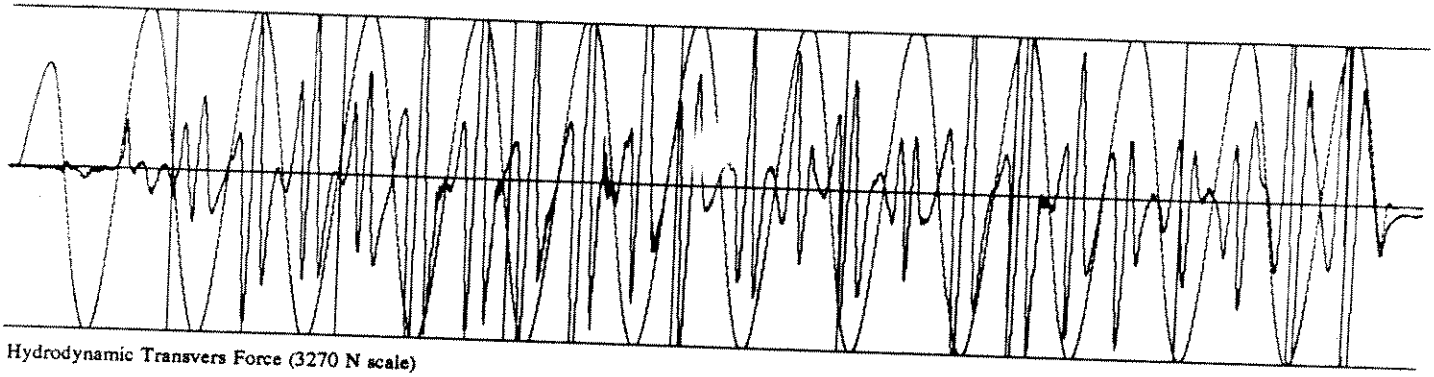

Hydrodynamic Transvers Force (3270 N scale)

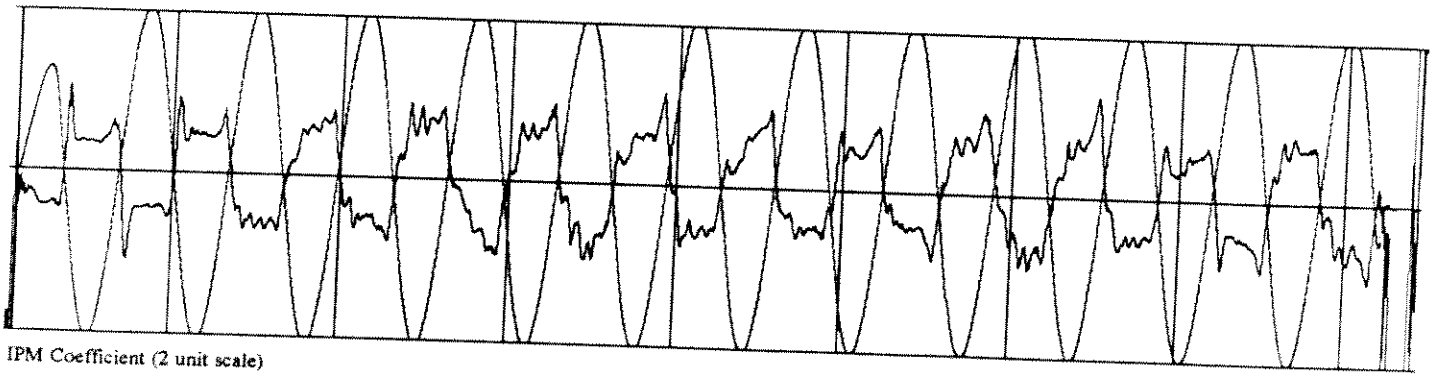

IPM Coefficient (2 unit scale)

PROCESSED DATA for RUN 293 points 1020 to 9450

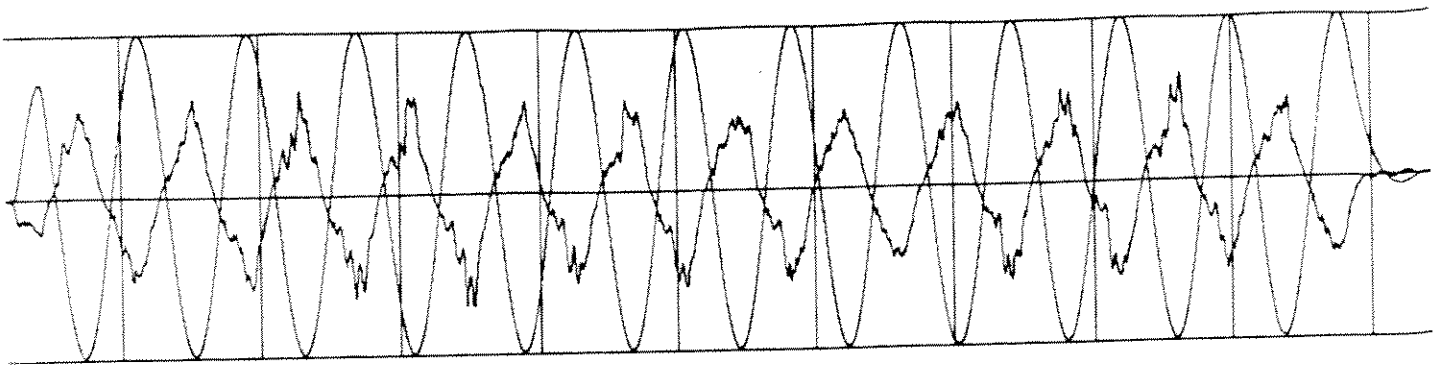

Hydrodynamic Inline Force (3270 N scale)

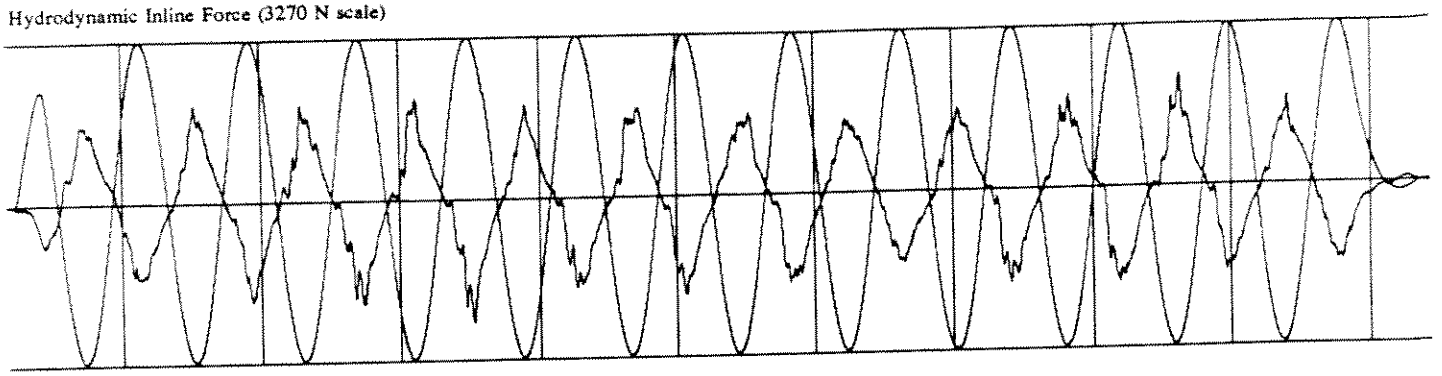

Defect Force (3270 N scale)

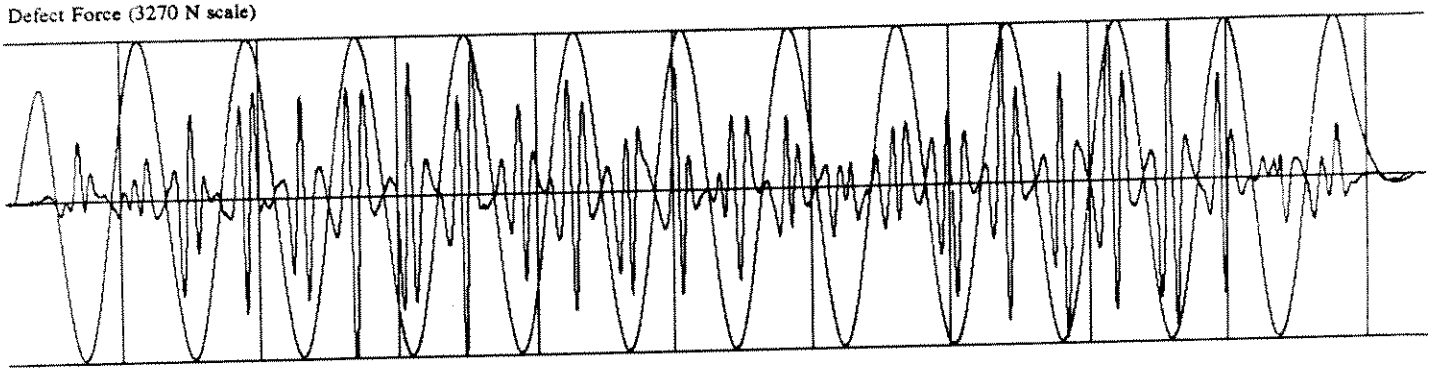

Hydrodynamic Transvers Force (3270 N scale)

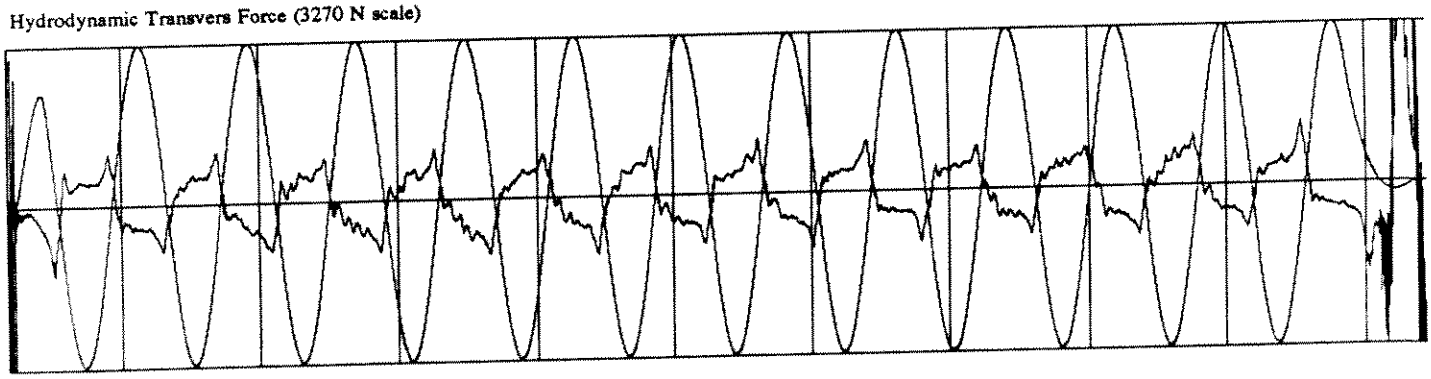

IPM Coefficient (2 unit scale)

PROCESSED DATA for RUN 355 points 1180 to 11430

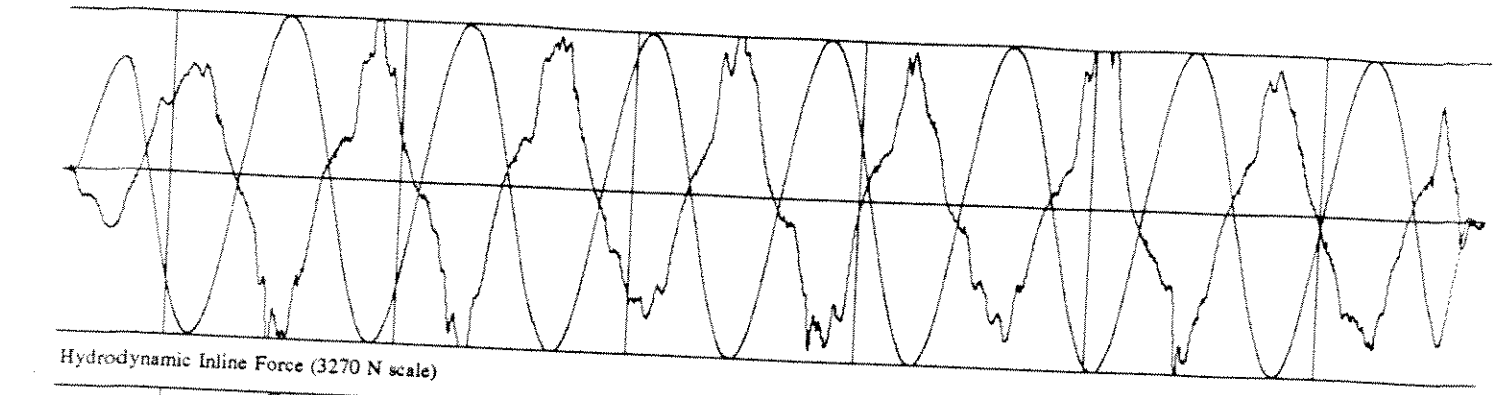

Hydrodynamic Inline Force (3270 N scale)

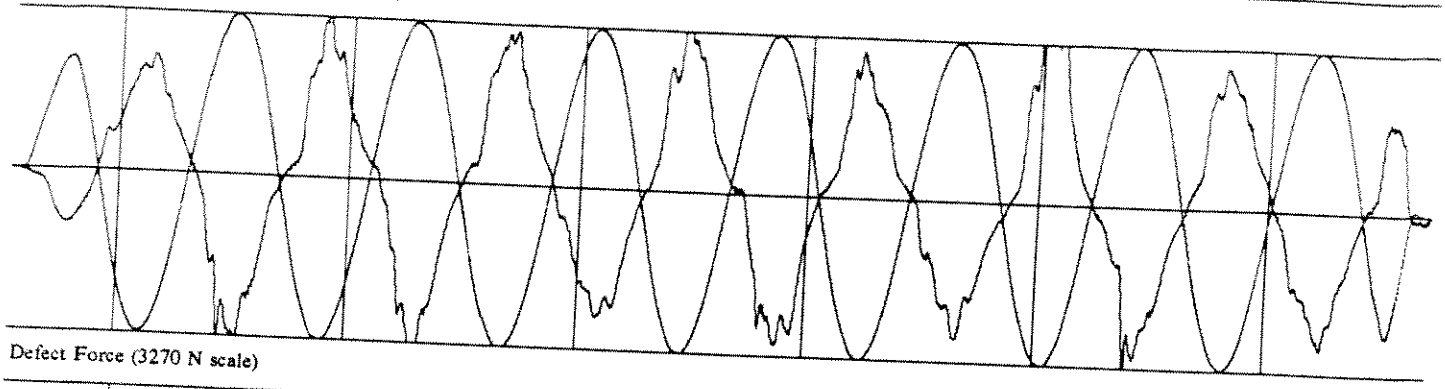

Defect Force (3270 N scale)

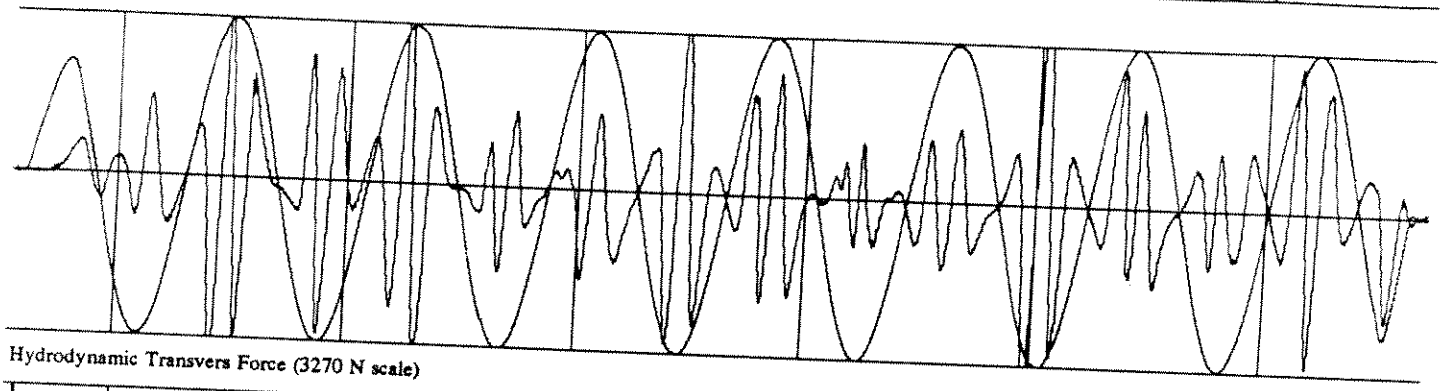

Hydrodynamic Transvers Force (3270 N scale)

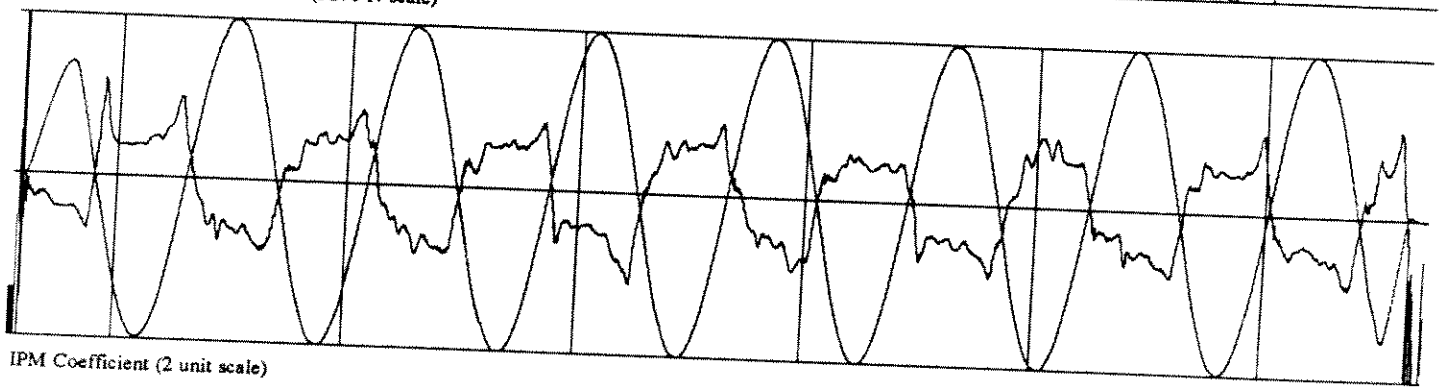

IPM Coefficient (2 unit scale)

PROCESSED DATA for RUN 294 points 1550 to 7700

APPENDIX D
REVIEW OF THE INERTIAL PRESSURE METHODOLOGY (IPM)

HYDRODYNAMIC LOADING

As an introduction to the IPM consider the concepts involved in the hydrodynamic loading of a cylinder. There are only two ways of exerting a force on a cylinder moving through a fluid. One is by pressure which is normal to the surface of the cylinder and the other is by shear which is tangent to the surface. For the high Reynolds Number flows encountered in offshore design the total integrated pressure force dominates. Thus the time varying force on a wave loaded cylinder is due to its pressure distribution and the familiar drag and inertial load components are derived from the integrated pressure force.

The scale of the pressure distribution is given by the Bernoulli equation for potential flow. For a cylinder, deviations from this pressure distribution are due to flow separation on the rear surface and return flow from previous wakes on the front. Pressure coefficients have long been used by aerodynamicists to account for such deviations from a potential flow.

THE INERTIAL PRESSURE METHOD

The Inertial Pressure Method (IPM) is a rational semiempirical approach to determining wave forces. The basis of the concept is that hydrodynamic loading on a body is derived from the instantaneous pressure distribution on the surface of the body. The pressure distribution can be represented by an instantaneous ideal pressure distribution which is modified by instantaneous empirical coefficients. The ideal pressure distribution is obtained from the Bernoulli-Euler equation applied to the potential flow about the body. The pressure distribution is integrated over the surface of the body to achieve an expression for the force acting on the body. The resulting equation, the IPM equation, can be used to empirically determine the instantaneous force coefficients (IPM Coefficients), or it can be used with instantaneous coefficients to determine forces.

In the following we present the development of the IPM equation following the above procedure, indicate how it is used, discuss the significance and dynamics of Theta-min, and contrast the forms of the IPM and Morison equations. We conclude with a brief reference to the correlations of the IPM coefficients that enable one to easily make use of time varying coefficients in practical computations.

DEVELOPMENT OF THE IPM EQUATION

To apply the IPM to a vertical cylinder moving along a straight line path consider the system of Figure 1 .

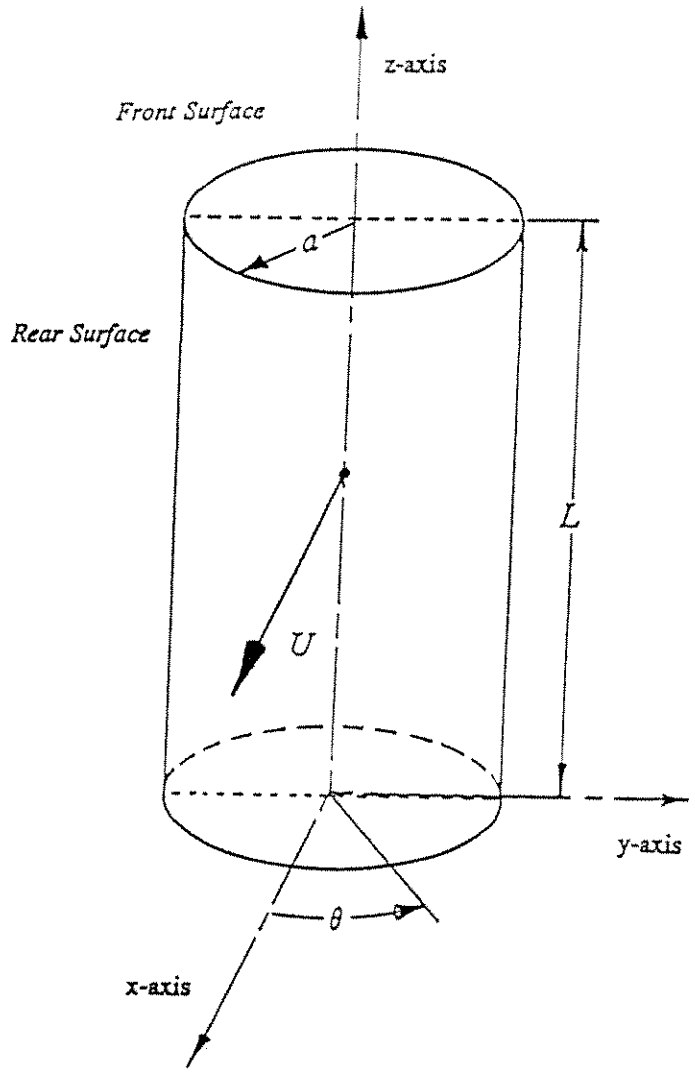

Figure 1

VERTICAL CYLINDER MOVING WITH VELOCITY U ALONG THE X-AXIS

For such a circular cylinder of radius a, confined to move along the x-axis with velocity U and acceleration $\dot{U}$, the potential flow pressure distribution, given by Lamb, is

$$P/\rho = a\dot{U}\cos\theta - 2U^2\sin^2\theta + F(t) \tag{1}$$

A more convenient form is achieved by referencing the pressure to the minimum pressure on the cylinder surface P_{min}, which occurs at the angular position on the surface θ_{min} (Theta-min). Using $\Delta P = P - P_{min}$, the potential flow pressure distribution can be written as:

$$\Delta P/\rho = a\dot{U}(\cos\theta - \cos\theta_{min}) - 2U^2(\sin^2\theta - \sin^2\theta_{min}) \tag{2}$$

This pressure acting over a differential segment, $L\,a\,d\,\theta$, of the cylinder surface yields the differential pressure force component in the x-direction:

$$dF_x = -\Delta P\ a\,L\cos\theta\ d\theta \tag{3}$$

Now to account for deviations from the potential flow pressure distribution consider the pressure coefficients C_f and C_r which modify the pressure on the "front" and "rear" halves of the cylinder. C_r is applied to the pressure on the surface for $-90° < \theta < 90°$ and C_f is applied to the pressure for $90° < \theta < 270°$.

Integration of the pressure force over the surface yields the x-component of the hydrodynamic force. Using the symmetry about the x-axis in performing the integration yields:

$$-F_x/a\,L = 2C_r\int_0^{90}\Delta P\cos\theta\ d\theta + 2C_f\int_{90}^{180}\Delta P\cos\theta\ d\theta \tag{4}$$

Evaluation of the integrals using the expression for ΔP results in an algebraic expression which can be written as:

$$F_x/\rho DL = -[(C_f+C_r)/2]\,\pi D\dot{U}/4 + (C_f - C_r)(4/3\,U^2 + R) \tag{5a}$$

with $D=2a$ and

$$R = -[a\dot{U}\cos\theta_{min} + 2U^2\cos^2\theta_{min}] \tag{5b}$$

The above IPM equation has a strong resemblance to the Morison equation. On contrasting the IPM and the Morison equations the following observations are of note:

For the drag term, the IPM coefficient is the difference in the front and rear pressure coefficients. Its value and sign change during a flow cycle with the reversal of the roles of the front and rear coefficients. Values of the IPM coefficient are observed to be between ±1. Corresponding instantaneous Morison drag coefficients are found by multiplying by 8/3.

For the inertial term, the IPM coefficient is the sum of the front and rear pressure coefficients. This sum yields the classic ideal value when the drag coefficient is 0 and decreases as the drag coefficient increases. This explicit coupling of the mass and drag coefficients has been implicitly noted by other authors over several decades.

Below we shall show how the IPM allows the computation of an empirical coefficient for each simultaneous observation of force and motion. Such IPM coefficient time series provide a clear detailed picture of the values and pattern required to precisely reproduce loading data.

Now consider an aspect of the above expression which is not found in the Morison methology, the quantity Theta-min. The expression for Theta-min, the minimum pressure angle, is obtained by setting to zero the differential of the pressure expression, Equation (1). This yields three conditions:

for $\dot{U}D/8U^2 \leq -1$ then $\theta_{min} = 0°$, (5c)

for $-1 < \dot{U}D/8U^2 < 1$ then $-\cos\theta_{min} = \dot{U}D/8U^2$, and (5d)

for $\dot{U}D/8U^2 \geq 1$ then $\theta_{min} = 180°$. (5e)

USING THE IPM ALGORITHM

The set of Equations (5) is referred to as the "IPM algorithm". With this algorithm it is possible to predict instantaneous hydrodynamic forces on a cylinder moving through a fluid with velocity U and acceleration $\dot{U}$. Using this algorithm, it is also possible to determine instantaneous drag and inertial coefficients from instantaneous force and kinematic data.

The procedure for using the algorithm is straight forward and can be facilitated by an understanding of some of the quantities which appear in these expressions. Below we have outlined a procedure for using the IPM algorithm which includes a discussion of some of the "new" quantities and concepts.

The three steps in using Equations (5) are:

(1) Compute the instantaneous quantity θ_{min}, Theta-min, from the instantaneous velocity and acceleration using Equation (5c), (5d), or (5e). Theta-min is determined by the kinematics of the motion only. A discussion of the behavior and importance of it will be given in a later section. Recall that it is the angular position on the cylinder surface where the potential flow pressure distribution would have a minimum value, and this angular position sweeps over the surface during the cycle. In parts of the flow cycle for which the velocity is large and the acceleration is small Equation (5d) would be used and the solution would tend to 90°. When the acceleration is dominant either Equation (5c) or (5e) is used and the values tend to 0° or 180° depending on the direction of the acceleration.

(2) With instantaneous values of Theta-min, velocity, and acceleration the quantity R is computed using Equation (5c). R is call the "interaction force term" and arises in our derivation from the use of the minimum pressure as a reference for the pressure distribution. The value of R is usually small because $cos\ \theta_{min}$ is small when the velocity is significant. When the acceleration is significant, $cos\ \theta_{min} \approx 1$, and R contributes as an inertial term multiplied by a drag coefficient. For most force predictions the R term can be neglected. We retain it however in determining IPM coefficients from force and kinematic data.

(3) Force predictions follow from Equation (5a) using instantaneous coefficient, kinematic, and R values. The Equation (5a) is identified as the "IPM equation"

MORISON AND IPM EQUATIONS

The similarity between the forms of the Morison equation and the IPM equation are significant and may be noted in the comparison below. These forms are both for a cylinder moving through a fluid.

Morison Equation:

$$F_x/\rho DL = - C_a\ \pi D\dot{U}/4 - C_d\ 1/2\ |U|U \qquad (6)$$

IPM Equation:

$$F_x/\rho DL = -(C_f+C_r)/2\ \pi D\dot{U}/4 + (C_f - C_r)(\ 4/3\ U^2 + R) \qquad (7)$$

In contrasting the expressions the following items should be noted:

(1) That the IPM pressure coefficients have the value of 1 when the surface's pressure is that of potential flow. When flow separation reduces the pressure below that of potential flow the coefficients become less than 1.

(2) That when potential flow occurs on both the rear and front surfaces $C_f = C_r = 1$ and the IPM inertial coefficient $(C_f + C_r)/2 = 1$ and the IPM drag term $(C_f - C_r) = 0$. For this "ideal" flow condition the IPM equation yields the classic expression for the hydrodynamic force on a moving cylinder:

$$F_x = -\rho(L\,\pi D^2/4)\,\dot{U} \tag{8}$$

which indicates an inertial force only. This force is equal to the product of cylinder acceleration and displacement mass and is in opposition to the acceleration. For motion of a cylinder in an ideal fluid the Morison equation inertial coefficient C_a is unity. Clearly the equivalency of the inertial terms and of the limiting values of their coefficients for these two equations has been established.

(3) That it appears both equations have two coefficients which must be supplied for force predictions. For the IPM equation, the deviation of pressure coefficients from unity controls the values of the drag and inertial coefficients. Consider the "deviation", δ, of the front coefficient from unity so $C_f = 1-\delta$. For this the value of the IPM drag coefficient $(C_f - C_r) = -\delta$ and the IPM inertial coefficient $(C_f + C_r)/2 = 1 - \delta/2$. A similar analysis considering the rear coefficient confirms that the value of $(C_f - C_r)$ is a measure of this "deviation" from the ideal flow pressure distribution and that this "deviation" results in a reduction of the inertial coefficient. Thus we observe that the drag and inertial coefficients are coupled so that the development of drag results in a reduction of the inertial coefficient. An empirical observation of this relationship has been reported by several investigators.

(4) That from the above only the IPM coefficient $(C_f - C_r)$ is needed. With it the deviation of the other coefficient $(C_f + C_r)$ from unity can be determined.

D-FORCE FORM OF EQUATIONS

Incorporating the above ideas into the Morison and IPM equations yields the useful forms given below.

Morison Equation:

$$F_x/\rho DL + \pi D\dot{U}/4 = C_a' \pi D\dot{U}/4 - C_d\, 1/2\, |U|U \qquad (9)$$

IPM Equation: *

$$F_x/\rho DL + \pi D\dot{U}/4 = (C_f - C_r)(\pi D|\dot{U}|/8 + 4/3\, U^2 + R) \qquad (10)$$

For the Morison equation we have replaced the inertial coefficient C_a with $(1 - C_a')$. The coefficient C_a' is referred to as the inertial correction.

For the IPM equation the use of the absolute value of acceleration is a consequence of the sign switching of the IPM coefficient. The IPM coefficient (C_f-C_r) is used as a single coefficient and not as separate values of C_f and C_r. The notation is somewhat confusing and cumbersome; however, we have retained it to emphasize that this coefficient is the difference in pressure coefficients on the front and rear surfaces. Also positive values of (C_f-C_r) are associated with $C_r < 1$ or separation on the rear surface, and the switching to negative values of (C_f-C_r) is associated with $C_f < 1$ or separation on the front surface.

Comparisons of the drag terms reveals that $C_d = 8/3\,(C_f-C_r)$. Note that nominal values of the IPM coefficient are less than 1.

The combination of terms (in-line hydrodynamic force and the ideal inertial force) on the left-hand side of the above equations is referred to as the "defect-force" or "D-Force". When a data reduction is performed the computation of the D-Force from force and kinematic data provides a useful measure of the drag contribution to the total force.

The above D-Force form of the IPM equation reveals the simplicity of determining instantaneous values of the IPM coefficient from instantaneous force and kinematic data. The D-Force divided by the kinematic term $(\pi D|\dot{U}|/8 + 4/3\, U^2 + R)$ yields the coefficient. It should be noted that this kinematic term is never zero so the coefficient is always finite.

---

* Note: An IPM expression for the transverse force has been derived using similar arguments. The IPM Transverse Force Coefficient is $(C_2 - C_1)$ and the force expression is:

$$F_y/\rho DL = (C_2 - C_1)(D|\dot{U}|/4 + 2/3\, U^2 + R)$$

COMMENTS ON THETA-MIN

A strong correlation between instantaneous values of Theta-min and the IPM coefficient has been noted in our previous studies and will be briefly treated in the final sections. The apparent reason for the correlation is that the IPM coefficient is a measure of the extent of flow separation and Theta-min is related to the potential for flow separation.

Recall that regions of adverse pressure gradient are necessary for separation and that the Theta-min position on the cylinder is the demarcation between segments of the cylinder subjected to "favorable" and "adverse" pressure gradients. Thus the pattern of Theta-min sweeping over the cylinder surface establishes conditions for flow separation and separation characterizes the value of the IPM coefficient. The sweeping of Theta-min can best be followed by considering the sinusoidal motion of a cylinder depicted in Figure 2 .

Beginning our observation as the cylinder moves through the null velocity with peak acceleration in the negative direction. At this point the value of $(\dot{U}D/8U^2)$ would be a large negative number. For this condition Eq.(5c) indicates Theta-min is at the 0° position and none of the surface is subjected to an adverse pressure gradient. Theta-min dwells in this position for a fraction of the cycle. The dwell time depends on the amplitudes of $\dot{U}$, D, and U^2. Eq.(5d) applies as the instantaneous value of $(\dot{U}D/8U^2)$ exceeds -1 and Theta-min sweeps away from 0° toward the 90° position. During this portion of the flow cycle a spreading region of adverse pressure exists between the $\pm\theta_{min}$ locations on the cylinder. This adverse pressure gradient would influence the flow on the rear surface. As U^2 achieves a maximum value, the acceleration becomes positive and Theta-min sweeps through 90°and on toward 180°. During this portion of the cycle a significant region of adverse pressure exists. This half cycle of negative motion for the cylinder concludes with $\theta_{min}=180°$ for a fraction of the motion for which $(\dot{U}D/8U^2)$ exceeds +1,Eq.(5e).

The dwell times of θ_{min} at 0° and 180° and the duration of the flow cycle when $\theta_{min} \simeq 90°$ are determined by $(\dot{U}D/U^2)$, which is the Iversen parameter, which is the reciprocal of the KC-Number. For small KC-Numbers the dwell at 0° and 180° is significant and the sweep through 90° is rapid. By contrast with large KC-Numbers the dwells at 0° and 180° are short and the minimum pressure is in the vicinity of 90°for most of the cycle. One can think of $cos\ \theta_{min}$ as an instantaneous KC-Number.

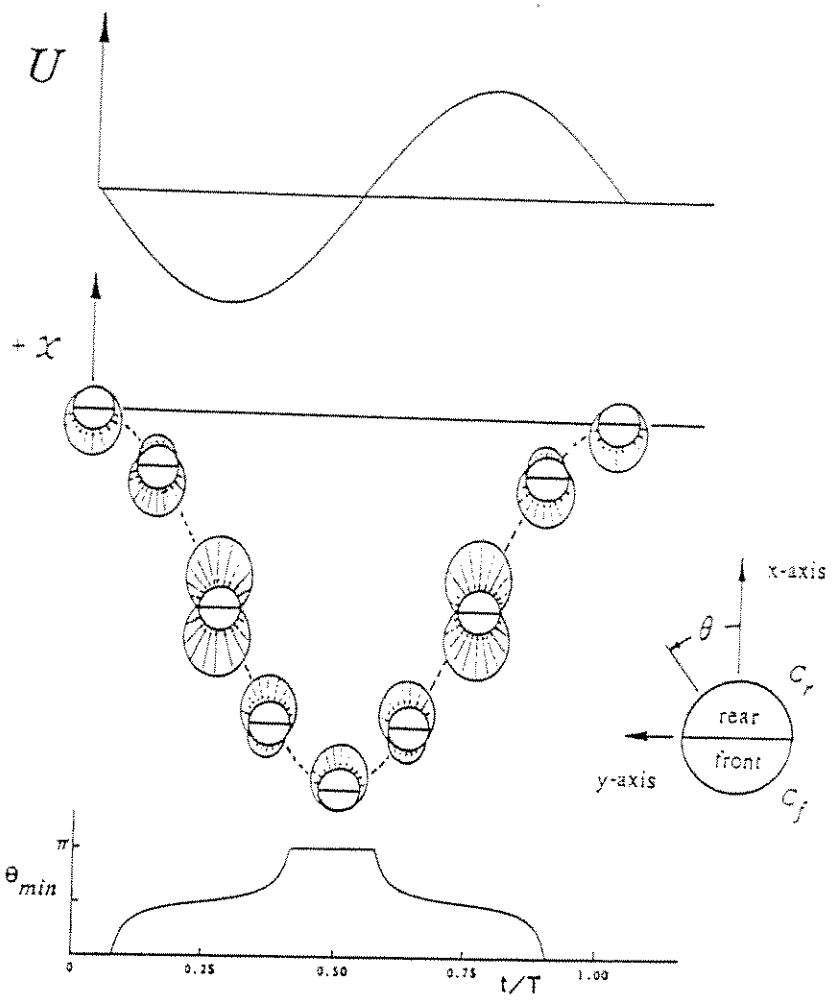

Figure 2

TIME SERIES REPRESENTATION FOR A MOVING CYLINDER

Relationship between the Velocity of a Cylinder and Its Position, Pressure Distribution, and Theta-min

IPM CORRELATIONS

The IPM's instantaneous coefficient time series is compatible with the Morison equation and can be interpreted in terms of the physics of the flow (separation, wake sweeping , etc). However, a more important feature has

been the establishment of the Theta-min Correlation, which is a correlation between instantaneous values of the IPM coefficient and the kinematic quantity Theta-min.

The quantity Theta-min is the location on a cylinder of the minimum potential flow pressure. This angular position sweeps back and forth over the cylinder surface (between 0° and 180°) during the flow cycle. It plays a key role in "turning on" the drag coefficient by determining when and where adverse pressure gradients exist on a cylinder. Adverse pressure gradients result in flow separation and build up of drag.

Figure 3 is an example of the Theta-min Correlation. Here the instantaneous values of the IPM coefficient and the Theta-min angle are cross plotted. This plot is for a "combined motion" flow involving multiharmonics. From this Figure it is clear that the drag does not "turn on" until Theta-min approaches 90°, the maximum velocity condition. The pattern in this figure shows inertial dominance early in the flow cycle where the drag is zero or slightly negative due to wake sweeping.

The persistence of this correlation pattern over a wide range of tests is central to using the IPM for predictions. With the pattern portrayed by the dashed lines in Figure 3, accurate force predictions have been achieved.

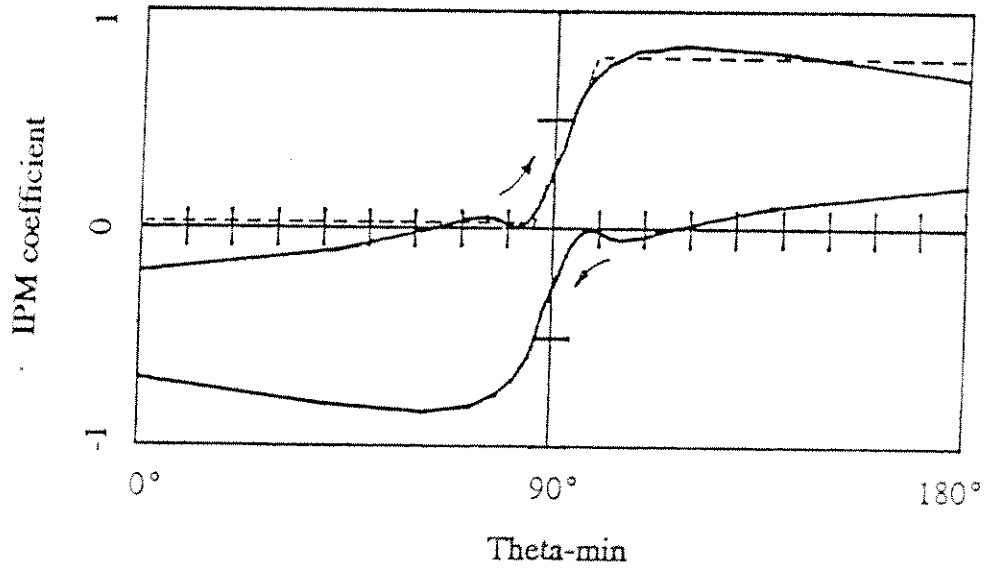

Figure 3

EXAMPLE OF THE THETA-MIN CORRELATION PATTERN

The IPM Coefficient, $(C_f - C_p)$, plotted versus Theta-min, θ_{min}, for a Combined Motion Test involving Multiharmonic Motion. The dashed line segments were effectively used to represent the pattern in force predictions. The progression around this plot is clockwise.

IPM WITH COMBINED MOTION

As a further illustration of the persistence of the Theta-min Correlation pattern, two records of SSPA data have been nearly superimposed for comparison in Figure 4 . These are plots of individual data points without filtering or smoothing. Both records represent the troublesome condition involving high steady currents combined with periodic motions. For such conditions no flow reversal occurs.

The level of correlation is such that the data points form the curves. For the lower plot the amplitude of motion equaled the cylinder diameter and the periodic velocity amplitude equaled the steady velocity. The upper plot is motion of half a cylinder diameter combined with a steady velocity twice the periodic velocity. The agreement is such that these plots could be interchanged.

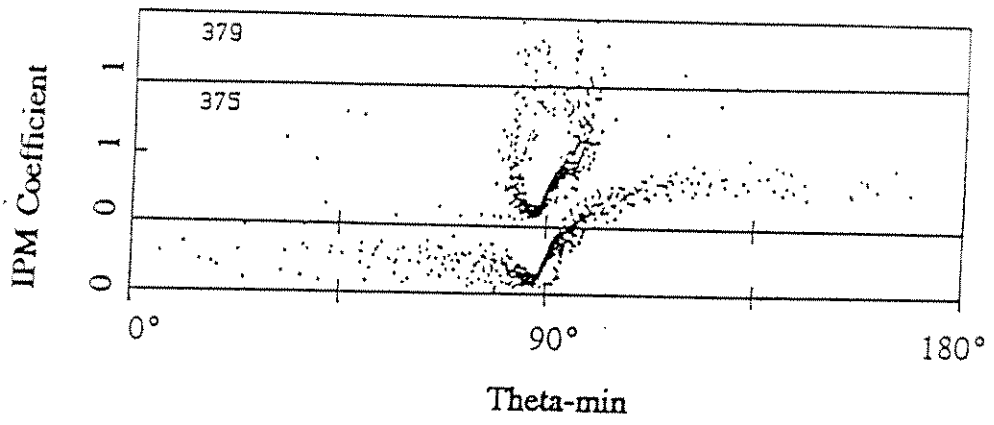

Figure 4

THETA-MIN CORRELATION PLOTS

A comparative superposition of IPM Coefficients from Two SSPA Combined Motion Runs involving large currents. For 375 the steady to periodic velocity ratio was 1 and the periodic KC-Number was 6.2 . For 379 the steady to periodic velocity ratio was 2 and the periodic KC-Number was 3.1 . For both the IPM correlation KC-Number was 27.